3D SEISMIC GEOMORPHOLOGY OF FLUVIAL SYSTEMS

Faisal A. Alqahtani

Department of Earth Science and Engineering

Imperial College London

Submitted in accordance with the requirements for
the degree of Doctor of Philosophy of Imperial College London

November 2010

Declaration

I declare that this thesis

3D SEISMIC GEOMORPHOLOGY OF FLUVIAL SYSTEMS

is entirely my own research under the supervision of Prof. Howard Johnson and Dr. Chris Jackson. The research was carried out in the Department of Earth Science and Engineering at Imperial College London. All published and unpublished material used in this thesis has been given full acknowledgement. None of this work has been previously submitted to this or any other academic institution for a degree or diploma, or any other qualification.

Faisal A. Alqahtani
PhD student
Department of Earth Science and Engineering
Imperial College London

Abstract

Fluvial sandstones constitute one of the major clastic petroleum reservoir types in many sedimentary basins around the world. This is especially true in the Tertiary basins of Southeast Asia, which display a wide range of fluvial channel reservoir types. This study is based on the analysis of high-resolution, shallow (seabed to *ca.* 500 m depth) 3D seismic data which provide exceptional imaging of the geometry, dimension and temporal and spatial distribution of fluvial channels. The Malay Basin comprises a thick (>8 km), rift to post-rift Oligo-Miocene to Pliocene basin-fill. The youngest (Miocene to Pliocene), post-rift succession is dominated by a thick (1-5 km), cyclic succession of coastal plain and coastal deposits, which accumulated in a humid-tropical climatic setting.

This study focuses on the Pleistocene to Recent (*ca*. 500 m thick) succession, which comprises a range of seismic facies, mainly reflecting changes in fluvial channel style and gross stratigraphic architecture. The succession has been divided into four seismic units (Unit 1-4), bounded by basin-wide stratal surfaces. Units 3 and 4 have been further divided into two sub-units. Two types of boundaries have been identified: 1) a boundary that is defined by a regionally-extensive erosion surface at the base of a prominent incised valley (e.g. Horizons C.1 and D.1); 2) a sequence boundary that is defined by more weakly-incised, straight and low-sinuosity channels which is interpreted as lowstand alluvial bypass channel systems (e.g. Horizons A, B, C, and D). Each unit displays a predictable vertical change of the channel pattern and scale, with wide low-sinuosity channels at the base passing gradationally upwards into narrow high-sinuosity channels at the top. The wide variation in channel style and size

is interpreted to be controlled mainly by the sea-level fluctuations on the widely flat and tectonically-quiescent Sundaland Platform.

Table of Contents

List of Figures

List of Tables

Acknowledgments

It is my pleasure to acknowledge the support of the many individuals and organisations who contributed to the successful completion of this study. First and foremost, I would like to express my deepest gratitude to my supervisors, Howard Johnson and Chris Jackson, for their advice, constant encouragement, and support. I have enormously benefited from their invaluable scientific and spiritual support throughout my study.

PETRONAS is gratefully acknowledged for providing 3D seismic and site survey data. I would especially like to thank: Rapi Som, Khairul Sulaiman, Nor Azhar Ibrahim, Rais, and Deva Ghosh for helpful discussion about the fluvial systems of Miocene to Recent succession.

A special thank goes to Exprodat, especially Alex Davis, Chris Jepps, and Gareth Smith for their help in using ArcGIS and developing a semi-automated methodology to quantify the channel morphometric parameters. Also I would like to thank King Abdul Aziz University for sponsoring my PhD study.

A special mention with sincere gratefulness goes to those who have made a big change on my life by supporting and encouraging me throughout my long period of study. This goes to my dearest parents who have waited so long to see this moment. Also I would like to thank my brothers and sisters for their support. A special thank to my wife and children who had to suffer a lot from my absence during my study and supported me throughout my study. Without their support I wouldn't be able to reach this point at all. I feel fortunate to have made so many good friends during my time in

the Department of Earth Science and Engineering. I wish to thank them all but too many to name. To you all, I dedicate this work.

Chapter 1
Introduction

1.1 Rational and Motivation

Fluvial channel sandstones form major productive reservoirs for hydrocarbons in many basins around the world. In these basins, exploration and production activities are increasingly concerned with predicting the origin and distribution of fluvial sandstone bodies, which include a wide variety of geometries and stacking patterns ranging from narrow, single-story sandstone bodies to wide and amalgamated multi-story sandstone bodies. Geometric quantitative data of fluvial channel sandstone bodies, including size, shape, orientation, spatial distribution, proportion and connectedness, are particularly important aspects of reservoir management that can help to determine reservoir volume productivity and ultimate recovery (Bryant and Flint, 1993; Reynolds, 1999). These data are also critical to building and conditioning 3D reservoir models in order to determine the most efficient well spacing and production strategy. Furthermore, studying the geometry of the fluvial sandstone bodies contributes directly to a better understanding of sequence stratigraphy and basin evolution, because these systems respond rapidly to changes in climate, tectonics and base-level (Schumm, 1977; Shanley and McCabe, 1994; Blum and Törnqvist, 2000).

Systematic vertical changes are indicated in many stratigraphic models of fluvial systems (e.g. Wright and Marriott, 1993; Shanley and McCabe, 1994). The Stratigraphic models infer predictable changes in fluvial architecture in response to a wide range of allocyclic

processes, including sea-level fluctuation, uplift, subsidence, faulting and climate. During base-level rise, channels change their size and geometries, typically becoming more highly-sinuous (meandering) with very well-developed point bars associated with lateral accretion surfaces. During the late highstand to early lowstand, when sea-level starts to fall, channels respond by typically becoming narrower with low to moderately-sinuous planform geometries.

Improvements in 3D seismic acquisition and processing can provide new insight into fluvial channel architectures, especially planform geometries. These data provide valuable qualitative and quantitative data of the subsurface reservoirs, which contribute directly to a better understanding of fluvial channel systems and their exploration and production potential. Furthermore, high-resolution 3D seismic data can also aid in the construction and conditioning of 3D reservoir geological models due to the lateral and vertical continuity of observations that cannot be obtained from other data sources (e.g. cores, well logs, outcrops; Figure 1.1).

This study is to evaluate the temporal and spatial variations in fluvial system architecture within the Pleistocene to Recent fill of the Malay Basin using high-quality, shallow 3D seismic data. The documentation of the dimensions and geometries of Pleistocene fluvial systems will help in the construction of a quantitative database which can be used to help constrain reservoir models for the deeper productive Miocene fluvial reservoirs in the Malay Basin and the broader Sunda Shelf. Furthermore, these seismically-derived quantitative data are used to establish relationships between the morphometric parameters and to develop empirical equations that can aid prediction of fluvial channel sand body dimensions.

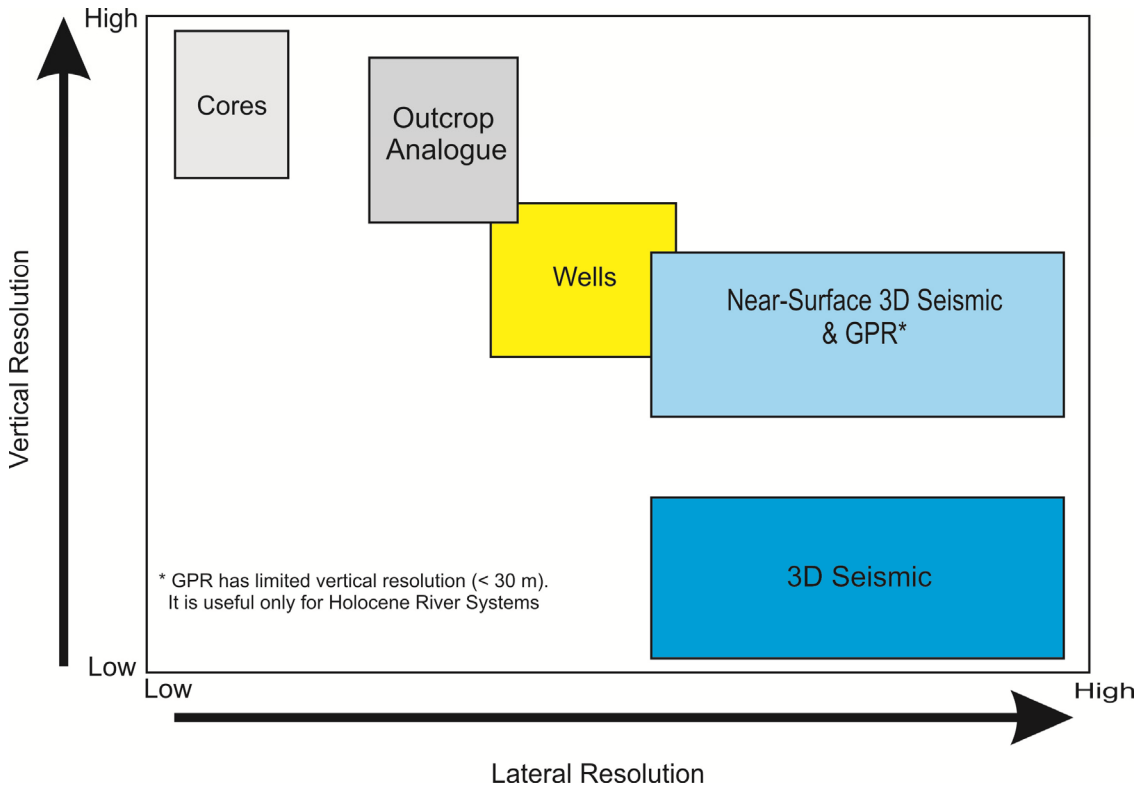

Figure 1.1: A schematic chart showing the various subsurface data types, including outcrops, cores, well logs, 3D seismic (deep) and near-surface 3D seismic that sample the reservoir volume plotted against the corresponding vertical and lateral resolutions. The vertical-based data (well logs and cores) and 2D outcrop can provide excellent information on the vertical extent of sediment bodies with, however, relatively low lateral resolution, compare to 3D seismic from deeper part. Near-surface 3D seismic data and Ground Penetrating Radar (GPR) can help bridge the data gaps between the vertical-based data and deep-3D seismic data by improving the vertical and lateral resolutions; however, the usefulness of GPR is vertically limited to depth of less than 30 m.

1.2 Thesis Aims and Objectives

The aim of this thesis is to describe and evaluate the size, geometry and architecture of fluvial systems within the Pleistocene to Recent succession of the Malay Basin. Most significantly, this study is on a basin-scale using a large 'mega-merge' 3D seismic dataset (11500 km^2), which allows investigation down to *ca*. 500 m below the present-day sea-bed. This dataset provides a unique analysis of fluvial architecture that cannot be

achieved from other data sources, such as a single 3D seismic survey, outcrops, well logs or cores. Specific objectives of this thesis are as follows:

1) Investigate temporal and spatial variations in fluvial system architecture, including an assessment of the controlling factors that determine the variability in the fluvial architecture.
2) Define the variability in 3D seismic expression and document the dimensions and geometries of fluvial systems observed in this study to classify the channels based on their cross-sectional view, planform geometry and morphometric parameters.
3) Construct a quantitative database which can be used to help constrain reservoir models for the productive Miocene fluvial reservoirs on the Sunda Shelf.
4) Describe and interpret the Late Pleistocene incised valley system on the Sunda Shelf, including the development of a model for such systems.
5) Test previous empirical equations developed on modern rivers against the fluvial systems observed within this study area, establish new empirical relationships between the channel morphometric parameters, and develop new empirical equations.

1.3 Study Area

The Malay Basin is situated in the centre of the Sunda Shelf, Southeast Asia, which is one of the largest intracontinental shelf areas in the world (i.e. *ca*. 125,000 km²) (Madon, 1999; Figure 1.2). The north-west southeast trending Malay Basin is 500 km long by 250 km wide, and is located between the Penyu and West Natuna basins to the south and the Pattani Basin to the north (Hutchison, 1989; Madon et al., 1999; Figure 1.2).

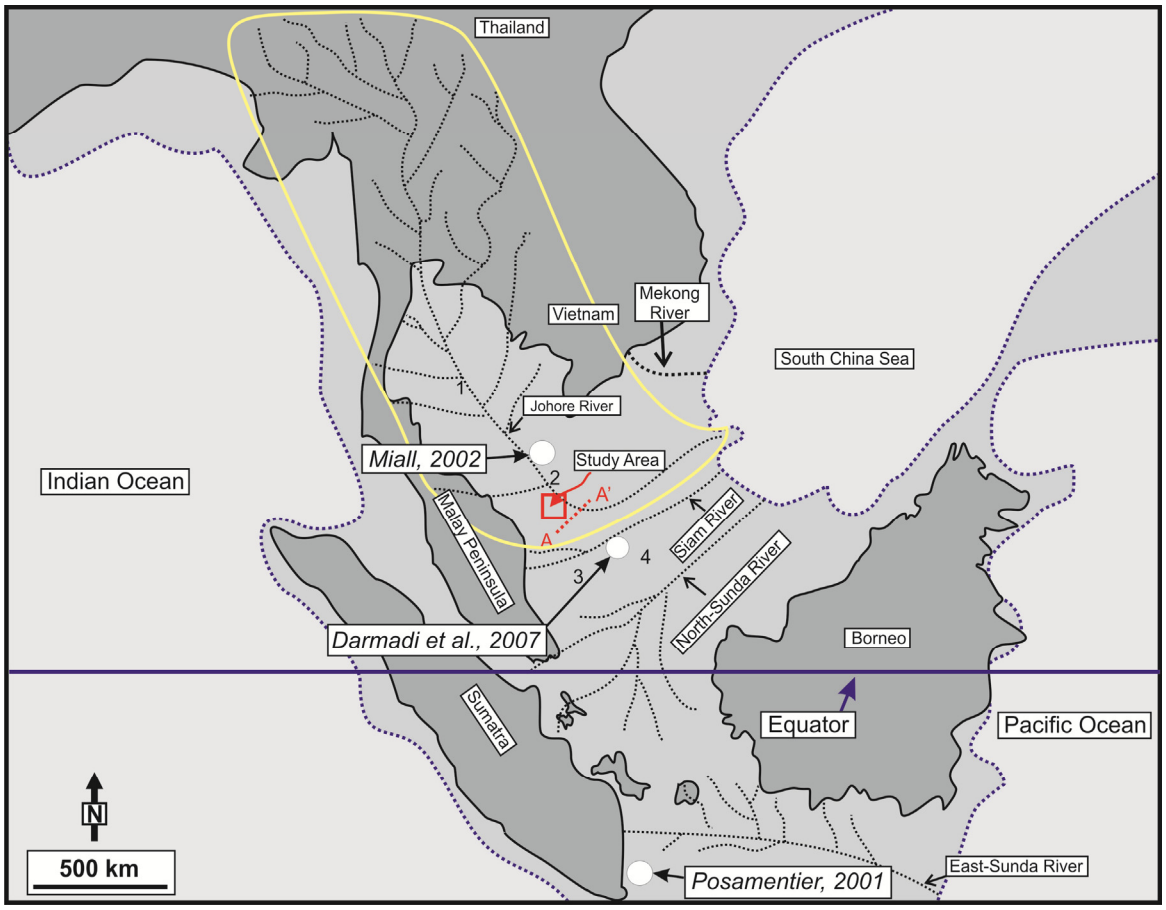

Figure 1.2: Location map of the study area within the Malay Basin (2) on Sunda Shelf, Southeast Asia. Locations of other basins (Pattani Basin (1); Penyu Basin (3); and West Natuna Basin (4)) within the Sunda Shelf are also shown. The study area is more than 700 km away from the shelf break and a few hundred kilometers basinward of the modern shoreline. The blue dashed-lines represent the shallow areas of the Sunda Shelf that were exposed during the sea-level falls. The black dashed-lines represent the paleo-drainage systems that are still detectable on the modern sea floor (edited from Molengraaff 1921; Tjia 1980; Voris, 2000). The water depth within the study area ranges from 50 to 80 m. The red solid-line represents the regional cross-section shown in Figure 1.4. The blue solid-line represents the equator line. Locations of previous studies of Posamentier (2001), Miall (2002) and Darmadi et al. (2007) that were conducted on SE Asia are shown.

1.3.1 Tectono-stratigraphic evolution

The Malay Basin formed as a result of tectonic extension during the Late Eocene to Early Oligocene, following the collision of India with the Asian continent (Tapponnier et al., 1986; Hutchison, 1989). The basin comprises a thick succession (>8 km) of Oligo-Miocene to Recent deposits, which overlie a pre-Tertiary basement consisting of metamorphic, igneous and sedimentary rocks (Figures 1.3 & 1.4). The structural evolution of the Malay Basin can be divided into three tectono-stratigraphic phases (Tjia, 1994; Madon, 1998; Negah et al., 1996 and Tjia and Liw, 1996): 1) a pre-Miocene syn-rift phase; 2) an Early to Middle Miocene post-rift phase dominated by thermally-induced subsidence and basin inversion; and 3) a Late Miocene to Recent phase dominated by thermally-induced subsidence but lacking significant basin inversion (Figure 1.4).

The pre-Miocene phase represents the initial extensional phase of basin development, when subsidence was controlled by normal faulting (Hamilton, 1979; Madon, 1999). Sedimentation was characterised by alternating sand-dominated and shale-dominated fluvio-lacustrine sequences within a series of isolated half-grabens (Madon, 1999). The Early to Middle Miocene post-rift phase was dominated by thermal subsidence that was accompanied by intermittent periods of compressional deformation. This resulted in local inversion of syn-rift half-grabens and re-activation of their bounding faults, which was particularly intense in the southern part of the basin (Madon, 1999). One consequence is that the south-western flank of the Malay Basin is slightly steeper than the north-eastern flank (Figure 1.4). During this post-rift thermal subsidence phase, deposition was characterised by coastal to shallow marine deposits. The Late Miocene to Recent phase was dominated by thermal subsidence, without any significant tectonic activity (Madon et

al., 1999). Deposition during this phase was mainly within coastal plain and shallow marine environments (i.e. Pilong Formation; Madon, 1999b).

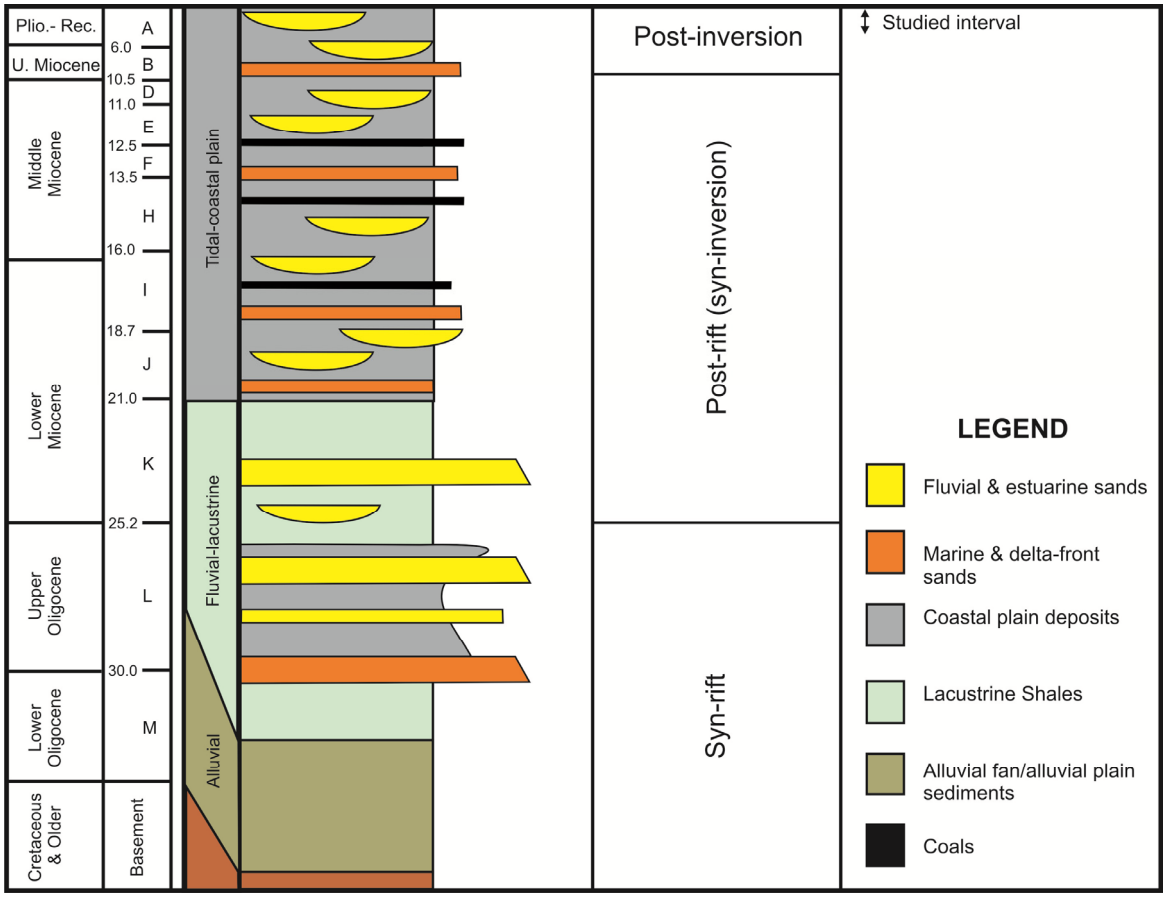

Figure 1.3: Generalised stratigraphic column of the Malay Basin showing the lithostratigraphic units. The studied interval is the upper part of Group A succession which is mainly composed of coastal plain deposits (Modified from Madon, 1999d).

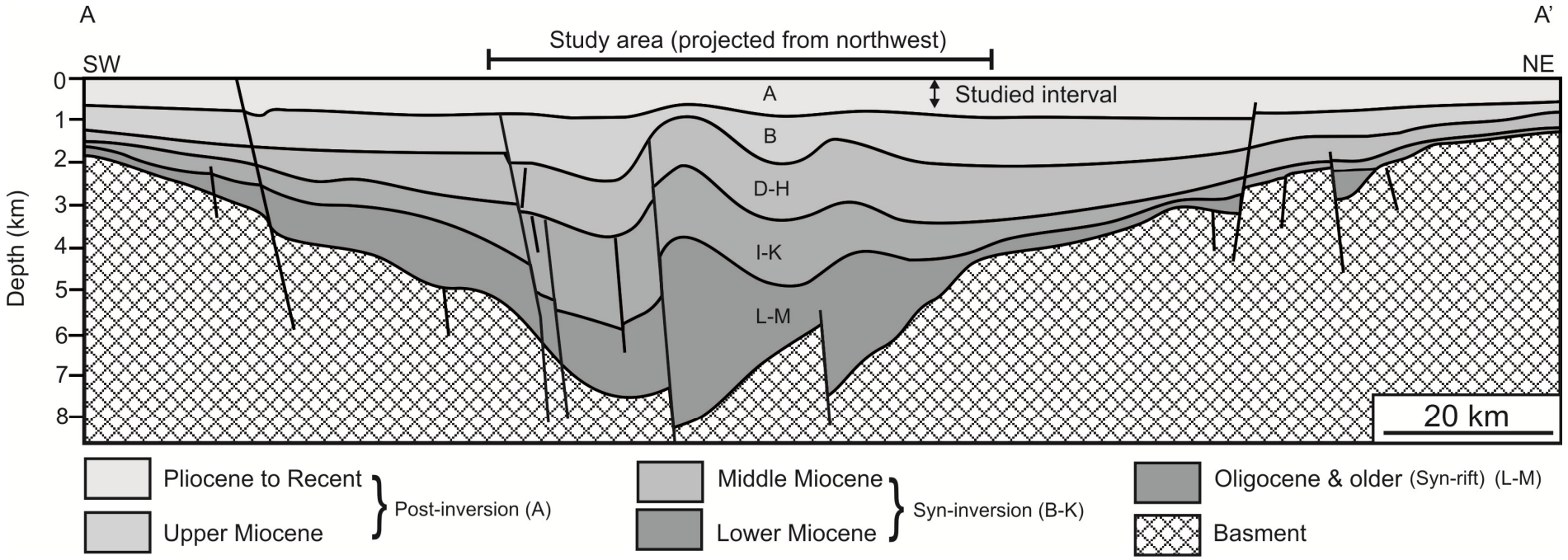

Figure 1.4: Regional cross-section of the Malay Basin. Location of this cross-section is shown in Figure 1.2. The studied interval lies within the Upper post-rift (post-inversion) Pliocene to Recent (Modified from Madon, 1999d).

1.3.2 Physiographic and paleoclimatic setting

The Sunda Shelf is one of the largest tropical shelf areas in the world (Hanebuth and Stattegger 2003). It is situated at the south-western margin of the South China Sea, the largest marginal sea of the Southeast Asia (Figure 1.2). The shelf is extremely broad (up to 800 km at its widest section) and has a very low-gradient (< 0.1º). The Sunda Shelf was tectonically stable during the Pliocene and Pleistocene (Madon, 1998). It is located at the equator and near the "West Pacific Warm Pool"; this suggests that the climate during the Last Glacial Maximum (LGM) was similar to the modern-day tropical climate of the Southeast Asia lowlands (Morley, 2000; Sun et al., 2000). However, monsoon-driven precipitation during the LGM was lower than during the Holocene, suggesting that vegetation patterns in lowland areas such as the Sunda Shelf were potentially affected by the dry winter-monsoon (Wang et al., 1999).

The present-day water depth within the study area ranges from 50 to 80 m and the average water depth across most of the Sunda Shelf is *ca*. 70 m. The shelf break occurs at *ca.* 180 to 220 m beneath the present-day sea-level. During the middle Pleistocene, the growth of continental glaciers decreased ocean volume and caused a maximum reduction in sea-level of *ca*. 160 m and *ca*. 120 m during the LGM (Gascoyne et al., 1979; Hopkins, 1982; Yang and Xie, 1984; Hanebuth et al., 2003; Hanebuth and Stattegger, 2003; Voris, 2000). Hence, most of the Sunda Shelf was subaerially exposed during the LGM, with the shoreline located close to the present-day shelf break (Hanebuth et al., 2003; Hanebuth and Stattegger, 2003; Voris, 2000). Consequently, the adjacent South China Sea was strongly reduced in size, forming a semi-enclosed marginal sea (Sathiamurthy and Voris, 2006).

Based on present-day bathymetric depth contours, Voris (2000) and Sathiamurthy and Voris (2006) presented a series of maps that estimated the exposed area of the Sunda Shelf during Pleistocene to Recent sea-level lowstands. These maps show several major submerged valleys, or paleo-'trunk' river systems, with associated tributaries (black dashed-lines in Figure 1.2). The most recent form is elongated depressions, up to several hundreds of kilometers in length and can be seen on the modern sea floor bathymetry map (Figure 1.2). One of these major trunk rivers, called the Johore River (Voris, 2000), ran south-eastwards through the Gulf of Thailand, the Malay Basin and ultimately to the South China Sea. Morley and Westaway (2006) also described a similar paleo-river system called the paleo-Chao Phraya River that ran through the Gulf of Thailand to South China Sea for much of the Cenozoic, including the Late Pleistocene. This river is thought to be synonymous with the Johore River. The area studied here is located close to the axis of the pre-Holocene Johore River (Figure 1.2).

The Johore/paleo-Chao Phraya River was one of the major sediment sources for the Malay Basin (Loe, 1997; Morley and Westaway, 2006). Adjacent local sediment sources from the Malay Peninsula were considerably smaller. The paleo-Chao Phraya River drained a large catchment area (*ca.* 750,000 km²), with its headwaters in northern Thailand. Clift (2006) suggested a reduction in sediment budget that was transported to the Sunda shelf through the Gulf of Thailand during the Late Miocene to Recent especially during LGM. This estimation was based on the reconstruction of the clastic mass accumulation on continental margins using well logs and seismic profiles, and from published data mainly derived from the work of Me´tivier et al. (1999). Furthermore, Hutchinson (1989) suggested that the basins in the Gulf of Thailand, including the Malay Basin, were supplied by vast quantities of clastic material from the rising mountain belts such as Himalaya and were transported by giant rivers such as the Mekong River. It is

possible that the Mekong River was also flowing through the Malay Basin during much of the Cenozoic times until it was diverted by the faulting during the Late Cenozoic (Hutchinson, 1989). The Mekong River now enters the Sunda Shelf from Vietnam. Sinsakul (1992) and Morley and Westaway (2006) concluded that during the LGM, when a reduction in sediment supply occurred, earlier highstand deltaic deposits inland of the modern coastline of the Gulf of Thailand were reworked and transported by the Johore /paleo-Chao Phraya River to the South China Sea.

1.4 Approaches and Methodologies

The main focus of this study has been the analysis of a 'mega merge' 3D seismic reflection dataset with a total areal extent of *ca.* 11500 km^2 (*ca.* 115 km wide by *ca.* 100 km long). Where possible, this has also been supplemented by higher resolution local site survey data. The following approaches and techniques have been utilised: 1) seismic facies analysis of the Pleistocene to Recent succession to divide the interval of interest into several seismic units; 2) generation of time and iso-proportional slices to image the fluvial systems in planview; 3) analysis of site survey data, including borings and high-resolution 2D boomer sections in order to determine the lithology and facies types; 4) application of geographic information software (GIS) to develop a quantitative methodology for measuring the morphometric parameters of the channels. Further details of the methodologies and techniques used in this study are discussed in Chapter 3.

1.5 Thesis Structures

This thesis consists of seven chapters. **Chapter 1** provides an introduction to the project and to the geological setting of the study area, including the motivation and the objectives of this research. **Chapter 2** reviews the most critical literature, focusing on three key aspects: 1) sequence-stratigraphic models of fluvial systems, including the vertical variability in fluvial channel architecture and style and the main geological controls. The formation and recognition of incised valleys and sequence boundaries are also discussed; 2) classification of the fluvial systems describing the relationship between planform geometry of the channels and the transported sediments; 3) methodologies and techniques used to determine the geometry of the fluvial channels, including the newly developed empirical equations and 3D seismic geomorphology. 3D seismic techniques and previous studies of 3D seismic geomorphology of fluvial systems are also illustrated. **Chapter 3** illustrates the methodologies and techniques used in this study including the new GIS methodology adopted for this study.

Chapters 4 to 6 discuss the analysis and the results of this research; each chapter is presented in the form of a paper, consequently the PhD supervisors (Chris Jackson and Howard Johnson) are included as co-authors. **Chapter 4** highlights the variability in 3D seismic expression, and investigates temporal and spatial variations in fluvial system architecture within the Pleistocene to Recent fill of the Malay Basin. The controlling factors that determine the variability in fluvial architecture are evaluated. **Chapter 5** describes a major Late Pleistocene incised valley, integrating 3D seismic and local site survey data. **Chapter 6** describes the morphometric parameters of 130 channels. These have been quantified to allow new empirical equations to be proposed that can be used in

the 3D reservoir modeling. Finally, **Chapter 7** discusses the main results of this study and relates them to the original aims and objectives.

Chapter 2

Overview of Fluvial Systems

2.1 Introduction

Fluvial sandstone reservoirs are complex and display a wide variety of stacking patterns. It is often assumed that meandering fluvial sandstone bodies are generally channel-like and isolated, whereas sheet-like fluvial reservoir sandstones are typically deposited in braided fluvial environments (Reading, 1996; Bridge and Tye, 2000). The complexity and vertical variability in fluvial channel architecture and style is indicated in most sequence-stratigraphic models of fluvial systems (e.g. Wright and Marriott, 1993; Shanley and McCabe, 1994), which attempt to explain the controlling factors that determine the changes and variability in fluvial systems.

In this chapter, three main aspects of fluvial architecture are discussed: 1) Sequence-stratigraphic evolution of the fluvial deposits, including a review of the vertical changes in fluvial architecture and the formation and recognition of incised valleys; 2) Classification of fluvial systems and the empirical relationship between the morphometric parameters of the channels; 3) Methodologies and techniques used to determine the geometry of the fluvial channels including the developed empirical equations and 3D seismic geomorphology.

2.2 Sequence-Stratigraphic Evolution of Fluvial Systems

Detailed understanding of the stratigraphic evolution of the fluvial deposits is still incomplete (Bridge and Tye, 2003), although several stratigraphic-sequence models for fluvial deposits have been proposed (e.g. Shanley and McCabe, 1991, 1993, 1994; Wright and Marriott, 1993; Posamentier and Allen, 1999; Figures 2.1 and 2.2). In these models, idealised vertical changes in fluvial channel type and architecture are predicted and related to key geological factors that control these vertical changes. To some extent, these models explain the importance and interaction of base-level change, climatic variability and tectonics.

2.2.1 Controls on Variability and Changes in Fluvial Systems

In detail, the vertical changes in fluvial channel architecture, style and size are controlled by numerous factors. Schumm (2005) divided these controlling factors into three types: 1) *upstream controls*, including tectonics, climate, lithology and the geological history; 2) *local controls*, including valley morphology, vegetation, active tectonics, tributaries and type of bedrock; and 3) *downstream controls*, which include base-level fluctuation and length (how far upstream the effects of the base level extend). Among these factors, base-level variations, syn-depositional tectonics and climate are considered to be the most significant factors. For channels that discharge into ocean basins, base-level corresponds to sea-level. Tectonics (uplift or subsidence) and base-level (sea-level) fluctuations are the main controls on the rate of accommodation space creation or destruction. In particular, these factors determine whether fluvial incision, aggradation or lateral migration occurs.

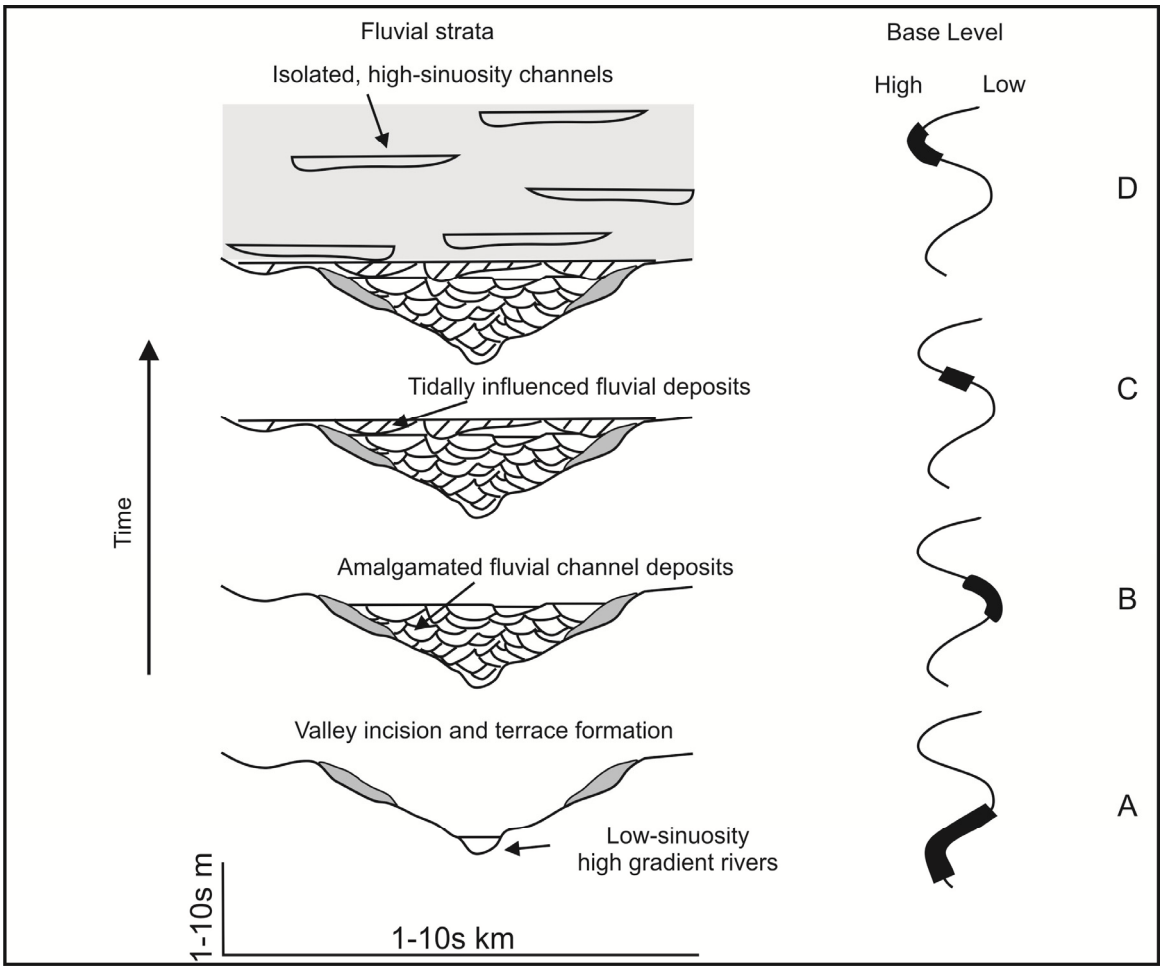

Figure 2.1: The fluvial sequence model of Shanley and McCabe (1991, 1993, 1994). It shows changes in fluvial architecture as a function of base level changes of nonmarine strata (modified from Shanley and McCabe, 1993).

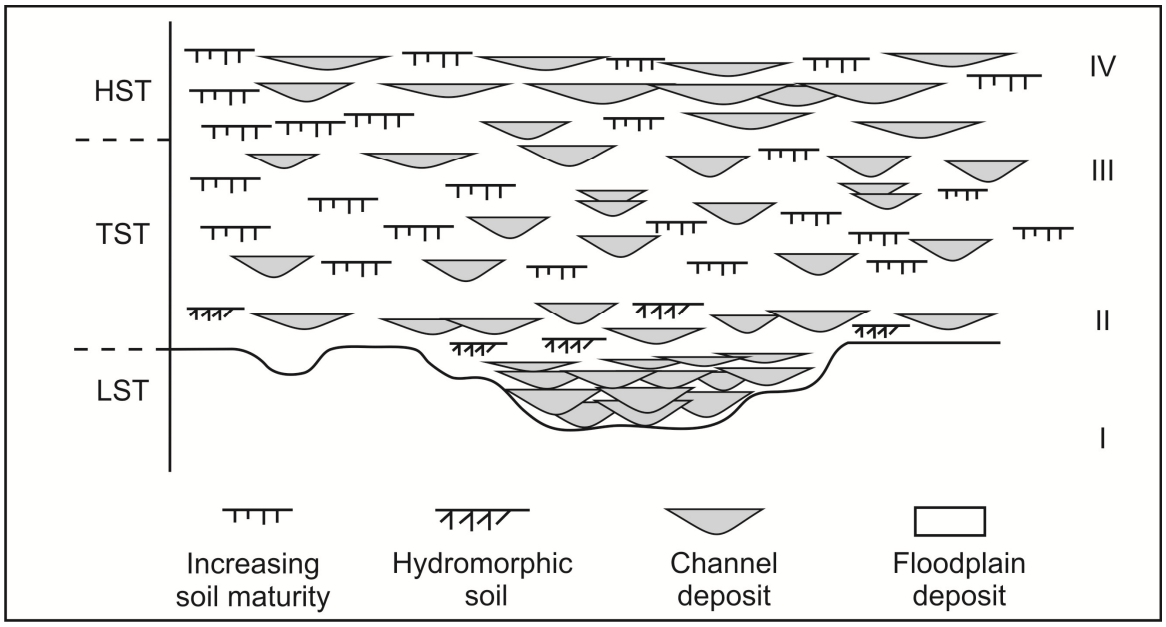

Figure 2.2: The fluvial sequence model of Wright and Marriott (1993; modified from Wright and Marriott, 1993).

Schumm (1993) indicated that deep river incision may occur in association with a significant fall in relative base-level, and that the geometric characteristics (e.g. width, depth, etc) of the fluvial incision are determined by the magnitude of the base-level fall (Posamentier, 2001). For example, when a significant fall in relative base-level occurs and a former shallow marine shelf is fully exposed, an incised valley may form (Van Wagoner et al., 1990; Posamentier and Allen, 1999; Posamentier, 2001; Figure 2.3 A). When a relative base-level does not expose the entire shelf, a lowstand alluvial bypass channel system and shelf delta may develop (Figure 2.3 B). Climate change may also have a significant influence on fluvial channel style by affecting the rate and calibre of sediment supply, vegetation cover, precipitation and discharge. However, climate is only rarely cited as a key control on the temporal and spatial evolution of fluvial systems (Ethridge and Schumm, 2007).

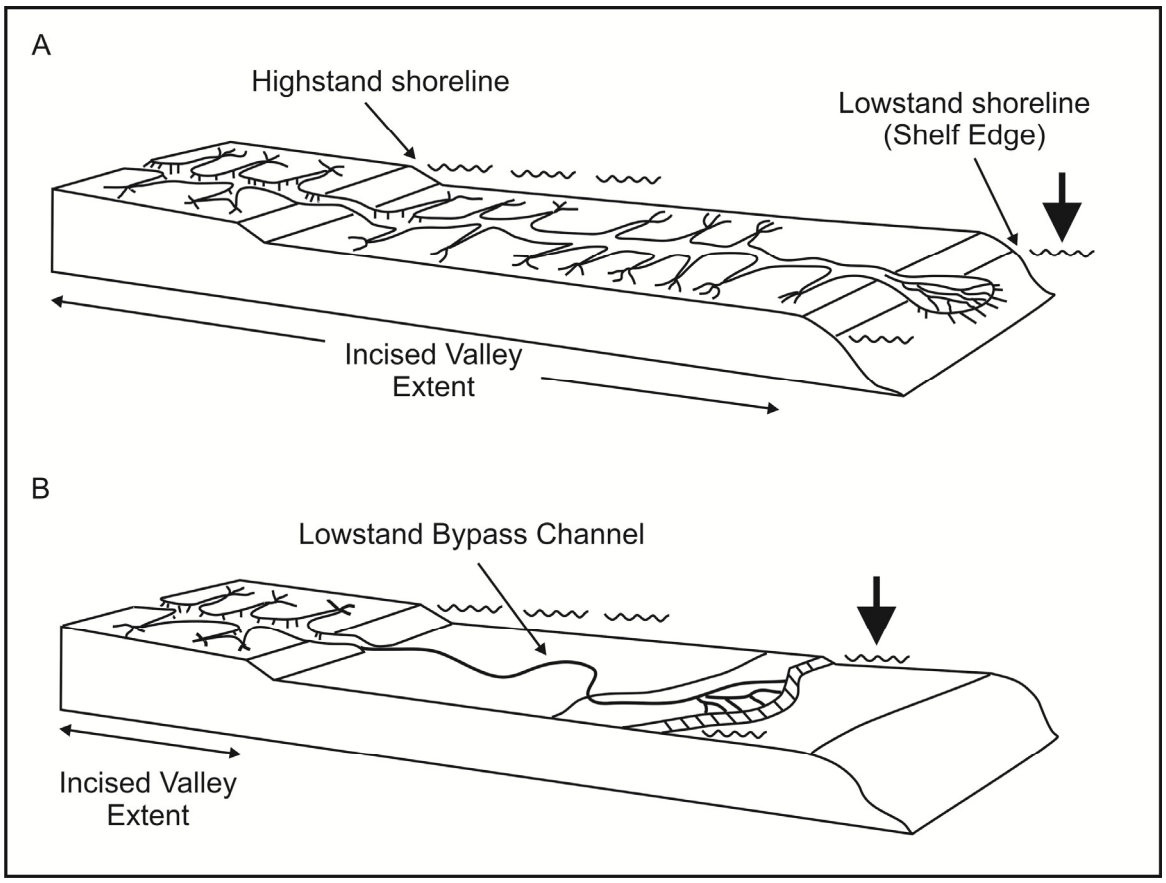

Figure 2.3: Two scenarios of incised valley **(A)** and Unincised Lowstand Alluvial Bypass Systems **(B)**. **A)** shows the formation of incised valley system on the entire shelf when the sea level fall fully exposes the shelf; **B)** shows the formation of Unincised lowstand alluvial bypass system when the sea-level fall does not fully expose the shelf (modified from Posamentier, 2001).

It is very common for a river to display different planform patterns along its course. The planform geometry changes include meander cut-off, avulsion, meander growth and shift and bar formation (Ethridge and Schumm, 2007). These changes cause rivers to reduce their sinuosity and length. It has been observed that braided rivers may become anastomosing and that meandering rivers can become straight in the downstream direction (Bridge, 2003; Ethridge and Schumm, 2007). The variability along a river course is mainly controlled by the downstream controls, including the base-level change. Fluvial systems respond relatively rapidly to changes in sea-level, which may be associated with the systems changing their sinuosity, width and/or depth along the river course (Blum and

Törnqvist, 2000; Schumm, 2005). Meandering rivers often decrease their sinuosity and become straighter when they reach the shoreline, indicating the influence of the sea level on the fluvial system. The Baram River, located in northwest Borneo is a type example of this.

2.2.2 Main Components of the Sequence-Stratigraphic Models of Fluvial Deposits

Sequence boundaries are defined as regional unconformities that separate the stratigraphic record into successions of conformable, genetically related strata (Vail et al., 1977). Two types of sequence boundaries have been identified (Vail et al., 1977; Van Wagoner et al., 1990). A *type 1 unconformity* develops when relative sea-level fall is greater than the rate of tectonic subsidence, leading to full exposure of the entire shelf, extensive subaerial erosion and formation of incised valleys. A *type 2 unconformity* develops when the relative seal-level falls slowly, leading to minor exposure, moderate fluvial incision and the development of lowstand alluvial bypass channel systems (Posamentier, 2001). This type of unconformity is much more difficult to identify in seismic and outcrop because they lack both deep erosion and major facies shifts (Miall, 1996). However, it can be identified by the presence of wide straight to low-sinuosity channels.

Incised valley systems are defined as fluvially-eroded, elongate topographic lows that are considerably wider than a single channel form (Dalrymple et al., 1994; Zaitlin et al., 1994). They typically are several kilometers wide and tens of meters deep (Zaitlin et al., 1994; Schumm and Ethridge, 1994). Incised valley systems have been scientifically and economically important since the introduction of the concept of sequence stratigraphy.

The incised valley fill, comprising the lowstand and transgressive deposits, contain significant hydrocarbon reservoirs in many basins around the world (Van Wagoner et al., 1990; Zaitlin et al., 1994). The recognition of the basal erosion surface of incised valleys provides important criterion for identifying sequence boundaries (Vail et al., 1977; Posamentier and Vail, 1988; Van Wagoner et al., 1990; Shanley and McCabe, 1993; Wright and Marriott, 1993).

Incised valley systems are formed by fluvial incision as a result of: 1) sea-level fall; 2) tectonic uplift; 3) climatic change resulting in increased discharge; or 4) stream capture that increases discharge in the combined system (Schumm and Ethridge, 1994; Thorne, 1994; Posamentier, 2001). In coastal settings, incised valleys are usually formed by fluvial incision during relative sea-level fall and shelf exposure and then filled during relative sea-level rise (Dalrymple et al., 1994; Nordfjord et al., 2006). Fluvial systems adjust relatively rapidly in response to changes in relative sea-level (e.g. Fisk and McFarlan, 1955); this may be associated with the systems changing their sinuosity, width and/or depth (Blum and Törnqvist, 2000; Schumm, 2005).

Zaitlin et al. (1994) has divided incised valleys into two different types based on the overall gradient of the fluvial-estuarine complex: 1) piedmont incised valleys; and 2) costal-plain incised valleys. Piedmont incised valleys are steeper and more structurally controlled. Additionally, three longitudinal segments of incised valleys that describe the relative degree of marine and fluvial influence were identified: 1) Segment 1 (marine incised valley), which is a seaward zone dominated by wave and/or tidal process; 2) Segment 2 (estuarine incised valley), which is an intermediate zone of mixed energy composing marine and non-marine deposits; and 3) Segment 3 (non-marine incised valley), which is a landward zone dominated by riverine sedimentation. These systems can be further divided into a “simple incised valley” or “compound incised valley” based

on the presence or the absence of multiple internal sequence boundaries within the incised valley fill (Zaitlin et al., 1994).

Incised valley systems have been recognised in shelf and/or shallow marine depositional settings and throughout the geological record from the Precambrian to Recent (Dalrymple et al., 1994; Zaitlin et al., 1994). Quaternary incised valley systems are very common features on many continental selves around the world (e.g. Posamentier and Allen, 1993; Reynaud et al., 1999; Nordfjord et al., 2006; Green, 2009; Paquet, et al., 2010). They have also been recognised on the Sunda Shelf using high-resolution 3D seismic data (e.g. Miall, 2002; Hanebuth and Stattegger, 2003; Darmadi et al., 2007; Kiel, 2009). However, the internal architecture and sedimentary fill of these valleys is not well documented. Furthermore, regional relationships between the incised valley and drainage area are rarely presented in ancient incised valleys.

Most of the incised valleys identified in literature are mainly incised into bedrock or into coastal and marine strata, and some contain marine units that implicate sea-level fluctuation in valley cutting and filling (Gibling, 2006). Valleys that incised into fluvial deposits are more difficult to identify, because it is very difficult to distinguish local deep scours from regional, valley-base scours (Best and Ashworth, 1997). There are several diagnostic criteria for identifying incised valleys (Reynolds, 1999; Hampson et al., 1997; Posamentier, 2001; Fielding and Gibling, 2005; Gibling, 2006): 1) the basal erosion surface that records the lowstand of relative sea-level (sequence boundary) must be of regional (basin wide) extent; 2) the basal erosion surface truncates underlying strata which may be present beneath the adjacent interfluves; 3) the basal surface is associated with small tributaries on the main valley interfluves.; 4) incised valley fill must have a distinctive internal architecture that is commonly multi-storey which records the progressive rise in base-level through the filling of the valley; therefore the facies within

the incised valley must be different from those adjacent to and below the erosional surface; 5) the depth and width of the incised valley has to be significantly larger than a 'normal' fluvial channel system; incised valleys are typically several kilometers wide and several tens of meters deep.

Identifying an incised valley and the associate erosional base (sequence boundary) using seismic data is not always easy. Posamentier (2001) pointed out that incised valleys can be identified and differentiated from other channels on seismic datasets based on the presence of small incised tributary valleys which are connected to the main trunk valley (Figure 2.3A). In contrast, lowstand alluvial bypass systems have no such associated tributaries. In addition, incised valleys are much larger than lowstand alluvial bypass channel systems (Figure 2.3B).

Directly above the erosional base of the incised valley, laterally amalgamated fluvial deposits are common. These deposits represent the late lowstand system tract (LST), when sea-level was starting to rise slowly (Wood and Hopkins, 1989; Shanley and McCabe, 1991, 1993). During this time, fluvial systems respond by depositing more sediment in response to the gradual base-level rise and show progressively increasing rates of aggradation (e.g. Posamentier and Allen, 1993). This results in multistory-multilateral channel bodies in the lower part of the incised valley fill and more isolated channel bodies in the upper part (cf. Martinsen et al., 1999; Wright and Marriott, 1993). Van Wagoner et al. (1990) and Zaitlin et al. (1994) stated that lowstand deposits are characterised by point bar deposits in distal and upper parts of the incised valley, which result from deposition by sinuous channels. In contrast, braided channel facies are more characteristic of early lowstand deposits and the upper reaches of the incised valley.

During continued sea-level rise (early transgressive systems tract (TST)), amalgamated fluvial sandstones are deposited (Shanley and McCabe, 1993; Olsen et al., 1995; Figure 2.1). Continued transgression causes the fluvial system to deposit more fine-grained sediment which results in more isolated sandstone bodies (cf. Wright and Marriott, 1993; Olsen et al., 1995; Figure 2.2). During rising base level, reduced fluvial gradients may also cause stream channel patterns to change to more meandering or anastomosing channel types, and crevasse deposits may increase as the river tries to maintain grade with base-level rise (Törnqvist, 1993; Blum and Törnqvist, 2000). Shanley and McCabe (1994) and Zaitlin et al. (1994) proposed that an increase in tidal deposits coincided with the period of maximum flooding. The distal parts of incised valleys may become estuaries when the valley is flooded during marine transgression.

The early highstand systems tract (HST) within much of the upper incised valley consists of thick sequences of isolated channel sands that are encased within fine-grained floodplain strata. One of the characteristic of the HST is the formation of interconnected and amalgamated sand bodies and river meander-belts, with poorly developed flood-plain deposits, due to the progressive loss of accommodation space in floodplain environments. This represents the progressive reduction in the rate of relative sea-level rise during the late HST period (Shanley and McCabe, 1993).

2.3 Channel Classification

Numerous river classification schemes have been developed and channels can be separated into two major groups depending on their 'freedom' to adjust their shape: (1) *confined channels*, which are bedrock-controlled and are relatively fixed over a relatively

significant period of time; and (2) *un-confined channels*, which are free to adjust and avulse (Schumm, 1977). Based on their planform geometry alone, alluvial channels have been traditionally classified as straight, meandering, and braided (Leopold and Wolman, 1957). Another popular classification is that single channels with varying sinuosity are divided into straight and meandering, and that multiple channels with varying sinuosity are divided into braided and anastomosing (Miall, 1977). Leopold and Wolman (1957) and Rust (1978) have used a sinuosity of 1.5 to separate high-sinuosity rivers from straight rivers. Schumm (1977, 1981) demonstrated that there is a strong relationships between the channel pattern and the type of the sediment transported by the channel, thereby allowing fluvial channels to be classified into three types: 1) *bed-load channels*, which are straight or of very-low sinuosity; 2) *mixed-load channels*, which are of moderate-sinuosity; and 3) *suspended load channels*, which are of high sinuosity.

Different attempts have been made to relate the morphological pattern of the channel to the sediment type. A strong empirical link between the mode of the sediment transport and planform and cross-sectional geometry of the channel has been recognised (Schumm, 1977). Most important is the separation between systems dominated by bedload transport, suspended-load transport and mixed-load transport. These relationships can be quantified in modern rivers, and they indicate qualitative trends that can be applied to the interpretation and classification of ancient fluvial depositional systems (Galloway and Hobday, 1996). In this classification, the main distinguishing features are as follows: 1) a bed-load river channel is defined by a channel that has a sinuosity from 1.0 to 1.3 and width-depth ratio of >40; 2) a mixed-load river channel is defined by a channel that has a sinuosity from 1.4 to 2.0 and width-depth ratio of >10, <40; and 3) a suspended load river channel is defined by a channel that has a sinuosity higher than 2.0 and width-depth ratio <10 (Figure 2.4). This classification was developed on the basis of using a database that

was limited to sand-bed alluvial rivers from the North American Great Plains in semiarid and subhumid regions and the Murrumbidgee River, Australia. This classification has not been tested on modern coastal plain rivers and does not include anastomosing channels (Ethridge and Schumm, 1978). By using aerial photographs from across USA, Schumm's classification has been expanded by Brick (1975, 1981, 1982, and 1983) to include other important variables that can be used to classify the rivers. These variables include both the degree and type of sinuosity, degree and type of braiding, and the degree and type of anastomosing.

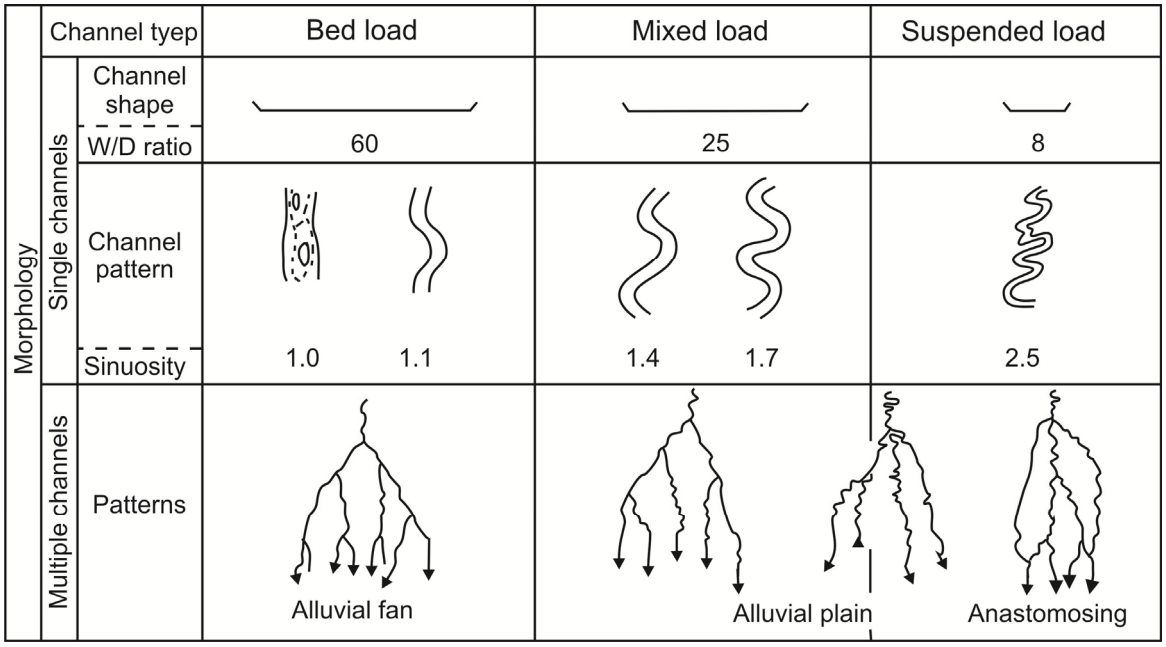

Figure 2.4: Schematic illustration of three channel classes defined by Schumm (1977). A strong empirical relationship between the channel patterns and the sediments being transported in the channel has been recognised.

Numerous attempts to reconstruct the morphologic and flow characteristics of ancient rivers have been based on empirical relationship developed for modern rivers. Many of these empirical relationships have been tested on data obtained from vertical profiles such

as outcrop and well logs, in order to link such factors as channel wavelength, channel width, meander belt width, sinuosity, discharge, etc. The vertical profile of outcrop and well logs provides information on sandstone bodies thickness, but these provide no information on lateral dimensions or planform geometry. Where closely-spaced wells and large and extensive outcrops are available, it may be possible to map entire bodies. However, this is rarely possible and more difficult to establish for the subsurface ancient river. Once the channel thickness (bankfull depth) is determined, several empirical equations can be used to estimate the channel width, meander belt width and sinuosity. These equations need to be tested on data obtained from ancient rivers that are seismically very well-imaged. These empirical equations are described later in this Chapter.

2.4 Basic Concept of Geometry of Fluvial Channels

2.4.1 Introduction

One of the main aims of studying fluvial geometry is to determine size, shape and orientation of channel sandstone bodies (Bridge and Tye, 2000; Bridge, 2003; Bridge, 2006; Gibling, 2006). Different approaches exist to examine the geometry of the sandstone bodies. Some studies have attempted to develop databases for different types of fluvial styles and hence to make statistical relationships between thickness (depth), width and length of sandstone bodies using data obtained from both modern and ancient deposits (e.g. Fielding and Crane, 1987; Bridge and Mackey, 1993; Reynolds, 1999; Gibling, 2006). Gibling (2006) reviews techniques and methods used by sedimentologists and geomorphologists to determine the geometry of fluvial sandstone bodies. This work is the most comprehensive study that used measurements of width, thickness (depth) and

length of the channel bodies and valley fills from more than 1500 published Quaternary and older bedrock examples. The calculated width-thickness ratio (W/T) from measurements of the width (W) and thickness (T) data from these examples were plotted on a log-log scale. The compilation of Gibling (2006) provides facies and dimensional information for different types of ancient channel bodies, which can be used to determine the width of the sandstone bodies where, as in most subsurface studies, thickness is the only parameter known. For example, Strong et al. (2002) used data provided by Fielding and Crane (1987) and Bridge and Mackey (1993) that can be applied to the deposits of meandering streams in order to determine the dimensions of the sandstone bodies of the Patachawarra Formation, Cooper Basin, South Australia. However, these data give a large range of widths (e.g. from 100 to 15,000 m), and thus can only be used as starting point for predicting specific ancient reservoir units (Miall, 2006).

The most critical dimension to be determined is the width of the subsurface sand bodies which then can be used to determine the rest of the morphometric elements of the channel system. Five methods can be used to determine the morphometric parameters of the fluvial channels (Bridge and Tye, 2000; Gibling, 2006; Miall, 2006): 1) well correlation; 2) outcrop analogues; 3) modern analogues; 4) empirical equations; and 5) 3D seismic geomorphology.

2.4.2 Well Correlation

Well correlation is the most common method for estimating the widths of the subsurface sandstone bodies. The validity of this method depends on correlation rules and strategies, well-spacing, well density and reservoir complexity (Bridge and Tye, 2000; Weber and

van Geuns, 1990). If the estimated widths of the sandstone bodies are less than the average well spacing, then individual channel bodies cannot be correlated by deterministic methods. In these cases, statistical (probabilistic/stochastic) approaches are used, based on sandstone proportions, net-to-gross ratio (NGR), and an appropriate database of W/T relationship (e.g. Johnson and Kroll, 1984). Stochastic modeling is a useful technique that can help to better represent the complex architecture of fluvial depositional systems (Keogh et al., 2007). Weber and van Geuns (1990) defined the relationship between the well density and the type of model that can be obtained. If the well density is sufficient to allow unique well correlations, a deterministic reservoir model can be obtained. In case of insufficient well density, a probabilistic model is required. In other cases, a mixed deterministic-probabilistic model is used where the well density is only partially sufficient for deterministic correlations.

In many cases the fluvial sandstone deposits are too narrow and thin to be correlated between adjacent wells (Gibling, 2006). Where the reservoirs are very narrow, closely-spaced wells would need to have been drilled to improve the spatial resolution. For example, Ebanks and Weber (1987) used subsurface data of close well-spacing to estimate the sandstone body width of meandering river deposits in Missouri, USA. With sufficiently close well-spacing, they were able to estimate the width and length of the sandstone bodies. Based on their estimation, the sandbody length was estimated to be 1.4 times the downflow dimensions. Cornish (1984) accomplished much the same thing for meandering rivers.

Determining the proportion of the sandstone bodies is a useful technique in correlating sandstone bodies between adjacent wells. Furthermore, it helps to determine the degree of amalgamation and connectedness of sandstone bodies. Fielding and Crane (1987) proposed that if sandstone proportions (NGR) of any stratigraphic interval exceeds 0.55,

the connectedness of the sandstone bodies will be improved as the degree of vertical and lateral amalgamation is high. Bridge and Tye (2000) proposed that with a NGR of less than 0.40, the reservoirs sandstones are expected to be isolated from one another whereas connectivity improves significantly with NGR of more than 0.40. Weber and van Geuns (1990) defined this value at 0.35 based on 3D reservoir modeling results. Furthermore, Shanley (2004) concluded with a NGR of > 0.70, fluvial deposits will display a high level of amalgamation. Where the calculated sandstone proportion is between 0.40 and 0.70, it is more difficult to generalize the degree of amalgamation and this would require separate modeling work to determine the degree of connectivity on a case by case bodies.

Weber and van Geuns (1990) observed three different types of clastic reservoir architecture based on well correlation: 1) Layer-Cake; 2) Jigsaw Puzzle; and 3) Labyrinth. The Layer-Cake reservoir type is a package of extensive sandstone bodies without any major discontinuity. Jigsaw Puzzle reservoir types are composed of a series of sandstone bodies representing two or more genetic units that fit together without major gaps. Labyrinth reservoirs represent packages of sandstone bodies that are shown as discontinuous lenses of sand. In general, sandstone reservoirs are not as discontinuous in three-dimensions as they appear in the 2D correlation panels. Thus, estimated widths of sandstone bodies using different approaches (described below) are critical to improve and guide the well correlation method.

2.4.3 Outcrop Analogues

Using outcrops as analogues for subsurface data is commonly used by researchers to provide more information that cannot be obtained from relatively sparse and incomplete

subsurface data. Outcrop analogues can give excellent information on the vertical and lateral extent of sediment bodies, and are ideally suited to match core data with sequence stratigraphy of rock successions. Furthermore, outcrops are the only source of geological analogue data that demonstrate what it is preserved in the geological record (Geehan, 1993). Data obtained from outcrop analogues can be used to constrain stochastic models and to build 3D fluvial reservoir models (Keogh et al., 2007).

Most subsurface studies have used one or more outcrop analogue to constrain the interpretation of subsurface data, because of the difficulties in determining dimensions of sandstone bodies (e.g. Lang et al., 2000). In addition, the third dimension, namely the length of the sandstone body, is virtually impossible to be estimated from subsurface data. Hence, the most useful information that can aid the interpretation of the geometry of the fluvial sandstone bodies can be obtained from a well-exposed outcrop. A few studies have attempted to determine the length of sandstone bodies (i.e. mid channel bar) using well-exposed outcrops. For example, Robinson and McCabe (1997) estimated sandstone body length in braided deposits in the Morrison Formation, Utah, to be a factor of 1.5 times sandstone body width. One of the most detailed studies of an outcrop analogue is that of Martinius (2000), who used two outcrops of Tertiary units in Spain to derive quantitative data of sandstone body dimensions and geometries.

Although new information, such as the width of the palaeochannels, can be determined using outcrop, determination of the paleochannel pattern may not be possible (North, 1996; Miall, 1996; Bridge and Tye, 2000; Tye, 2004). Moreover, using outcrops as analogues for subsurface data is not always practical (Geehan, 1993; Bridge and Tye, 2000; Tye, 2004). For example outcrops usually give limited horizontal (plan-view) information and may not always reflect the proper preservation potential of sequences. Selecting a suitable ancient analogue for the subsurface reservoir study depends on the

quality of the outcrop and on the understanding of geometry of the subsurface sandstones and the depositional model used during the interpretation (Bridge and Tye, 2000; Lang et al., 2000). Furthermore, most outcrops are not extensive enough to provide useful quantitative data (i.e. width, meander belt width, etc) that can be used to build 3D models for subsurface reservoirs. Finally, data from subsurface studies are usually limited (e.g. limited lithology information due to lack of available cores) which makes it more difficult to find a suitable outcrop for a subsurface reservoir study.

However, considerable insights into reservoir characterisation and appropriate reservoir analogues can be obtained by using different techniques, including field petrophysics, shallow seismic, and GPR and borehole data in selected, well-exposed outcrops. GPR datasets from outcrops have been used as analogues for subsurface reservoirs to provide both qualitative and quantitative data (Thomson et al., 1995; Bristow and Jol, 2003). GPR can be useful in defining larger scale geometrical features (e.g. channel width and surface patterns) and internal features (e.g. lateral accretion and bar forms). However, GPR has limited vertical resolution (< 30 m deep below the surface).

2.4.4 Modern Analogues

Modern analogues enable researchers to closely examine the depositional processes and the geometry of sediment bodies (Lang et al., 2000). Using these modern examples as analogues, the dimensions of sandstone bodies can be determined using aerial photographs and field surveys. One of the advantages of using modern analogues is that researchers can revisit the same spot several times allowing for observations of sediment accumulation rates and/or erosion and seasonal variations (Lang et al., 2000). To validate

this method, modern analogues are required to show similarity in sedimentary processes, including sedimentary structures and grain size to the subsurface reservoirs. Several studies have been attempted to use modern analogues to obtain quantitative and qualitative data of the geometry of sandstone bodies.

Swanson (1976) attempted to determine the key fluvial variables such as channel width, meander wavelength, etc., using aerial photographs of modern meandering rivers. Tye (2004) proposed a new method for determining the dimensions of subsurface reservoirs using satellite and aerial photographs of modern depositional environments to measure channel width and length. Statistical methods were then used to examine the relationships between the width and length of the channel. The results were used as input for object-based 3D reservoir modelling. Tye (2004) argued that one problem of his geomorphological approach was that it failed to include the erosional relationships between the channel-belt units. This is because modern and recent systems cannot provide information on the long-term preservation of modern sediments (Miall, 1996). In addition, the effects of the compactional modification and digenesis cannot be determined from the modern systems (Lang et al., 2000). The only source of such information is the rock record itself. The internal structure of the channel deposits and bars beneath the surface cannot be resolved by using the surface maps and aerial photographs of modern systems. Shanley and McCabe (1994) and Shanley (2004) stated that although much information can be obtained from modern systems, the interplay of subsidence rate, base level change and sediment supply plays a far greater control on the degree of connectivity of fluvial channels rather than the short-term processes that are commonly observed when studying modern systems.

GPR partly overcomes this issue. This technique can provide high-resolution images of the shallow subsurface that helps to link the architecture of shallow subsurface (< 30 m)

and surface channels. Some studies have used GPR as a tool to determine the internal architecture of the channels and bars (e.g. Best et al., 2003; Lunt and Bridge, 2004; and Bridge, 2006). However, GPR still cannot reveal the long-term preservability of present-day deposits.

2.4.5 Empirical Equations

Empirical equations relate maximum channel thickness, channel depth, channel width and channel-belt width using data derived from modern rivers. These equations have long been used to predict the width of subsurface channel sandstone bodies (e.g. Leeder, 1973; Collinson, 1978; Lorenz et al., 1985 and 1991; Fielding and Crane, 1987; Bridge, 1997; Bridge and Tye, 2000; Dalrymple, 2001; Shanley, 2004; Table 2.1). Bridge and Tye (2000) evaluated different techniques, including theoretical, experimental and field studies in order to determine the best technique that can be used to assess the dimensions of ancient fluvial deposits based on cores and wireline logs. They used the empirical equations of Bridge and Mackey (1993), but included new parameters such as meander wavelength and sinuosity, that were not included in the original equations. In order to estimate the width of the sandstone bodies, the dimensions of paleochannels and channel belts need to be determined. The two most commonly estimated dimensions are width and depth. Paleochannel depth is considered to be the same as the maximum bankfull channel depth.

Table 2.1: Summary of empirical equations developed by different researchers to estimate channel depth (*h* or *dm*), channel width (*W*) and meander belt width (*Wm*).

Source	Maximum (*h*) or mean (*dm*) bankfull depth	Bankfull width (*W*)	Sandbodies width (*Wm*)
Leeder (1973)	*h*=thickness of complete un-truncated channel bar	$W=6.8h^{1.54}$	----------
Collinson (1978)	*h*=thickness of complete un-truncated channel bar	Same as Leeder (1973)	$Wm=65.5h^{1.57}$
Lorenz et al. (1985)	*h*=thickness of complete un-truncated channel bar, decompacted by an arbitrary 10% as proposed Ethridge and Schumm (1978)	Same as Leeder (1973)	$Wm=7.44W^{1.01}$
Fielding & Crane (1987)	Same as Lorenz et al. (1985)	Same as Leeder (1973)	$Wm=12.1dm^{1.85}$ case 2A (for best solution fit) $Wm=0.95dm^{2.07}$ case 1B (for meandering deposit fit, lower limit) $Wm=64.6\ dm^{1.54}$ case 2B (for meandering deposit fit, upper limit)
Bridge & Mackey (1993)	$dm=0.57\ h$	$W=8.88dm^{1.82}$ $W=15.85dm^{1.58}$	$Wm=59.9dm^{1.8}$ $Wm=45.76h^{1.52}$ $Wm=192\ h^{1.37}$
Bridge (1997)	$dm=16Sm\text{-}34Sm$ *Sm*=mean of cross-set thickness	Same as Bridge and Mackey (1993)	Same as Bridge and Mackey (1993)
Bridge and Tye (2000)	Same as Bridge (1997)	Same as Bridge and Mackey (1993)	Same as Bridge and Mackey (1993)

Maximum bankfull channel depth can be estimated from the thickness of lateral accretion sets or epsilon beds in outcrop (Ethridge and Schumm, 1978; Allen, 1979; North, 1996; Bridge, 1997; Bridge and Tye, 2000). However, it is not possible to identify epsilon beds from core or wireline logs. Bridge and Tye (2000) estimated maximum bankfull depth from wireline logs and cores by using the thickness of decompacted (un-truncated)

complete channel bar and channel-fill sequences. Unfortunately, it is not always easy to identify un-truncated channel-fills from core and wireline logs. Moreover, the thickness of channel sandstones is not always as large as the bankfull channel depth due to post-depositional compaction that reduces the channel-fill thickness during burial (Bridge and Tye, 2000; Bridge, 2003). Ethridge and Schumm (1978) suggested that 10% to be added to estimates of channel-fill thickness (and bankfull depth estimates) to account for post-depositional, burial-related compaction.

Another method involves independent estimates from the relationship between dune height and cross-bed set thickness and the known relationship between dune height and water depth. In order to use this method, the thickness of many cross-bed sets needs to be measured. Once the mean and standard deviation are calculated, these values are used to estimate the mean dune height using equations proposed by Leclair and Bridge (2001). The estimated dune height is used in a number of empirical equations to determine the maximum bankfull depth (Bridge and Tye, 2000). For examples, Yalin (1964) and Allen (1970) proposed the following equations:

$$d/hm = 6$$

$$d = 11.6\ hm^{0.84}$$

where d is bankfull depth and hm is dune height (Yalin, 1964). These equations also help to determine the empirical relationship between dune height and depth.

However, the observed thickness (maximum bankfull thickness) is probably less than the original maximum thickness due to the compaction that reduces the channel-fill thickness during the burial. Ethridge and Schumm (1978) suggested adding 10% to the channel-fill thickness because the sands compact up 10% of their thickness.

Once reasonable estimates of paleochannel depths are determined, paleochannel widths can be estimated using empirical equations (Leeder, 1973; Bridge and Mackey, 1993). Leeder (1973) developed an empirical relationship between the channel depth and the channel width for channels with sinuosity more than 1.7. Channel width can be estimated from the equation of:

$$Wc=6.8h^{1.54}$$

where the Wc is the channel width and the h is the channel thickness (channel depth). This relationship is invalid for low-sinuosity channels (Leeder, 1973).

Estimated widths and depths can be used to construct approximations of sandstone bodies distribution and continuity from 2D well log correlation panels. This helps to avoid simplistic, often false assumptions commonly made in correlating well logs by using core description, isopach mapping and log patterns (Bridge and Tye, 2000). An example of this is shown in Figure 2.5, which illustrates two interpretations of the same fluvial channel belts in the Travis Peak Formation, North Appleby Field, East Texas Basin (Zone 1). Figure 2.5 A) shows the initial interpretation by Tye (1991) based on core description and isopach mapping. The widths of sandstone bodies were overestimated by Tye (1991) because no quantitative data were obtained. Bridge and Tye (2000) reinterpreted the geometry of the fluvial channels based on using empirical equations proposed by Bridge and Mackey (1993; Table 1; Figure 2.5 B). The maximum bankfull depth ranges from 6 to 10 m and thus the mean bankfull depth is estimated to be 3-5 m. The sandstone bodies are then predicted to be 436-1741 m wide suggesting narrower sandstone bodies.

Log-log plots of estimated channel-belt width and bankfull depth can be made to compare estimates with data from modern rivers (Tye, 2004; Gibling, 2006). Shanley (2004) used the estimated dimensions of the sandstone bodies of the Upper Cretaceous Lance

Formation, in the Jonah Field, Wyoming, using empirical equations proposed by different authors (Table 1) and plotted them on log-log plots. If the plan-view paleochannel pattern of these fluvial deposits can be identified, parameters such as sinuosity, radius of curvature, wavelength, channel width, meander belt width, area, and volume of specific point bars can be estimated (e.g. Ebanks and Weber, 1987; Cornish, 1984; Fachmi and Wood, 2003). However, several empirical equations have been proposed to estimate these parameters (e.g. Leopold and Wolman; 1960; Carlston, 1965; Collinson, 1978; Lorenz et al., 1985; Fielding and Crane, 1987).

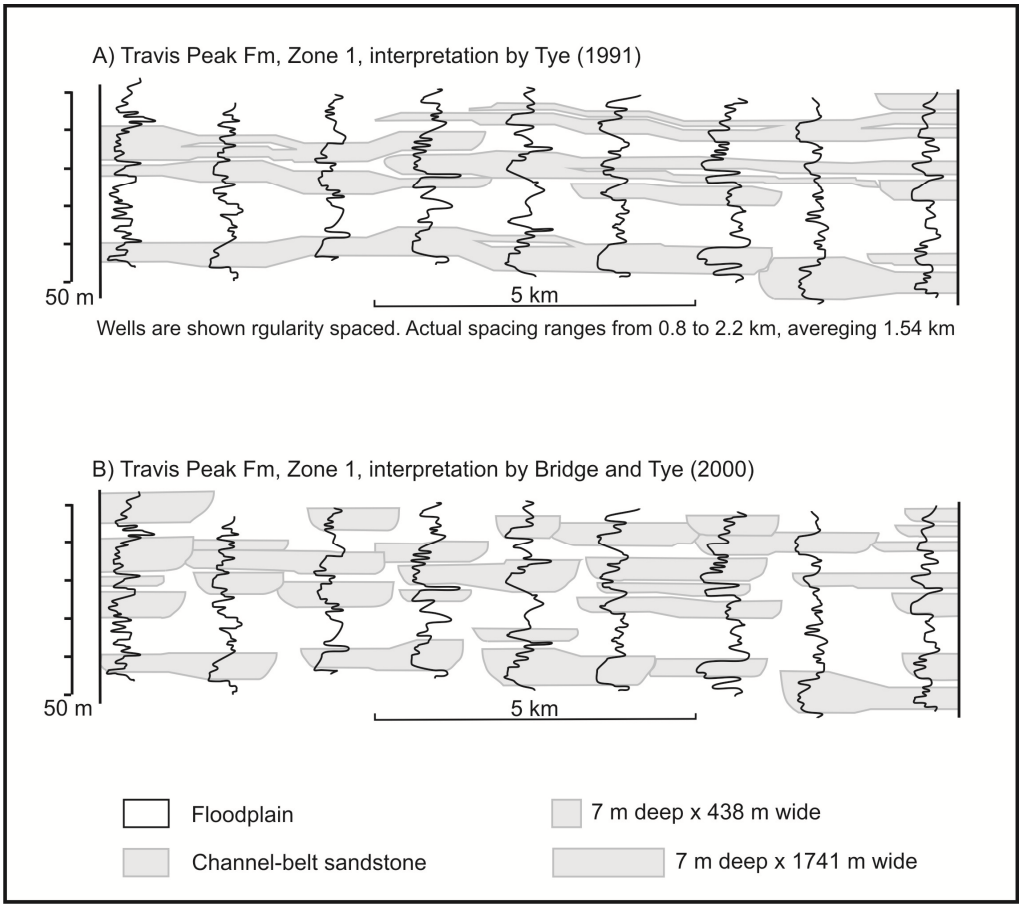

Figure 2.5: Two interpretations of fluvial channel belts in the Travis Peak Formation, North Appleby field, east Texas Basin (Zone 1). **A)** Initial interpretation by Tye (1991) based on core description and isopach mapping. **B)** A reinterpretation by Bridge and Tye (2000) based on using empirical equations. The results of these equations (widths of sandstone bodies = 436-1741 m) suggest that channel sandstones are narrower than interpreted before **(A)**.

The meander belt width is measured as the width between two lines that bound the outermost visible meander-loop sets. It represents the dimensions that defines the width of the sandstone bodies and the ‘‘container’’ within which individual channels migrate. One way to estimate the meander belt width for ancient channels is from the channel width. Lorenz et al. (1985) established an empirical relationship between the channel width and meander belt width which can be estimated from:

$$Wm=7.44Wc^{1.01}$$

Where the Wm is the meander belt width and the Wc is the channel width. This relationship was mainly based on the combined data of Leopold and Wolman (1960) and Carlston (1965). Meander belt width can also be estimated from the channel depth. Based on the quantitative data collated by Carlston (1965), Collinson (1978) established the following empirical relationship relating the meander belt width and channel depth:

$Wm=64.6h^{1.54}$.

Fielding and Crane (1987) complied published data on channel depth and meander belt width to produce the following relationship:

$Wm=12.1\ h^{1.85}$

This relationship was based on the use of the best-fit line for all the collected data.

The meander wavelength is defined as the length between the uppermost and lowermost inflection points. Leopold and Wolman (1960) established empirical relationship between the meander wavelength and channel width for high-sinuosity channels. This relationship is summarised as:

$Lm=10.9Wc^{1.01}$

Where Lm is the meander wavelength. Another relationship between the meander wavelength and channel depth were proposed by Leeder (1973) and Collinson (1978) as:

$Lm=74.1h^{1.54}$

Brice (1984) suggested that the ratio of the meander wavelength to the channel width is *ca.* 10 and the ratio of meander wavelength to radius of curvature is *ca.* 5.

The empirical equations described above have improved the quantitative estimations of the channel dimensions and connectedness of the sandstone bodies (Bridge and Tye, 2000). These equations can help to reduce the number of wells that are planned to be drilled in any new oil and gas field at an early stage by estimating dimensions of sandstone bodies and connectedness of the sandstones bodies using data obtained from a discovery well and a core. However, Miall (2006) argued that because the numerical models are generated based on input of data that are generalised for the whole range of fluvial styles, and is commonly composed of a small range of sandstone body dimensions, these models are commonly unrealistic. Moreover, these models can only be used as a starting point for the prediction of specific reservoir units (North, 1996). As stated above, the plan form geometry of the paleochannels cannot be determined using vertical-based data alone (North, 1996; Miall, 1996; Bridge and Tye, 2000 Tye, 2004). Thus, 3D seismic data are required to aid the interpretation of the geometry of the fluvial channel sandstone bodies. Analysis of high-resolution seismic data is potentially the best method for imaging planform pattern of subsurface channel sandstone bodies (Bridge and Tye, 2000).

2.4.6 3D Seismic Geomorphology

Since the publication of AAPG Memoir 26 in 1979, the application of seismic stratigraphy has been increasingly applied to the subsurface using 2D and 3D seismic data. Continuous improvements in 3D seismic technology and visualisation software have allowed direct imaging of depositional elements at varying scales and in numerous depositional settings. The most recent advances in this subject have been in deep marine (e.g. Kolla et al., 2001; Posamentier and Kolla 2003; Posamentier, 2004) and coastal plain settings (e.g. Posamentier, 2001; Miall, 2002; Carter, 2003; Darmadi et al., 2007). The

study of depositional systems using 3D seismic reflection data has been termed 'seismic geomorphology' (*sensu* Posamentier, 2000; see also Cartwright and Huuse, 2005; Davies et al., 2004; Posamentier et al., 2007). This analytical approach has been proven to be a powerful technique in visualising the external form and internal architecture of subsurface rock volumes and in predicting the sequence stratigraphic evolution and infill of sedimentary basins. Furthermore, it can provide new views of fluvial architecture and much more valuable qualitative and quantitative data of the subsurface reservoirs. These data can contribute directly to a better understanding of fluvial channel systems and, thereby, will have important implications for exploration and production. Finally, high-resolution 3D seismic data can also aid in the construction and conditioning of 3D reservoir geological models due to the lateral and vertical continuity of observations that cannot be obtained from other sources of data (e.g. cores, well logs, outcrops).

Maximising the value of 3D seismic interpretations requires integration of the 3D seismic with well logs, cores and rock property information. This enables critical information on lithofacies and depositional settings to be calibrated with the 3D seismic data and thus can provide important implications for the interpretation of the sedimentary rocks. This type of study has been called 'seismic sedimentology' by Zeng and Hentz (2004). These improvements are major advances, although there are limitations. For example, the vertical and lateral resolution of 3D seismic data plays a major role in limiting the usefulness of the 3D seismic interpretations.

The depositional sub-environments and depositional elements can be interpreted directly from the 3D seismic volume (Posamentier, 2004). Consequently, the lithological distribution pattern, particularly that of reservoir facies, can be more precisely determined. Moreover, the best quality 3D seismic data allows different river types (meandering, braided, and anastomosing channels) and their deposits to be distinguished.

This can improve our ability to better understand the depositional and stratigraphic evolution and infill of sedimentary basins (Ethridge and Schumm, 2007).

2.4.6.1 3D Seismic Interpretation Techniques

Several 3D seismic interpretation techniques have been used since 3D seismic data was first introduced. The initial step when first analysing 3D seismic dataset is to start picking horizons with strong reflections and/or horizons that can be interpreted as continuous stratal surfaces. However, picking horizons is not always straightforward. For example, in some depositional sequences such as coastal-plain fluvial sequences, the seismic events are discontinuous with no significant amplitude anomaly (Zeng, 2007). In these cases, where the horizons are discontinuous, significant errors may be observed and an accurate interpretation may be difficult to obtain (Zeng and Hentz, 2004). However, once the horizons are consistently picked, different visualisation tools can be used to rapidly interrogate the 3D seismic volume.

A technique that is widely used for imaging a depositional surface is slicing through the 3D seismic volume. Different slicing techniques can be used through a 3D seismic data volume (Posamentier et al., 2007). These techniques include time slices (horizontal), horizon slices (parallel to stratal surfaces), proportional slices and dipping planar slices. Slicing through a 3D seismic volume can provide optimum images of stratigraphic features if the slices are generated as near as possible to the target interval and parallel to a well-mapped horizon (Posamentier et al., 2007).

A time slice is a horizontal seismic section taken at certain two-way travel time (twt) levels through a 3D seismic volume. The time slice can be useful, but only if the seismic

reflections are parallel and nearly horizontal and the stratigraphy is essentially flat (Zeng and Hentz, 2004). It also is useful in the determination of structural features. If the seismic reflections are not flat nor near horizontal, a stratal slice is sufficient. When the seismic reflections are uniformly divergent, then proportional slices yield the best result. In case the reflections are uniformly dipping, then dipping planar slices are useful (Posamentier et al., 2007).

Once horizon maps and/or horizon slices have been generated, amplitude and attribute mapping techniques can be applied. Amplitude and attribute maps can be generated along a horizon or for an interval between two horizons using the attribute calculations. The amplitude and attribute maps can provide important information about the depositional element at those surfaces (horizons). Using an amplitude map, the depositional element can be revealed by the virtue of different impedance characteristics of that element relative to the surrounding strata (Posamentier et al., 2007). There are different types of interval attributes such as maximum positive polarity amplitude, maximum absolute polarity amplitude, the ratio of positive maximum to negative maximum amplitude, and total cumulative amplitude (Posamentier et al., 2007).

Another attribute technique involves analysis of volume-based attributes (Posamentier et al., 2007). This mapping technique is useful when no such information can be obtained from horizon slices due to difficulties in defining a reference horizon that can be used as a datum. Different volume attribute maps can be generated using this technique such as coherence, continuity and discontinuity maps. The coherence, continuity and discontinuity maps are generated where the similarities or dissimilarities between two adjacent traces can be mapped. These maps have, at first, been used for detecting subsurface faults only; however, these maps were found to be useful for determining the channel edges and geo-bodies (Brown, 2003; Posamentier et al., 2007). Other techniques

such as voxbody analysis and volume co-rendering can provide useful information about the distribution of geo-bodies and thus the stratigraphic and geomorphologic characteristics of depositional elements (Posamentier et al., 2007).

The applications of these techniques have improved our ability in interpreting subsurface geology. Calibrating the planview images (surface maps) with seismic cross-sections is a very important step to accurately interpret the geomorphic features observed on the surface maps. Furthermore, it is very important to image the planview of the buried surfaces which are unique for most ancient deposits that aid the interpretation of depositional environments and thus the dimensions of sandstone bodies.

2.4.6.2 Applications of 3D Seismic Geomorphology

3D seismic stratigraphic analysis techniques have been widely applied to deep-water turbidities and submarine fan deposits (e.g. Beauboeuf and Fridmann, 2000; Posamentier et al., 2004; Kolla et al., 2001; Posamentier and Kolla 2003; Fowler et al., 2004; Morgan, 2004; Steffens et al., 2004). In contrast, few similar studies have been completed using 3D seismic to evaluate subsurface fluvial systems (e.g. Isa et al., 1992; Posamentier, 2001; Miall, 2002; Carter, 2003; Darmadi et al., 2007; Zeng, 2007; Wood, 2007). This is because the deep-water deposits are good-quality reservoirs with high well productivities. The deep-water deposits usually contain giant accumulations that are composed of thick sandstone and thick shale which makes it easy to distinguish sandstone from shale especially where coal seams are absent. The coal seams which are common within the fluvial succession add more difficulties in interpreting 3D seismic data. In addition, developments in the resolution of 3D seismic and well technologies in offshore areas with

improved geological concepts (e.g. fan models, sequence and seismic stratigraphy, basin topography, etc.) have major influence on the successes of deep-water exploration. The following sections illustrate different examples of 3D seismic geomorphological studies of fluvial systems.

An early study was completed by Isa et al. (1992), who documented a single, wide (500 m) meandering channel associated with point bars from the Late Pleistocene of the Malay Basin. Miall (2002) also studied Pleistocene fluvial systems in the northern part of the Malay Basin to determine the architecture of these fluvial systems. Wide range of channel types were recognised including meandering, braided low-sinuosity channels and incised valleys (Figure 2.6). This study was one of the first studies that evaluated braided channels using 3D seismic data (Ethridge and Schumm, 2007). Miall (2002) provided quantitative data on several Pleistocene to Recent channel systems that are clearly imaged. He used these data to compare the channel systems within the Malay Basin to modern rivers and led him to conclude that no large rivers flowed through the Malay Basin. A simple reservoir model and a sequence stratigraphic model have been developed to illustrate the vertical changes in the fluvial architecture size and style within the Pleistocene succession of the Malay Basin (Figure 2.7). The main conclusion of Miall (2002) study is that the changes of fluvial styles are controlled by both the sea-level fluctuation and subsidence rate which determine the generation/destruction of the accommodation space. In addition, the variations in fluvial styles and size suggested that simplistic models that show uniform fluvial styles are not always applicable.

Wide range of channel types, crevasse splays and floodplain deposits were documented by Hedage et al. (1994) who used seismic vertical profiling (SVP) as the primary measurement tool to describe thin-bedded reservoirs within the Frio Formation, South Texas. Burnett (1996) used time slices to image fluvial systems of the Upper

Pennsylvanian Cisco system of West Central Texas, and clearly imaged meandering channel sandstone bodies.

Using time slices derived from 3D seismic dataset from the offshore northwest Java Sea, Posamentier (2001) examined Miocene to Pleistocene alluvial systems. He documented both incised and 'non-incised' valley systems. In addition, meandering channels and point bars with meander scrolls and were observed within the incised valleys. Based on these observations, Posamentier (2001) suggested that in areas that are tectonically active the incised valleys are formed only if the sea-level falls below the shelf edge and the shelf is fully exposed. Moreover, when the rate of the sea-level fall is insufficient, and therefore the shelf is not fully exposed, lowstand alluvial bypass channel systems and shelf delta are developed (Figure 2.3).

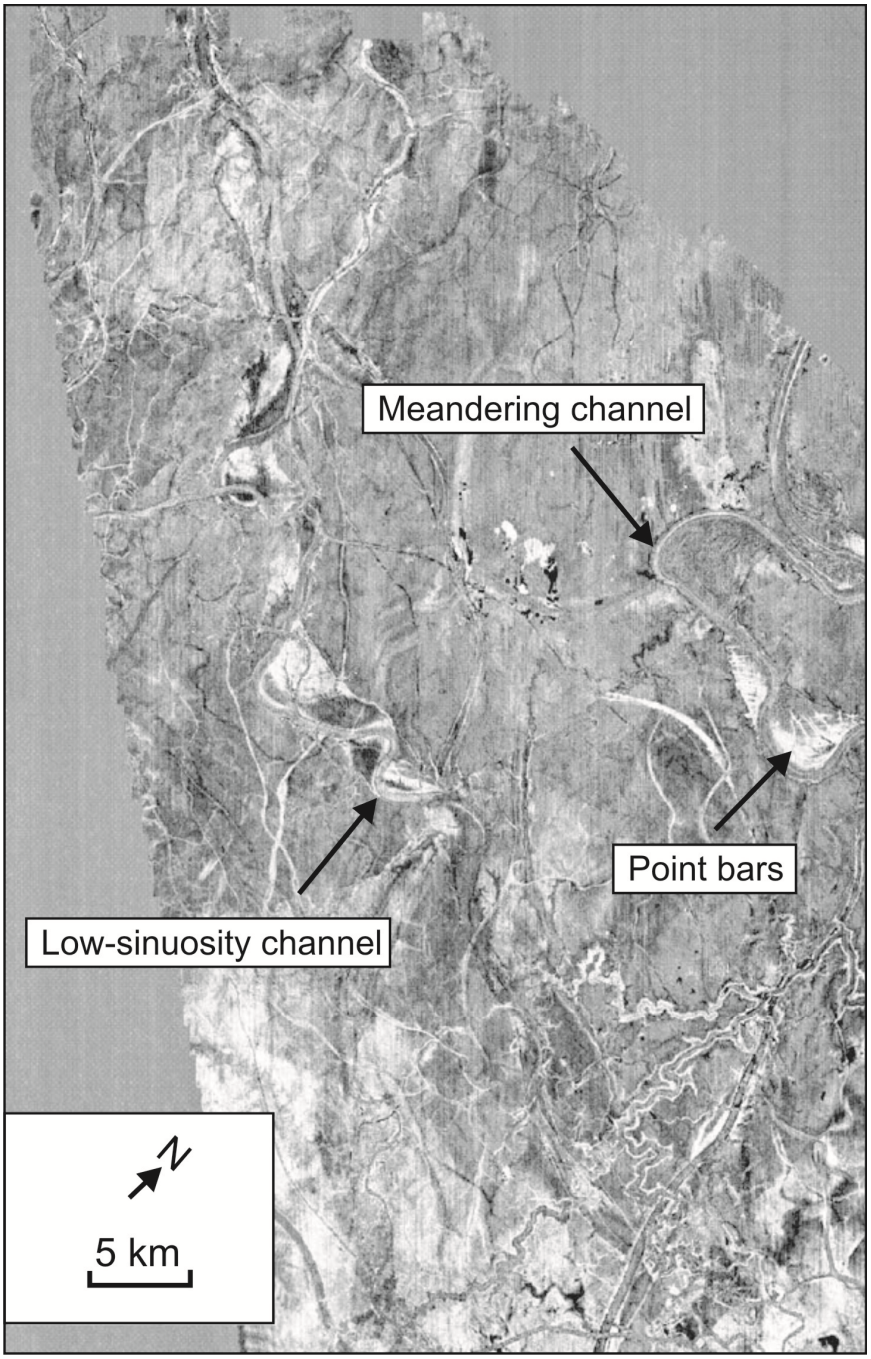

Figure 2.6: A time slice at 196 ms showing wide range of fluvial systems observed within the Late Pleistocene fluvial systems of the Malay Basin (modified from Miall, 2002).

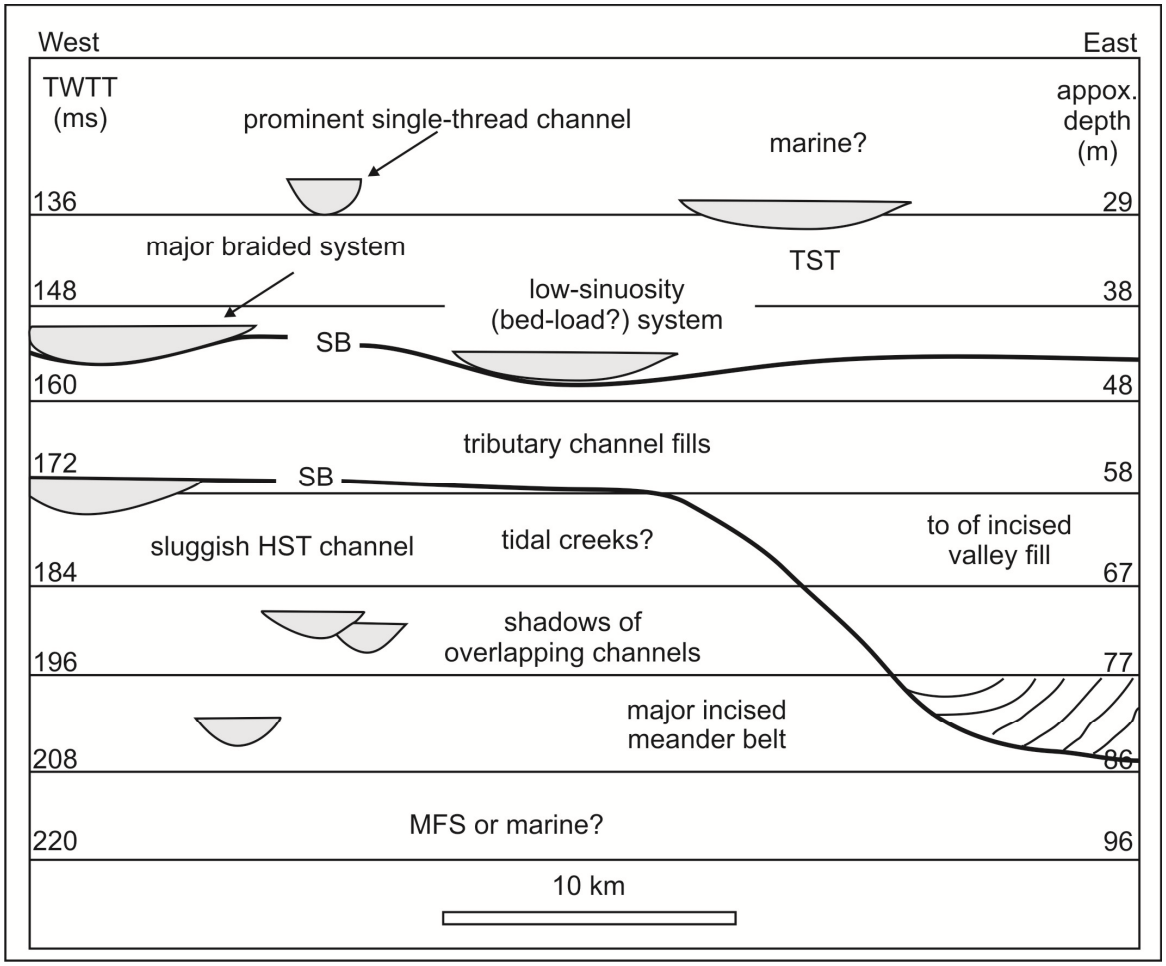

Figure 2.7: A sequence stratigraphic model developed on the basis of time slices analysis. The position of the lower sequence boundary is based primarily on the existence of incised valley (modified from Miall, 2002).

Nakanish et al. (2003) integrated 3D seismic data with well logs to investigate the fluvial systems of the Late Jurassic Birkhead Formation, Eromango Basin, South Australia and recognised abandonment channels on amplitude maps. Similar study but with exceptional high-resolution images was conducted by Carter (2003). Carter (2003) used these data to examine the four Oligocene-Miocene meandering-point bars reservoirs from the Widuri Field, Java Sea. A highly sinuous meandering channel and related features, such as point bar accretion were clearly imaged (Figure 2.8). He further suggested that these deposits are parts of lowstand bypass channel systems and are not part of an incised valley fill.

Furthermore, Carter (2003) used quantitative measurements from seismic data to improve the developed reservoir model and hence to target new well locations. Martinez et al. (2004) used 3D seismic and well logs to examine the Late Miocene Messinian unconformity on the Ebro continental margin, where a meandering channel and an incised valley were identified.

Darmadi et al. (2007) used 3D seismic data, including horizontal time slices along with seismic section, to examine the fluvial architectures of the Pliocene to Holocene Muda Formation on the Sunda Shelf, offshore Indonesia. Different channel style and size from major meandering rivers to small tributaries and floodplain drainage channels were clearly imaged. In this study, predictable vertical changes in fluvial channel architecture styles and size are indicated. Darmadi et al. (2007), concluded that the variability in channel pattern within the Pleistocene succession in West Natuna Basin is controlled mainly by variations in discharge during gradual aggradation and that the sea-level fluctuation had less of an influence. This interpretation has been also proposed by Kiel (2009) which was mainly based on the fact that the study area is *ca.* 1000 km away from the shelf break which has been estimated as the paleo-shoreline in the Sunda Shelf by Darmadi et al. (2007).

Rabelo et al. (2007) used a new method called GeoTime, which is a 3D seismic volume that is created between two near-isochronous geological surfaces, to examine the fluvial depositional environments. This method allowed imaging a meandering channel and thus helps to quantitatively estimate the morphometric parameters such as the meander belt width. Zeng (2007) reviewed the methods of seismic geomorphological imaging. He used these methods to examine Pliocene fluvial systems in the coastal-plain of offshore Louisiana and show how the seismic images improved by using stratal and proportion slices. A meandering river, point bar, channel fill and abandonment channels were clearly

imaged. These images have been further used by Wood (2007) to quantitatively measure the morphometric parameters of these channel systems. Wood (2007) plotted these parameters against each other to establish empirical relationship between these parameters. Wood (2007) was able to classify the channels following Schumm (1977) into three channel classes which are bed-load, and mixed-load, and suspended-load channels.

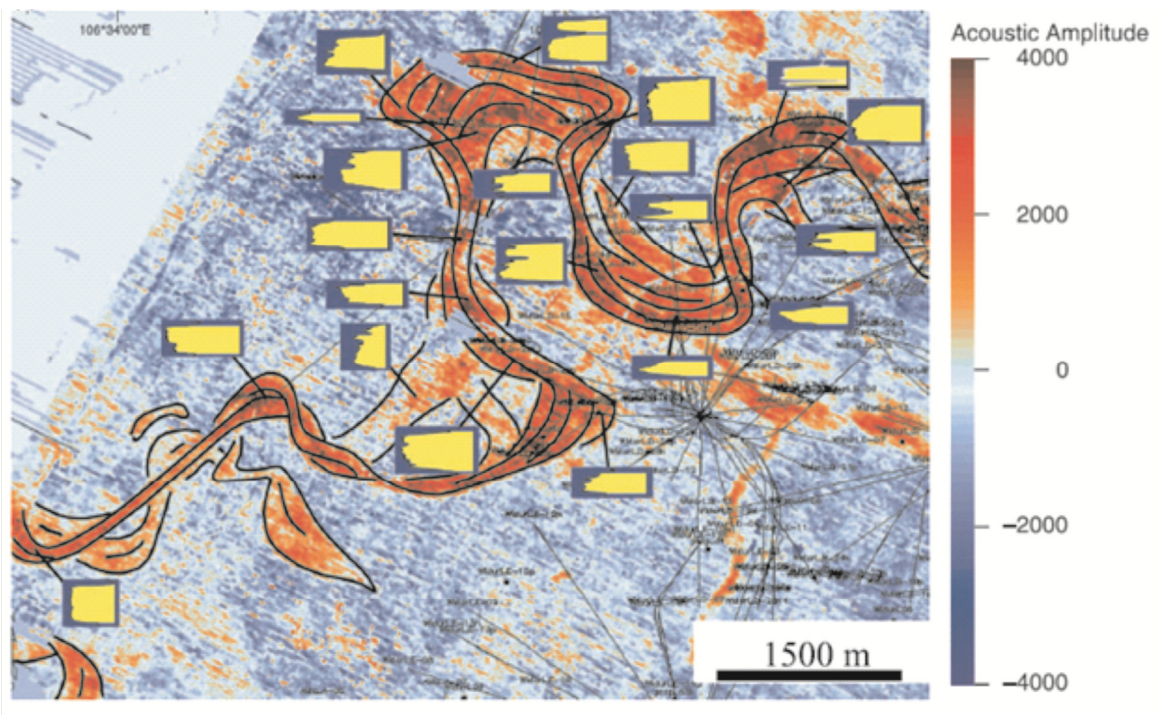

Figure 2.8: Amplitude map showing large meandering channel with interpreted internal architecture and gamma-ray signatures of Widuri Reservoirs, Java Sea (after Carter, 2003).

Chapter 3

Data Sources and Methodology

3.1 Data Sources

The data utilised in this study consists of a 3D seismic reflection dataset with a total areal extent of *ca*. 11500 km^2 (*ca*. 115 km wide by *ca.* 100 km long); supplemented locally by site survey data (Figure 3.1). The data sources used in this study are described in the following sections.

3.1.1 3D Seismic Dataset

The seismic dataset comprises ten separate seismic surveys that have been merged into a single interpretable 3D volume. The dataset is zero-phase processed with SEG normal polarity, in which a positive (peak) event (black seismic reflection on seismic sections) represents a downward increase in acoustic impedance, and a negative (trough) event (white seismic reflection on seismic sections) represents a downward decrease in acoustic impedance (Brown, 2004). In-line and cross-line spacing within these surveys are 9.38 m and 12.5 m, respectively. The vertical record length is 600 milliseconds two-way time (ms twt). The vertical sampling interval for all surveys is 2 ms, except for one survey which has a sampling interval of 1 ms. The dominant seismic frequency ranges from 60-70 Hz. Unfortunately, only limited well data are available to calibrate the seismic data, as most wells within the area targeted the deeper, productive Miocene succession. However,

depth and thickness measurements were converted from the milliseconds two-way time (ms twt) to metres by using velocity information (i.e. check-shot data) from one reference well (Tunggal-1; Figure 3.1) which does contain these data. This well indicates that the average velocity of the shallow part of the basin fill is *ca*. 1880 m sec^{-1}. Based on the estimation of the frequency and velocity, the vertical resolution ranges from *ca.* 6.7 to 7.8 m and the lateral resolution ranges from *ca.* 11.5 to 15.5 m.

The quality of the seismic data within the studied interval is generally excellent, although exact amplitude values vary between different surveys due to variations in the acquisition and processing parameters. Fortunately, this does not unduly hamper the overall imaging and mapping of fluvial systems. There are also marked 'acquisition footprints' in the upper parts of several of the individual datasets within the merged survey. These appear as amplitude stripes on horizontal 'time' slices and as small breaks or discontinuities along reflection events in seismic cross-sections. Finally, some of the individual surveys within the mega-merge survey have not been optimally merged as observed by minor (< 4 ms) vertical offset of reflection events. Fortunately, most of these minor issues can be overcome by using a combination of map-view and cross-section images, thereby ensuring that only true geological features were interpreted.

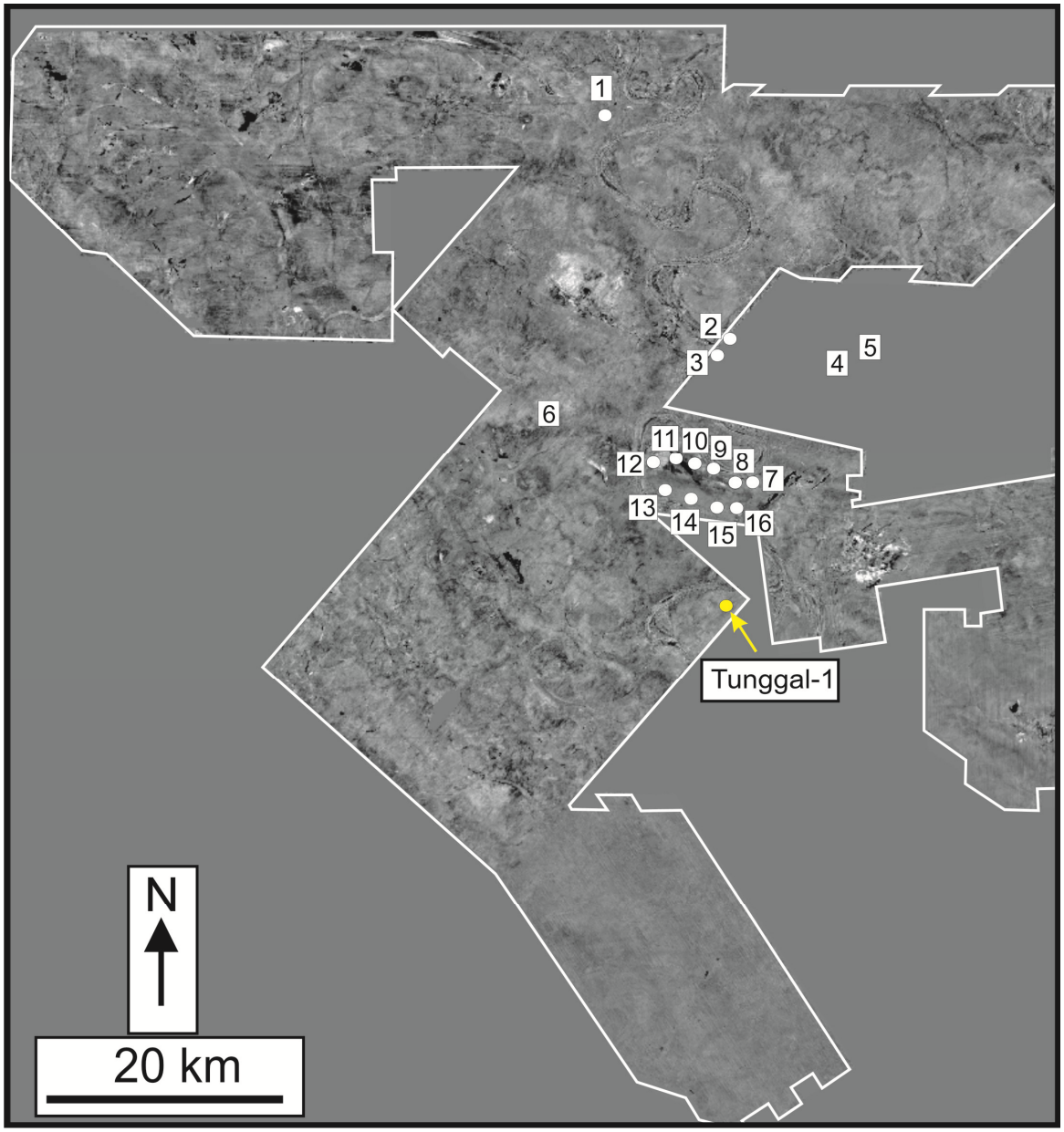

Figure 3.1: Base map of the study area based on a horizontal 'time' slice at 400 ms. The volume consists of ten surveys that have been merged to make a single interpretable volume. The yellow-circle represents the location of the well (Tunggal-1) that was used in the time-depth conversion. The white-circles represent the locations of the borings used in this study (see Table 3.1 for more details).

3.1.2 Site Survey Dataset

Site survey data from 56 locations have been analysed in this study. The site survey data consists of the following data types:

1) Sixteen platform borings, which are 30-150 metres in length, provide information on the lithology and facies of the stratigraphic fill of the incised valley (Table 3.1 and Figure 3.1). The geographic coordinates of these borings were imported into ArcGIS and then superimposed onto a time-slice at 108 ms twt such that their locations with respect to the studied incised valley could be visualised.
2) 40 km^2 of high–resolution, multi-channel, 2D seismic data (typical individual line length of 2 km) with frequencies of up to 250 Hz; although these data theoretically provide a higher vertical resolution of stratigraphic layering (e.g. *ca.* 2 m) than the standard 3D seismic data (e.g. *ca.* 6.8-7.8 m), this is often not the case. In addition, these 2D data are spatially-limited, thus these data are not widely used in this study.
3) Boomer data, which is analogous to seismic reflection data but has a dominant frequencies range of 2-7 kHz (compared to 250 Hz for the high-resolution 2D seismic data and 60-70 Hz for the 3D seismic data). These data provide very high-resolution images (vertical resolution of *ca.* 300-500 cm) of the internal architecture of the uppermost part (maximum of 60 m below seabed) of the incised valley fill.
4) Side-scan sonar data, which provide detailed images of seabed irregularities that may be related to shallowly-buried, pre-Holocene fluvial channels and valleys.
5) Echo sounder data, which provides detailed water depth information by using high-frequency (200 kHz) transducer sources.

6) Geotechnical cores, which provide lithological information up to 3 m below the seabed.

Table 3.1: lists the platform boring analysed in this study. Location of these borings relative to the incised valley (IV) is illustrated.

No.	Borehole name	Total depth (m)	Field	Water depth at well location (m)	Location
1	Melor	150	Melor Field	76.3	Within IV
2	Tangga Barat-1A	150	Tangga Field	70.9	Within IV
3	Tangga Barat-1B	150	Tangga Field	70.8	Within IV
4	BH Tangga	150	Tangga Field	65.3	Outside IV
5	Tangga Deep-1	30	Tangga Field	63.3	Outside IV
6	Bujang Deep-1	30	Bujang Field	66.1	Outside IV
7	Dulang A-Primary	150.6	Dulang Field	74.5	Within IV
8	Dulang A-Secondary	151.6	Dulang Field	74.7	Within IV
9	Dulang B	150.3	Dulang Field	79	Within IV
10	Dulang WP-B	60	Dulang Field	78.4	Within IV
11	Dulang WP-C	60	Dulang Field	75.7	Within IV
12	Dulang WP-D	60	Dulang Field	74.6	Within IV
13	Dulang SPM-1	30	Dulang Field	74.6	Within IV
14	Dulang SPM-2	45	Dulang Field	77.2	Within IV
15	Dulang SPM-3	45	Dulang Field	75.6	Within IV
16	Dulang SPM-C	45.6	Dulang Field	77.3	Within IV

3.2 Methodology

3.2.1 3D Seismic Analysis

Based on seismic facies analysis and reflection continuity, seven horizons have been mapped throughout the study area. Time-structure maps and isochron maps have been constructed. Interpretation of depositional features and geomorphological patterns observed within these seismic units has been achieved by the use of a combination of horizontal 'time' slices and 'iso-proportional' slices (*sensu* Zeng et al., 1998; Brown, 2004; Posamentier et al., 2007). Time slices are seismic slices that are taken horizontally through the original reflectivity 3D seismic volume whereas iso-proportional slices are obtained by slicing between two parallel or non-parallel, horizontal or dipping reflection events (see Zeng et al., 1998; Brown, 2004; Posaminter et al., 2007; Figure 3.2A). Horizontal 'time' slices are only useful when the geological features of interest and the stratigraphic timelines along which they are developed are horizontal to sub-horizontal; this only occurs in the upper part of the studied succession (Figure 3.2A). In the middle and lower parts of the studied interval where the seismic reflections are not horizontal (due to post-depositional deformation), iso-proportional slices have been utilised (Figure 3.2A).

Ten interpretive maps were constructed that illustrated the range of fluvial channel styles at various stratigraphic levels within the dataset. Each map is composed of observations from a succession of time and/or iso-proportional slices taken from either the lower half or the upper half of each mapped seismic unit; hence each map illustrates the type of channels that are observed in either the base or the top part of each unit (Figure 3.2B). It should be noted that the number of channels shown on these maps at any one stratigraphic level should be considered a 'minimum'; this reflects a lack of or only partial imaging of

channels which are at or below seismic resolution, and high 'fragmentation' of channels due to incision by younger channels. Mapping and interpretation of the stratigraphic occurrence of channels is challenging as channels commonly incise downwards from a variety of stratigraphic levels and are superimposed on individual seismic slices. Moreover, seismic 'multiples' from shallower channels may mask channels imaged at lower stratigraphic levels.

3.2.2 Site Survey Analysis

Sixteen lithological logs have been constructed using the platform borings and shallow cores (Appendix 8.3); from these logs an idealised log, which represents the bulk lithologies and sedimentological characteristics observed within the stratigraphic interval of interest, has been created. This log has then been tied to the seismic data using depth information in order to determine the lithological and sedimentological characteristics, and depositional facies which infilled the studied incised valley. This lithological information has also been used to interpret the boomer section.

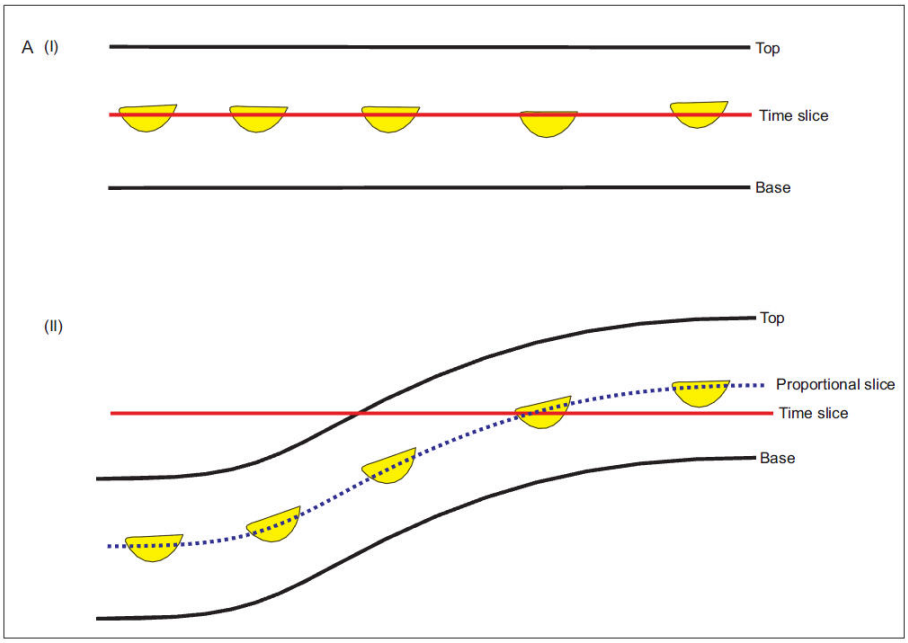

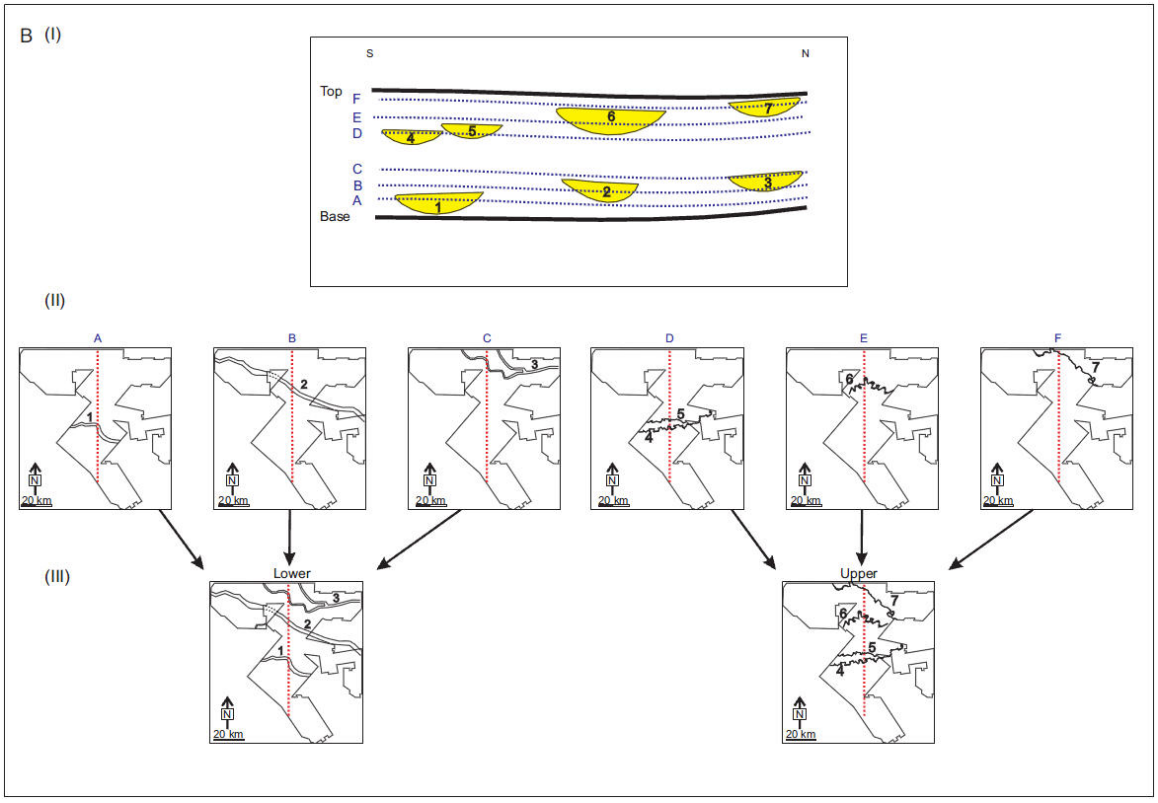

Figure 3.2: A) shows the differences between the horizontal 'time' slice (I) and iso-propositional slices (II). Time slices are horizontal slices that are taken through the original reflectivity 3D seismic volume (I) where the iso-proportional slices are obtained by slicing between two non-parallel reflections (II); **B)** shows the methodology used in creating the interpretive planview maps presented in this study. These maps are composed of successive iso-proportional slices. (I) a schematic cross-section through the study area showing an individual unit and range of channels (1-7) that are bounded by the top and base of the unit. The blue dashed-lines (A-F) represent the iso-proportional slices that have been generated at different stratigraphic level .The 2D horizontal map-views of these slices are shown in (II). These horizontal map-views are then combined to make two interpretive planview maps that represent the type of the channels that are observed within the lower half and upper half of the unit.

3.2.3 GIS Methodology

3.2.3.1 Introduction

Standard seismic interpretation and visualisation software are not designed to allow extraction of quantitative, spatially-referenced data from seismic reflection volumes. Therefore, seismic interpretation software has been integrated with geographic information system (GIS) software to develop a methodology that can be used to measure and document the various geometric parameters of the studied fluvial systems. In particular, dataset limitations notwithstanding, the ten interpretive maps are treated as 'paleo-satellite', Google Earth-type images, and they have been imported into ArcGIS for quantitative analysis. A semi-automatic data extraction workflow has been developed, which is efficient, fast and flexible.

3.2.3.2 Measuring Morphometric Parameters

The morphometric parameters examined in this study include channel width (*CW*), channel depth (*CD*), meander belt width (*MBW*), meander wavelength (*ML*), channel length (*La*), sinuosity (*SI*), and radius of curvature (RC). All of these parameters have been determined using interpretative maps in ArcGIS. The exception to this is depth which was measured directly from vertical slices through the seismic volume. The geometry of a total of 130 channels has been documented and the associated parametric data has been used to establish empirical relationships between these parameters. In this study, these parameters have been measured following the most widely accepted methodology to measure modern rivers using aerial photographs by different authors (e.g. Schumm, 1977, Ethridge and Schumm 2007, Wood 2007; Figure 3.3A).The geometric

parameters are measured differently depending on the data used in the analysis. Descriptors of these geometric parameters and how these parameters are measured in both modern and ancient rivers are given in the following sections.

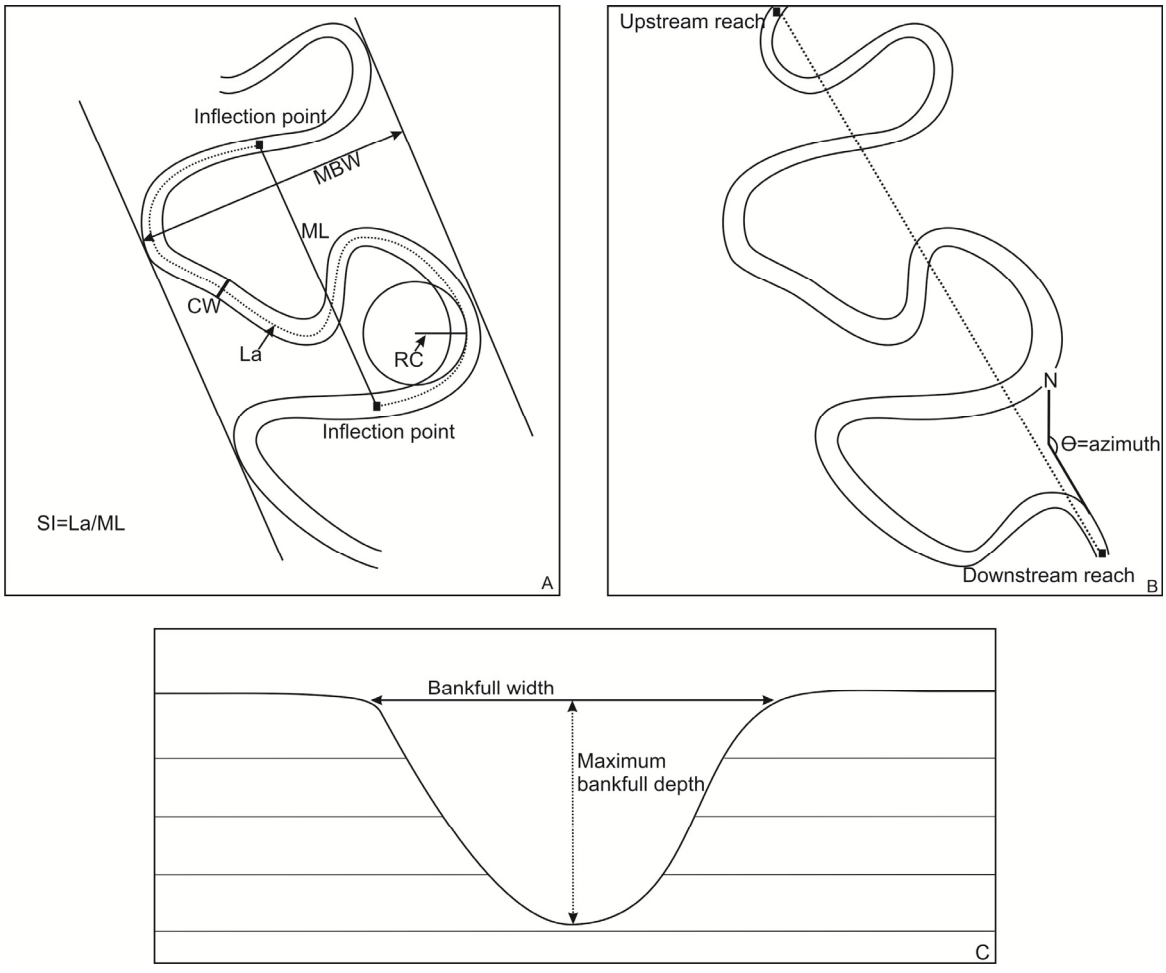

Figure 3.3: Schematic drawing showing the methodology adopted to measure the morphometric parameters of the fluvial systems **(A & C)** and the channel orientation **(B)**. The morphometric parameters include channel width (*CW*), channel depth (*CD*), meander belt width (*MBW*), radius of curvature (*RC*), meander wavelength (*ML*), and channel length (*La*). Sinuosity (*SI*) is calculated as the length along the channel course (*La*) divided by the meander wavelength (*ML*). The channel orientation is determined by defining the azimuth of a line that has been drawn between two points of the upstream and downstream reaches; **C)** Schematic drawing showing the methodology adopted to measure the channel depth (*CD*) from the seismic cross-section.

3.2.3.2.1 *Channel Depth (CD)*

CD is a measure of the maximum depth of the channel-related incision. This parameter is measured directly from vertical seismic sections and is defined as the vertical distance between the top and base of the channel-related incision (Figure 3.3C); however, in case where the channel is only visible on time and/or iso-proportional slices, *CD* can be measured by the number of time or iso-proportional slices over which the channel feature appears (e.g. given a 2 ms vertical sampling interval, a channel observed on 4 timeslices would be 6 ms 'thick'). *CD* is measured every 500 m.

3.2.3.2.2 *Channel Width (CW)*

CW is measured directly from the interpretive planview maps and is defined as the horizontal distance between the erosional margins that bound the channel (Figure 3.3A). *CW* is measured every 500 m on lines which are perpendicular to the channel centerline (channel length (*La*)).

3.2.3.2.3 *Meander Belt Width (MBW)*

MBW describes the width of a fluvial sandbody that forms in response to lateral migration of numerous individual channel systems; in practice, this value defines the width of the 'container' within which the individual channels migrate. *MBW* is measured directly from the interpretive maps as the width between two lines that bound outermost visible meander-loop sets (Figure 3.3A). Like *CW*, *MBW* is measured on a line which is perpendicular to the valley centreline every 500 m along the valley axis.

3.2.3.2.4 *Meander Wavelength (ML)*

ML is defined and measured as the length between the upstream and downstream inflection points that define a single, complete meander bend (Figure 3.3A).

3.2.3.2.5 *Channel Length (La)*

La is measured as the length of the centreline along the channel course between the uppermost and lowermost inflection points (Figure 3.3A). *La* is measured and used with *ML* to calculate channel sinuosity (*SI*).

3.2.3.2.6 *Sinuosity (SI)*

SI is an important parameter in describing the overall map-view style (e.g. meandering, braided and straight) of a fluvial system. *SI* is calculated by dividing the channel length (*La*) on meander wavelength (*ML*) for discrete meander segments of the channel.

3.2.3.2.7 *Radius of Curvature (RC)*

RC is calculated by measuring the radius of a best-fit circle located within a meander bend (Figure 3.3A).

3.2.3.2.8 *Channel Orientation (CO)*

The overall trend or orientation for each channel has been determined by defining the azimuth of a line that has been drawn between two points of the upstream and

downstream reaches at the limits of the dataset (Figure 3.3B). Since the ultimate source of sediment supply (i.e. the Malay Peninsula and Thailand) and the ultimate depocentre (i.e. the South China Sea) for most if not all of the channels observed within the Malay Basin are known, the upstream and downstream reaches of each channel have been defined. After determining the orientations of all the channels observed on the interpretive maps, these data have been plotted on rose diagrams to assess the vertical changes in channel orientation for Pleistocene to Recent fluvial systems.

3.2.3.3 GIS Workflow

A semi-automated GIS methodology to determine the morphometric parameters has been developed. A workflow has been put together using ArcGIS goeprocessing tools and ET Geowizards extension. This workflow takes around 30 minutes to run. Once the start polygons which define the channel and the meander belt (steps 1-3 described below) have been generated, the tools take seconds to run. The workflow consists of ten simple steps as follows:

1) Importing the time or iso-proportional slices into Arcview software with its geographical coordinates using the Georeferencing tool (Figure 3.4).
2) Digitising the channel edges using the Editing tool (red polygon in Figure 3.4).
3) Digitising the meander belt using the Editing tool (black polygon in Figure 3.4).
4) Creating the centerline of meander belt (valley axis) using ET Geowizards tool (blue-line in Figure 3.5A).
5) Creating perpendicular lines (every 500 m) to the valley axis centerline using ET Geowizards tool (green-line in Figure 3.5B).

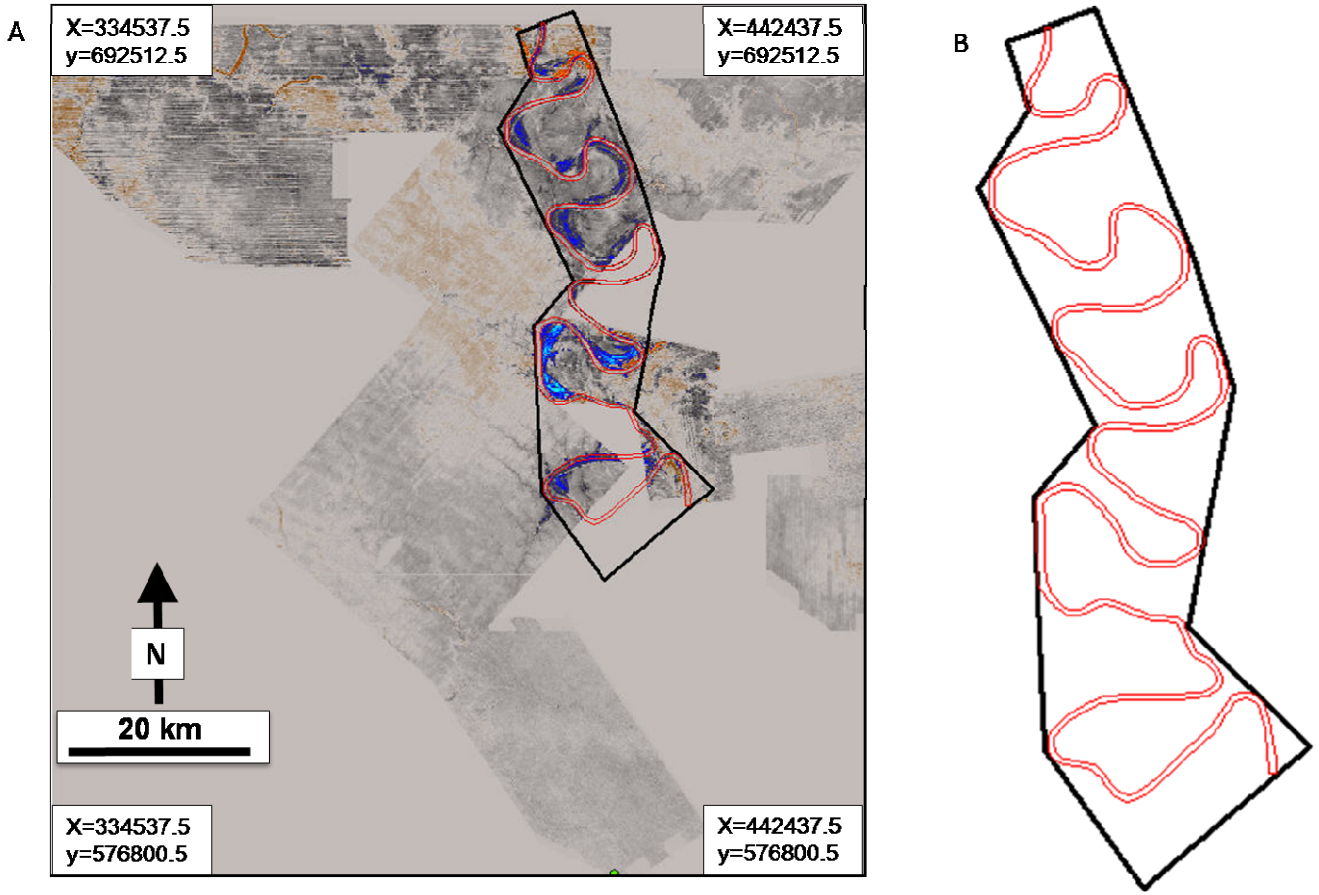

Figure 3.4: A) A time slice of 108 ms showing a large meandering channel used in the development of the methodology. This time slice has been imported into ArchGIS using its geographical coordinates (shown on the corners of this Figures). The banks (red polygon) and the meander belt (black polygon) of the channel have been digitised; **B)** close-up image of the digitised channel banks and meander belt.

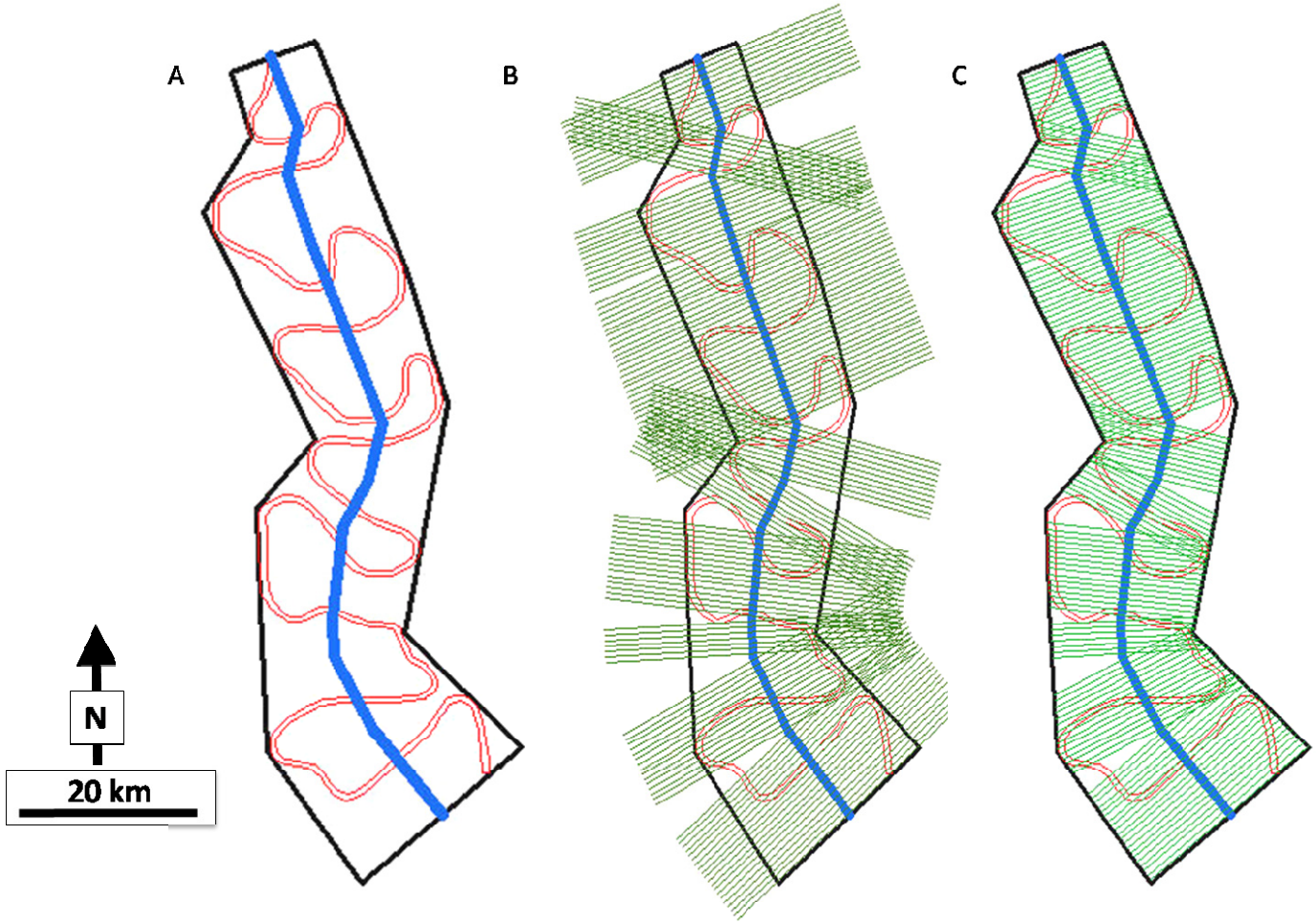

Figure 3.5: A) shows the created centerline (blue line) of meander belt (valley axis); **B)** shows the created perpendicular lines (green lines) to the valley axis; **C)** the clipped perpendicular lines which represents the widths of the meander belt.

6) Clipping the perpendicular lines to the meander belt boundaries using ET Geowizards tool. These clipped lines represent the meander belt width (*MBW*) (Figure 3.5C).
7) Creating the channel centerline using ET Geowizards tool (thin black-line in Figure 3.6A).
8) Creating perpendicular lines (every 500 m) to the channel centerline using ET Geowizards tool (green-line in Figure 3.6B). These lines have been clipped to the channel banks. These clipped lines represent the channel width (*CW*).
9) Creating point intersections where the channel centerline intersects with valley axis centerlines using ET Geowizards tool (black dots in Figure 3.7A & B). This results in dividing the channel centerline and valley axis centerlines into small segments. The segments along channel centerlines represent half channel length (½ *La*) whereas the segments along valley axis centerline represent half wavelength (½ *ML*) (Figure 3.7C). There are two methods to calculate the *ML* and *La*: a) By multiplying the ½ *ML* and ½ *La* by two; or b) By summing the length of every two segments of ½ *ML* and ½ *La* (Figure 3.7D). The *ML* and *La* is used to calculate the sinuosity (*SI*).
10) Creating circles that best-fit the meander bends using Editing tool (blue circle in Figure 3.8). The radii of these circles represent the radius of curvature (RC).

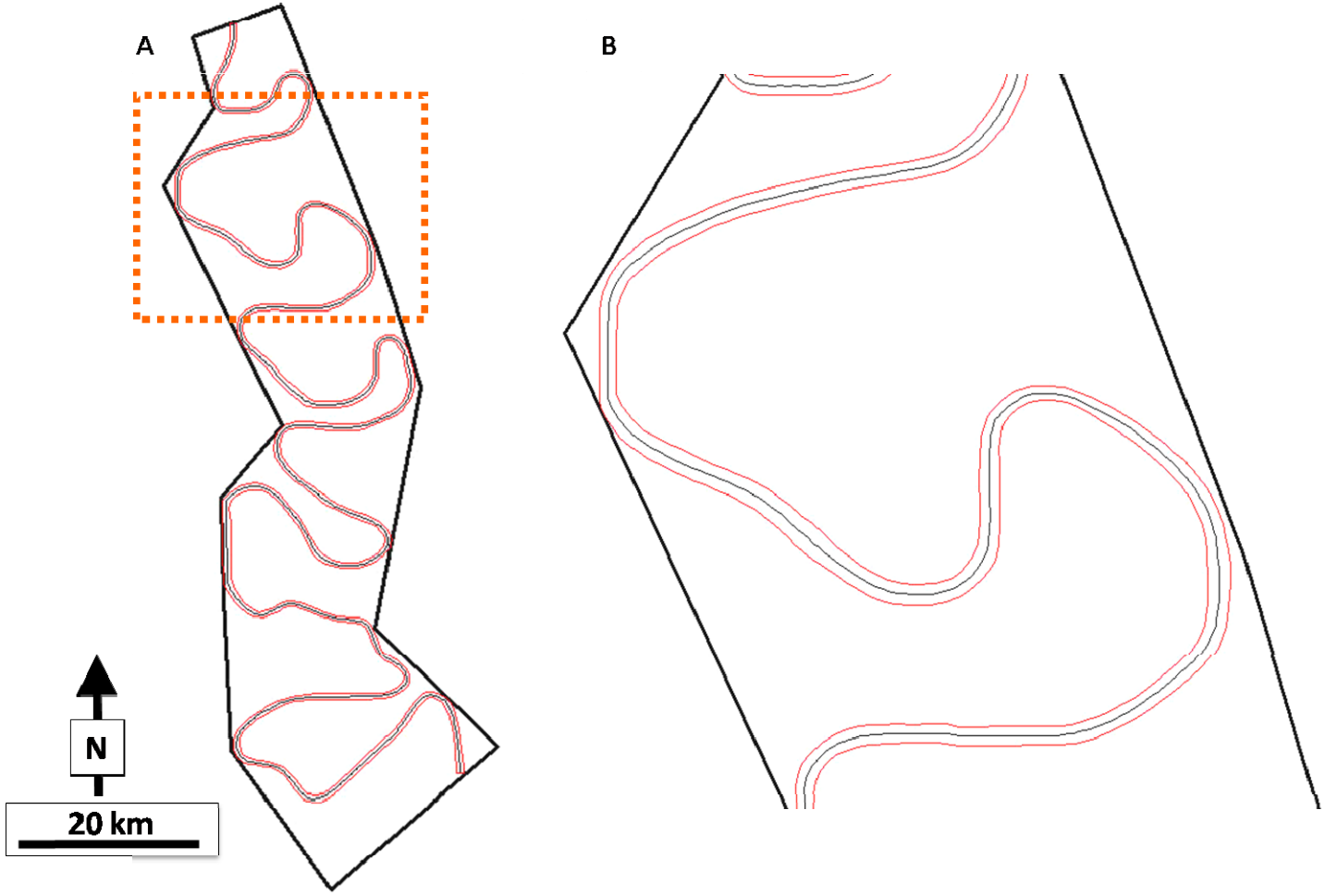
A
B
N
20 km

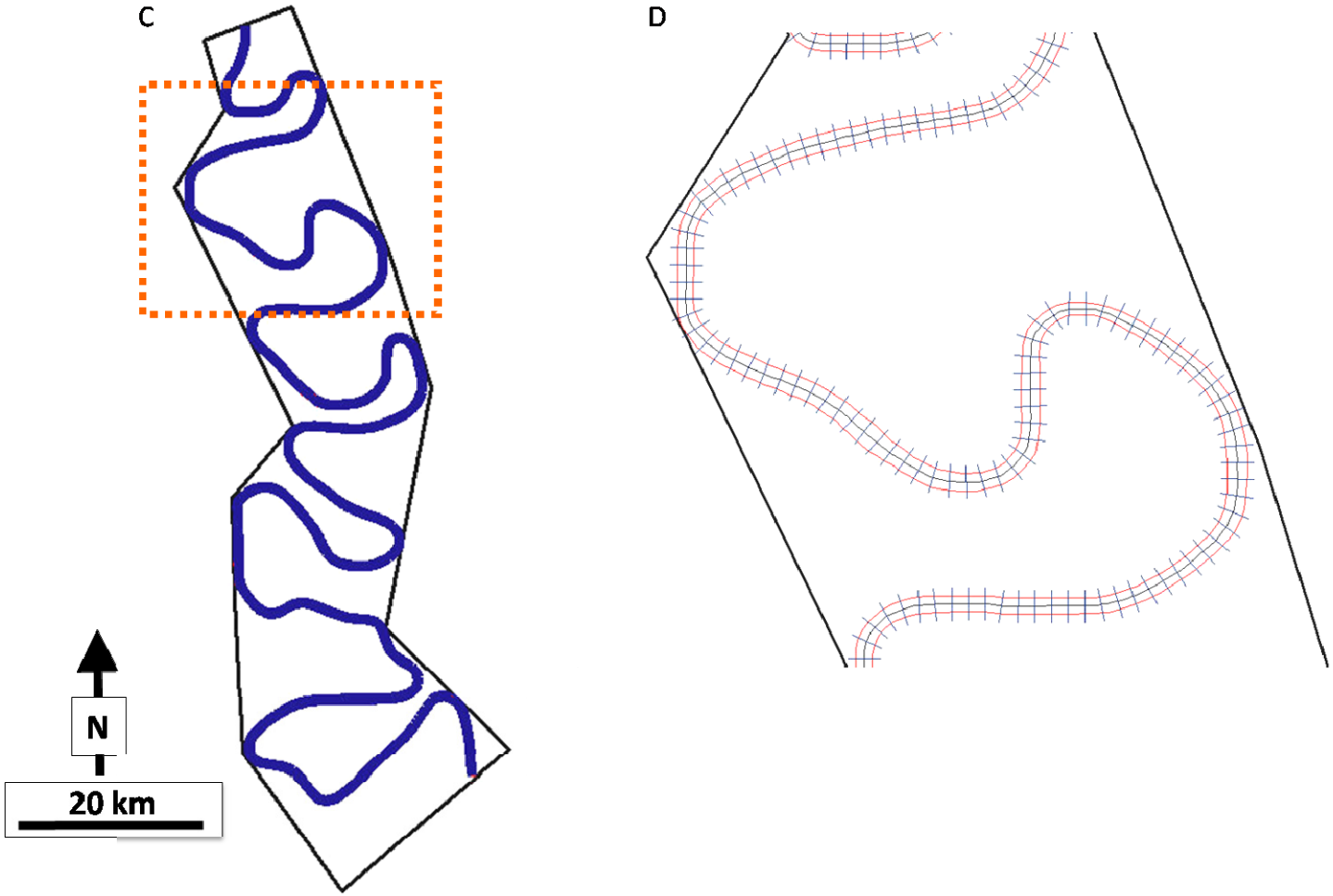

Figure 3.6: A & B) shows the created channel centerline (black line); **C & D)** shows the created perpendicular lines (blue lines) to the channel centerline. These lines have been clipped to represent the channel width.

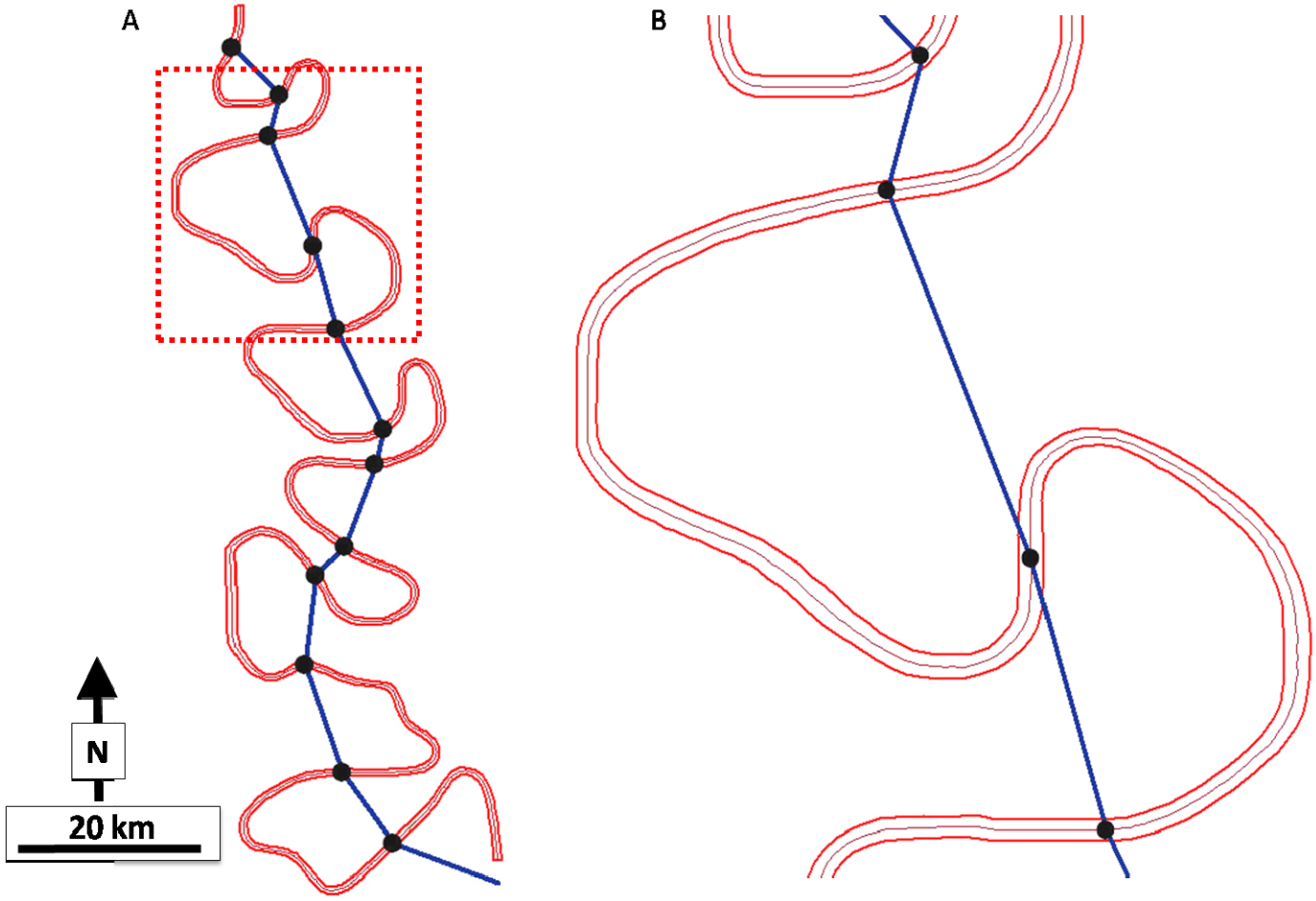
A
B
N
20 km

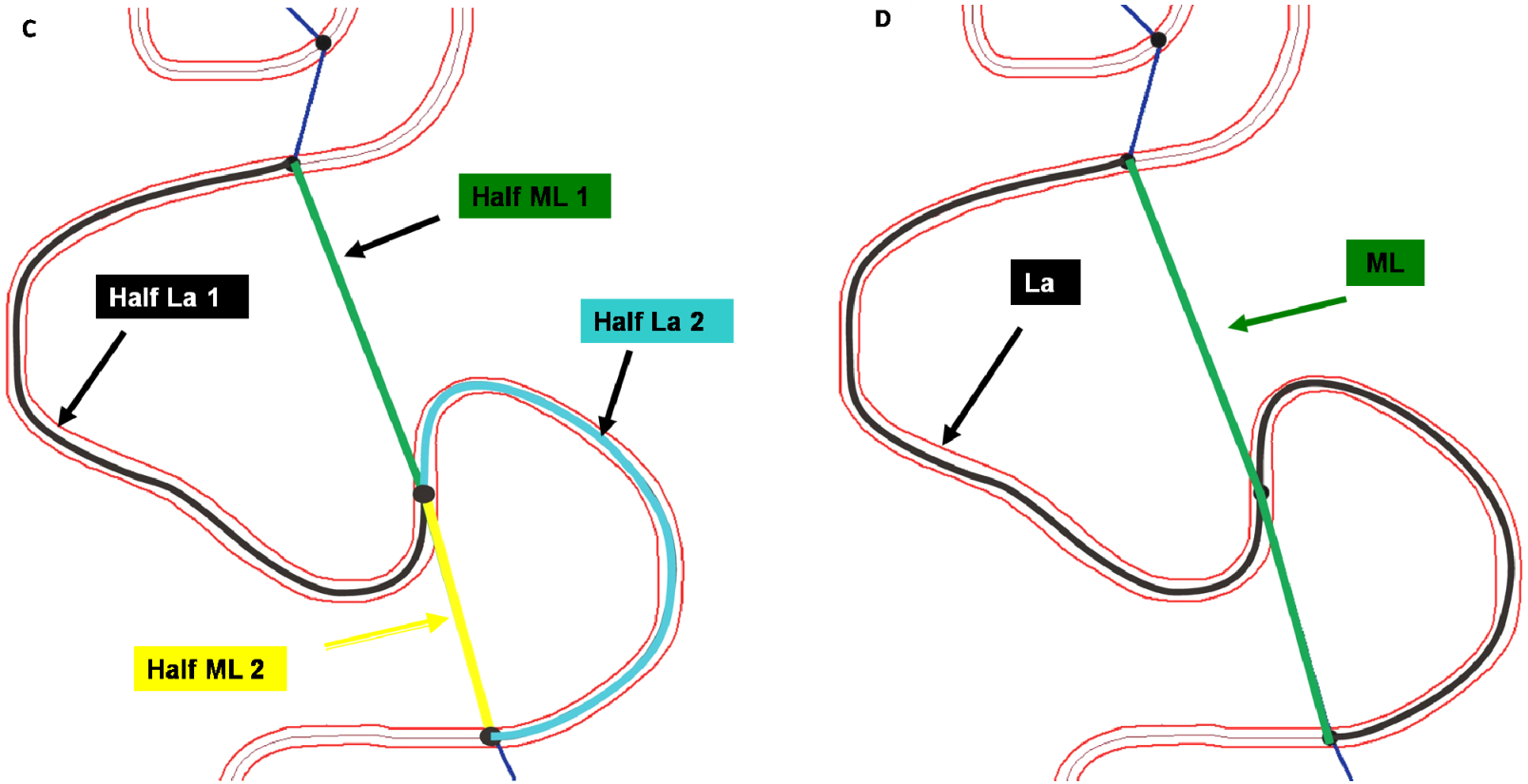

Figure 3.7: **A & B)** shows the created point intersections (black dots) where the channel centerline intersects with the meander belt (valley axis) centerline; **C)** shows the half meander wavelength (½ *ML* represented as segments along the valley axis centerline) and the half channel length (½ *La* represented as segments along the channel centerline); **D)** shows the calculated *ML* and *La* for a single channel segment.

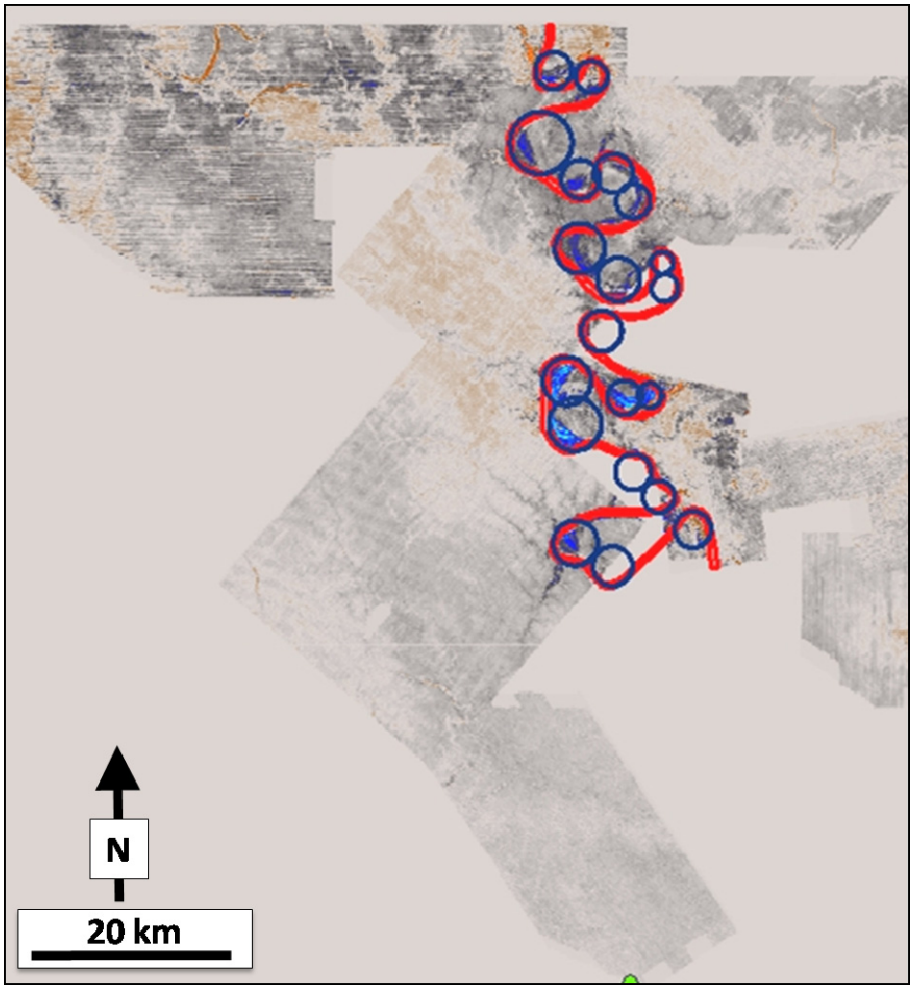

Figure 3.8: shows the created circles (blue circles) that best-fit the meander bend. The radius of a best-fit circle around the meander bend is used to calculate the radius of curvature (*RC*).

Chapter 4

3D Seismic Geomorphology of Fluvial Systems of the Pleistocene to Recent in the Malay Basin, Southeast Asia

4.1 Abstract

Fluvial sandstones constitute one of the major clastic petroleum reservoir types in many sedimentary basins around the world. This is especially true in the Tertiary basins of Southeast Asia, which display a wide range of fluvial channel reservoir types. This study is based on the analysis of high-resolution, shallow (seabed to *ca.* 500 m depth) 3D seismic data which provide exceptional imaging of the geometry, dimension and temporal and spatial distribution of fluvial channels. The Malay Basin comprises a thick (>8 km), rift to post-rift Oligo-Miocene to Pliocene basin-fill. The youngest (Miocene to Pliocene), post-rift succession is dominated by a thick (1-5 km), cyclic succession of coastal plain and coastal deposits, which accumulated in a humid-tropical climatic setting.

This study focuses on the Pleistocene to Recent (*ca*. 500 m thick) succession, which comprises a range of seismic facies, mainly reflecting changes in fluvial channel style and gross stratigraphic architecture. The succession has been divided into four seismic units (Unit 1-4), bounded by basin-wide stratal surfaces. Units 3 and 4 have been further divided into two sub-units (Older which are sub-units 3.1 and 4.1 and sub-units 3.2 and 4.2 which are the younger). Two types of boundaries have been identified: 1) a boundary

that is defined by a regionally-extensive erosion surface at the base of a prominent incised valley (e.g. Horizons C.1 and D.1); 2) a sequence boundary that is defined by more weakly-incised, straight and low-sinuosity channels which is interpreted as lowstand alluvial bypass channel systems (e.g. Horizons A, B, C, and D). Each unit displays a predictable vertical change of the channel pattern and scale, with wide low-sinuosity channels at the base passing gradationally upwards into narrow high-sinuosity channels at the top. The wide variation in channel style and size is interpreted to be controlled mainly by the sea-level fluctuations on the wide flat and tectonically-quiescent Sundaland Platform. However, climate control may have a significant impact on the channel style and size by affecting the discharge and the types of sediment load

This study demonstrates how a better understanding of fluvial reservoir variability can be obtained through the analysis of high-resolution, shallow 3D seismic data (seabed to *ca.* 500 m), which can provide exceptional imaging of fluvial channel planform shapes and other geometrical properties and dimensions.

4.2 Introduction

Fluvial channel sandstones form major productive reservoirs for hydrocarbons in many basins around the world. These fluvial sandstones are complex and may display a wide variety of stacking patterns, ranging from narrow, single-story sandstone bodies to broad, multi-lateral/multi-story sandstone bodies. It is often assumed that reservoir sandstones comprised of meandering river deposits are generally channel-like and isolated, whereas sheet-like fluvial reservoir sandstones are typically deposited in braided fluvial environments (Reading, 1996; Bridge and Tye, 2000). The complexity and vertical

variability in fluvial channel architecture and style is indicated in most sequence-stratigraphic models of fluvial systems (e.g. Wright and Marriott, 1993; Shanley and McCabe, 1994).

The variability in fluvial channel type and geometry is controlled by numerous factors including base-level, climate, tectonic, sediment types, and hydrology. Schumm (2005) described three dominant factors that control the architectural variability in fluvial systems: 1) *upstream controls*, including tectonics, climate and bedrock lithology of the source area; 2) *local controls*, including valley morphology, vegetation, active tectonics, tributaries and type of bedrock; and 3) *downstream controls*, which include base-level fluctuations and length of upstream extent. Among these factors, base-level variations, syn-depositional tectonics and climate are considered to be the most significant factors that influence the overall fluvial channel architecture and size. For channels that discharge into marine basins, base-level corresponds to sea-level. Tectonics (uplift or subsidence) and base-level fluctuations are the main controls on the rate of accommodation creation or destruction. Therefore, these factors determine whether fluvial incision, aggradation or lateral migration occurs. Climate change may also have a significant influence on fluvial channel style by affecting the rate and caliber of sediment supply, vegetation cover, precipitation and discharge; however, climate is only rarely cited as a key control on the temporal and spatial evolution of fluvial systems (Blum and Törnqvist, 2000; Ethridge and Schumm, 2007).

It has long been recognised that fluvial systems may change their sinuosity, width and/or depth in response to changes in base-level (Blum and Törnqvist, 2000; Schumm, 2005). For example, Schumm (1993) indicated that deep river incision may occur in association with a significant fall in relative base-level, and that the geometric characteristics (e.g. width, depth, etc) of the fluvial incision is determined by the magnitude of the base-level

fall (see also Posamentier, 2001). When a significant fall in relative base-level occurs and a former shallow marine shelf is fully exposed, an incised valley may form (e.g. Van Wagoner et al., 1990; Posamentier and Allen, 1999; Posamentier, 2001). When a relative base-level fall does not expose the entire shelf, a lowstand alluvial bypass channel system and associated shelf delta may develop (Posamentier, 2001).

Continuous improvements in 3D seismic technology and visualisation software have allowed direct imaging of depositional elements at varying scales and in numerous depositional settings, most notably in deep marine (e.g. Kolla et al., 2001; Posamentier and Kolla 2003; Posamentier, 2004) and coastal plain settings (e.g. Posamentier, 2001; Miall, 2002; Carter, 2003; Darmadi et al., 2007). The study of depositional systems using 3D seismic reflection data has been termed 'seismic geomorphology' (*sensu* Posamentier, 2000; see also Cartwright and Huuse, 2005; Davies et al., 2004; Posamentier et al., 2007). This analytical approach has been proven to be a powerful technique in visualising the external form and internal architecture of subsurface rock volumes and in predicting the sequence stratigraphic evolution and infill of sedimentary basins. Furthermore, high-resolution 3D seismic data can also aid in the construction and conditioning of 3D reservoir geological models due to the lateral and vertical continuity of observations that cannot be obtained from other sources of data (e.g. cores, well logs, outcrops).

This study highlights the variability in 3D seismic expression, and investigates temporal and spatial variations in fluvial system architecture within the Pleistocene to Recent fill of the Malay Basin on the Sunda Shelf, situated offshore eastern Malay Peninsula, SE Asia (Figure 4.1). A number of previous studies have utilised 3D seismic data to understand the geometry and evolution of fluvial systems at several locations around the Sunda Shelf (e.g. Isa et al., 1993; Miall, 2002; Darmadi et al., 2007; Kiel, 2009). This study differs from these previous studies by investigating a much larger (i.e. *ca*. 11500 km^2) 3D

seismic dataset than utilised previously (e.g. 680-4000 km^2). This 'mega-merge' 3D seismic dataset images down to *ca*. 500 m below the present-day sea-bed and provides a unique opportunity to evaluate the Pleistocene-Quaternary, fluvial to coastal plain succession on a basin-scale; critically, such an overview cannot be achieved from interpreting a single 3D seismic survey. In regions such as the Sunda Shelf, where climate has remained relatively uniform over the last *ca*. 20 Myr, the shallow parts of large 3D seismic datasets provide an extremely valuable source of analogue data for the deeper, prospective, but more poorly-imaged Miocene succession. In particular, the documentation of the dimensions and geometries of Pleistocene fluvial systems will help in the construction of a quantitative database which can be used to help constrain reservoir models for the productive Miocene fluvial reservoirs on the Sunda Shelf (see Chapter 6). These data can also be used to improve the reconstruction of the type, evolution and controls on Pleistocene river systems on the Sunda Shelf.

4.3 Geological Setting

4.3.1 Tectono-stratigraphic evolution

The Malay Basin is situated in the centre of the Sunda Shelf, Southeast Asia, which is one of the largest intracontinental shelf areas in the world (i.e. *ca*. 125,000 km^2) (Madon, 1999; Figure 4.1). The north-west southeast trending Malay Basin is 500 km long by 250 km wide, and is located between the Penyu and West Natuna basins to the south and the Pattani Basin to the north (Hutchison, 1989; Madon et al., 1999; Figure 4.1). The basin formed as a result of tectonic extension during the Late Eocene to Early Oligocene, following the collision of India with the Asian continent (Tapponnier et al., 1986;

Hutchison, 1989). The basin comprises a thick succession (>8 km) of Oligo-Miocene to Recent deposits, which overlie a pre-Tertiary basement consisting of metamorphic, igneous and sedimentary rocks (Figures 4.2 & 4.3). The structural evolution of the Malay Basin can be divided into three tectono-stratigraphic phases (Tjia, 1994; Madon, 1998; Negah et al., 1996 and Tjia and Liw, 1996): 1) a pre-Miocene syn-rift phase; 2) an Early to Middle Miocene post-rift phase dominated by thermally-induced subsidence and basin inversion; and 3) a Late Miocene to Recent phase dominated by thermally-induced subsidence but lacking significant basin inversion (Figure 4.3).

The pre-Miocene phase represents the initial extensional phase of basin development, when subsidence was controlled by normal faulting (Hamilton, 1979; Madon, 1999). Sedimentation was characterised by alternating sand-dominated and shale-dominated fluvio-lacustrine sequences within a series of isolated half-grabens (Madon, 1999). The Early to Middle Miocene post-rift phase was dominated by thermal subsidence that was accompanied by intermittent periods of compressional deformation. This resulted in local inversion of syn-rift half-grabens and re-activation of their bounding faults, which was particularly intense in the southern part of the basin (Madon, 1999). One consequence is that the south-western flank of the Malay Basin is slightly steeper than its north-eastern flank (Figure 4.3). During this post-rift phase, deposition was characterised by coastal to shallow marine deposits. The Late Miocene to Recent phase was dominated by thermal subsidence, without any significant tectonic activity (Madon et al., 1999). Deposition during this phase was mainly within coastal plain and shallow marine environments (i.e. Pilong Formation; Madon, 1999b).

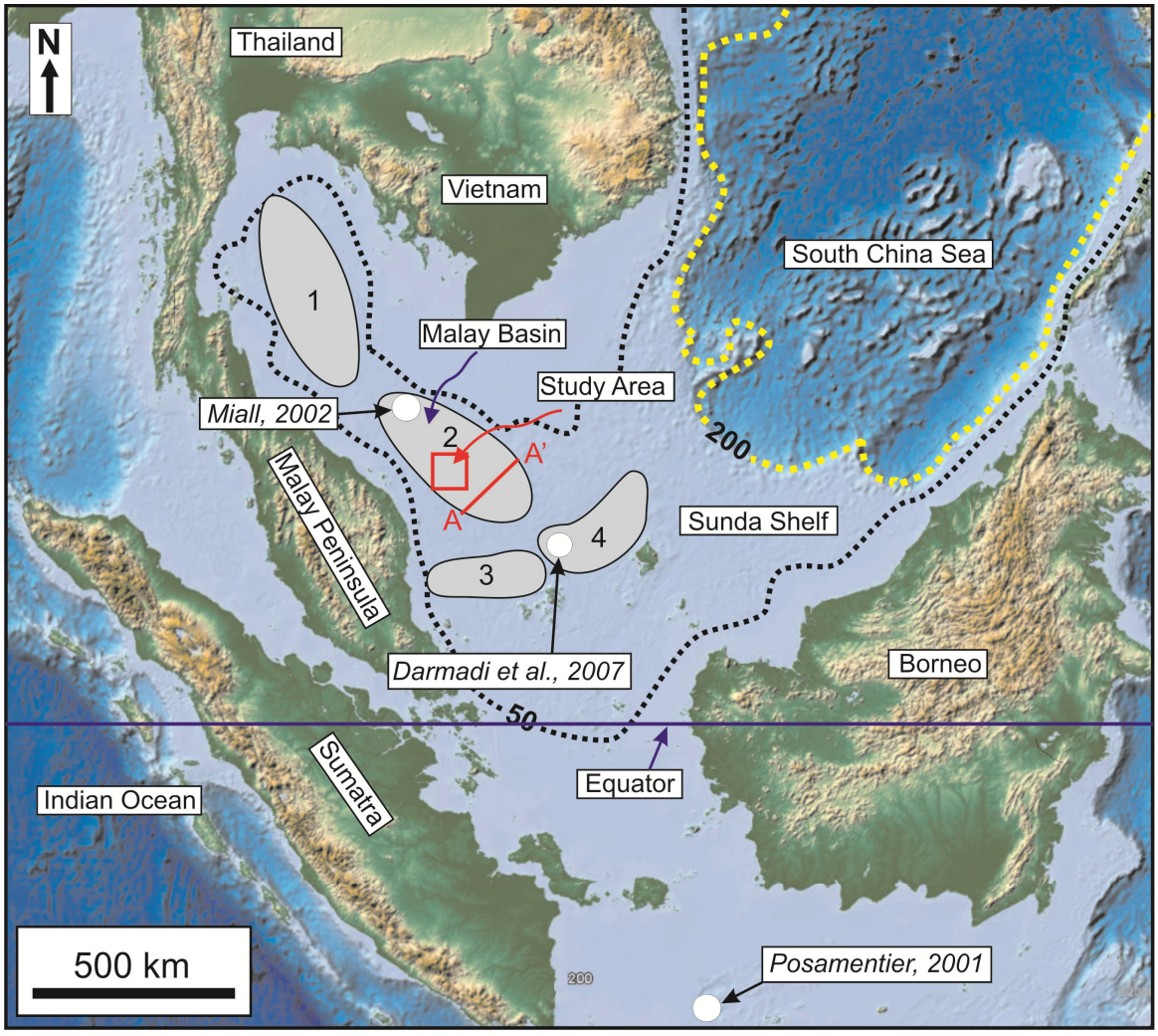

Figure 4.1: Location map of the study area within the Malay Basin (2) on the Sunda Shelf, Southeast Asia. The other basins are Pattani Basin (1), Penyu Basin (3), and West Natuna Basin (4). The yellow and black dashed-lines represent the present-day depth contours at 200 and 50 m, respectively. The water depth within the study area is mainly from 50 to 80 m. The red solid-line represents the regional cross-section shown in Figure 4.3. The blue solid-line represents the equator line. Locations of previous studies of Posamentier (2001), Miall (2002) and Darmadi et al. (2007) that were conducted on SE Asia are shown. Bathymetry data was obtained from National Geophysical Data Centre (NGDC) (http://www.ngdc.noaa.gov).

4.3.2 Physiographic and palaeoclimatic setting

The Sunda Shelf is one of the largest tropical shelf areas in the world (Hanebuth and Stattegger, 2003). It is situated at the south-western margin of the South China Sea, the

largest of the Southeast Asian marginal seas (Figure 4.1). The shelf is extremely broad (up to 800 km at its widest section) and has a very low gradient (< 0.1º). The Sunda Shelf was tectonically stable during the Pliocene and Pleistocene (Madon, 1998). The study area is located close to the Equator and near the "West Pacific Warm Pool"; this suggests that the climate during the Last Glacial Maximum (LGM) was similar to the present-day tropical climate of the Southeast Asia lowlands (Morley, 2000; Sun et al., 2000). However, monsoon-driven precipitation during the LGM was lower than during the Holocene, suggesting that vegetation patterns in lowland areas, such as the Sunda Shelf, were potentially affected by the dry winter-monsoon (Wang et al., 1999).

The present-day water depth within the study area ranges from 50 to 80 m and the average water depth across most of the Sunda Shelf is *ca*. 70 m. The shelf break occurs at *ca*. 180 to 220 m beneath the present-day sea-level. During the middle Pleistocene, the growth of continental glaciers decreased ocean volume and caused a maximum reduction in sea-level of *ca*. 160 m and *ca*. 120 m during the LGM (Gascoyne et al., 1979; Hopkins, 1982; Yang and Xie, 1984; Hanebuth et al., 2003; Hanebuth and Stattegger, 2003; Voris, 2000). Hence, most of the Sunda Shelf was subaerially exposed during the LGM, with the shoreline located close to the present-day shelf break (Hanebuth et al., 2003; Hanebuth and Stattegger, 2003; Voris, 2000). Consequently, the adjacent South China Sea was strongly reduced in size, forming a semi-enclosed marginal sea (Sathiamurthy and Voris, 2006).

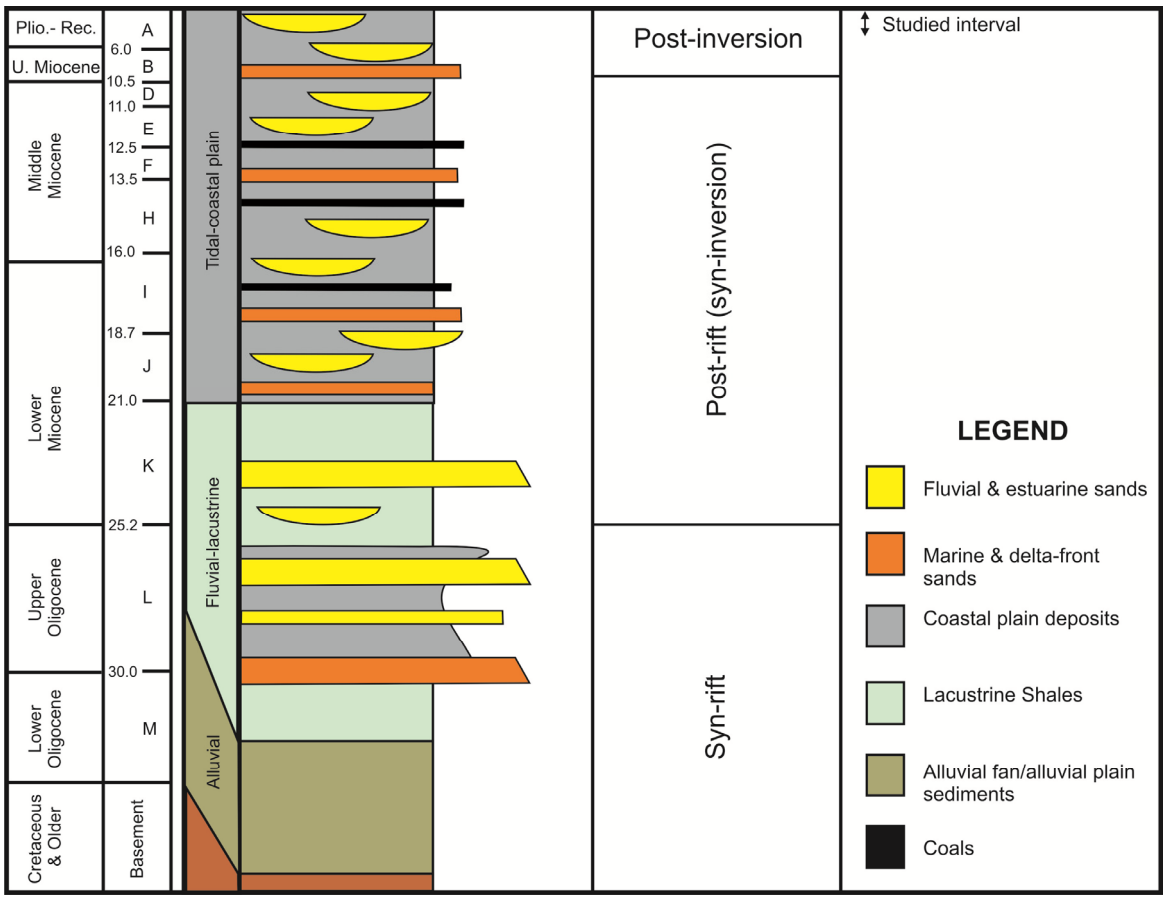

Figure 4.2: Generalised stratigraphic column of the Malay Basin. The second column contains the main regional stratigraphic intervals (labelled A-M) and their approximate ages (in Myr). The studied interval is the upper part of Group A succession which is mainly composed of coastal plain deposits (Modified from Madon, 1999d).

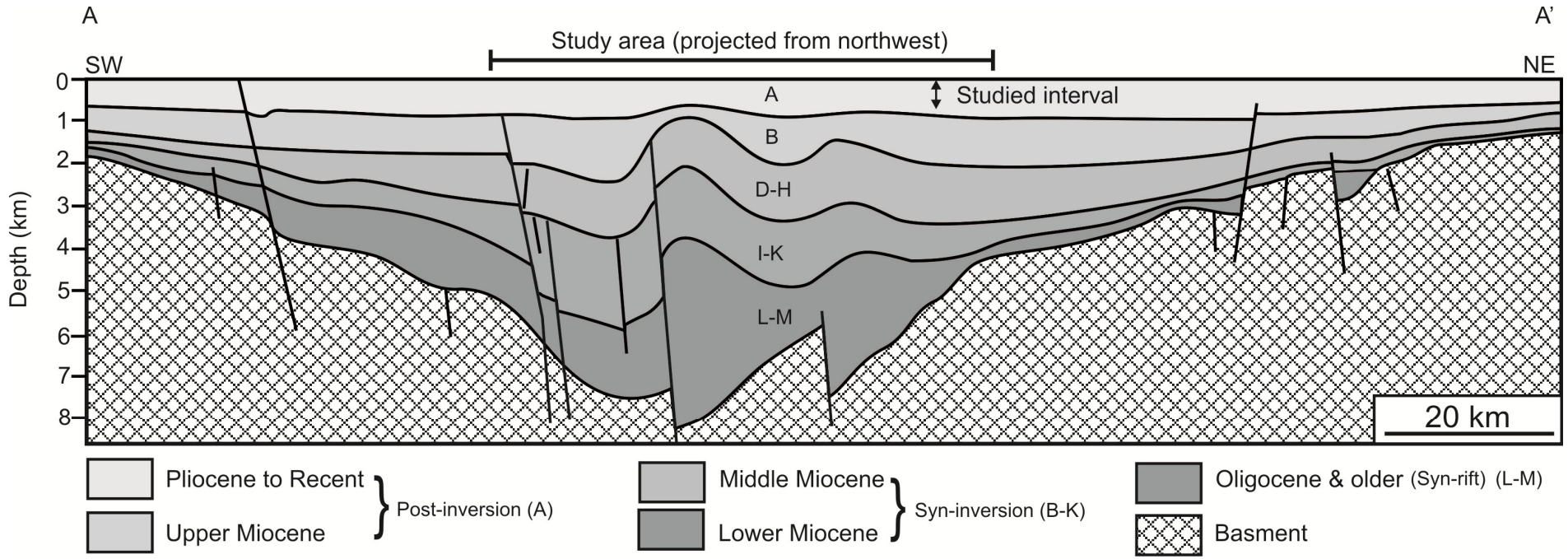

Figure 4.3: Regional cross-section of the Malay Basin. The main regional stratigraphic intervals are labelled A-M (Figure 4.2). Location of this cross-section is shown in Figure 4.1. The studied interval lies within the Upper post-inversion Pliocene to Recent (Modified from Madon, 1999d).

4.4 Data Sources and Methodology

The data utilised in this study consists of a 3D seismic reflection dataset with a total areal extent of *ca*. 11500 km^2 (*ca*. 115 km wide by *ca.* 100 km long; Figure 4.4). The seismic dataset comprises ten separate seismic surveys that have been merged into a single interpretable 3D volume. The dataset is zero-phase processed with SEG normal polarity, in which a positive (peak) event (black seismic reflection on seismic sections) represents a downward increase in acoustic impedance, and a negative (trough) event (white seismic reflection on seismic sections) represents a downward decrease in acoustic impedance (Brown, 2004). In-line and cross-line spacing within these surveys are 9.38 m and 12.5 m, respectively. The vertical record length is 600 milliseconds two-way time (ms twt). The vertical sampling interval for all surveys is 2 ms, except for one survey which has a sampling interval of 1 ms. The dominant seismic frequency ranges from 60-70 Hz. Unfortunately, only limited well data are available to calibrate the seismic data, as most wells within the area targeted the deeper, productive, Miocene succession. However, depth and thickness measurements were converted from the milliseconds two-way time (ms twt) to metres by using velocity information (i.e. check-shot data) from one reference well (Tunggal-1; Figure 4.4) which does contain these data. This well indicates that the average velocity of the shallow part of the basin fill is *ca*. 1880 m sec^{-1}. Based on the estimation of the frequency and velocity, the vertical resolution ranges from *ca.* 6.7 to 7.8 m and the lateral resolution ranges from *ca.* 11.5 to 15.5 m.

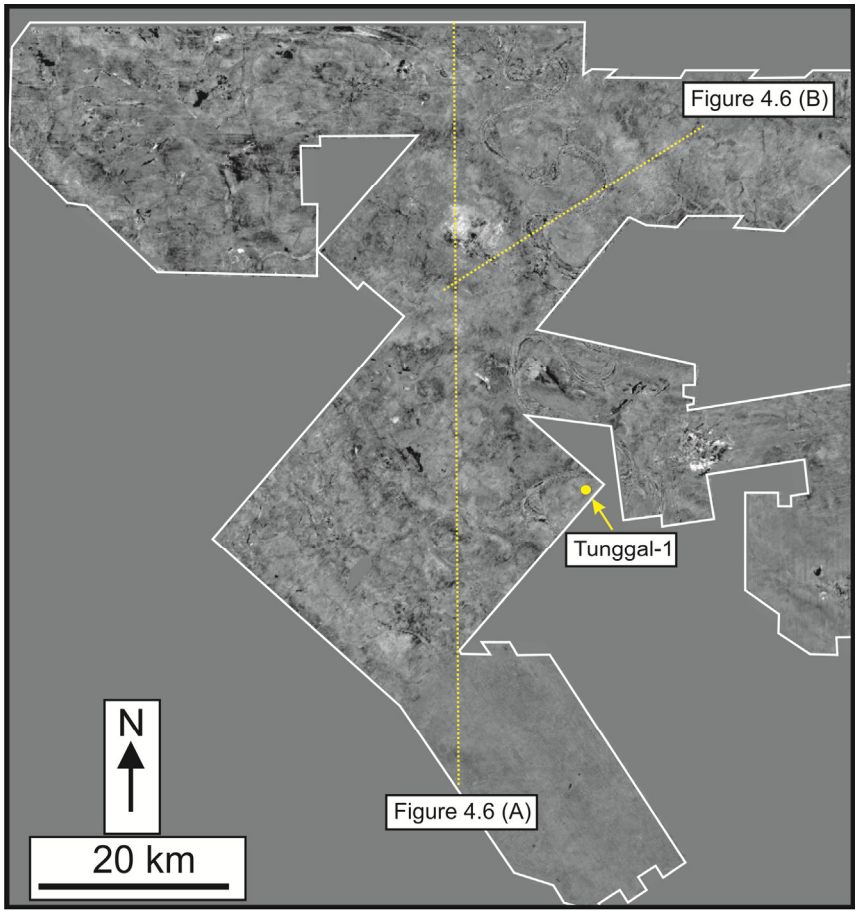

Figure 4.4: Base map of the study area based on a horizontal 'time' slice at 400 ms. The volume consists of ten surveys that have been merged to make a single interpretable volume. The yellow-circle represents the location of the well (Tunggal-1) that was used in the time-depth conversion. The yellow-dashed lines illustrate the locations of the seismic sections shown on Figures 4.6.

The general quality of the seismic data within the studied interval is generally excellent, although exact amplitude values vary between different surveys due to variations in the acquisition and processing parameters. Fortunately, this does not unduly hamper the overall imaging and mapping of fluvial systems. There are also marked 'acquisition footprints' in the upper parts of several of the individual datasets within the merged survey. These appear as amplitude stripes on horizontal 'time' slices and as small breaks or discontinuities along reflection events in seismic cross-sections. Finally, some of the individual surveys within the mega-merge survey have not been optimally merged as

observed by minor (< 4 ms) vertical offset of reflection events. Fortunately, most of these minor issues can be overcome by using a combination of map-view and cross-section images, thereby ensuring that only true geological features were interpreted.

Interpretation of depositional features and geomorphological patterns has been achieved by the use of a combination of horizontal 'time' slices and 'iso-proportional' slices (*sensu* Zeng et al., 1998; Brown, 2004; Posamentier et al., 2007). Time slices are seismic slices that are taken horizontally through the original reflectivity 3D seismic volume whereas iso-proportional slices are obtained by slicing between two parallel or non-parallel, horizontal or dipping reflection events (see Zeng et al., 1998; Brown, 2004; Posamentier et al., 2007; Figure 4.5A). Horizontal 'time' slices are only useful when the geological features of interest and the stratigraphic timelines along which they are developed are horizontal to sub-horizontal; this only occurs in the upper part of the studied succession (Figure 4.5A). In the middle and lower part of the studied interval where the seismic reflections are not horizontal (due to post-depositional deformation), iso-proportional slices have been utilised (Figure 4.5A).

Ten interpretive maps were constructed that illustrated the range of fluvial channels styles at various stratigraphic levels within the dataset. Each map is composed of observations from a succession of time and/or iso-proportional slices taken from either the lower half or the upper half of each mapped seismic unit; hence each map illustrates the type of channels that are observed in either the base or the top part of each unit (Figure 4.5B). It should be noted that the number of channels shown on these maps at any one stratigraphic level should be considered a 'minimum'; this reflects a lack of or only partial imaging of channels which are at or below seismic resolution, and high 'fragmentation' of channels due to incision by younger channels. Mapping and interpretation of the stratigraphic occurrence of channels is challenging as channels commonly incise downwards from a

variety of stratigraphic levels and are superimposed on individual seismic slices. Finally, seismic 'multiples' from shallower channels may mask channels imaged at lower stratigraphic levels.

4.5 Seismic Stratigraphic Analysis

4.5.1 Stratigraphic Framework

Based on seismic facies analysis and reflection continuity, the Pleistocene to Recent succession has been divided into four seismic units (Units 1-4; Table 4.1; Figure 4.6). The horizons bounding these units have been mapped throughout the study area (Horizons A-E; Figure 4.6). Two additional horizons, Horizons C.1 and D.1, have been mapped within the upper part of Unit 3 and Unit 4, respectively, to allow further sub-division of these units into two sub-units (i.e. sub-units 3.1, 3.2, 4.1 and 4.2; see Table 4.1 and Figure 4.6). Horizons C.1 and D.1 are both strongly erosive. Figure 4.6C is a schematic stratigraphic cross-section which illustrates the stratigraphic template and nomenclature used, and the vertical variability of fluvial channels within this framework.

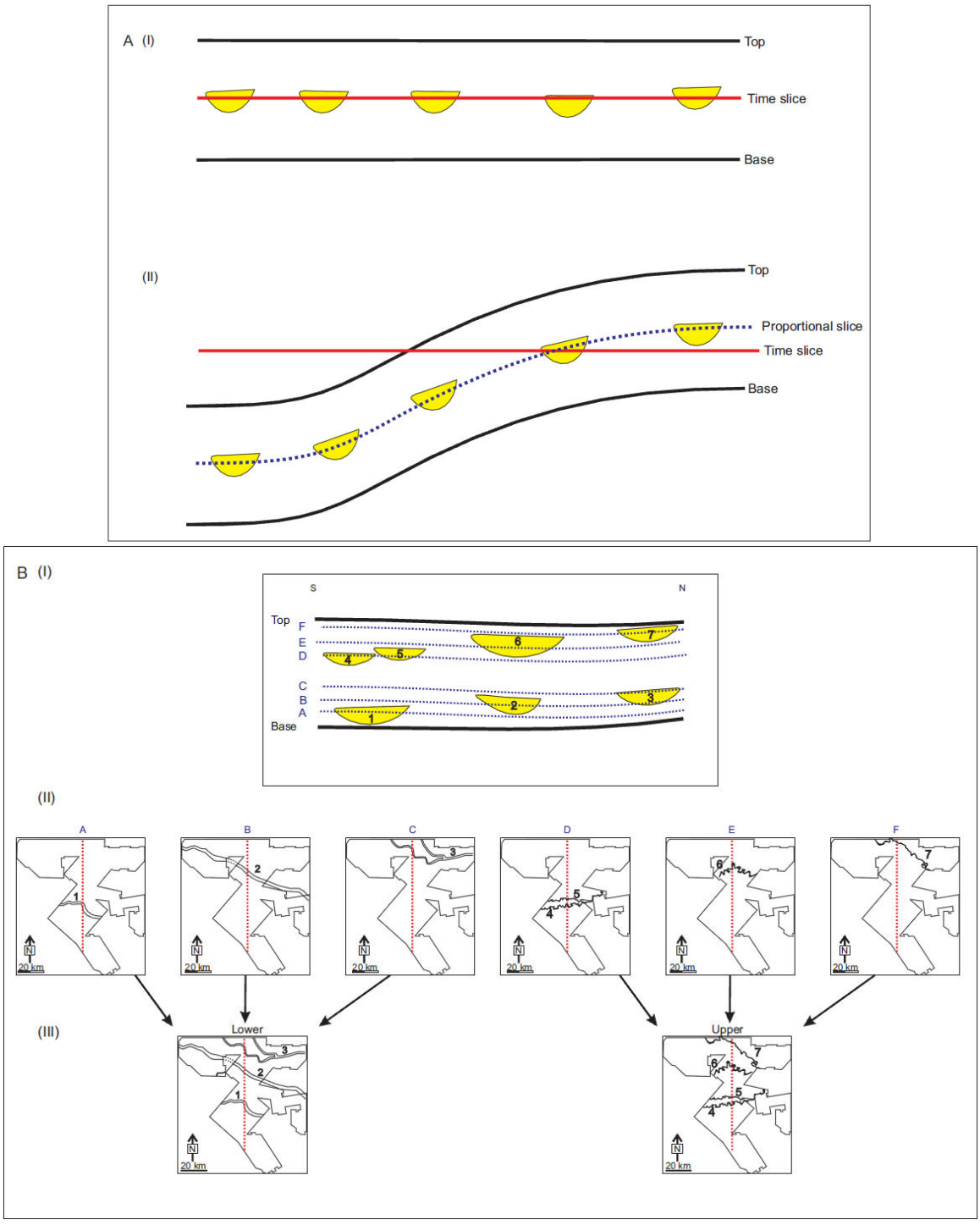

Figure 4.5: A) shows the differences between the horizontal 'time' slice (I) and iso-propositional slices (II). Time slices are horizontal slices that are taken through the original reflectivity 3D seismic volume (I) where the iso-proportional slices are obtained by slicing between two non-parallel reflections (II); **B)** shows the methodology used in creating the interpretive planview maps presented in this study. These maps are composed of successive iso-proportional slices. (I) a schematic cross-section through the study area showing an individual unit and range of channels (1-7) that are bounded by the top and base of the unit. The blue dashed-lines (A-F) represent the iso-proportional slices that have been generated at different stratigraphic level .The 2D horizontal map-views of these slices are shown in (II). These horizontal map-views are then combined to make two interpretive planview maps that represent the type of the channels that are observed within the lower half and upper half of the unit.

Table 4.1: lists the seismic units and sub-units which are identified within the Pleistocene to Recent succession within the Malay Basin. The basic information data including isochron range and average, channel width (*CW*), channel depth (*CD*) and sinuosity (*SI*) of the channel systems that have been observed in the lower and upper parts of each unit are illustrated.

Unit No.	Base horizon	Top horizon	Thickness range (ms twt)	Average thickness (ms twt)	(m)	Channel parameters Strat. Level	*CW* (m)	*CD* (m)	*SI*	Incised valley parameters width (m)	depth (m)	*SI*	Interpretive Planview Map
4.2	D.1	E	82-192	110	104	confined	600	25	3	13000-18000	55-78	1.1	Figure 4.13 A
						unconfined	320-600	15-32	1.1.15	---------	---------	-------	
4.1	D	D.1	108-228	120	112	'U'	75-220	8-20	1.3-1.5	---------	---------	-------	Figure 4.12 B
						'L'	300-1300	15-30	1-1.3	---------	---------	-------	Figure 4.12 A
3.2	C.1	D	228-290	6	58	confined	150-250	12-25	2.5-3	3500-6500	35-60	1.1	Figure 4.11
						unconfined	450-715	18-30	1-1.2	---------	---------	-------	
3.1	C	C.1	250-330	80	75	'U'	75-212	8-23	1.5-2.5	---------	---------	-------	Figure 4.10 B
						'L'	350-1100	15-32	1-1.17	---------	---------	-------	Figure 4.10 A
2	B	C	330-420	90	85	'U'	75-250	10-23	1.4-2.3	---------	---------	-------	Figure 4.9 B
						'L'	580-3000	30-50	1-1.25	---------	---------	-------	Figure 4.9 A
1	A	B	420-575	155	145	'U'	75-200	8-18	1.6-2.7	---------	---------	-------	Figure 4.8 B
						'L'	450-2100	22-30	1-1.2	---------	---------	-------	Figure 4.8 A

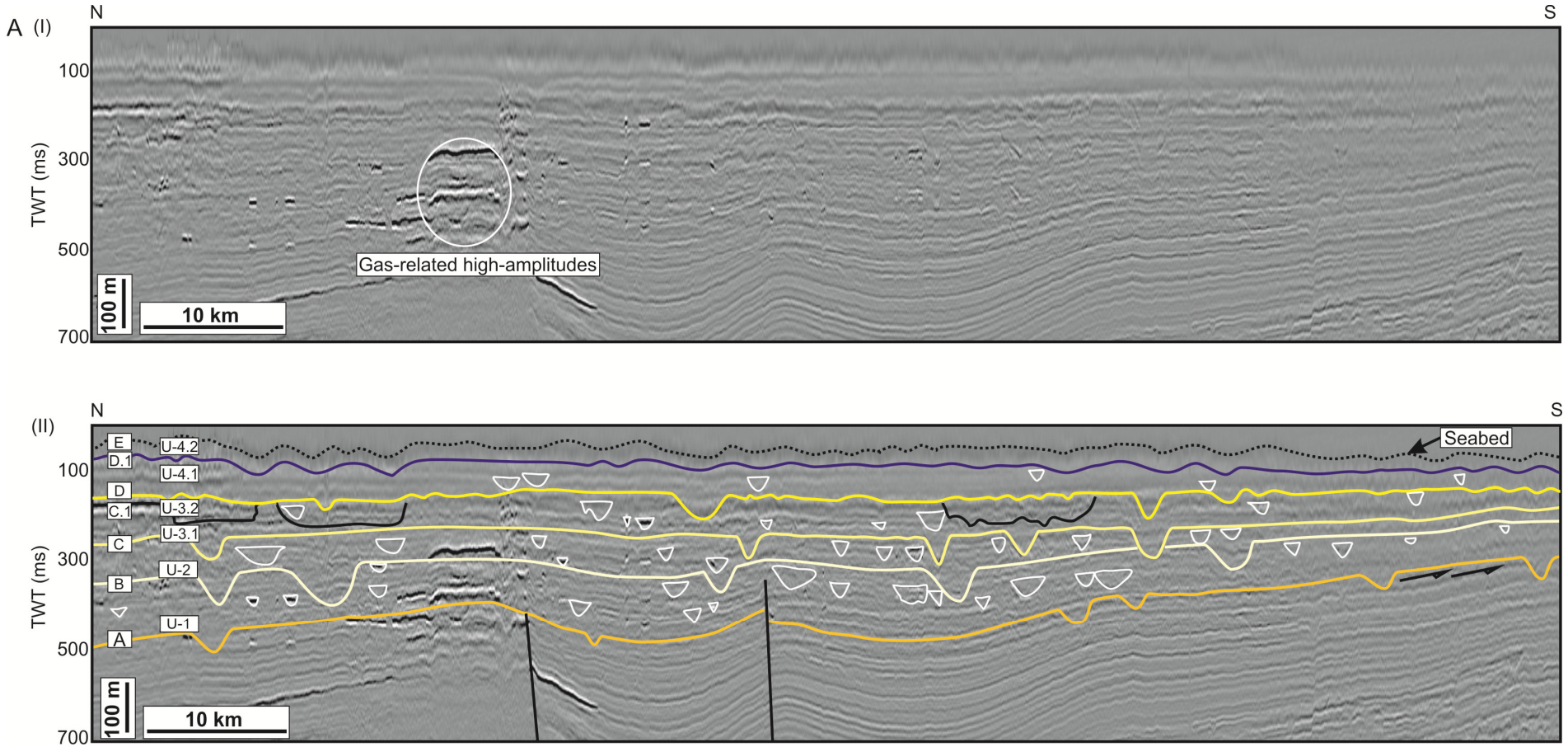
A (I)
N
S
100
300
500
700
TWT (ms)
Gas-related high-amplitudes
100 m
10 km
(II)
N
S
Seabed
E
D.1
D
C.1
C
B
A
U-4.2
U-4.1
U-3.2
U-3.1
U-2
U-1
100
300
500
700
TWT (ms)
100 m
10 km

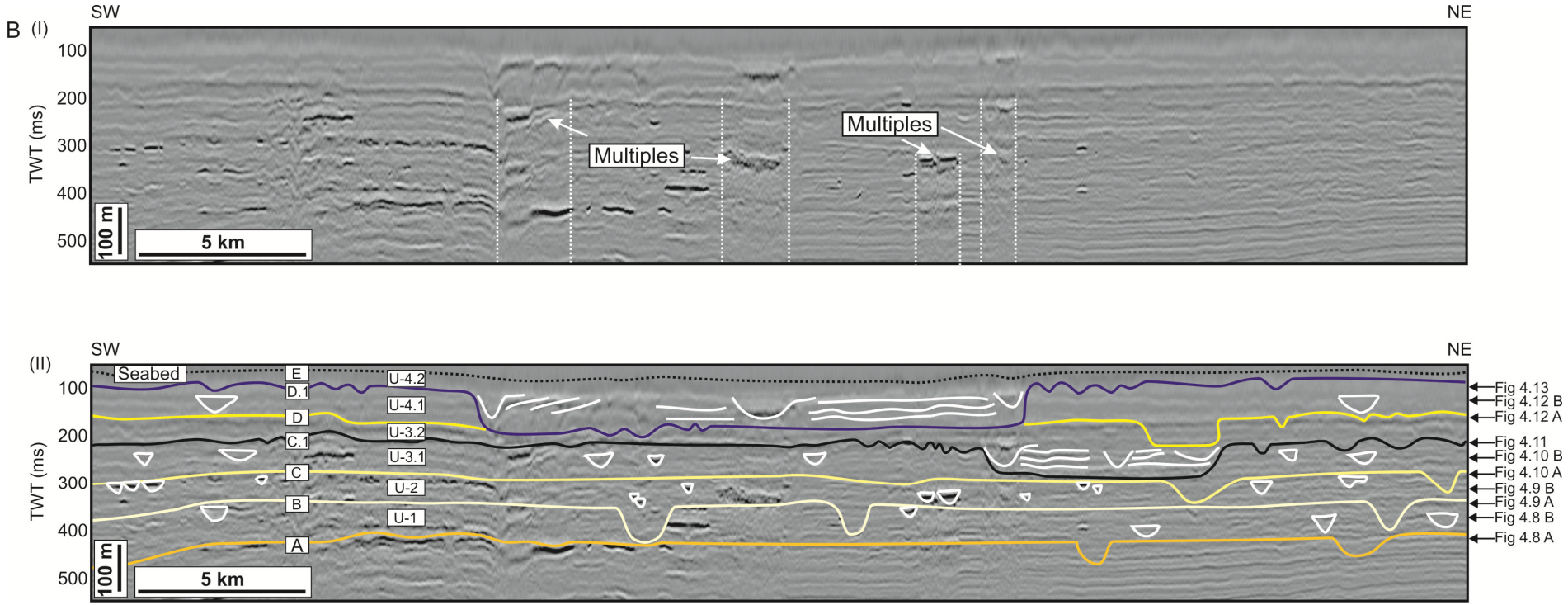
B (I)
SW
NE
100
200
300
400
500
TWT (ms)
Multiples
Multiples
100 m
5 km
(II)
SW
NE
Seabed
E
D.1
D
C.1
C
B
A
U-4.2
U-4.1
U-3.2
U-3.1
U-2
U-1
100 m
5 km
Fig 4.13
Fig 4.12 B
Fig 4.12 A
Fig 4.11
Fig 4.10 B
Fig 4.10 A
Fig 4.9 B
Fig 4.9 A
Fig 4.8 B
Fig 4.8 A

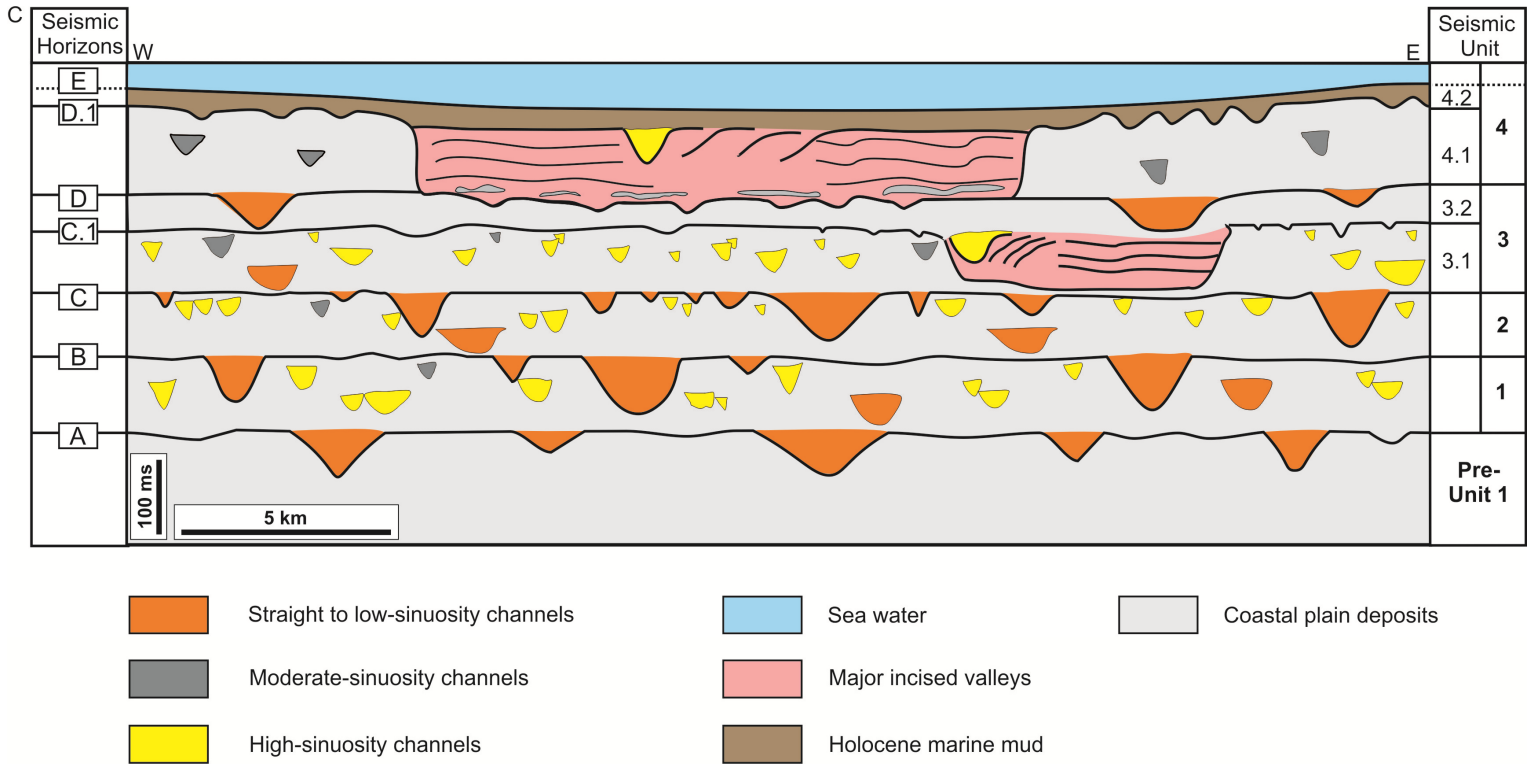

Figure 4.6: A) (I) Un-interpreted and (II) interpreted regional seismic section through the 3D seismic dataset illustrating the seismic units (1-4) and the bounding surfaces (Horizons A-E). Major channel systems are also shown as white 'u' or 'v' shapes. The main bounding surfaces (Horizon A-D) are characterised by prominent incisions. Note the angular discordance between Horizon A and underlying unit at the basin margin (right side of cross-section). Location of this section is shown in Figure 4.4; **B)** Un-interpreted (I) and interpreted (II) seismic section showing the seismic units (1-4) and the bounding surfaces (Horizon A-E). Two additional horizons (Horizon C.1 and D.1) have been picked to show deep and wide incision features. These two horizons divide Unit 3 and 4 into sub-units. Major channel systems are also shown. Note the seismic expression within these deep incisions is different from those adjacent strata. Interpretive planview maps of horizontal 'time' and iso-proportional slices (Figure 4.8-4.13) used in this study are shown on the right-hand side of this seismic section as figure numbers. Location of this section is shown in Figure 4.4; **C)** A schematic cross section through the Pleistocene to Recent succession within the Malay Basin showing the seismic units (1-4) and the sub-units 3.1, 3.2, 4.1, and 4.1, the bounding surfaces (A-E) and the channel types observed within each unit. Note the systematic vertical changes in channel patterns and scale in each individual unit.

4.5.2 Seismic Characteristic of the Channel Systems

A wide range of fluvial channel styles and morphologies have been observed at multiple stratigraphic levels within the Pleistocene succession. In cross-section, these channels are characterised by different seismic expressions and six main types have been identified (Table 4.2; Figure 4.7): 1) *Type-1:* characterised by a V-shaped channel morphology, 24-38 ms twt (22-35 m) deep, infilled with variable amplitude, laterally-continuous seismic reflections (Figure 4.7A & B); 2) *Type-2:* characterised by a V-shaped channel morphology, 16-32 ms twt (15-30 m) deep, infilled with low amplitude, laterally-discontinuous (chaotic) seismic reflections (Figure 4.7C); 3) *Type-3:* characterised by a U-shaped channel morphology, 32-54 ms twt (30-50 m) deep, infilled with variable amplitude, laterally-continuous seismic reflections (Figure 4.7D); 4); *Type-4:* characterised by a narrow, shallow (13-22 ms twt (12-20 m) deep), u-shaped channel morphology, with a clear erosional base but too shallow to have a discernable seismic facies infill (Figure 4.7E); and 5) *Type-5:* characterised by a laterally discontinuous, high-amplitude 'doublet' that is significantly higher than the encasing seismic reflection event; this type of channel lacks an erosional base and is too shallow (8-13 ms twt (6-12 m) deep) to have a discernable seismic facies infill (Figure 4.7F); 6) *Type-6:* characterised by a very broad and very deep (38-80 ms twt (35-78 m)), u- or v-shaped channel morphology, infilled with wide range of seismic facies, including chaotic seismic facies overlain by laterally-continuous facies, horizontal or dipping, variable amplitude reflections (Figure 4.6B).

Table 4.2: illustrate the types of the channel morphologies observed within the Pleistocene to Recent succession. The description and the morphometric parameters including channel width (*CW*), channel depth (*CD*) and sinuosity (*SI*) of these types of channel systems are described.

Channel Type	Seismic facies description	Comments	Morphometric parameters				Examples
			CW (m)	*CD* (ms twt)	*CD* (m)	*SI*	
Type-1	v-shaped, infilled with variable-amplitude, laterally-continuous seismic reflections	common in association with large, low-sinuosity channels	450-1500	24-38	22-35	1-1.3	Figure 4.7 A & B
Type-2	v-shaped, infilled with low-amplitude, chaotic seismic reflections	common in association with large, highly sinuous channels	300-600	16-32	15-30	2.5-3.5	Figure 4.7 C
Type-3	u-shaped, infilled with variable-amplitude, laterally-continuous seismic reflections	common in association with major low-sinuosity channels	1500-3000	32-54	30-50	1-1.12	Figure 4.7 D
Type-4	Narrow, shallow, u-shaped, with a clear erosional base and sub-seismic infill	common in association with medium-scale, high-sinuosity channels	150-300	13-22	12-20	2-3	Figure 4.7 E
Type-5	Laterally discontinuous, high-amplitude, seismic reflection 'doublet' lacking on erosional base and with a sub-seismic infill	very common in association with moderate-sinuosity channels and narrow, highly-sinuosity channels	75-200	8-13	6-12	1.5-2	Figure 4.7 F
Type-6	Broad, deep and u-shaped, filled with a wide range of seismic facies	commonly associated with incised valleys and association channel fills	3500-13000	38-80	35-78	1.1-1.2	Figure 4.6 B

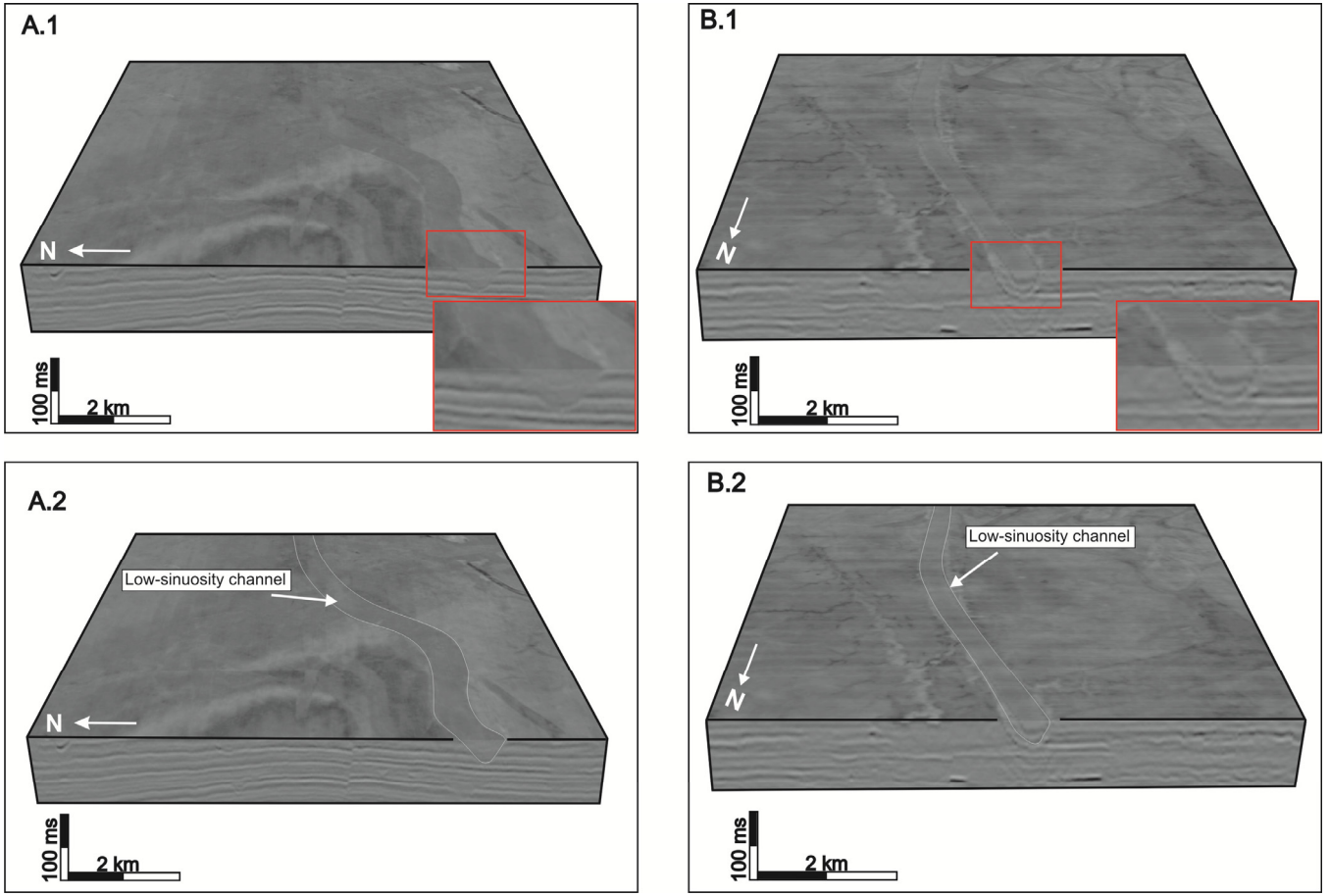
A.1
N
100 ms
2 km
B.1
N
100 ms
2 km
A.2
Low-sinuosity channel
N
100 ms
2 km
B.2
Low-sinuosity channel
N
100 ms
2 km

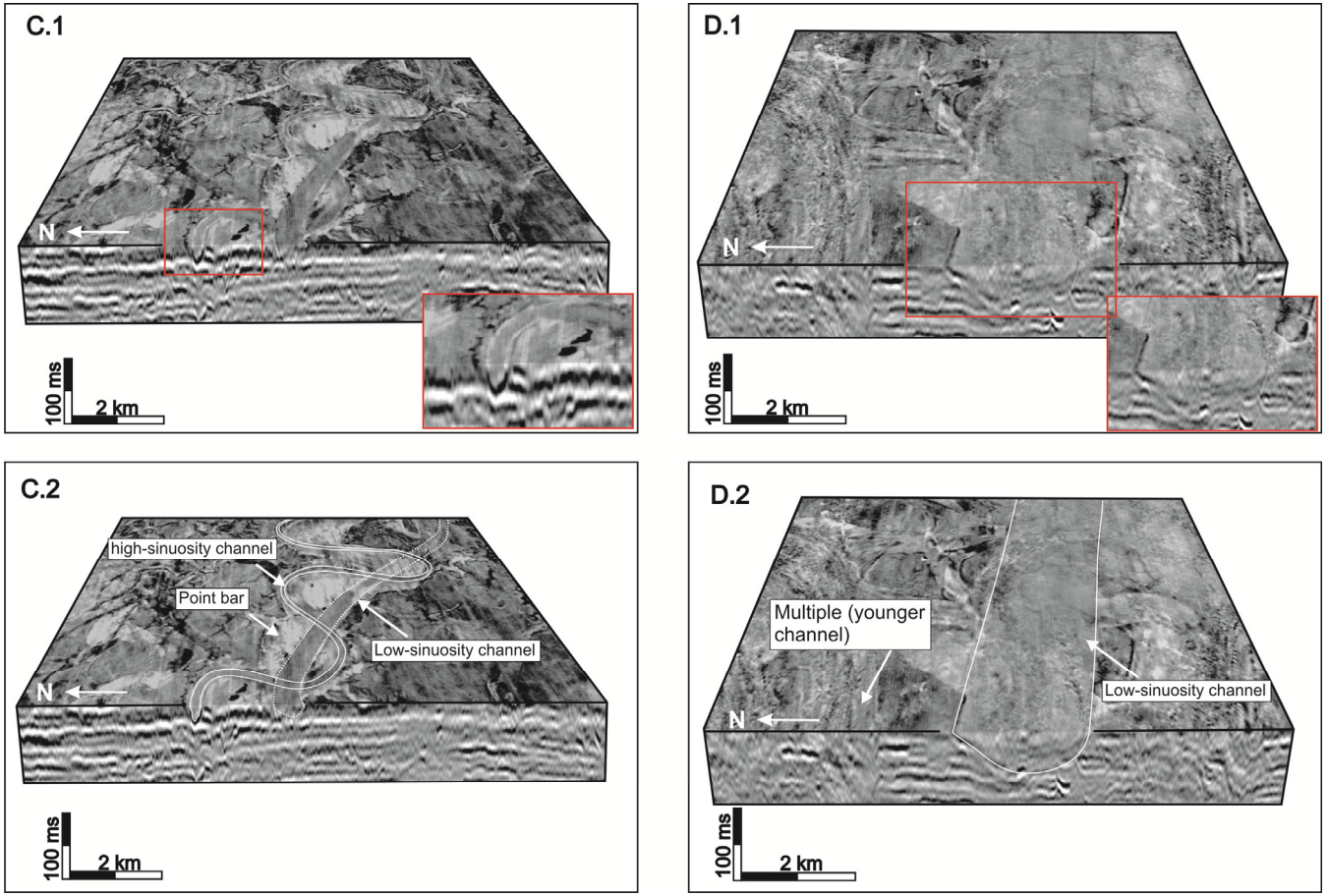
C.1
N
100 ms
2 km
D.1
N
100 ms
2 km
C.2
high-sinuosity channel
Point bar
Low-sinuosity channel
N
100 ms
2 km
D.2
Multiple (younger channel)
Low-sinuosity channel
N
100 ms
2 km

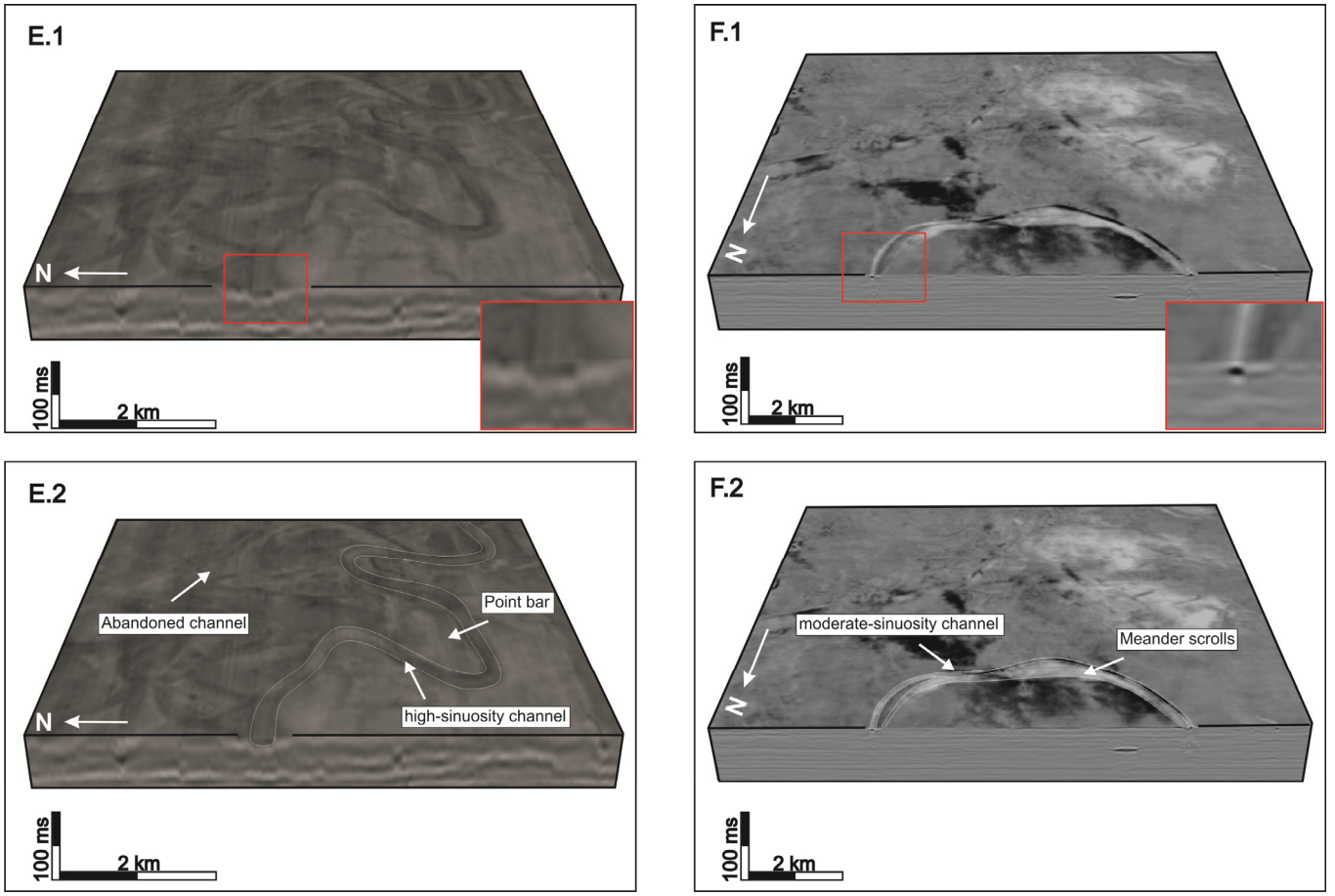

Figure 4.7: 3D seismic cubes showing the horizontal and vertical seismic expression of different types of channels. Six main types of channel morphologies have been recognised: 1) *Type-1:* V-shaped channel morphology, infilled with variable amplitude, laterally-continuous seismic reflections (low-amplitude **(A)** and high-amplitude **(B)**); 2) *Type-2:* V-shaped channel morphology infilled with low amplitude, laterally-discontinuous (chaotic) seismic reflections **(C)**; *Type-3:* U-shaped channel morphology, infilled with variable amplitude, laterally-continuous seismic reflections **(D)**; 3); *Type-4:* Narrow and shallow, u-shaped channel morphology with clear erosional base but with sub-seismic infill **(E)**; *Type-5:* Laterally discontinuous, high-amplitude 'doublet' that is significantly higher than the encasing seismic reflection event but which lacks erosional base and sub-seismic infill **(F)**; and 6) *Type-6:* very broad and very deep u-shaped channel morphology infilled with wide range of seismic facieses including chaotic seismic facies overlain by laterally-continuous facies and *Type-2* channel morphologies along with dipping surfaces (see Figure 4.6 B). Locations of these 3D cubes are shown on Figures 4.8-4.13.

These types of channel morphologies are associated with different channel styles. In more detail, *Type-1* and *Type-3* channel morphologies are commonly associated with straight to low-sinuosity channels; however, wide, straight to low-sinuosity channels are associated with *Type-3* channel morphologies. *Type-2* channel morphologies are commonly associated with large, highly-sinuous channels, especially those confined within incised valleys. *Type-4* channel morphologies are very common in association with medium-scale, highly-sinuous channels, whereas *Type-5* channel morphologies are very common in association with small-scale channels which are characterised by high and moderate sinuosities. In planview, these channels are usually associated with accretion surfaces; however, these accretion surfaces are extremely subtle in vertical seismic sections. *Type-6* channel morphologies, with variable seismic expressions, are limited to the fills of large incised valleys developed in the upper part of the studied interval. Within this type, a wide range of seismic expression including chaotic, laterally-continuous seismic facies, and *Type-2* channel morphologies which is associated with the large highly-sinuous channels are observed.

4.5.3 Evaluation of the Depositional Sequences

As described above, four seismic units have been identified within the Pleistocene to Recent succession. The vertical and lateral distribution of the channel types illustrated above is described in the following sections, and interpreted in terms of the key controls on channel evolution outlined in the Introduction.

4.5.3.1 Unit 1

Description: The base of Unit 1 is defined by Horizon A, which is a high-amplitude, laterally-continuous seismic reflection. Moderate relief is observed along Horizon A due to tectonically-driven, inversion-related uplift across two structural highs located in the middle of the study area (Figure 4.6A). Horizon A is mainly characterised by *Type-1* channels, which are up to 38 ms twt (35 m) deep and up 2.5 km wide (Figures 4.6 and 4.7A). Channels in the lower part have a low sinuosity index (SI=1.05 to 1.18) and are mainly orientated WSW-ESE (Figure 4.8A). Although, *Type-1* channels are the dominant channel types in Unit 1, large (up to 2.5 km wide), *Type-3* channels have been observed that are associated with smaller (0.5-1 km wide by 25-30 ms twt (20-25 m) deep), low-sinuosity (SI=1.15) tributaries. Two larger *Type 3* channels (widths of up to 3 km and with sinuosities of 1.05) are located in the north-eastern part of the study area and are oriented NW-SE.

Within Unit 1, channels vary in size and sinuosity. The upper part of Unit 1 is characterised by highly-sinuous channels (SI >2; Figure 4.8B). The largest highly-sinuous channels are 250 to 300 m wide, with meander belt width of 6-9 km with radius of curvature of 1-1.8 km and are associated with well-developed scrolls (Figure 4.8B). These channels are characterised by *Type-2* and *Type-4* morphologies (Figure 4.5; see also examples from Figure 4.7C & E). Towards the top of this unit and the base of next unit (Horizon B), channels become smaller and less sinuous. Several smaller moderate-sinuosity channels (SI=1.3-1.5) are recognised. These channels range from 75-160 m wide with meander belts of < 1 km wide.

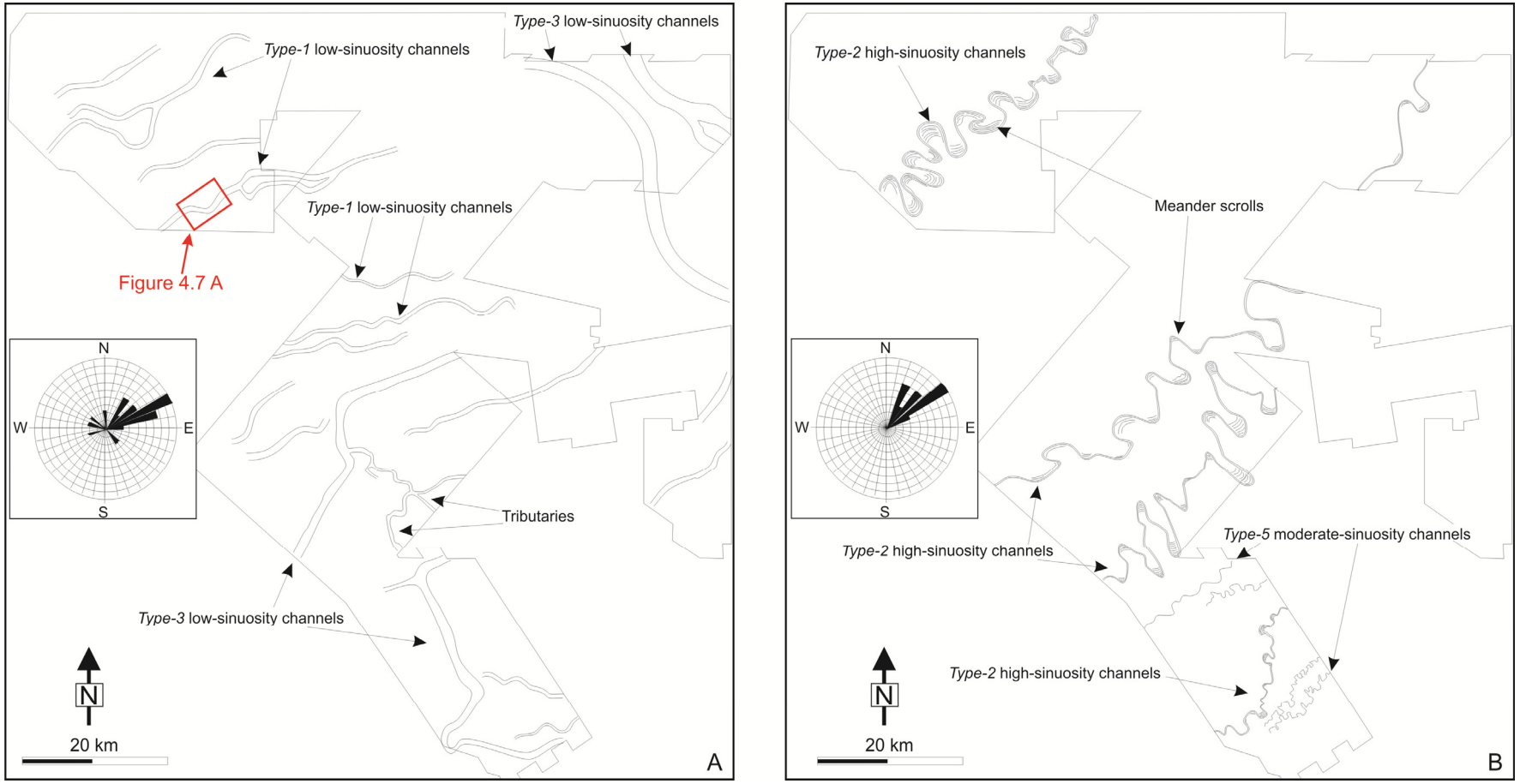

Figure 4.8: Two interpretive planview maps within Unit 1; **A)** shows the type of channels observed within the lower part of Unit 1 which is dominated by wide, straight to very low-sinuosity channels. These channels were flowing from the high elevated areas towards the axial zone of the basin. Location of Figure 4.7A is also shown; **B)** shows the type of channels observed within the upper part of Unit 1 which is dominated by highly sinuous channels with well-developed scroll bars. Channel orientations are represented as a rose diagram for each part of Unit 1.

Interpretation: Correlation of Horizon A with other areas suggests that this horizon marks the base of the Pleistocene succession within the Malay Basin. The presence of the truncated reflections at the base of the Unit 1 along the SW margin of the study area is interpreted to reflect tectonically-induced tilting of the basin (Figure 4.5A). Furthermore, prominent fluvial incisions and the presence of low-sinuosity channels at the base of this unit indicate fluvial erosion and suggest that this horizon is a sequence boundary that was formed during a relative sea-level lowstand. The chaotic seismic facies within Unit 1 reflects the variable nature of coastal plain deposits, including laterally-discontinuous fluvial channel sandstone bodies. In contrast, the relatively high-amplitude and laterally-continuous seismic facies of the underlying deposits suggests much less lithological variability. In the context of the Malay Basin, the latter seismic response is typical of shallow marine depositional systems (e.g. Ghosh et al, 2010).

In detail, the straight and low-sinuosity channels in the lower part of Unit 1 were broadly flowing eastwards from the high elevated areas in the west and south towards the axial zone of the basin in the east (Figure 4.8A). These rivers may have drained into a larger fluvial system in the axial zone of the basin (e.g. NE corner of Figure 4.8A). Unfortunately, this interpretation cannot be tested as seismic data quality in the middle part of the study area is poor due to the presence of anomalously high-amplitude zones interpreted to be related to the presence of hydrocarbons trapped within the structural highs. Based on the lack of smaller dentritic tributaries, channels in the lower part of Unit 1 may form part of a 'lowstand alluvial bypass system' (*sensu* Posamentier, 2001), formed during relative sea-level fall. Such systems have been documented on the Java Sea Shelf and are interpreted to form when the magnitude of relative sea-level fall is not great enough to expose wider parts of the previously-flooded continental shelf (e.g. the Sunda Shelf). The large rivers (> 2.5 km wide) in the middle of the study area were

elongated, possibly due to an overall increase in discharge from the smaller tributary channels. These fluvial rivers would have been filled when the sea-level started to rise slowly during the late lowstand.

In contrast to the relatively straight channels within the lower part of Unit 1, channels in the upper part of Unit 1 are dominated by highly-sinuous, meandering channel forms which are associated with point bar deposits (Figure 4.8B). Based on sequence-stratigraphic concepts, these meandering channels may be interpreted as having formed during sea-level rise after the preceding sea-level fall (Shanley and McCabe, 1994).

4.5.3.2 Unit 2

Description: The base of Unit 2 is defined by Horizon B which is a high-amplitude, laterally-continuous reflection (Figure 4.6). Unit 2 is characterised by laterally-discontinuous (chaotic) seismic facies. In cross-section, Horizon B is characterised by prominent incisions which are 16-48 ms twt (15-45 m) deep and 0.5-3 km wide; these are associated with *Type-1* and *Type-3* channel morphologies (Figures 4.6, 4.7A & D). Channels in the lower part of Unit 2 are straight and have a low sinuosity index (SI=1.03 to 1.15; Figure 4.9A). The largest channels are associated with smaller tributaries and are oriented NW-SE whereas the smaller ones are oriented SW-NE. These tributaries are characterised by *Type-1* channel morphologies and have a low sinuosity index (SI=1.10), with channels up to 32 ms twt (30 m) deep and 800 m wide with no dendritic patterns being observed.

Within the upper part of Unit 2, a wide range of channel sizes and styles are observed, ranging from low- to high-sinuosity channels (Figure 4.9B). A large (27 ms twt (25 m) by

1 km wide), NE-SW-trending, low-sinuosity (SI=1.25) *Type-1* channel is observed in the north-western part of the study area (e.g. Figure 4.7C). In addition, three E-W-trending, high-sinuosity (SI up to 2) *Type-2* channels, which are up to 20 ms twt (18 m) deep and up to 370 m wide are observed. These systems have meander belt widths of up to 6 km, with a radius of curvature of 2 km, and have very well-devolved scrolls (e.g. Figure 4.7C). Finally, seven W-E oriented, moderately-sinuous, *Type-4* channels, <15 ms twt (13 m) deep and <100 m wide, and with meander belt widths of <3.5 km are developed; these too have very high-amplitude scrolls (Figure 4.7F).

Interpretation: In a similar manner to Unit 1, the discontinuous nature of the seismic facies within Unit 2 is interpreted to reflect the variable nature of coastal plain deposits; this includes laterally-discontinuous fluvial channel sandstone bodies as evidenced by the clear fluvial morphologies observed in map-view. The prominent incisions observed along Horizon B at the base of Unit 2 are interpreted as being related to fluvial erosion; given that underlying meandering systems at the top of the Unit 1 were interpreted to have been deposited during sea-level rise and/or highstand, Horizon B may represent a sequence boundary formed during a subsequent period of relative sea-level fall.

In detail, the larger, straight, low-sinuosity channels which lack dentritic tributaries may represent lowstand alluvial bypass channel systems (*sensu* Posamentier, 2001) which flowed south-eastwards from the elevated areas along the western basin margin towards the ultimate depositional basin located in the South China Sea in the east. The large-scale geometric characteristics (e.g. scale, sinuosity, etc) of these river systems may be similar to those of Brahmaputra River, India (Figure 4.9D); however, based on limited vertical seismic resolution, it is not possible to identify smaller, in-channel depositional elements such mid-channel bars within the low-sinuosity channels within the lower part of Unit 2.

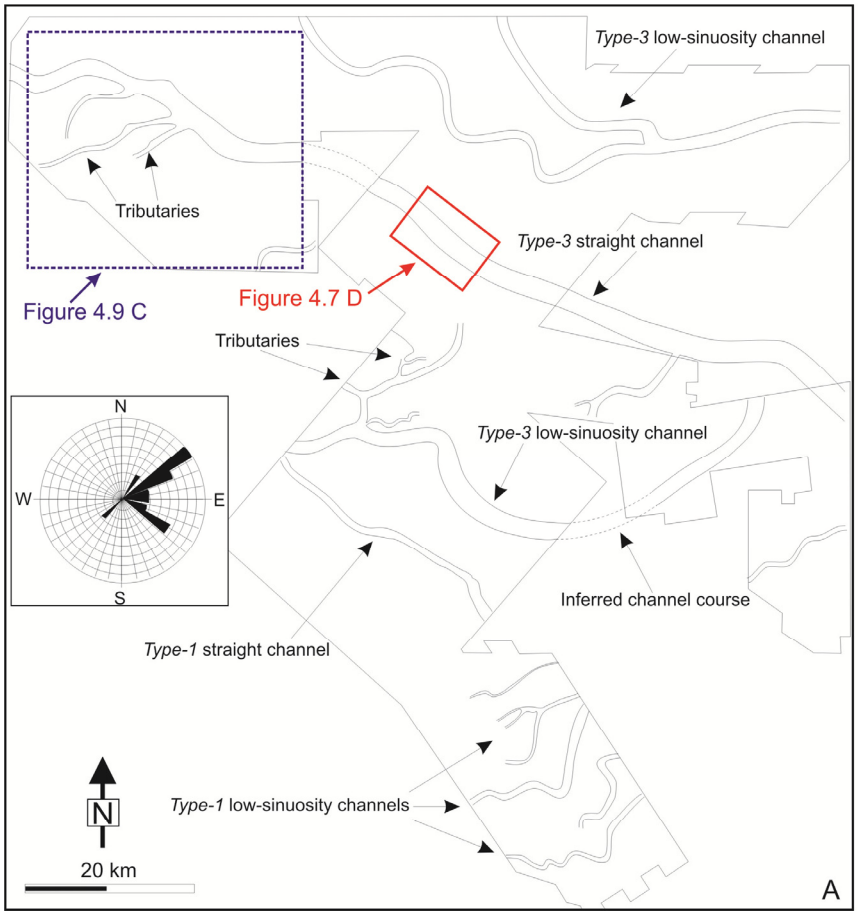
Type-3 low-sinuosity channel
Tributaries
Figure 4.9 C
Figure 4.7 D
Type-3 straight channel
Tributaries
N
W
E
S
Type-3 low-sinuosity channel
Inferred channel course
Type-1 straight channel
N
Type-1 low-sinuosity channels
20 km
A

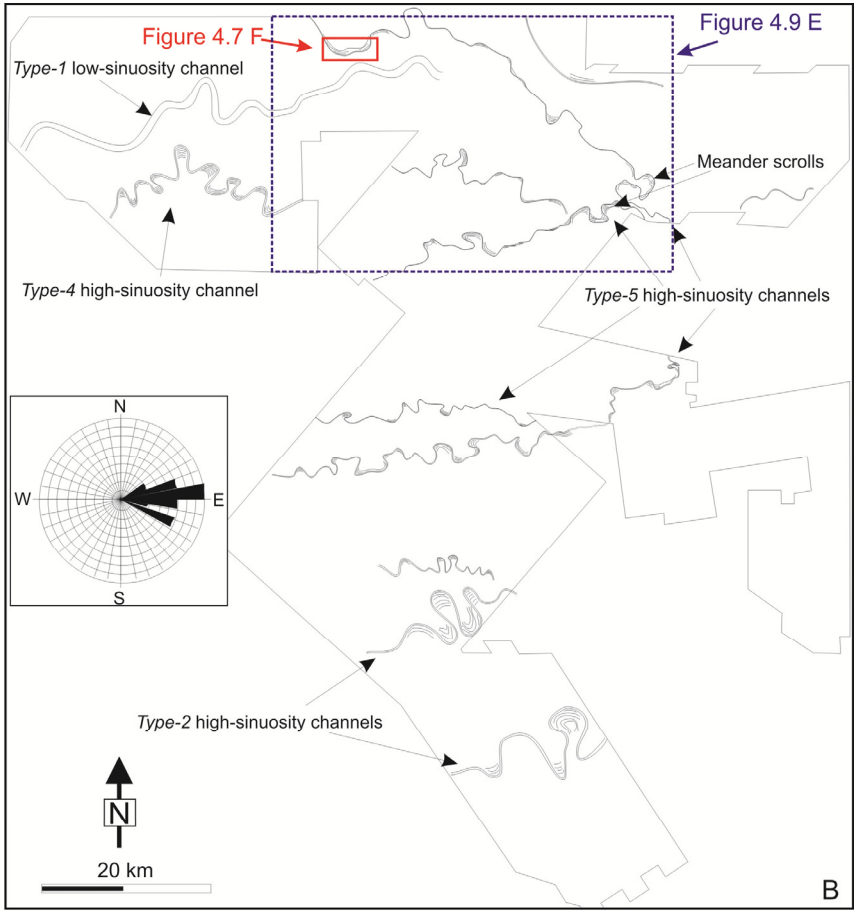
Figure 4.7 F
Figure 4.9 E
Type-1 low-sinuosity channel
Meander scrolls
Type-4 high-sinuosity channel
Type-5 high-sinuosity channels
N
W
E
S
Type-2 high-sinuosity channels
N
20 km
B

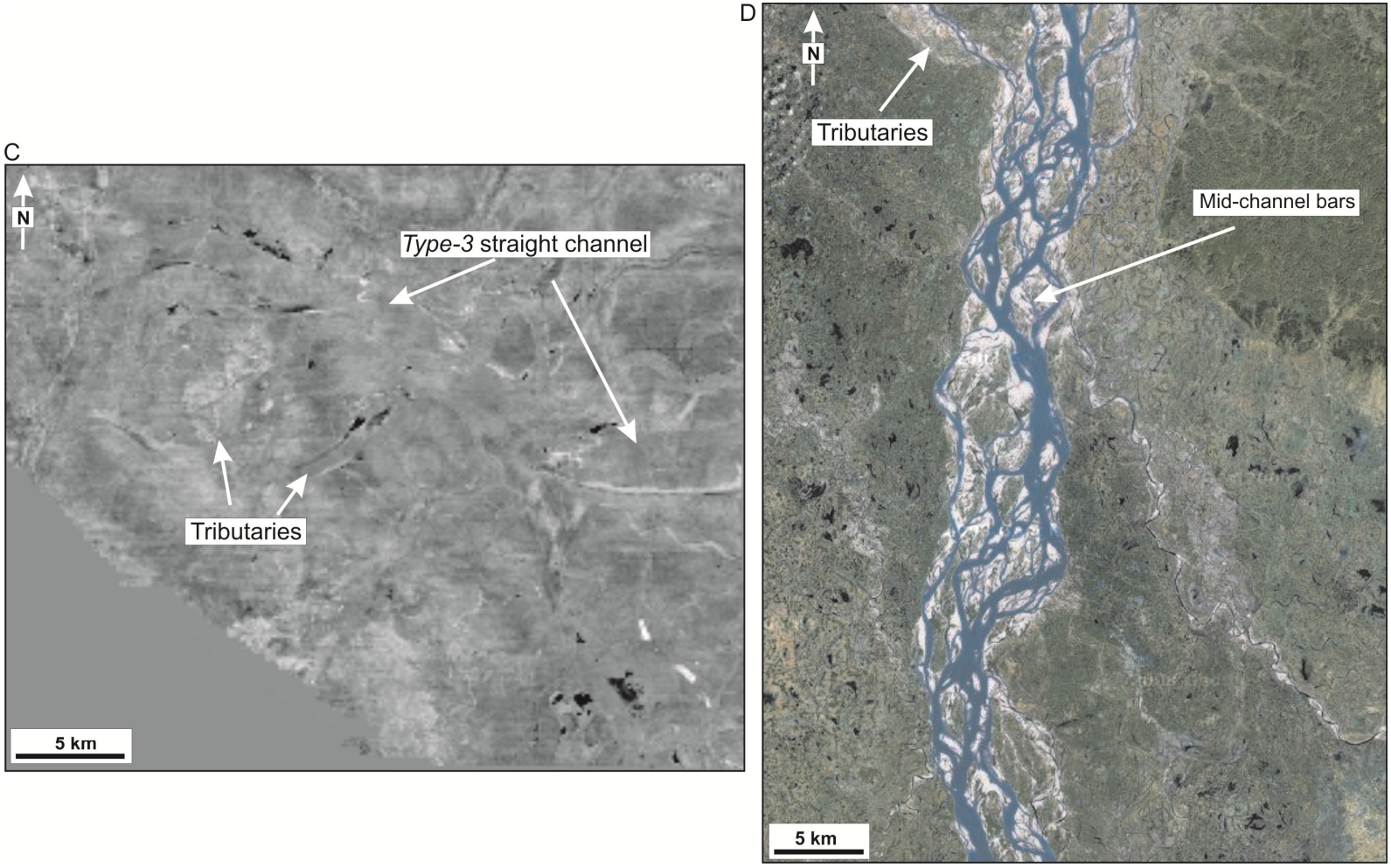
C
N
Type-3 straight channel
Tributaries
5 km
D
N
Tributaries
Mid-channel bars
5 km

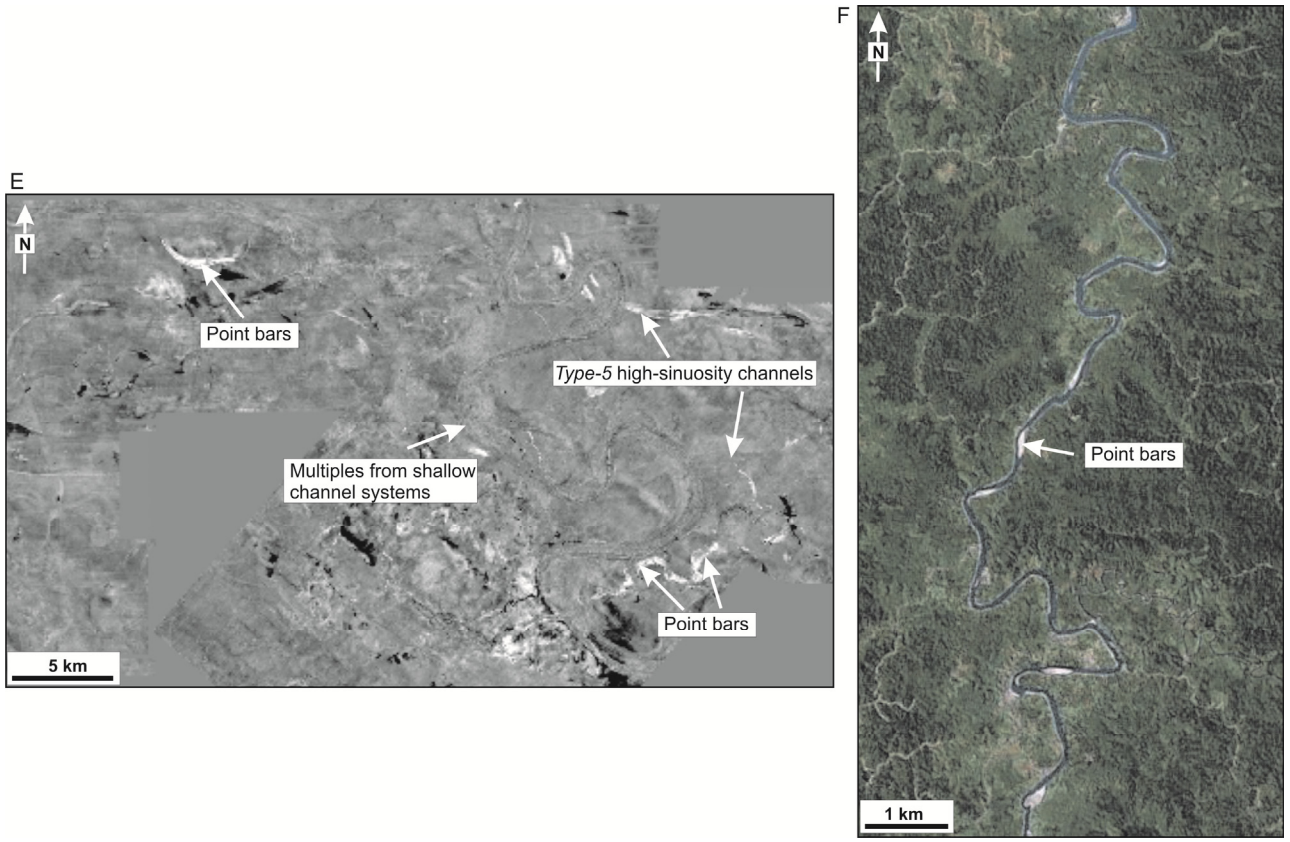

Figure 4.9: Two interpretive planview maps within Unit 2; **A)** shows the type of channels observed within the lower part of Unit 2 which is dominated by wide straight and very low-sinuosity channels. The major channels were broadly flowing to SE towards the South China Sea. The low-sinuosity channels in the southern part were flowing to NE towards the axial zone of the basin. Location of Figure 4.7 D and Figure 4.9C is shown; **B)** shows the type of channels observed in the upper part of Unit 2 which is dominated by small-scale, high-sinuosity channels with well-developed scroll bars; however, a large low-sinuosity channel has been observed in the northern part of the study area. Most of the channels were flowing to the east. Location of Figure 4.7 F and Figure 4.9 E is shown. Channel orientations are represented by a rose diagram for each part of the Unit; **C)** shows a part of iso-proportional slice illustrating part of the large straight channels; **D)** shows a part of the modern Brahmaputra River, India with channel width of 2-3.8 km, depth of 23 m and sinuosity index of 1.1. This modern river can be used as a modern analogue for river shown in Figure 4.9 C; **E)** shows a part of iso-proportional slice illustrating several moderately sinuous channels observed within the upper part of Unit 2; **F)** shows a part of the modern Kinabatangan River, Indonesia that has similar characteristics (width of 100-160 m; Depth of 5-8 m, meander belt width of 2 km and SI of 1.8) to those observed within the upper part of Unit 2. Note the sandy side bars associated with this modern river which looks similar to those imaged in Figure 5.9 E.

The smaller channels flowing north-eastwards from the elevated areas in the south towards the axial zone of the basin in the east suggesting that these channels possibly drained into those larger channels (Figure 4.9A). Like similar channels in Unit 1, these channels may represent lowstand alluvial bypass systems which formed when the magnitude of relative sea level fall was insufficient to fully expose the Sunda Shelf; however, sea-level fall-induced incision was great enough to form a channel 45 m deep and 3 km wide. The major channels located in the middle of the study area were elongated (up 3 km), possible due to an overall increase in discharge from the smaller tributary channels. The fluvial rivers would have been filled when the sea-level started to rise slowly during the late lowstand

The upper part of Unit 2 is dominated by highly-sinuous meandering rivers with associated point bar deposits. These meandering channels have different sizes and are of varying sinuosity; these differences may be caused by the type of sediment load and the discharge (c.f. Schumm, 1993). The filling of these meandering rivers started during continued sea-level rise. The Kinabatangan River, Indonesia, is a modern river that is similar in plan-view geometry and scale to the moderately-sinuous rivers observed within Unit 2 (Figure 4.9F). Note the relatively sand-rich point bars which may be a modern example of the high amplitude point bars associated with moderately-sinuous channels within Unit 2 (Figure 4.9E).

4.5.3.3 Unit 3

Unit 3 has been divided into two sub-units: 1) a lower unit (sub-unit 3.1) which is characterised by variable amplitude, laterally-continuous seismic facies; and 2) an upper

unit (sub-unit 3.2) which is characterised by laterally-discontinuous (chaotic) seismic facies. Full descriptions and interpretations of these sub-units are given below.

4.5.3.3.1 *Sub-unit 3.1*

Description: The base of sub-unit 3.1 is defined by Horizon C which is high-amplitude, laterally-continuous reflection (Figure 4.6). In cross-section, Horizon C is characterised by prominent incisions associated with low-sinuosity, *Type-1* and *Type-3* channel morphologies of varying scales (Figure 4.7A & D and 4.10A). For example, a W to E-flowing, low-sinuosity channel, up to 37 ms twt (35 m) deep and 2.5 km wide has been recognised in the northern part of the study area (Figure 4.10A). This channel is associated with a network of smaller tributaries, although no distinct dendritic patterns can be observed. In addition, a series of smaller (i.e. 22 to 32 ms twt (20 to 30 m) and 0.3 to 1.5 km wide), low-sinuosity channels which are oriented SW-NW have been observed through the study area at this stratigraphic level.

Within sub-unit 3.1, a wide variety of channel size and style have been observed. A large, E-flowing, low-sinuosity channel, up to 25 ms twt (23 m) deep and 1 km wide is recognised (Figure 4.10B). This channel is flanked by high amplitudes and in cross section is characterised by a *Type-1* channel morphology (see example in Figure 4.7B). Most of the channels within the upper part of sub-unit 3.1 have a high sinuosity index (SI up to 3), with channel depths typically being < 18 ms twt (15 m) and widths of up to 300 m. Meander belt widths are up to 5 km and radius of meander curvature is up to 1.3 km. These channels are characterised by *Type-3* and *Type-4* channel morphologies and, although varying orientations are observed, the majority of these systems appear to flow

towards the E (Figure 4.7C & E). Several abandoned channels are clearly imaged in association with these highly-sinuous channels (Figure 4.10B).

Interpretation: Prominent incisions along Horizon C at the base of sub-unit 3.1 are interpreted to be related to fluvial erosion and, in a similar manner to that interpreted for lower unit-bounding horizons (e.g. Horizon A and B), suggest that this horizon may represent a sequence boundary formed during relative sea-level fall.

In detail, the major low-sinuosity channel in the northern part of the study area was elongated, possible due to an increase in the discharge from the relatively smaller tributaries. The major channel immediately overlying Horizon C at the base of sub-unit 3.1 is interpreted to represent a lowstand alluvial bypass channel system that flowed eastwards from the elevated areas along the basin margin in the west towards the ultimate depositional basin in the South China Sea. The smaller channels were flowing north-eastwards from the basin margin in the south towards the axial zone of the basin in the east; this may imply that these channels drained into that larger channel which is located in the middle part of the study area (Figure 4.10A). These lowstand alluvial bypass systems formed in response to a relative the sea-level fall which did not fall below the shelf edge and the entire Sunda Shelf was not exposed. The fluvial channels would have been filled when the sea-level started to rise slowly during the late lowstand

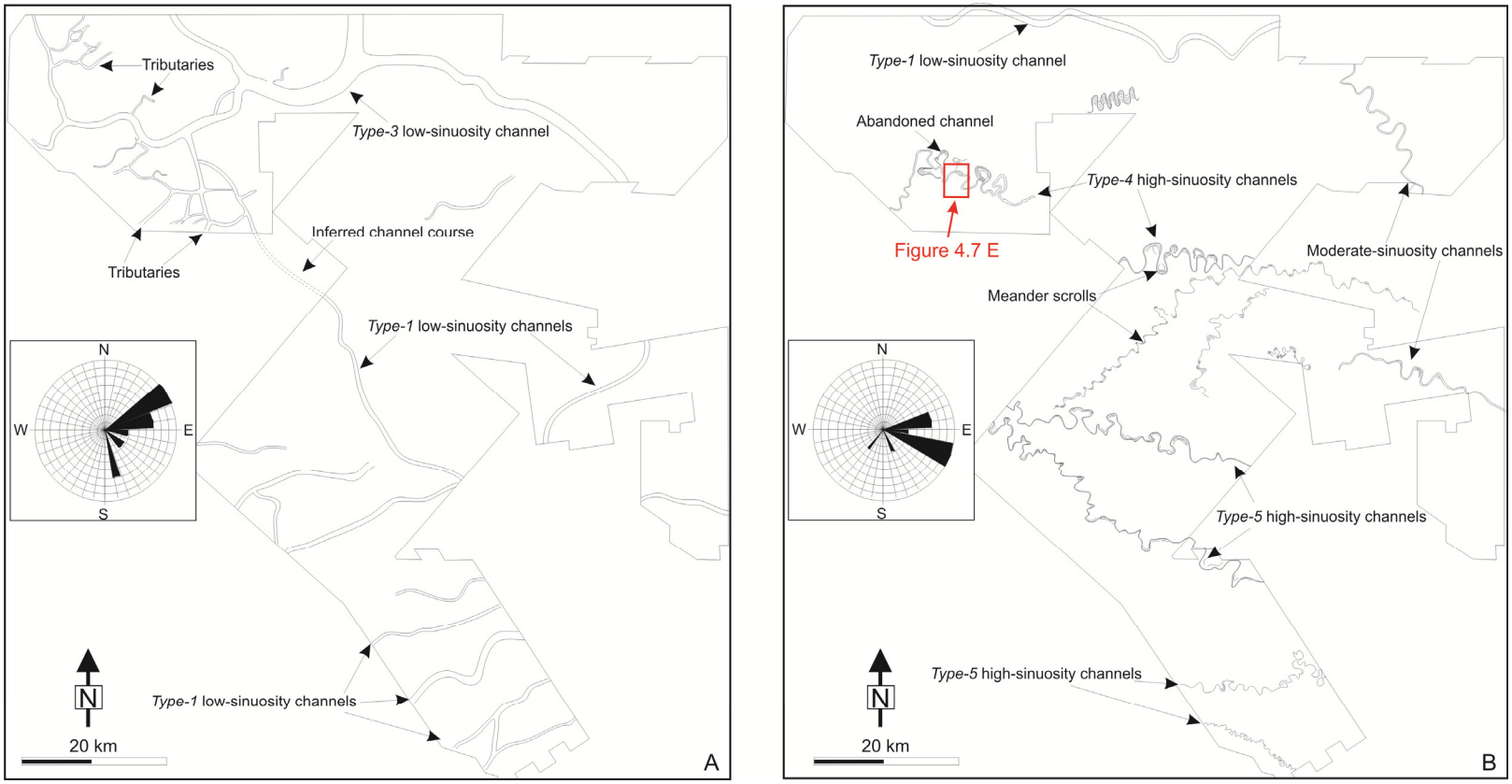

Figure 4.10: Two interpretive planview maps within sub-unit 3.1 **A)** shows the type of channels observed within the lower part of sub-unit 3.1 which is dominated by wide straight and very low-sinuosity channels. The major channels were broadly flowing to SE towards the South China Sea and the low-sinuosity channels in the southern part were flowing to NE towards the axial zone of the basin; **B)** shows the type of channels observed in the upper part of sub-unit 3.1 which is dominated by medium-scale, highly sinuous channels with well-developed scroll bars; however, a large low-sinuosity channel has been observed in the northern part of the study area. Most of the channels were flowing to SE. Location of Figure 4.7 E is shown. Channel orientations are represented by a rose diagram for each sequence.

Directly above these low-sinuosity channels, a low-sinuosity channel is recognised in the northern part of the study area (Figure 4.10B); this is interpreted as a braided river system formed during the latter part of the of sea-level lowstand associated with sub-unit 3.1. The highly-sinuous channels in the upper part of this sub-unit are mainly characterised by small- and medium-scale meandering channels associated with point bar deposits. These point bars are recognised by high amplitudes which are associated with very-well developed meander scrolls. These meandering channels flowed broadly eastwards towards the South China Sea. In association with the larger meandering rivers, abandoned channels were clearly imaged. This could be caused by continued sea-level rise (cf. Bridge, 2003).

4.5.3.3.2 *Sub-unit 3.2*

Description: The base of sub-unit 3.2 is defined by Horizon C.1 which is a high-amplitude reflection with significant topographic relief (Figure 4.6B). This horizon is characterised by three major incisions (depths 38 to 62 ms twt (35–58 m) and widths of 3.5 and 6.5 km) with *Type-6* channel morphologies. These incision features are located in the middle of the study area (Figure 4.11A). At the margins of these major incision features more subtle incision features which are <50 m and <75 m wide are observed. Different seismic facies have been observed within these incisions, including laterally-continuous seismic reflections and smaller 'v'-shaped incisions (*Type-2* and *Type-4* channel morphologies) associated with inclined seismic reflections which dip inwards towards the incisions.

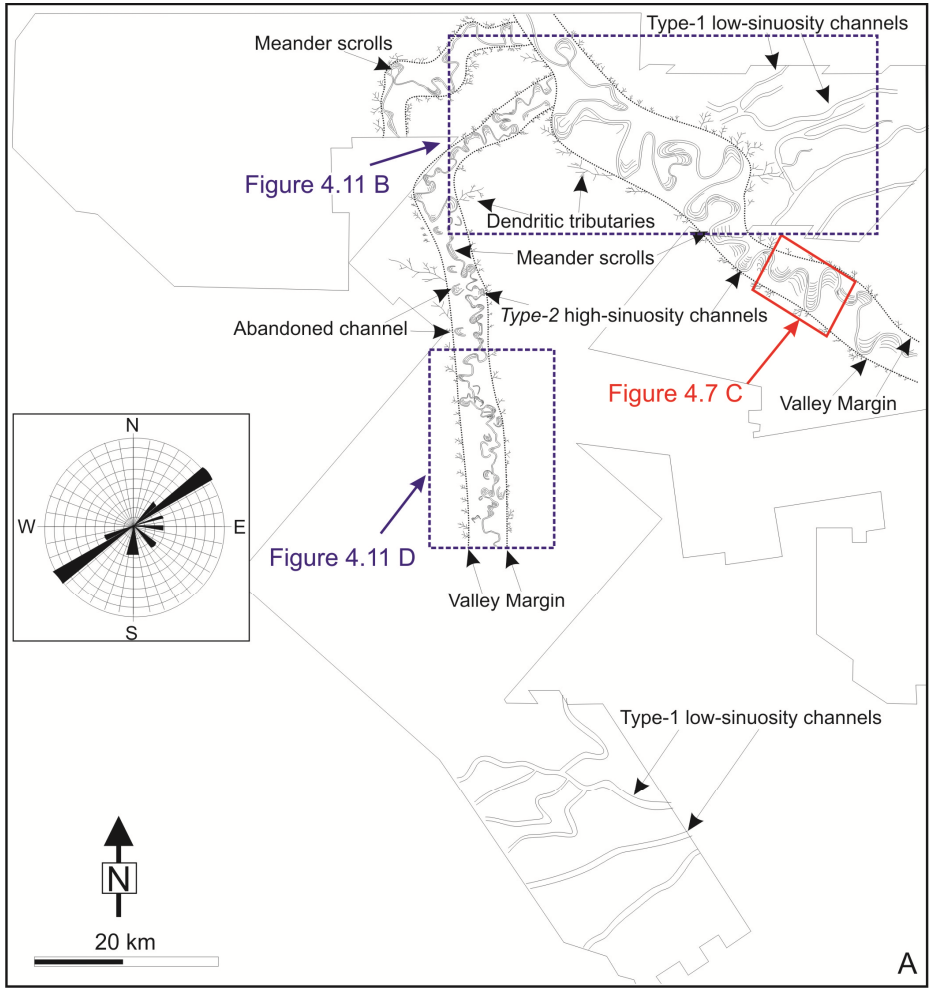
Type-1 low-sinuosity channels
Meander scrolls
Figure 4.11 B
Dendritic tributaries
Meander scrolls
Type-2 high-sinuosity channels
Abandoned channel
Figure 4.7 C
Valley Margin
N
W
E
S
Figure 4.11 D
Valley Margin
Type-1 low-sinuosity channels
N
20 km
A

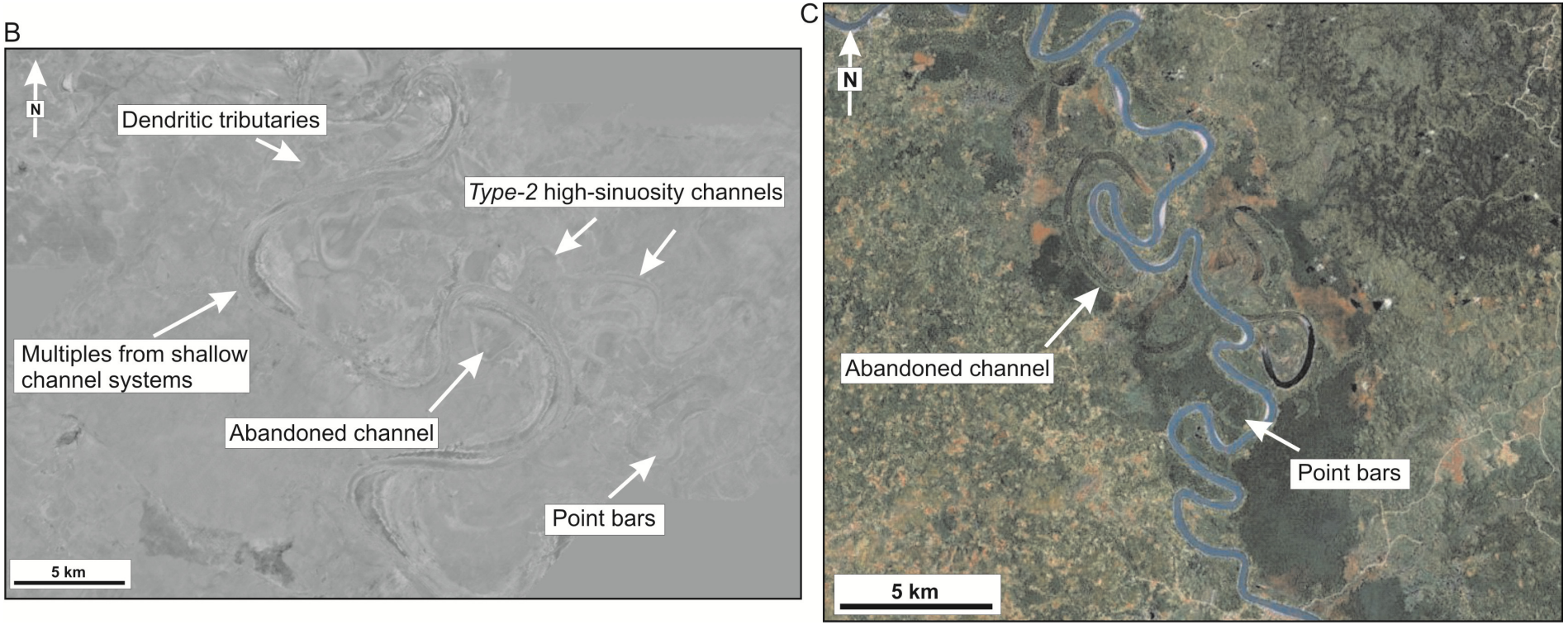
B
N
Dendritic tributaries
Type-2 high-sinuosity channels
Multiples from shallow channel systems
Abandoned channel
Point bars
5 km
C
N
Abandoned channel
Point bars
5 km

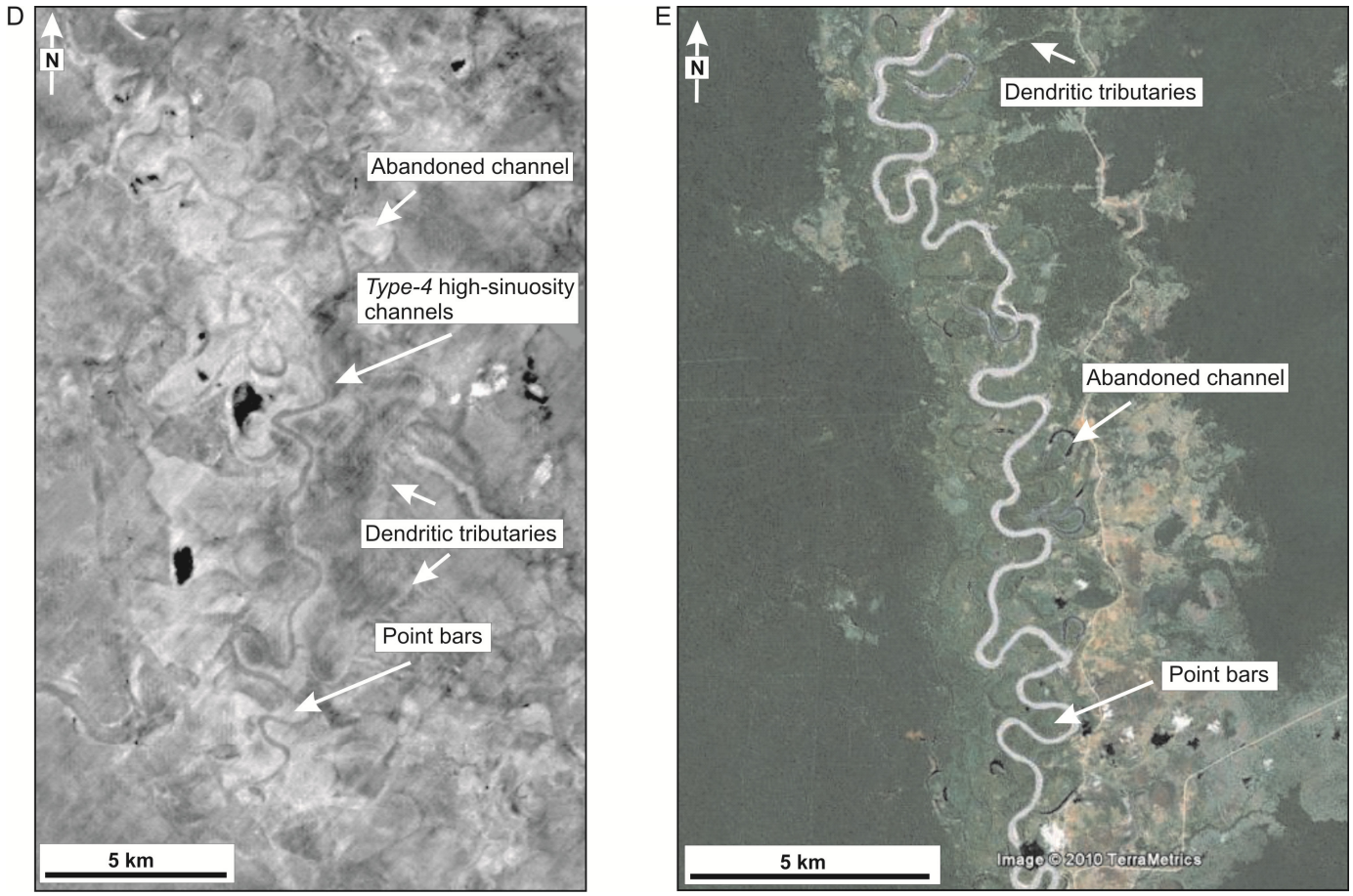

Figure 4.11: A) An interpretive planview map within sub-unit 3.2 showing three high-sinuosity channels with very well-developed scroll bars that are confined to the walls of these incisions. At the margins of these incisions, small tributaries are shown. Straight and low-sinuosity channels have been observed on the NE and SE part of the study area. These channels were flowing towards the axial zone of the basin. Locations of Figures 4.7 C, 4.11B and 4.11D are shown. Channel orientations are represented by a rose diagram; **B)** shows a part of iso-proportional slice illustrating a major highly sinuous meandering river; **C)** is a part of the modern Mahakam River, Indonesia. Similar channel morphometric parameters (width of 300-450 m, depth of 8-15 m, meander belt width of 7-8.5 km, and SI of 2.9) are observed in both rivers; **D)** shows a part of iso-proportional slices showing a confined highly-sinuous meandering river associated with many abandoned channels; **E)** is a part of the modern Barito River, Indonesia that has characteristics (width of 150-250, depth of 6-8 m, meander belt width of 700 m, and SI of 2.7) that similar to those observed to the ancient river showing in Figure 4.11D.

In planview, these v-shaped incisions are seen to be the cross-sectional expression of highly-sinuous channels confined within the broader incisional features (*Type-2* channel morphologies; Figure. 4.11A). One such channel, which occupies the largest incision feature, is up to 400 m wide, 28 ms twt (25 m) deep, has a meander belt width of up to 6.5 km up and a radius of curvature of 1.7 km (Figure 4.7C and 4.11A & B). This channel and two other highly-sinuous channels with widths of 150-200 m and depths of <18 ms twt (15 m) flowed to SE and S (Figure 4.11A). In the north-eastern and southern part of the study area, several low-sinuosity channels with widths of up to 600 m and depths of 22 ms twt (20 m) have been identified.

Interpretation: The deep incision features developed along Horizon C.1 are interpreted to be incised valleys that formed when the sea-level fall fell below the shelf break and the Sunda Shelf was exposed. This interpretation is supported by the presence of the smaller dentritic tributaries that drain into the main valleys (Figure 4.11; Posamentier, 2001). The erosional surface at the base of the incised valleys (Horizon C.1) is interpreted to represent another sequence boundary within Unit 3. These incised valleys are significantly larger than the lowstand alluvial bypass channel systems identified within the underlying depositional units (i.e. Units 1 and 2).

Incised valleys at the base of sub-unit 3.2 are interpreted to have been back-filled during the subsequent relative sea-level rise. Due to limited seismic imaging of the basal portion of these valleys coupled with the potential thin nature of the associated deposits, it is not possible to determine whether a lowstand braided channel is located in the lower part of the incised valleys as proposed by fluvial sequence stratigraphic models (e.g. Shanley and McCabe, 1994). If such deposits are truly absent, this may imply that these systems were dominated by bypass during relative sea-level fall and no such lowstand systems were

deposited. The majority of the incised valleys are filled by highly-sinuous meandering rivers associated with point bar deposits and well-developed meander scrolls (Figures 4.7C; 4.11). These meandering rivers may have formed and deposited sediment during the transgression succeeding the earlier relative sea-level fall. Figure 4.11D & F illustrate portions of the Mahakam and Barito Rivers, Indonesia. These rivers have similar geometric characteristics (e.g. sinuosity, depth, width, meander belt width) to those observed within sub-unit 3.2.

The low-amplitude, laterally-continuous reflections developed on the top of these incised valleys are interpreted as a marine mud drape deposited after the relative sea-level rise during the subsequent highstand after the incised valleys were drowned.

4.5.3.4 Unit 4

Unit 4 has been divided into two sub-units: 1) a lower unit (sub-unit 4.1) which is characterised by low-amplitude, laterally-continuous seismic facies; and 2) an upper unit (sub-unit 4.2) which is characterised by laterally-discontinuous (chaotic) seismic facies. These sub-units are described and interpreted below.

4.5.3.4.1 *Sub-unit 4.1*

Description: The base of sub-unit 4.1 is defined by Horizon D which is a high-amplitude, reflection event, along which prominent incisions with T*ype-1* channel morphologies are observed. These channels are up to 32 ms twt (30 m) deep (Figure 4.7A & D). In planview, these incised features are of low to very low-sinuosity (SI 1-1.3), with channel

widths of 300-1300 m (Figure 4.12A). Most channels flowed towards the south-east. In the middle of the study area, a major channel (22 ms twt (20 m) deep and 1 km wide increases in its sinuosity eastwards. In the southern part of the study area, several straight to low-sinuosity channels which range from 400 to 700 m wide and 12 to 15 m deep are identified.

Within sub-unit 4.1, above the basal channel systems, channels vary in size and sinuosity. For example, in the upper part of this sub-unit, several moderately-sinuous (SI ranges from 1.3 to 1.5), relatively small channels are recognised (Figure 4.12B). These channels are characterised by *Type-3* and *Type-4* channel morphologies (see example in Figure 4.6E) which are up to 22 ms twt (20 m) deep and up to 320 m wide. These channels become less sinuous toward the SE and channels in the middle of the study area appear to be partly eroded at the base of the deeply-incised feature of sub-unit 4.1.

Interpretation: Prominent incisions along Horizon D at the base of sub-unit 4.1 are interpreted to be related to fluvial erosion and, in a similar manner to that interpreted for lower unit-bounding horizons (e.g. Horizon A, B and C), suggest that this horizon may represent a sequence boundary formed during relative sea-level fall. These lowstand alluvial bypass channel systems flowed south-eastward towards the South China Sea.

Towards the top of sub-unit 4.1, fluvial channels become smaller and more sinuous. However, these channels do not have particularly high sinuosity indices and are not associated with well-developed point bars, perhaps suggesting that these channels formed during the early stages of a marine transgression following the preceding relative sea-level fall.

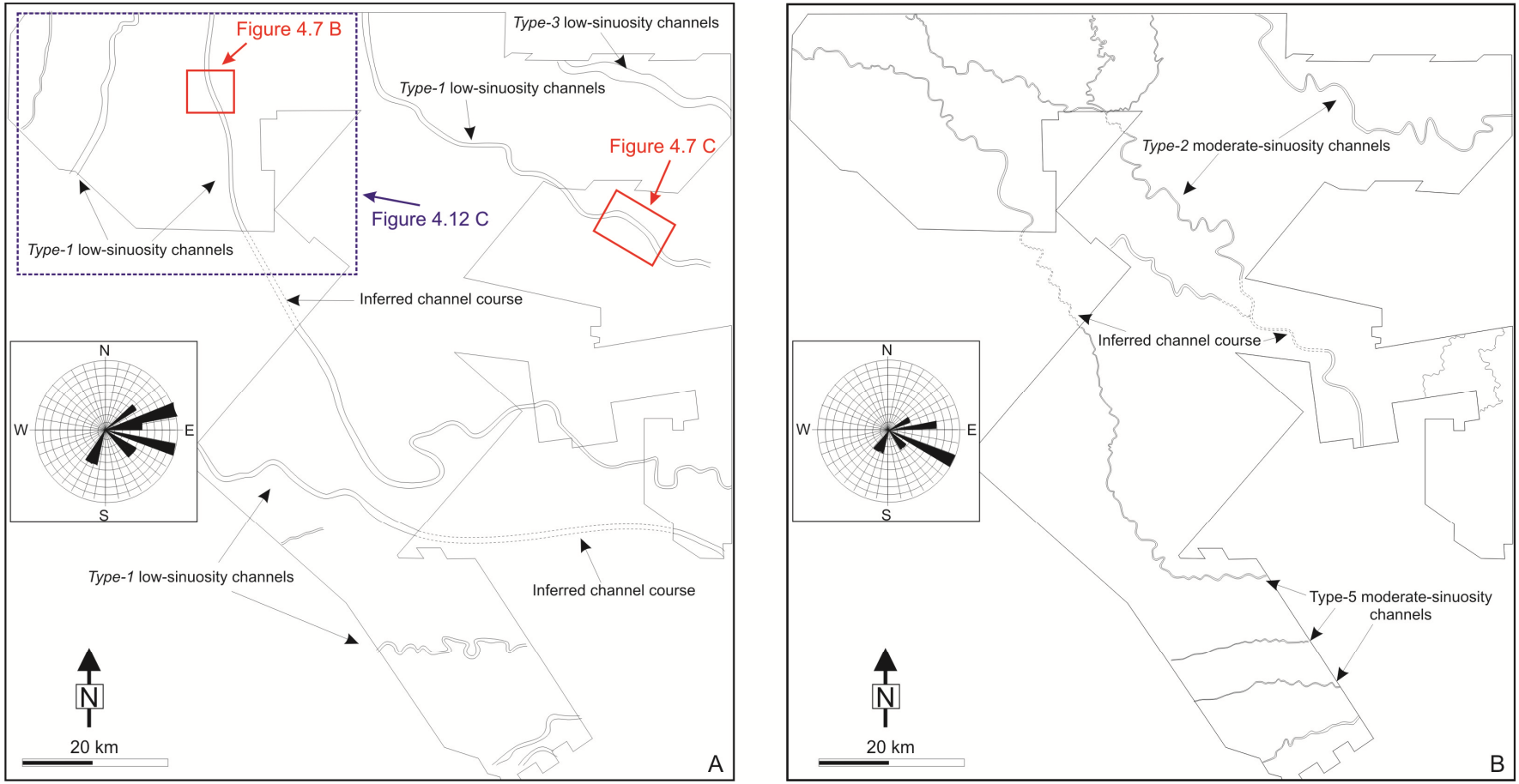
Figure 4.7 B
Type-3 low-sinuosity channels
Type-1 low-sinuosity channels
Figure 4.7 C
Figure 4.12 C
Type-1 low-sinuosity channels
Inferred channel course
N
W
E
S
Type-1 low-sinuosity channels
Inferred channel course
N
20 km
A
Type-2 moderate-sinuosity channels
Inferred channel course
N
W
E
S
Type-5 moderate-sinuosity channels
N
20 km
B

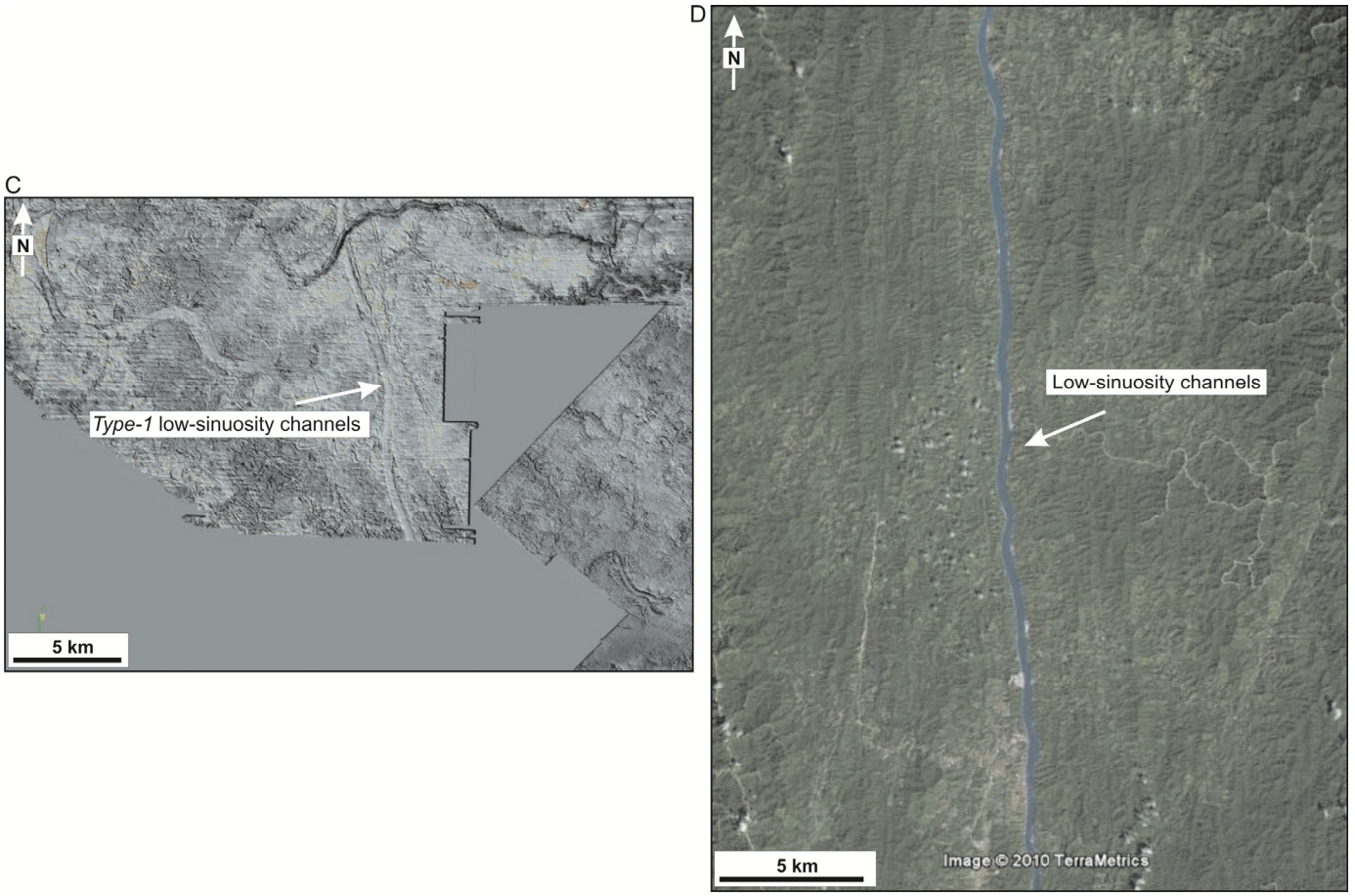

Figure 4.12: Two interpretive planview maps within sub-unit 4.1; **A)** shows the type of channels observed within the lower part of sub-unit 4.1 which is dominated by wide straight and very low-sinuosity channels. The major channels were broadly flowing to SE towards the South China Sea. The low-sinuosity channels in the southern part were flowing to NE towards the axial zone of the basin. Location of Figures 4.7B & C and 4.12 C are shown; **B)** shows the type of channels observed in the upper part of sub-unit 4.1 which is dominated by medium-scale, moderate-sinuosity channels with no scroll bars. Some parts of the channels in the middle part of the study area were eroded off by the latest deep incision of sub-unit 4.2. Channel orientations are represented by a rose diagram for each part of this sub-unit; **C)** shows a part of a combination of time and coherence slice illustrating a large low-sinuosity channel; **D)** is a part of the modern Rajang River, Malaysia showing a low-sinuosity channel with width of 320-410 m, depth of 23 m, and SI of 1. This river looks similar to the ancient river imaged in Figure 4.12C.

4.5.3.4.2 *Sub-unit 4.2*

Description: The base of sub-unit 4.2 is defined by Horizon D.1; this is a high-amplitude reflection along which a 83 ms twt (80 m) deep and 13 km wide incision with a *Type-6* channel morphology is identified in the middle of the study area (Figure 4.12). Incision at the base of this feature results in the erosion of some of the channels systems within the underlying sub-unit 4.1. In cross section, the seismic facies within this incision are different from those outside the incision. Outside this deep incision, ~50 m wide, incised features with 'v'-shaped channels are recognised (Figure 4.13). In planview, these channels have a pronounced dentritic pattern (Figure 4.13). At the bottom of the major incisional feature, a series of lenticular bodies are observed. These bodies are overlain by flat-laying reflections, and a channel with a *Type-2* morphology which is associated with inclined (up to 7°) reflections. This *Type-2* channel is highly-sinuous and is 27 ms twt (25 m) deep, 600 m wide and has a meander belt width of 13 km. This channel flowed towards the SE and is fully confined within the deep incision. A neck-cut off abandoned channel was clearly imaged in the downstream part of the channel (Figure 4.13). In the southern part of the study area, relatively large (depths of 17-34 ms twt (15-30 m) and widths of 400 to 900 m), low-sinuosity channels which flowed towards the SE are developed.

Interpretation: The large incisional feature developed along Horizon D.1 is significantly larger than those lowstand alluvial bypass channel systems observed in underlying stratigraphic units. These features are, therefore, interpreted as an incised valley formed due to a relative sea-level fall and Horizon D.1 is interpreted as a sequence boundary. Furthermore, based on its stratigraphic occurrence towards the top of the Pleistocene succession and by comparison to other similar systems documented in nearby basins

(Posamentier, 2001; Miall, 2002, Darmadi et al., 2007), this valley is interpreted to have formed during the Last Glacial Maximum when sea-level fell below the shelf edge and the whole Sunda Shelf was exposed. The presence of smaller small dentritic tributaries at the valley margin supports the interpretation of this large incisional feature as an incised valley (cf. Posamentier, 2001). Lenticular bodies developed immediately above the erosional base of the incised valley may represent the lowstand deposits which may have accumulated within a lowstand braided river system (e.g. Shanley and McCabe, 1994).

After formation of the erosional base and initial deposition, the incised valley became occupied by a large sinuous river system which appears to represent the major system occupying the axial zone of the Malay Basin during Late Pleistocene times. This channel is similar in geometry to portions of the downstream part of the Mississippi river, although it is slightly smaller. This channel is bigger than most if not all the meandering rivers in Southeast Asia. Low-sinuosity channels in the southern part of the study area which flowed to the southeast could be large tributaries that fed the main incised valley. During subsequent sea-level rise at the shelf-edge, the main trunk river within the incised valley appears to have responded by becoming more sinuous (Figure 4.13A & B). This meandering river was associated with point bars and is interpreted to have developed during the main transgressive period.

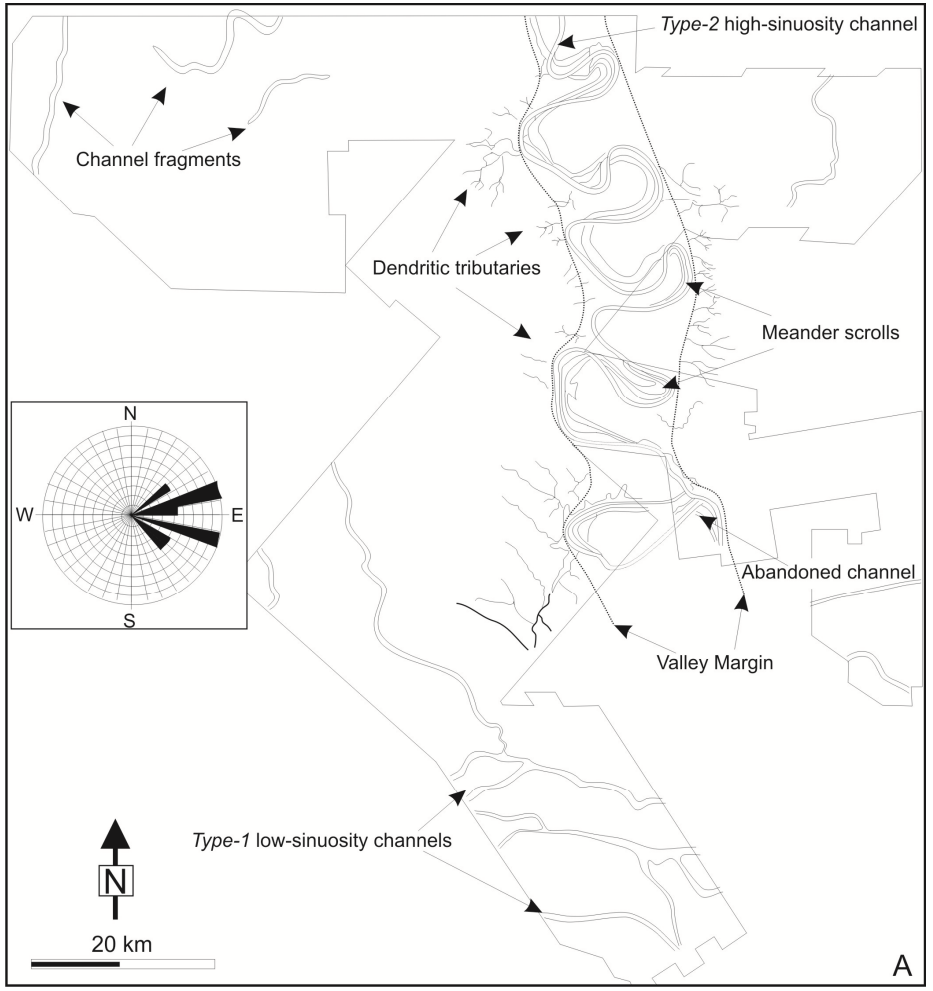
Type-2 high-sinuosity channel
Channel fragments
Dendritic tributaries
Meander scrolls
N
W
E
S
Abandoned channel
Valley Margin
Type-1 low-sinuosity channels
N
20 km
A

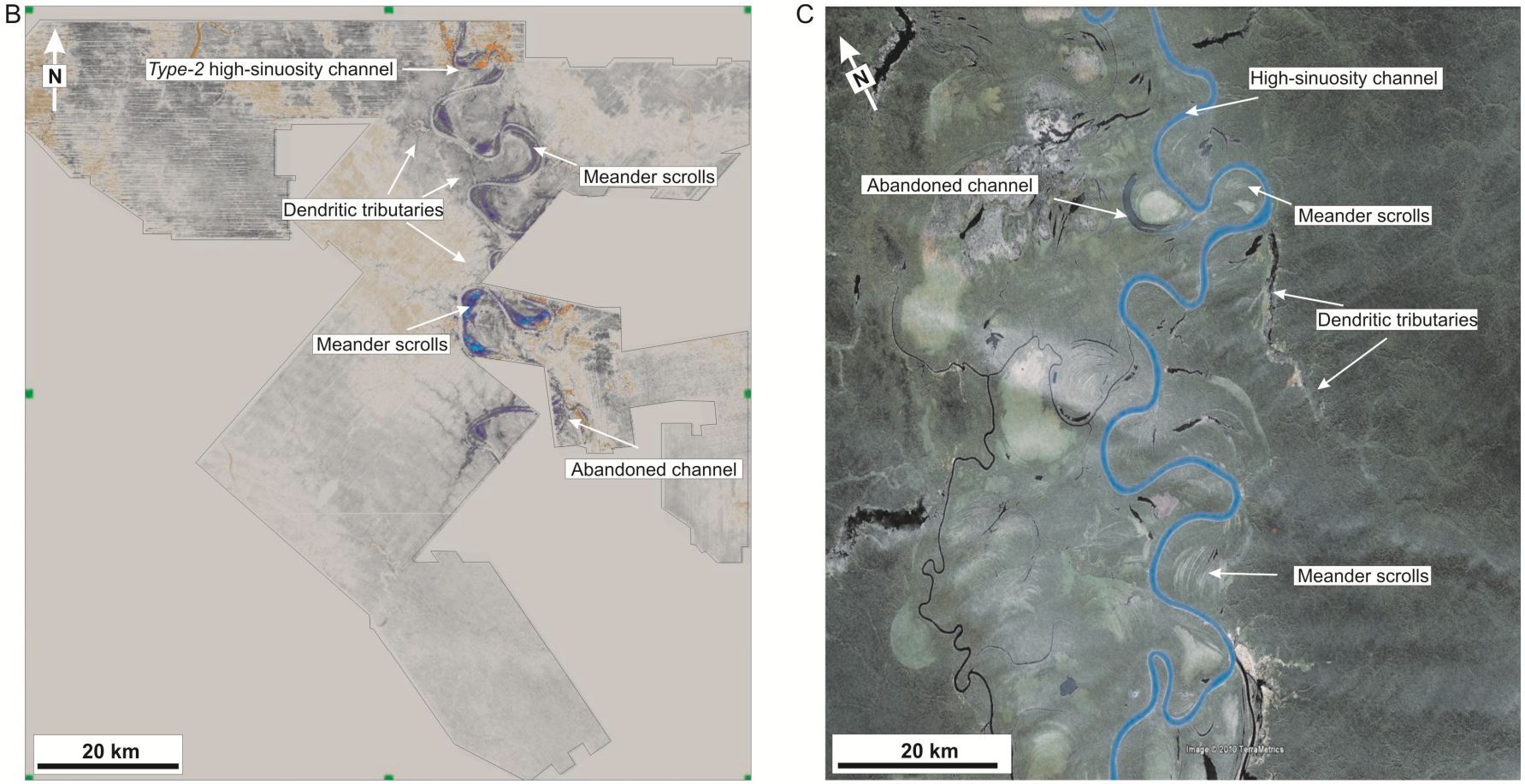

Figure 4.13: A) an interpretive planview map within sub-unit 4.2; **B)** Time slice at 108 ms twt showing a large high-sinuosity channel with very well-developed scroll bars which is confined to the walls of the incision. At the margins of these incisions, small tributaries are shown. Channel orientations are represented by a rose diagram; **C)** Illustrates portion of the Purus River which is one of the main tributary river of the Amazon. This river has similar geometric characteristics (width of 500-750, depth of 10-15 m, meander belt width of 14-24 km, and SI of 2.8) that similar to that observed in the time-slice 108 (B).

A neck-cut off and associated abandoned channel observed in the southern part of the study area suggests that a continued sea-level rise may have caused the channel to reduce its sinuosity via this mechanism (Schumm, 2005). Furthermore, this meandering river became low-sinuosity channel toward the South China Sea which is seen in another dataset (not shown in this study) within the southern part of the Malay Basin (Rapi, 2010, pers. comm.). Figure 4.13C illustrates portion of the Purus River which is one of the main tributary river of the Amazon. This river has similar geometric characteristics (e.g. sinuosity, depth, width, meander belt width) to this large meandering river.

4.6 Discussion

4.6.1 Sea-level fall and the formation and recognition of incised valleys

Sequence boundaries are defined as regional unconformities that separate the stratigraphic record into packages of conformable, genetically-related strata (Vail et al., 1977). Two types of sequence boundaries have been identified (Vail et al., 1977; Van Wagoner et al., 1990); (i) *type 1* which develop when relative sea-level fall is more rapid and of higher magnitude than the rate of tectonic subsidence; in this case the shelf may be fully exposed, subaerial erosion occurs and incised valleys form; and (ii) *type 2* which develop when relative sea-level is slow and of moderate magnitude, and only minor exposure and limited subaerial erosion occurs. Fluvial systems associated with this type of sea-level fall have been termed as lowstand alluvial bypass systems (Posamentier, 2001). This type of unconformity is much more difficult to identify in seismic and outcrop because they are not characterised by deep erosion or major facies shift (Miall, 1996); however, Type 2

unconformities can be defined on the basis of identifying a marked and stratigraphically rapid switch from high-sinuosity to low-sinuosity channels.

Most previously identified incised valleys are incised into bedrock or into coastal and marine strata. Many contain fully marine deposits, implicating sea-level fluctuations in valley cutting and filling (Gibling, 2006). Valleys incised into fluvial deposits are more difficult to identify as it is more difficult to distinguish locally deep scours located at, for example, channel confluences, and more regional valley-base scours (Best and Ashworth, 1997). Based on these difficulties several diagnostic criteria have been suggested for identifying incised valleys (Hampson et al 1997; Posamentier, 2001; Fielding and Gibling, 2005): 1) the basal erosion surface that records the lowstand of relative sea-level (sequence boundary) must be of regional (basin wide) extent; 2) the basal erosion surface truncates underlying strata which may be present beneath the adjacent interfluves; 3) the basal surface is associated with the presence of small tributaries on the main valley interfluves.; 4) incised valley fills must have a distinctive internal architecture that is commonly multi-storey which records the progressive rise in base-level through the filling of the valley; therefore the facies within the incised valley must be different from those adjacent to and below the erosional surface; 5) the depth and width of the incised valley has to be significantly larger than expected for a 'normal' fluvial channel system. Geometrically, incised valleys are typically several kilometres wide and several tens of meters deep (Zaitlin et al., 1994; Reynolds, 1999; Gibling, 2006).

Identifying an incised valley and the associate erosional base (sequence boundary) using seismic data is difficult; however, Posamentier (2001) indicated that incised valleys can be identified and differentiated from 'large' river systems on seismic datasets based on the presence of small incised tributary valleys which link to the main trunk valley. In contrast, lowstand alluvial bypass systems have no such associated tributaries. In

addition, the sizes of these incised valleys are much larger than the sizes of those lowstand alluvial bypass channel systems (e.g. width (18000 vs. 3000 m) and depth (80 vs. 45 m)).

Given that; (i) the Malay Basin is located in the centre of the Sunda Shelf, a relatively large distance from the main sediment source area(s) (Figure 4.1); and (ii) the low-gradient Sunda Shelf was tectonically quiescent during the Pleistocene to Recent (Madon et al., 1999), it is considered unlikely that climatic variations and/or tectonics are the primary controls on the variation in channel architecture observed within the Pleistocene succession in this study (see discussion by Miall, 2002). Based on available data it is not possible to determine exactly how far the predominantly non-marine Malay Basin was from coeval paleo-shoreline(s) during the Pleistocene. However, a series of maps presented by Voris (2000) suggest that the Sunda Shelf was exposed during the Late Pleistocene to Recent and indicate that the study area within the Malay Basin was not far (i.e. a few hundreds of kilometres away) from the paleo-shoreline. It is considered most likely, therefore, that sea-level was the major factor controlling the types and stratigraphic organisation of fluvial channels within the Pleistocene to Recent succession within the Malay Basin.

Based on 3D seismic data from the Java Sea, Posamentier (2001) distinguished incised valleys and 'non-incised' lowstand alluvial bypass channel systems. According to Posamentier (2001), incised valleys can be defined by the presence of small dentritic tributaries that fed the main valley system, whereas lowstand alluvial bypass channel systems have no such associated tributaries. Both types of channel systems have been recognised in this study and other studies conducted on the Sunda Shelf (e.g. Miall, 2002; Darmadi et al, 2007). The development of incised valleys or lowstand alluvial bypass systems depends on the magnitude of the relative sea-level fall. For example, when the

sea-level fall is large and sufficient to expose the entire shelf, an incised valley may form. Valleys such as this are clearly observed in the Late Pleistocene succession in the present study area. Posamentier's (2001) interpretation was based on seismic slices; here, we identify incised valleys in both cross-section (Figure 4.6B) and horizontal slices (Figures 4.11 & 4.13) and demonstrate pronounced and deep incision features. Additionally, truncations at the valley margins are observed.

In this study lowstand alluvial bypass channel systems are characterised by relatively wide, straight to very low-sinuosity (SI 1-1.2) channels. Similar channel types have also been observed by Miall (2002), Darmadi et al. (2006) and Wood (2007). On the Sunda Shelf and within the Malay Basin, such channel systems are 0.5- 3.5 km wide, 25-45 m deep and are straight or of low-sinuosity (SI 1-1.2). Tributaries with dentritic planview patterns are not typically observed in association with these channel systems. These channel systems are interpreted to form when relative sea-level fall is not rapid or of sufficiently large magnitude to expose the entire shelf. Given that the Sunda Shelf has a very low-gradient present-day and presumably in the Pleistocene, it is suggested that any minor relative sea-level fall may expose some if not all of the shelf area. This minor relative sea-level fall along with the low-gradient shelf may lead to the formation of the wide and deep channel systems. Furthermore, the major alluvial bypass channel systems were elongated as these channels had to widen due to increasing in the discharge from the attached tributary channels. Darmadi et al. (2007), concluded that the variability in channel pattern within the Pleistocene succession in West Natuna Basin is controlled mainly by variations in discharge during gradual aggradation and that the sea-level fluctuation had less of an influence. This interpretation has been also proposed by Kiel (2009) which was mainly based on the fact that the study area is *ca.* 1000 km away from the shelf break which has been estimated as the paleo-shoreline in the Sunda Shelf by

Darmadi et al. (2007); However, in this study the sea-level changes is interpreted to be the main controlling factor and may have driven the overall stratigraphic changes within the Pleistocene succession within the Malay Basin Although, relative sea-level variations are the main controlling factor that determine the channel style and size, sediment loads and discharge which is controlled by climate may play a significant role in determining the variability of the channel types and sizes among each stratigraphic level. Furthermore, the lowstand alluvial bypass channel systems were flowing from the high elevated areas in the west which may reflect high regional stream gradients during early lowstand. Due to a lack of age constraints on the studied stratigraphy in this study (Malay Basin) and that of Darmadi et al. (2007) (West Natuna Basin) it was difficult to confidently tie observations from both areas. However, based on the fact that both successions were deposited in a tectonically inactive basin, the sea-level changes may have driven stratigraphic changes in a similar manner in both areas

In view of these observations, the surfaces bounding the bases of the main Pleistocene seismic-stratigraphic units identified in this study (i.e. Horizons A, B, C, C.1, D, and D.1) are interpreted to represent sequence boundaries. Two types of sequence boundaries have been identified. 1) *Type-1:* these are characterised by numerous prominent 'v' and/or 'u'-shaped incised features filled with variable-amplitude, chaotic or laterally-continuous reflections (Horizon A, B, C, and D; Figure 4.6); and 2) *Type-2*: these are characterised by either a single or a very few, wide and deep incisions filled with a range of seismic facies (Horizon C.1 and D.1). This latter type of surface is associated with significant topographic relief and numerous smaller incised features at the margin of the main deep incisions (Figure 4.6B). Such unconformities can typically be easily recognised in coastal and shallow marine deposits where the influence and impact of relative sea-level variations, as expressed by abrupt facies shifts, are most pronounced. In contrast, in

alluvial strata, identification of these unconformities is more difficult, as it can be difficult to distinguish locally deep fluvial scours from true erosional surfaces at the base of the valleys formed in response to relative sea-level changes (Best and Ashworth, 1997).

4.6.2 Vertical changes in fluvial style and sequence-stratigraphic models

The Pleistocene to Recent succession of the Malay Basin displays a wide range of fluvial channel architectures and size within a relatively limited stratigraphic interval. Systematic vertical changes in fluvial channel architecture and styles have been observed within each individual unit and sub-unit of the Pleistocene to Recent succession of the Malay Basin. At the base of each unit, several straight and low-sinuosity channels are observed. Toward the top of the each unit, the channels change their pattern and size to typically become smaller and of higher sinuosity.

Systematic vertical changes are indicated in many stratigraphic models of fluvial systems (e.g. Wright and Marriott, 1993; Shanley and McCabe, 1994). The variability and changes in fluvial architecture are controlled by several factors including sea-level fluctuation, tectonics and climate. During base-level rise and transgression, channels change their scales and styles, typically becoming more highly-sinuous (meandering) with very well-developed point bars associated with lateral accretion surfaces. During the late highstand, when sea-level starts to fall, channels respond by changing their sinuosity and size, typically becoming narrower and being characterised by low to moderately-sinuous channels.

Despite various controlling factors, Schumm (1977, 1981) demonstrated that there is a strong relationships between the channel pattern and the type of the sediment transported

by the channel, thereby allowing fluvial channels to be classified into three types: 1) bed-load channels which are straight or of very-low sinuosity; 2) mixed-load channels which are of moderate-sinuosity; 3) suspended-load channels which are of high sinuosity. Based on Schumm's (1977) classification, low-sinuosity channels may be filled with sands. Miall (2002) suggested that these lowstand channels may provide the greatest volume of potential porous reservoir. The highly-sinuous meandering channels observed towards the top of the units have variable amplitude, unlike the straight and low-sinuosity channels which have low-amplitude, laterally-continuous facies. For example, the channel point bars are of significantly higher amplitude than the fill of the channel itself, suggesting that the point bars are of a different lithology to the channel (Figure 4.7C). However, no well logs or cores are available to determine the lithology responsible for these changes in seismic facies although, by comparison to other examples, it may be speculated the point bars are sandstone-rich indicating good-quality reservoirs whereas the channels are mudstone-rich (cf. Miall, 2002; Carter, 2003; Darmadi et al., 2007).

4.7 Conclusions

The Pleistocene to Recent successions within the Malay Basin which is about 500 m thick were divided into four seismic units. The bounding surfaces (sequence boundaries) of these sequences are characterised by prominent fluvial incisions. Two different types of incisions have been identified; deep incised valley systems that are associated with smaller tributaries feeding the main valley and weakly incised channel systems that are interpreted as lowstand alluvial bypass channel systems have been recognised. A wide variety of channel style and size have been observed within each individual unit. The major controlling factor that determines the channel types and their sizes are the sea-level

fluctuations; however, effects of climate on discharge are also noticed. There are systematic vertical changes in the channel pattern and sizes in response to the sea-level variations. It has been observed that the lower part of each unit is characterised by wide and deep straight and low-sinuosity channels overlain by meandering rivers with well-developed point bar deposits. These meandering channels change their sinuosity toward the top of the unit to become less-sinuous with few or no meander point bar deposits.

Two major deep and wide incised valleys were identified within the Late Pleistocene succession. Within these incised valleys, two large meandering channels with very well-developed accretion surfaces of point bar deposits are confined to the valley margins. These meandering channels were located in the middle part of the study area which indicates that these valleys are the major channels that occupied the axial zone of the Malay Basin. The formation of these valleys was caused by the significant falls in the sea-level that widely exposed the entire Sunda Shelf.

Chapter 5

3D Seismic Geomorphology of a Late Pleistocene Incised Valley Complex on the Sunda Shelf, Southeast Asia

5.1 Abstract

Analysis of the shallow (<500 ms) part of a mega-merge 3D seismic reflection survey, supplemented with very high-resolution site survey data including platform borings and boomer data, has enabled identification and characterisation of a large (up to 18 km wide by 80 m deep) incised valley within the Late Pleistocene succession on the Sunda Shelf, offshore eastern Malaysia. The base of this incised valley fill comprises coarse-grained sediments, including pebbles, gravels and possibly cobbles. These deposits are overlain by fine-grained sands and interbedded sands and clay with shell fragments and terrestrially-derived organic material. Inclined heterolithic stratification (IHS) is the dominant macro-scale sedimentary structure developed within this interval. In the upper part of the incised valley a large (up to 800 m wide and 23 m deep), highly-sinuous channel, with very well-developed lateral accretion surfaces, is exceptionally well imaged in the 3D seismic data. The valley fill is capped by *ca.* 16 m of clay, which contains shell fragments and some lenticular sand layers.

It is estimated that the Late Pleistocene incised valley was formed at or near the Last Glacial Maximum (LGM) when a significant sea-level fall of *ca*. 120 m exposed the low-gradient (<0.1º) Sunda Shelf. This incised valley represented an axial drainage system

which ran along the length of the Malay Basin during the latest Pleistocene. It is speculated that this valley extended >1200 km from the Gulf of Thailand in the north to the South China Sea in the east, and formed part of the Johore/palaeo-Chao Phraya river system that drained into the South China Sea during the Late Pleistocene.

5.2 Introduction

Incised valleys are defined as fluvially-eroded, elongate topographic lows that are typically significantly wider (e.g. up to several kilometres) and deeper (e.g. up to several tens of metres) than that associated with a single channel form (Dalrymple et al., 1994; Schumm and Ethridge, 1994; Zaitlin et al., 1994; Hampson et al., 1997; Reynolds, 1999). Incised valley systems are economically important as the contained lowstand and transgressive deposits may represent significant hydrocarbon reservoirs in many sedimentary basins (Van Wagoner et al., 1990; Zaitlin et al, 1994). The recognition of the erosional surfaces at the base of incised valley systems provides important criterion for the identification of sequence boundaries when applying sequence-stratigraphic concepts to ancient sedimentary succession (Vail et al., 1977; Posamentier and Vail, 1988; Van Wagoner et al., 1990; Shanley and McCabe, 1993; Wright and Marriott, 1993).

Incised valley systems are formed by fluvial incision as a result of: 1) relative or eustatic sea-level fall; 2) tectonic uplift; 3) climatic change (e.g. increased rainfall) resulting in increased discharge; or 4) stream capture which results in increased discharge in the composite drainage system (Schumm and Ethridge, 1994; Thorne, 1994; Posamentier, 2001). In coastal settings, incised valleys usually form in response to fluvial incision during relative sea-level fall and shelf exposure; they are then typically filled during the

subsequent relative sea-level rise (Dalrymple et al., 1994). Fluvial systems respond relatively rapidly to changes in relative sea-level (e.g. Fisk and McFarlan, 1955); this may be associated with the systems changing their sinuosity, width and/or depth (Blum and Törnqvist, 2000; Schumm, 2005). In particular, Schumm (1993) indicated that deep river incision may occur in association with a significant fall in relative base-level, and that the geometric characteristics of the fluvial incision (e.g. width, depth, etc) are determined by the magnitude of the base-level fall (Posamentier, 2001). When a significant fall in relative sea-level occurs and a former shallow marine shelf is fully or widely exposed, an incised valley may form (Van Wagoner et al., 1990; Posamentier and Allen, 1999; Posamentier, 2001). When a relative sea-level does not expose the entire shelf, lowstand alluvial bypass channel systems (*sensu* Posamentier, 2001) and associated shelf delta may develop.

Zaitlin et al. (1994) has divided incised valleys into two different types based on the overall gradient of the contained fluvial-estuarine complex: 1) piedmont incised valleys; and 2) coastal-plain incised valleys. Piedmont incised valleys are typically steeper and more structurally-controlled. Additionally, Zaitlin et al. (1994) identified three longitudinal segments of incised valleys fills that describe and define the degree of the effects of marine and fluvial processes; these include: 1) *Segment 1* – this is the *marine incised valley*, which is a seaward zone dominated by wave and/or tidal process; 2) Segment 2 – this is the *estuarine incised valley*, which is an intermediate zone of mixed energy associated with both marine and non-marine deposits; and 3) Segment 3 – this is the *non-marine incised valley*, which is a landward zone dominated by riverine sedimentation. Incised valleys systems can be further divided into a "simple incised valleys" or "compound incised valleys" based on the presence or the absence of multiple internal sequence boundaries within the incised valley fill (Zaitlin et al., 1994).

Incised valley systems have been recognised throughout the geological record (Dalrymple et al., 1994; Zaitlin et al., 1994). However, much of our understanding of their form, genesis and fill comes from analysis of Quaternary incised valley systems, which are very common features on many continental selves around the world (e.g. Posamentier and Allen, 1993; Reynaud et al., 1999; Nordfjord et al., 2006; Green, 2009; Paquet, et al., 2010). Quaternary incised valleys have been recognised on the Sunda Shelf, Southeast Asia using high-resolution 3D seismic reflection data (e.g. Miall, 2002; Hanebuth and Stattegger, 2003; Darmadi et al., 2007; Kiel, 2009). However, the internal architecture and sedimentary fill of these valleys is not well documented. Furthermore, the regional relationship of these incised valleys to the larger fluvial drainage area on Sunda Shelf is not presented in these case studies.

The main objective of this paper is to describe the form and fill, and interpret the genesis of a major incised valley system on the Sunda Shelf, Southeast Asia. This analysis is based on the shallow portion (<500 ms) of a high-resolution, 'mega-merge' 3D seismic reflection dataset, supplemented by high-resolution site survey data which includes platform borings and boomer data (see below). Integrating these data provides a unique opportunity to evaluate the form, fill and genesis of the major incised valley system on the Sunda Shelf. The valley system under investigation was part of a regionally extensive drainage network (*ca*. 750,000 km²) that extended throughout the Malaysian-Thailand part of the Sunda Shelf during the Late Pleistocene.

5.3 Geological Setting

5.3.1 Tectono-stratigraphic evolution

The Malay Basin is situated in the centre of the Sunda Shelf, Southeast Asia, which is one of the largest intracontinental shelf areas in the world (*ca*. 125,000 km²) (Madon, 1999; Figure 5.1). The north-west southeast trending Malay Basin is 500 km long by 250 km wide and is located between the Penyu and West Natuna basins to the south, and the Pattani Basin to the north (Hutchison, 1989; Madon et al., 1999; Figure 5.1). The basin formed as a result of tectonic extension during the Late Eocene to Early Oligocene, following the collision of India with the Asian continent (Tapponnier et al., 1986; Hutchison, 1989). The basin comprises a thick succession (>8 km) of Oligo-Miocene to Recent deposits, which overlie pre-Tertiary 'basement' consisting of metamorphic, igneous and sedimentary rocks (Figures 5.2 and 5.3). The structural evolution of the Malay Basin can be divided into three tectono-stratigraphic phases (Tjia, 1994; Madon, 1998; Negah et al., 1996 and Tjia and Liw, 1996): 1) a pre-Miocene syn-rift phase; 2) an Early to Middle Miocene post-rift phase, dominated by thermally-induced subsidence and basin inversion; and 3) a Late Miocene to Recent phase, dominated by thermally-induced subsidence after the main period of basin inversion (Figure 5.3).

The pre-Miocene extensional phase represents the initial phase of basin development, when subsidence was controlled by normal faulting (Hamilton, 1979; Madon, 1999). Sedimentation was characterised by alternating sand-dominated and shale-dominated fluvio-lacustrine sequences within a series of isolated half-graben (Madon, 1999). The Early to Middle Miocene post-rift phase was dominated by thermal subsidence that was accompanied by intermittent periods of compressional, inversion-related deformation. This resulted in local inversion of syn-rift half-graben and re-activation of their bounding

faults; this was particularly intense in the southern part of the basin and is associated with the south-western flank of the Malay Basin being slightly steeper than the north-eastern flank (Figure 5.3) (Madon, 1999). During this post-rift phase, deposition was characterised by coastal to shallow marine sequences.

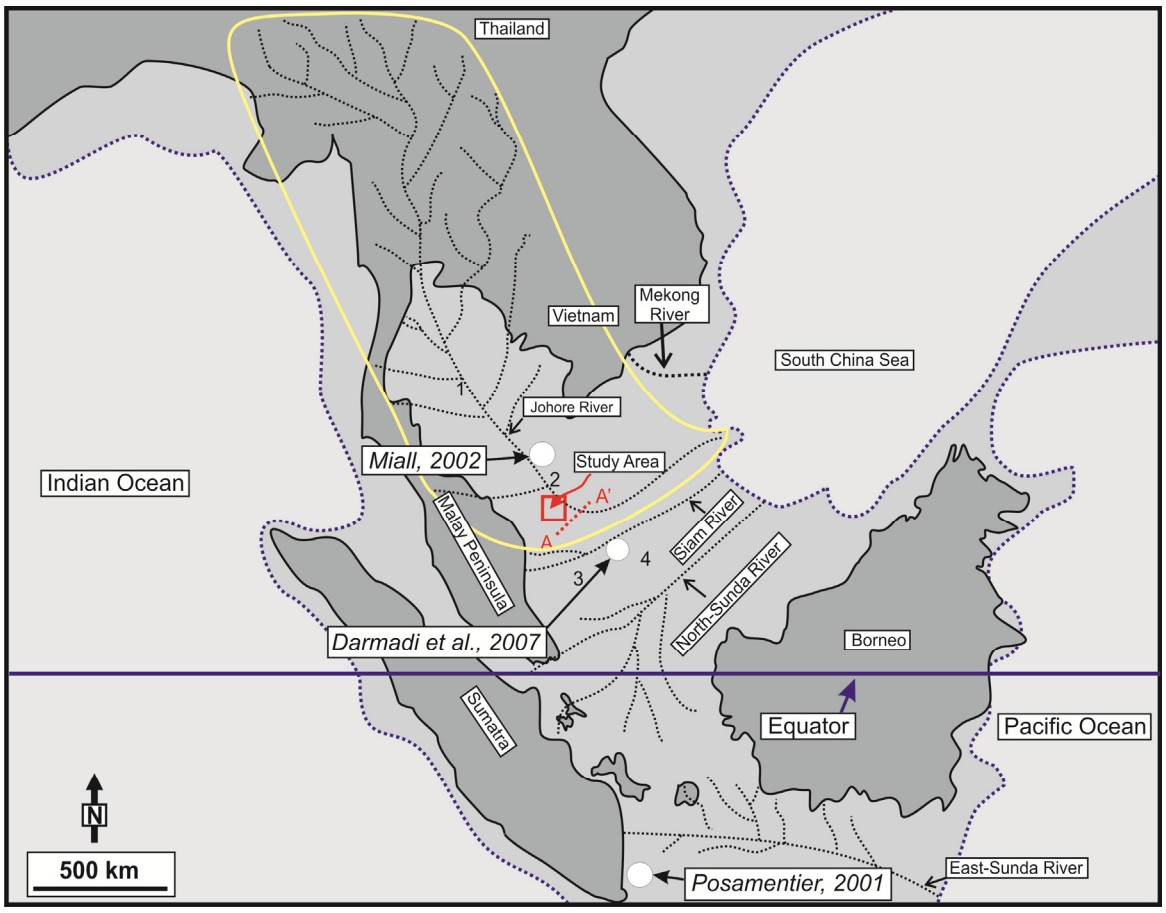

Figure 5.1: Location map of the study area within the Malay Basin (2) on Sunda Shelf, Southeast Asia. Locations of other basins (Pattani Basin (1); Penyu Basin (3); and West Natuna Basin (4)) within the Sunda Shelf are also shown. The study area is *ca*. 700 km away from the shelf break and a few hundred kilometres basinward of the modern shoreline. The blue dashed-lines represent the shallow areas of the Sunda Shelf that were exposed during the sea-level falls. The second major modern river system (~ 70 km west of the Chao Phraya) in Thailand is the Maeklaeng river which enters the present Gulf of Thailand was the left-bank tributary of the extended Paleo-Chao Phraya river system during the Pleistocene lowstands (Morley and Westaway, 2006). The black solid-lines represent the paleo-drainage systems that are still detectable on the modern sea floor (edited from Molengraaff 1921; Tjia 1980; Voris, 2000). The water depth within the study area ranges from 50 to 80 m indicating that during the lowstand, the Sunda Shelf was widely exposed. The red solid-line represents the regional cross-section shown in Figure 5.3. The blue solid-line represents the equator line. Locations of previous studies of Posamentier (2001), Miall (2002) and Darmadi et al. (2007) that were conducted on SE Asia are shown.

The Late Miocene to Recent phase was dominated by thermally-induced subsidence, without any significant tectonic activity (Madon et al., 1999). Deposition during this phase was mainly within coastal plain and shallow marine environments (i.e. Pilong Formation, Madon, 1999b).

5.3.2 Physiographic and paleoclimatic setting

The Sunda Shelf is one of the largest tropical shelf areas in the world (Hanebuth and Stattegger 2003). It is situated at the south-western margin of the South China Sea, the largest marginal sea of Southeast Asian (Figure 5.1). The shelf is extremely broad (up to 800 km at its widest point) and has a very low-gradient (<0.1º). The Sunda Shelf was tectonically stable during the Pliocene and Pleistocene (Madon, 1998). It is located at the equator, near the "West Pacific Warm Pool"; this suggests that the climate during the Last Glacial Maximum (LGM) was similar to the tropical climate which characterises the Southeast Asia lowlands present-day (Morley, 2000; Sun et al., 2000). However, monsoon-driven precipitation during the LGM was lower than during the Holocene, suggesting that vegetation patterns in lowland areas, such as the Sunda Shelf, were potentially affected by the dry winter-monsoon (Wang et al., 1999).

The present-day water depth within the study area ranges from 50-80 m, with the average water depth across much of the Sunda Shelf being *ca*. 70 m. The shelf break occurs at *ca.* 180-220 m beneath present-day sea-level. During the middle Pleistocene, the growth of continental glaciers decreased ocean volume and caused a reduction in sea-level of between *ca*. 160 m and *ca*. 120 m during the LGM (Gascoyne et al., 1979; Hopkins, 1982; Yang and Xie, 1984; Hanebuth et al., 2003; Hanebuth and Stattegger, 2003; Voris,

2000). Hence, most of the Sunda Shelf was subaerially exposed during the LGM, with the shoreline interpreted to have been located close to the present-day shelf break (Figure 5.1; Hanebuth et al., 2003; Hanebuth and Stattegger, 2003; Voris, 2000). Consequently, the South China Sea was significantly smaller than it is present day and formed a semi-enclosed marginal sea (Sathiamurthy and Voris, 2006).

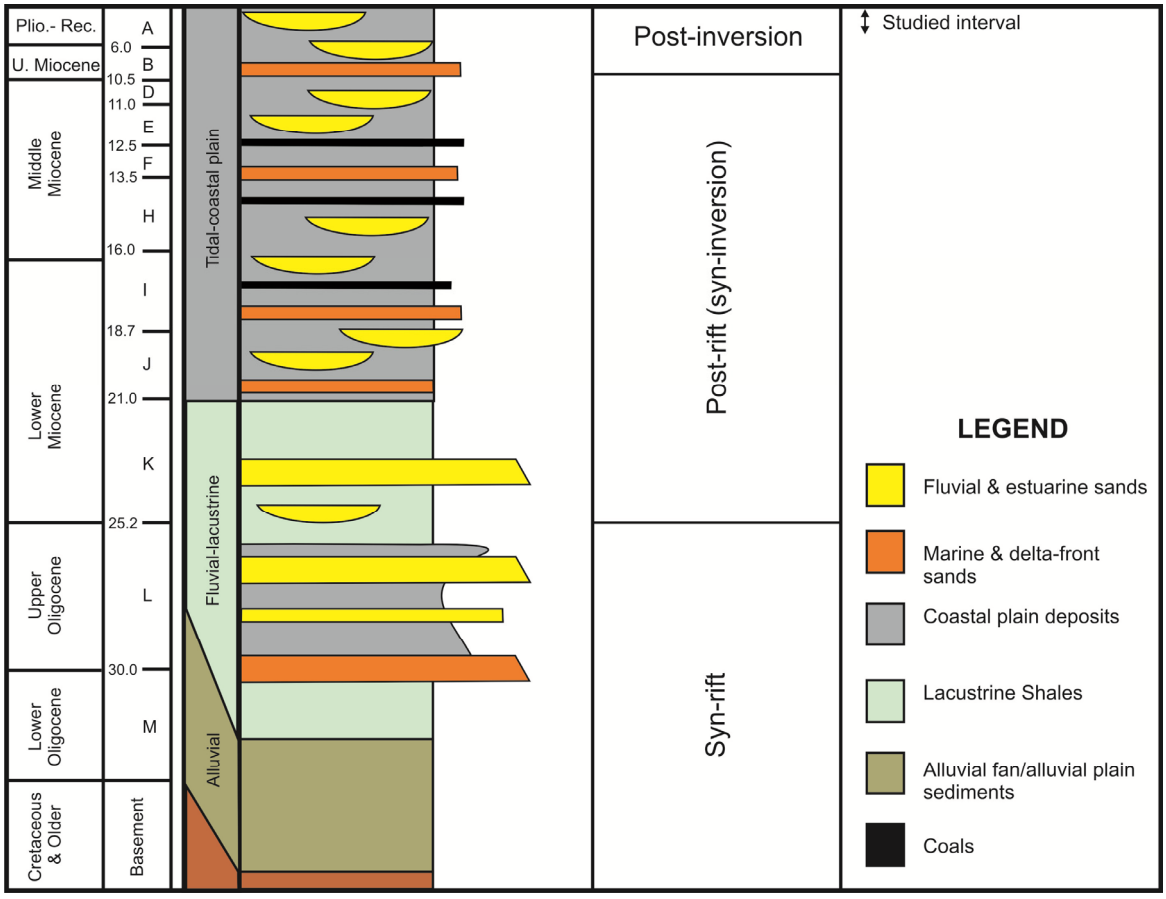

Figure 5.2: Generalised stratigraphic column of the Malay Basin. The studied interval is the upper part of Group A succession which is mainly composed of coastal plain deposits (Modified from Madon, 1999d).

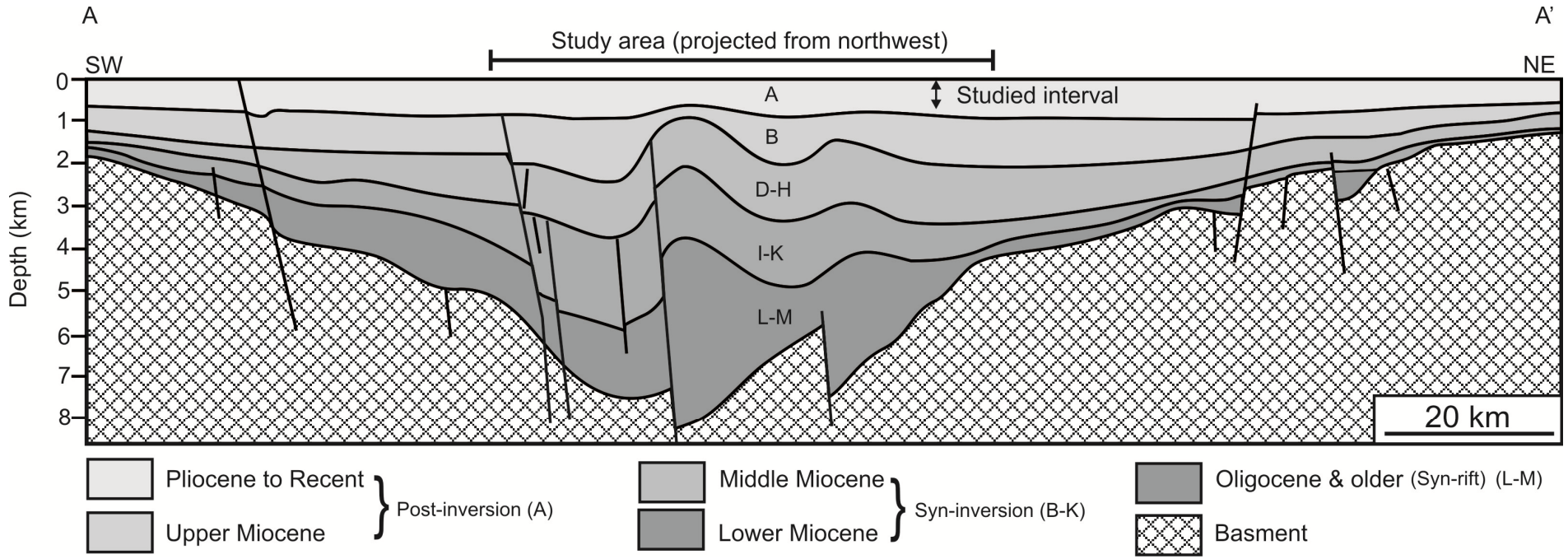

Figure 5.3: Regional cross-section of the Malay Basin. The main regional stratigraphic intervals are labelled A-M. Location of this cross-section is shown in Figure 5.1. The studied interval lies within the Upper post-inversion Pliocene to Recent (Modified from Madon, 1999d).

Based on present-day bathymetric contours, Voris (2000) and Sathiamurthy and Voris (2006) presented a series of maps that estimated the exposed area of the Sunda Shelf during Pleistocene to Recent sea-level lowstands. These maps highlight several major submerged valleys, or paleo-'trunk' river systems with associated tributaries (black dashed-lines in Figure 5.1). These valleys are typically expressed on the modern sea floor as elongate depressions that are up to several hundreds of kilometres in length (Figure 5.1). One of these major trunk rivers, called the Johore River (Voris, 2000), ran south-eastwards through the Gulf of Thailand, the Malay Basin and ultimately to the South China Sea. Morley and Westaway (2006) also described a similar paleo-river system called the paleo-Chao Phraya River, which ran through the Gulf of Thailand to South China Sea during much of the Cenozoic and including the Late Pleistocene; this river is thought to be synonymous with the Johore River. Importantly, the present study area is located close to the axis of the pre-Holocene Johore River (Figure 5.1).

Although sediment may have been sourced from the Malay Peninsula to the west, the Johore River/paleo-Chao Phraya probably represented one of the major sediment sources for the Malay Basin (Loe, 1997; Morley and Westaway, 2006). The paleo-river drained a large catchment area (*ca.* 750,000 km²) located in the northern part of Thailand. Clift (2006) suggested a reduction in sediment budget that was transported to the Sunda shelf through the Gulf of Thailand during the Late Miocene to Recent especially during LGM; this estimate is based on a reconstruction of the clastic mass accumulation on continental margins derived from well logs and seismic profiles, and from data published by Me´tivier et al. (1999). Furthermore, Hutchinson (1989) suggested that the basins in the Gulf of Thailand, including the Malay Basin, were supplied by vast quantities of clastic material derived from rising mountain belts such as Himalayas and were transported by giant rivers such as the Mekong River. It is believed that the (paleo) Mekong River

flowed through the Malay Basin during much of the Cenozoic until it diverted to the east by the faulting during the Late Cenozoic (Hutchinson, 1989). The Mekong River now enters the Sunda Shelf through Vietnam. Sinsakul (1992) and Morley and Westaway (2006) concluded that during the LGM, when a reduction in sediment supply occurred, much of the earlier highstand deltaic deposits inland of the modern coastline of the Gulf of Thailand were reworked by the Johore River/paleo-Chao Phraya river and deposited in the South China Sea.

5.4 Data Sources and Methodology

This study used a 3D seismic reflection dataset with a total areal extent of *ca*. 11500 km^2 (*ca.* 115 km wide by *ca.* 100 km long) and site survey data (see below) from sixty-five locations (Figure 5.4).

5.4.1 3D seismic data

The seismic dataset comprises ten separate seismic surveys that have been merged into a single 3D volume (so-called 'mega-merge' survey). The dataset is zero-phase processed with SEG normal polarity, in which a positive (peak) event (red or yellow reflection on seismic sections) represents a downward increase in acoustic impedance, and a negative (trough) event (blue or black white reflection on seismic sections) represents a downward decrease in acoustic impedance (Brown, 2004). In-line and cross-line spacing within these surveys are 9.38 m and 12.5 m, respectively. The vertical record length is 600 milliseconds two-way time (ms twt). The vertical sampling intervals of all surveys is 2

ms, except within one survey which has a sampling interval of 1 ms. The dominant seismic frequency ranges from 60-70 Hz. Unfortunately, only limited well data are available to calibrate the seismic data, as most wells within the area targeted the deeper, productive, Miocene succession. However, depth and thickness measurements were converted from the milliseconds two-way time (ms twt) to metres by using velocity information (i.e. check-shot data) from one reference well (Tunggal-1; Figure 5.4). This well indicates that the average velocity of the shallow part of the basin fill is *ca*. 1880 m sec^{-1}. Based on estimates of the frequency and velocity, the vertical resolution of the seismic data ranges from *ca*. 6.7 to 7.8 m. The lateral resolution of the data ranges from *ca.* 11.5 to 15.5 m.

The quality of the seismic data within the studied interval is generally excellent, although exact amplitude values vary between different surveys due to variations in the acquisition and processing parameters. Fortunately, this does not unduly hamper the overall imaging and mapping of fluvial systems. There are also marked 'acquisition footprints' in the upper parts of several of the individual datasets within the merged survey. These footprints appear as amplitude 'stripes' on horizontal seismic 'timeslices' and as small discontinuities along reflection events on seismic cross-sections. Finally, some of the individual surveys within the mega-merge survey have not been optimally merged as observed by minor (<4 ms) vertical offset of correlative reflection events. Fortunately, most of these minor issues can be overcome by using a combination of map-view and cross-section images, thereby ensuring that only true geological features are interpreted.

Interpretation of depositional features has been achieved by the use of 'timeslices' (i.e. horizontal seismic slices taken through the original reflectivity 3D seismic volume; *sensu* Zeng et al., 1998; Brown, 2003; Posamentier et al., 2007; see also Figure 4.5A in Chapter 4). Time slices are only useful when the geological features of interest, and the

stratigraphic timelines along which they are developed, are horizontal to sub-horizontal; this in the case in the shallow, undeformed part of the succession studied here (Figure 5.5). To fully document the form and fill of the incised valley, time slices have been examined at 2 ms intervals.

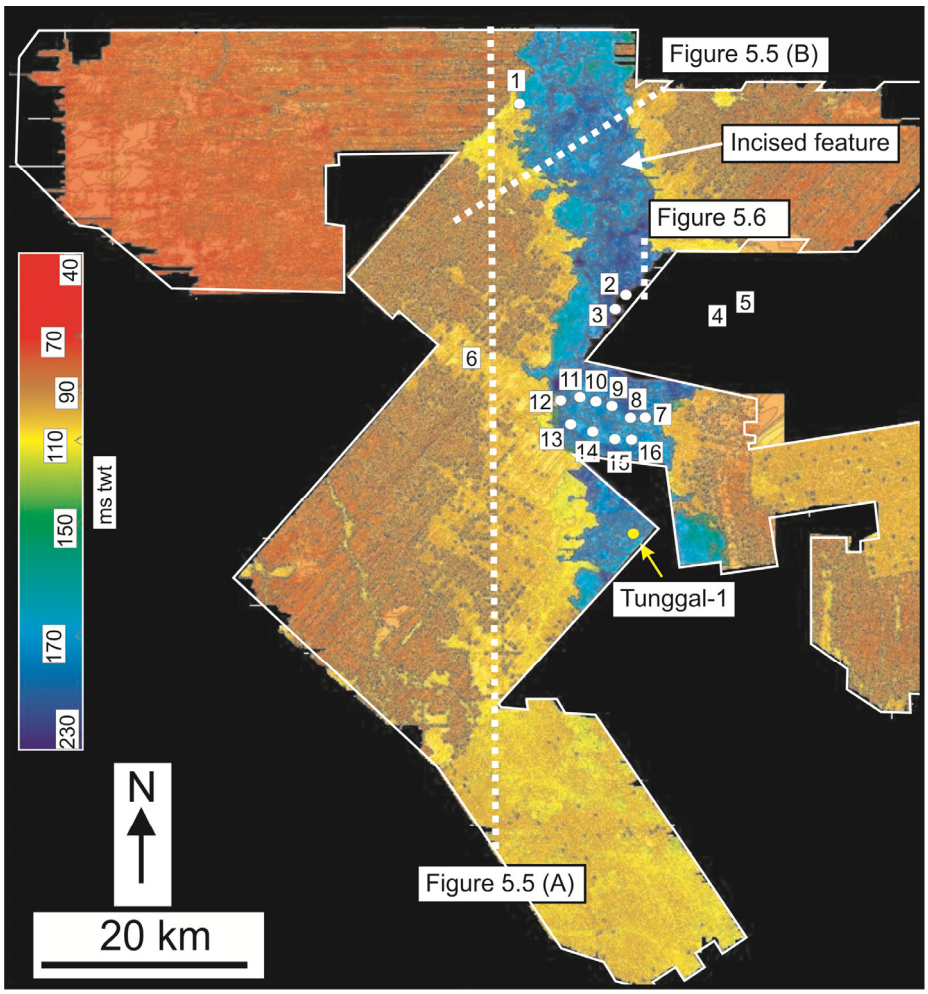

Figure 5.4: Time-structure map along Horizon (D.1) showing a significant relief (blue area) in the central part of the study area. The seismic data used in this study consist of ten surveys that have been merged to make a single interpretable volume. The yellow-circle represents the location of the well (Tunggal-1) that was used in the time-depth conversion. The white-circles represent the locations of the borings used in this study (see Table 5.1 for more details). The white-dashed lines and the white sold-line illustrate the locations of the seismic sections shown on Figures 5.5 and boomer section shown on Figure 5.6, respectively.

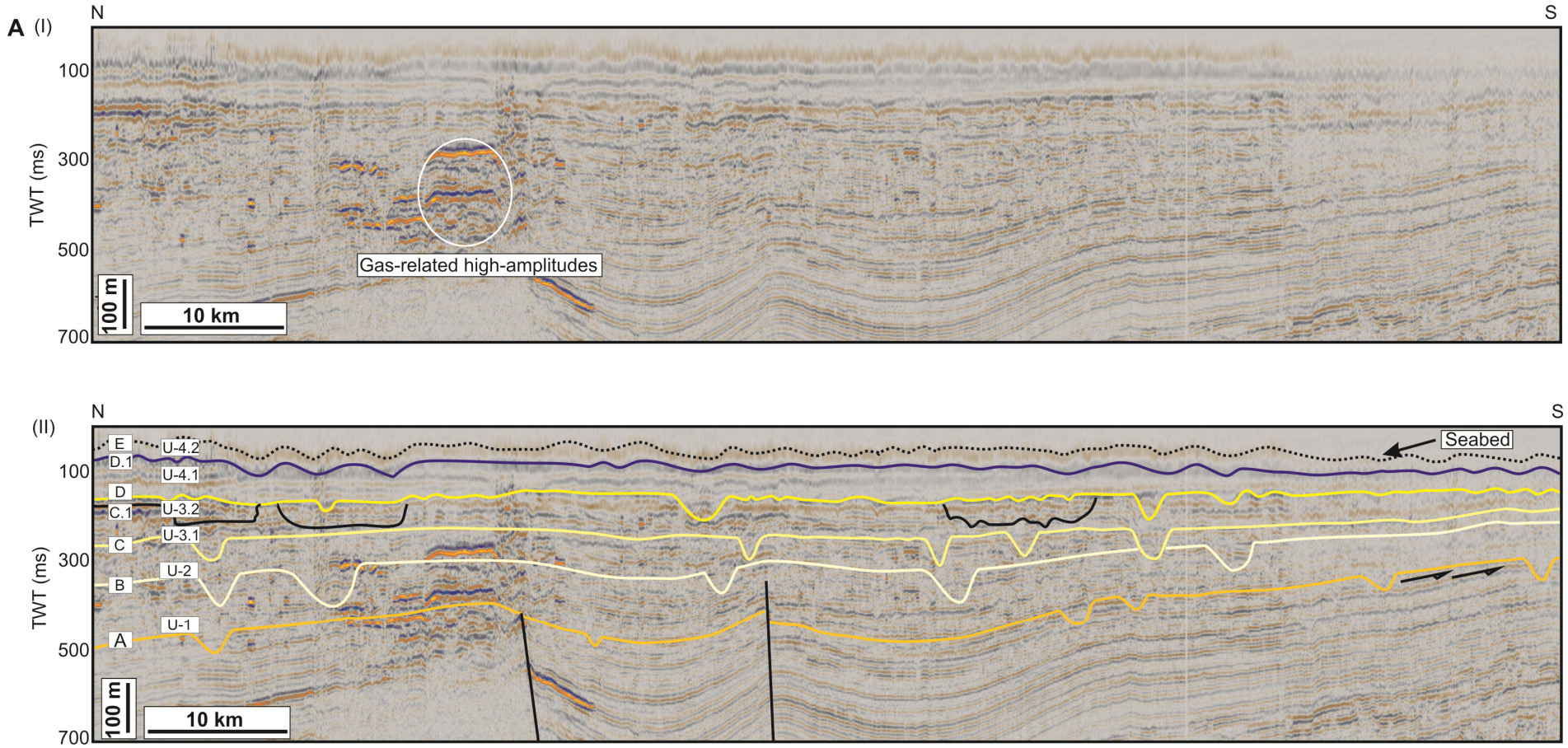
A (I)
N
S
100
300
500
700
TWT (ms)
Gas-related high-amplitudes
100 m
10 km
(II)
N
S
E
D.1
D
C.1
C
B
A
U-4.2
U-4.1
U-3.2
U-3.1
U-2
U-1
Seabed
100
300
500
700
TWT (ms)
100 m
10 km

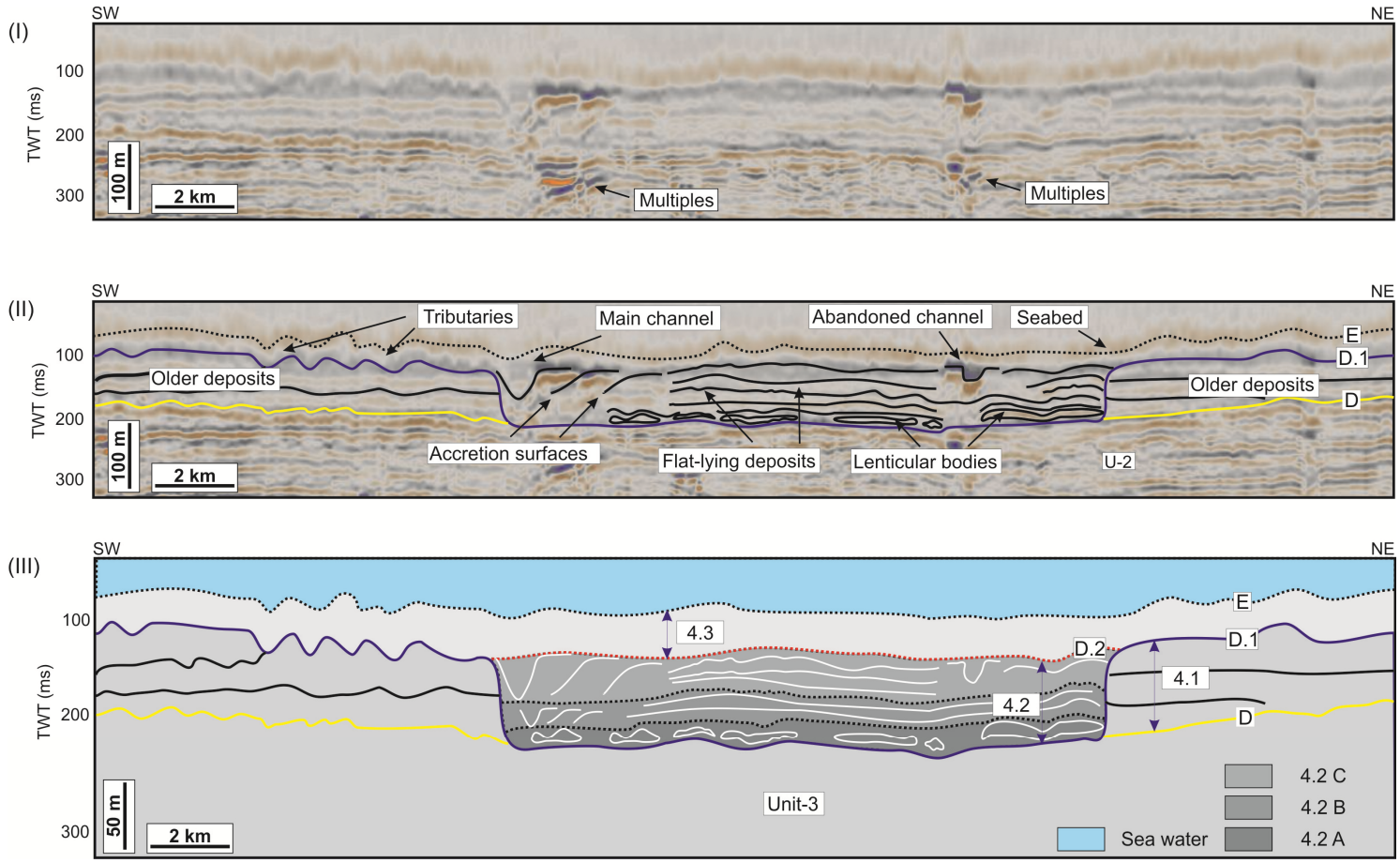

Figure 5.5: A) (I) Un-interpreted and (II) interpreted regional seismic section through the 3D seismic dataset illustrating the seismic units (1-4) and the bounding surfaces (Horizons A-E). Major channel systems are also shown as white 'u' and 'v' shapes. The main bounding surfaces (Horizon A-D) are characterised by prominent incisions. Note the angular discordance between Horizon A and underlying unit at the basin margin (right side of cross-section). Location of this section is shown in Figure 5.4. **B)** (I) Un-interpreted and (II & III) interpreted seismic section through the 3D seismic dataset illustrating the sub-units of Unit 4 and the bounding surfaces (D, D.1,D.2 & E). Note the seismic expression within the deep incision is different from the adjacent strata. V-shaped channel morphology associated with accretion surfaces which is underlain by lenticular bodies is also shown. Truncations at the valley margin are recognised. Location of this section is shown in Figure 5.4.

Mapping of the stratigraphic occurrence of channels is challenging as channels commonly incise downwards from a variety of stratigraphic levels and may be superimposed on a succession of seismic slices. In addition, seismic 'multiples' from shallower channels may mask channels imaged at lower stratigraphic levels. However, through analysis of a combination of seismic sections and timeslices, only true geological features were interpreted.

5.4.2 Site Survey Data

Site survey data from 65 locations have been analysed in this study. The site survey data consists of the following data types:

1) Sixteen platform borings, which are 30-150 metres in length, provide information on the lithology and facies of the stratigraphic fill of the incised valley (Table 5.1 and Figure 5.4; Appendix 8.3). The geographic coordinates of these borings were imported into ArcGIS and then superimposed onto a time-slice at 108 ms twt to such that their locations with respect to the studied incised valley could be visualised.
2) 40 km^2 of high–resolution, multi-channel, 2D seismic data (typical individual line length of 2 km) with frequencies of up to 250 Hz; although these data theoretically provide a higher vertical resolution of stratigraphic layering (e.g. *ca.* 2 m) than the standard 3D seismic data (e.g. *ca.* 6.8-7.8 m), this is often not the case. In addition, these 2D data are spatially-limited, thus these data are not widely used in this study.

3) Boomer data, which is analogous to seismic reflection data, but which has a dominant frequency range of 2-7 kHz (compared to 250 Hz for the high-resolution 2D seismic data and 60-70 Hz for the 3D seismic data). These data provide very high-resolution images (vertical resolution of *ca.* 300-500 cm) of the internal architecture of the uppermost part (maximum of 60 m below seabed) incised valley fill (Figure 5.6).
4) Side-scan sonar data, which provide detailed images of seabed irregularities that may be related to shallowly-buried, pre-Holocene fluvial channels and valleys.
5) Echo sounder data, which provides detailed water depth information by using high-frequency (200 kHz) transducer sources.
6) Geotechnical cores, which provide lithological information up to 3 m below the seabed.

Sixteen lithological logs have been constructed using the platform borings and shallow cores; from these logs an idealised log, which represents the bulk lithologies and sedimentological characteristics observed within the stratigraphic interval of interest, has been created (Figure 5.7). This log has then been tied to the seismic data using depth information in order to determine the lithological and sedimentological characteristics, and depositional facies which infilled the studied incised valley. This lithological information has also been used to interpret the boomer section (Figure 5.6).

5.5 Stratigraphic Framework

Based on seismic facies analysis, the Pleistocene to Recent succession has been divided into four seismic units (Units 1-4; Figure 5.5). The horizons bounding these units have

been mapped throughout the study area (Horizons A-E; Figure 5.5). Two additional horizons, Horizons C.1 and D.1, have been mapped within the upper part of Unit 3 and Unit 4, respectively, to allow further sub-division these units into two sub-units (i.e. sub-units 3.1, 3.2, 4.1 and 4.2; see Tables 5.2 & 5.3 and Figure 5.5B & C). Horizons C.1 and D.1 are both strongly erosive.

Table 5.1: lists the platform boring analysed in this study. Location of these borings relative to the incised valley (IV) is illustrated.

No.	Borehole name	Total depth (m)	Field	Water depth at well location (m)	Location
1	Melor	150	Melor Field	76.3	Within IV
2	Tangga Barat-1A	150	Tangga Field	70.9	Within IV
3	Tangga Barat-1B	150	Tangga Field	70.8	Within IV
4	BH Tangga	150	Tangga Field	65.3	Outside IV
5	Tangga Deep-1	30	Tangga Field	63.3	Outside IV
6	Bujang Deep-1	30	Bujang Field	66.1	Outside IV
7	Dulang A-Primary	150.6	Dulang Field	74.5	Within IV
8	Dulang A-Secondary	151.6	Dulang Field	74.7	Within IV
9	Dulang B	150.3	Dulang Field	79	Within IV
10	Dulang WP-B	60	Dulang Field	78.4	Within IV
11	Dulang WP-C	60	Dulang Field	75.7	Within IV
12	Dulang WP-D	60	Dulang Field	74.6	Within IV
13	Dulang SPM-1	30	Dulang Field	74.6	Within IV
14	Dulang SPM-2	45	Dulang Field	77.2	Within IV
15	Dulang SPM-3	45	Dulang Field	75.6	Within IV
16	Dulang SPM-C	45.6	Dulang Field	77.3	Within IV

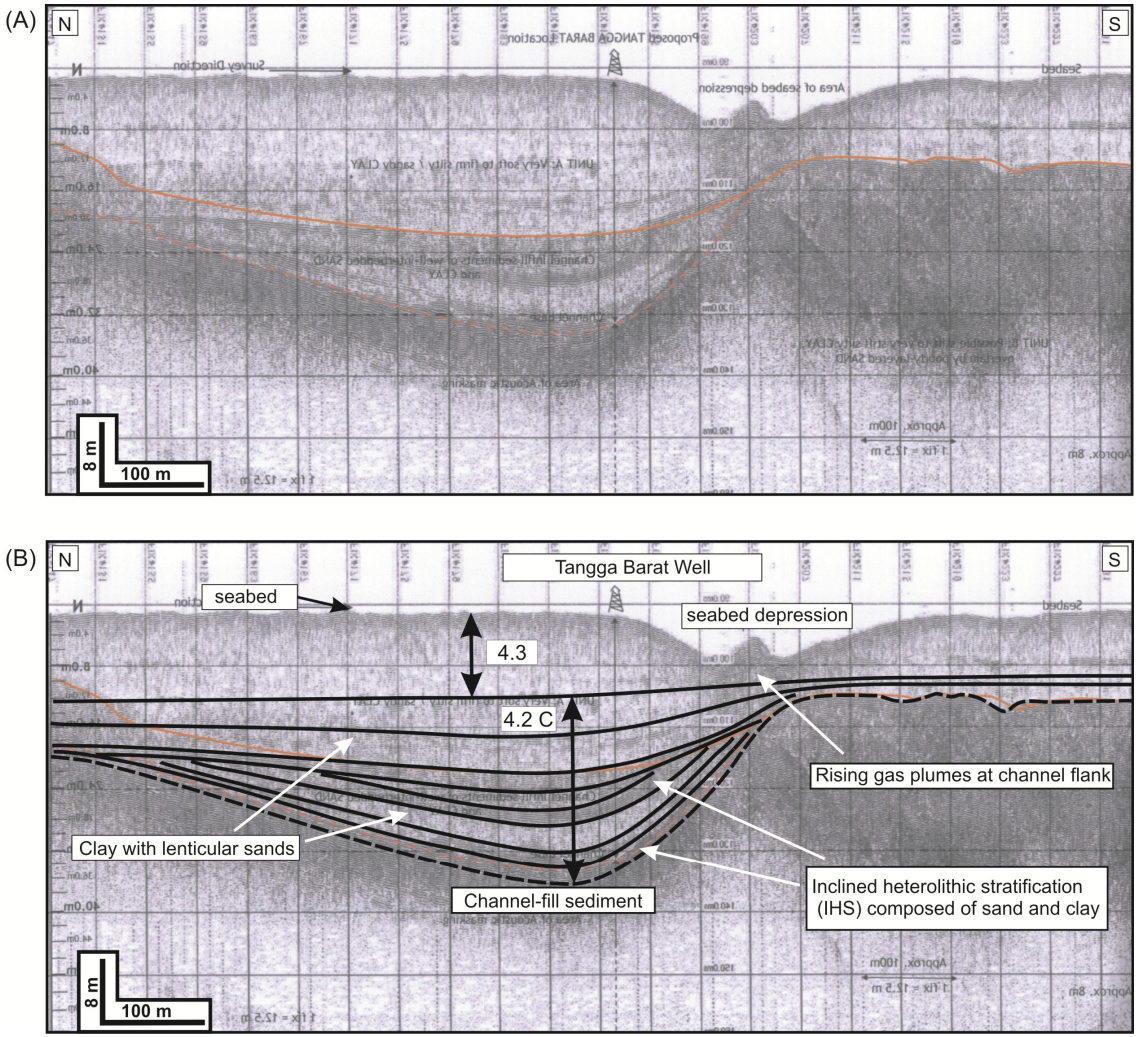

Figure 5.6: Uninterpreted **(A)** and interpreted **(B)** high-quality imaging of boomer data showing the v-shaped morphology of the highly-sinuous channel identified at the top of the incised valley. IHS of the channel fill is clearly imaged. Note the seabed depression caused by the rising gas plumes at the channel flanks. Location of this section is shown on Figure 5.4.

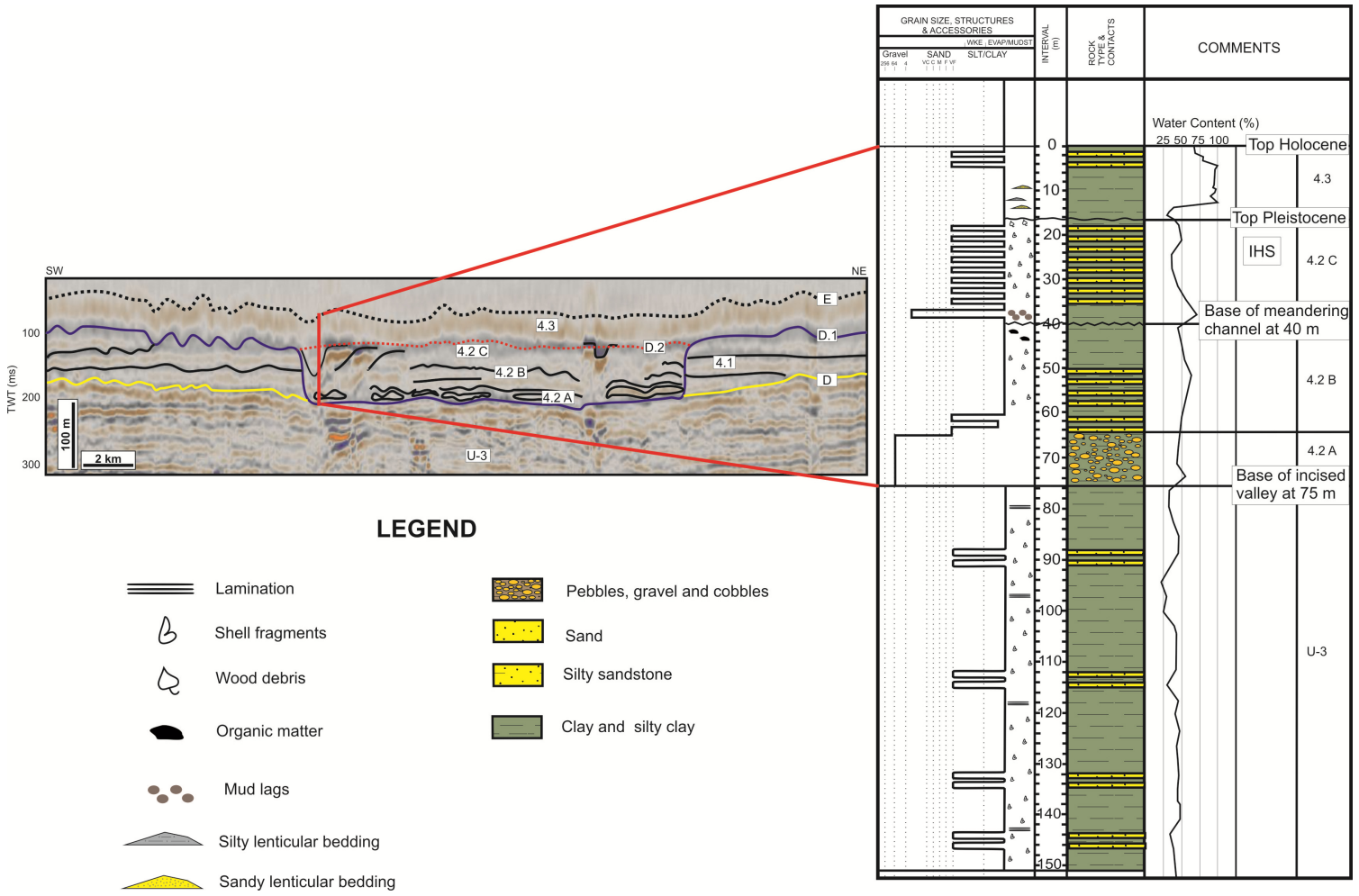

Figure 5.7: An idealised lithological log of the Late Pleistocene to Recent succession has been calibrated with the seismic data in order to determine the fill lithology of the Late Pleistocene incised valley. Gravels and cobbles with well-interbedded sands and stiff clay are observed at the base of the incised valley. The highly-sinuous channel at the top of the incised valley is mainly filled with stiff clay with inclined heterolithic stratification (IHS). These IHS are clearly imaged in the boomer section shown on Figure 5.6. Thick soft clay (16 m) capped the incised valley.

Table 5.2: lists the seismic units and sub-units which are identified within the Late Pleistocene succession within the Malay Basin. The basic information data including isochron range and average, channel width (CW), channel depth (CD) and sinuosity (SI) of the channel systems that have been observed in the lower and upper parts of each unit are illustrated.

Unit No.	Base horizon	Top horizon	Thickness range (ms twt)	Average thickness (ms twt)	Average thickness (m)	Channel parameters				Incised valley parameters		
						Stratigraphic Level	CW (m)	CD (m)	SI	width (m)	depth (m)	SI
4.3	D.2	E	100-82	18	16	NO channels observe				----------	------	----
4.2	D.1	D.2	192-100	92	87	Inside IV	600	25	3	13000-18000	55-87	1.2
						Outside IV	320-600	15-32	1.1.15	----------	------	----
4.1	D	E.1	228-108	120	112	U	75-320	8-20	1.3-1.5	----------	------	----
						L	300-1300	15-30	1-1.3	----------	------	----

Table 5.3: lists the sub-units identified within sub-unit 4.2. The basic information data including isochron range and average, channel width (CW), channel depth (CD) and sinuosity (SI) of the channel systems that have been observed in the lower and upper parts of each unit are illustrated.

Sub-unit No.	Average thickness (ms twt)	Average thickness (m)	Seismic facies character	Channel Parameters		
				CW (m)	CD (m)	SI
4.2 C	25-32	23-30	Type-2 channel morphology associated with dipping surfaces	600	25	3
4.2 B	22-30	20-28	Laterally-continuous reflections with no observed channel morphology	----------	------	----
4.2 A	12-15	10-13	Lenticular, discontinuous seismic facies	----------	------	----

Sub-unit 4.1 which is the oldest is characterised by laterally-continuous seismic facies. Sub-unit 4.2 which represents the main fill of the incised feature is characterised by a wide range of seismic facies which corresponds to a wide range of lithology. Based on these variations of seismic facies and lithology, sub-unit 4.2 has been further divided into three sub-units (i.e. sub-units 4.2A, 4.2B, and 4.2C; Table 5.3; Figures 5.5B). Sub-unit 4.3 is youngest and it caps sub-unit 4.2A schematic stratigraphic cross-section which illustrates the stratigraphic template and nomenclature used, and the vertical variability of fluvial channels within this framework are shown Figure 5.5B.

5.5.1 Seismic Facies Analysis of the Depositional Sequences

The vertical and lateral distribution of the channel and valley types identified within Unit 4 is described in the following sections.

5.5.1.1 Unit 4

As discussed above, Unit 4 has been divided into three sub-units (Tables 5.2; Figure 5.5B): 1) Sub-unit 4.1 (the oldest) is characterised by low-amplitude, laterally-continuous seismic reflections; 2) Sub-unit 4.2 is characterised by wide range of seismic facies, including chaotic and laterally-continuous seismic facies along with prominent, v-shaped channel-like incisions associated with inclined reflection events; and 3) Sub-unit 4.3 (the youngest) is characterised by low-amplitude, laterally-continuous seismic reflections. A full description of the seismic facies within these sub-units is given below. In addition,

the corresponding sedimentological character of these units is described, based on data derived from the platform borings and shallow cores.

5.5.1.1.1 *Sub-unit 4.1*

Description: The base of sub-unit 4.1 is defined by Horizon D. This is a high-amplitude reflection event along which prominent incisions, with v-shaped channel morphologies, are observed. These channels are up to 32 ms twt (30 m) deep (Figure 5.5). In planview, these channel features are 300-1300 wide and of low to very low-sinuosity (SI 1-1.3) (Figure 5.8A). Most channels flowed towards the south-east. In the middle of the study area, a major channel (22 ms twt (20 m) deep and 1 km wide) is observed which increases in sinuosity eastwards (from SI=1 to SI=1.2). In the southern part of the study area, several very low- to low-sinuosity channels (SI=1-1.15), which are 400-700 m wide and 12-15 m deep, are identified.

Within sub-unit 4.1, above the basal channel systems described above, channels of varying size and sinuosity are developed. For example, in the upper part of this sub-unit, several moderately-sinuous (SI=1.3-1.5), relatively small channels (22 ms twt (20 m) by 320 m wide) are recognised (Figure 5.8B). These channels are characterised by ‘v’ and ‘u’-shaped channel morphologies (Figure 5.5). These channels become less sinuous toward the SE, and appear to be partly eroded by the late deeply-incised feature of sub-unit 4.1 in the middle of the study area.

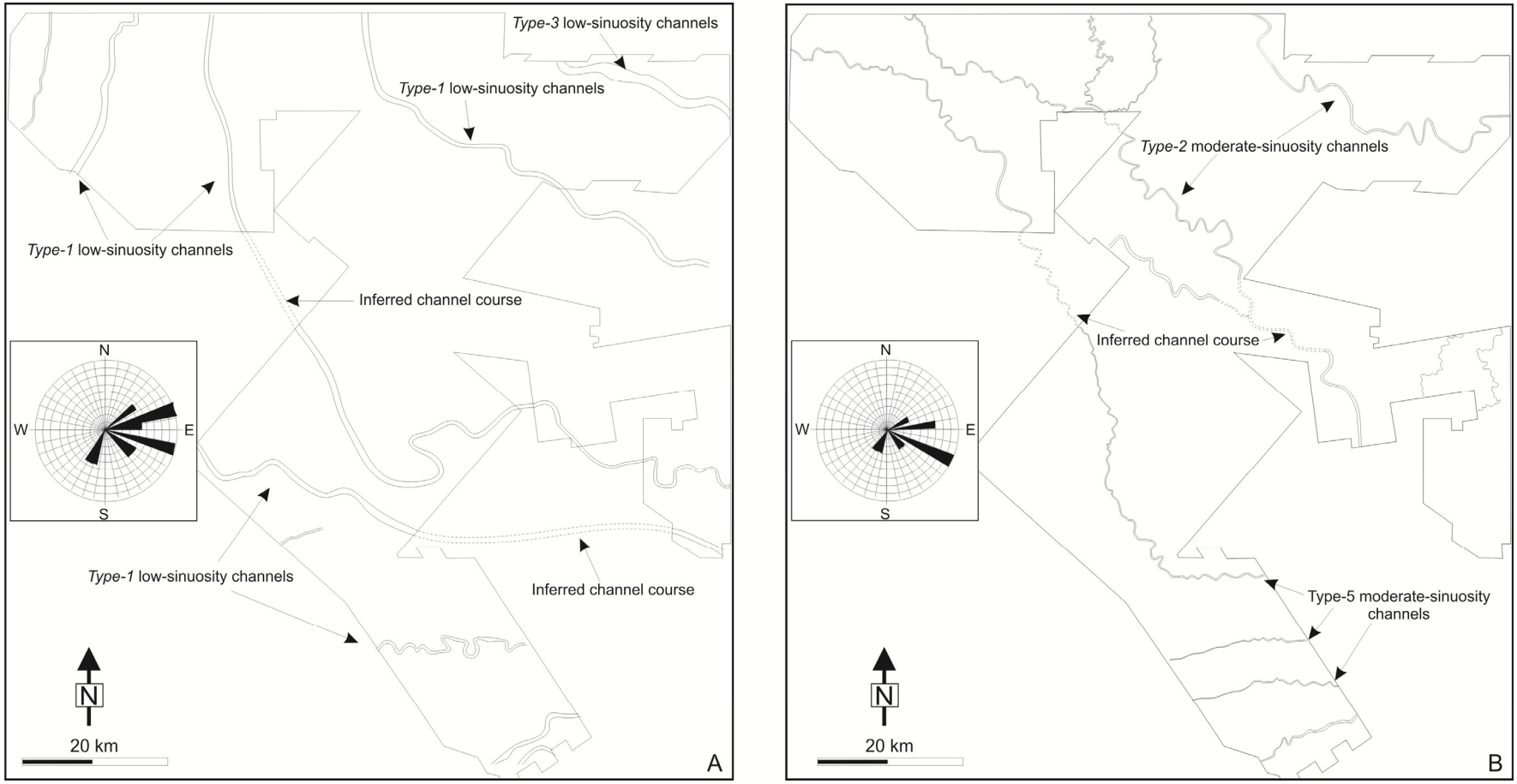

Figure 5.8: Two interpretive planview maps within sub-unit 4.1; **A)** shows the type of channels observed within the lower part of sub-unit 4.1 which is dominated by wide straight and very low-sinuosity channels. The major channels were broadly flowing to SE towards the South China Sea. The low-sinuosity channels in the southern part were flowing to NE towards the axial zone of the basin; **B)** shows the type of channels observed in the upper part of sub-unit 4.1 which is dominated by medium-scale, moderate-sinuosity channels with no scroll bars. Some parts of the channels in the middle part of the study area were eroded off by the latest deep incision of sub-unit 4.2. Channel orientations are represented by a rose diagram for each part of this sub-unit.

Lithology: Unfortunately, all the platform borings are located outside of the seismically-defined channels described above, hence the lithological fill of these channel is unknown; however, sub-unit 4.1 is dominated by very stiff, dark-grey, silty clays with some layers of fine-grained sands. The precise thicknesses of these fine-grained sands are not documented, although many of these units appear to be <1 m thick. Shell fragments are common in the middle part of this sub-unit. The upper part of sub-unit 4.1 which is beneath the adjacent interfluves and directly below Horizon D.1 is characterised by stiff, dark greenish-grey, silty clay, with traces of organic material. It is noted that shell fragments and organic material are absent in the lower part of this sub-unit.

5.5.1.1.2 *Sub-unit 4.2*

Description: The base of sub-unit 4.2 is defined by Horizon D.1; this is a high-amplitude reflection, along which a broad (13 km wide), deep (83 ms twtt (80 m)), N-S-trending, 'u'-shaped incision is identified in the middle of the study area (Figure 5.5B). Incision at the base of this feature results in the erosion of some of the channels systems within the underlying sub-unit 4.1. Outside of the main, deep, valley-like incision developed along Horizon D.1, smaller (*ca*. 50 m wide) incised features with 'v'-shaped channel morphologies are recognised (Figure 5.5B). In planview, these channels trend broadly perpendicular and link in to the main N-S-trending valley-related incision. In addition, they have a pronounced dendritic pattern, with progressively smaller incisions branching off larger incisions with increasing distance from the main valley-like incision (Figure 5.9A & C). In the southern part of the study area, relatively large (depths of 17-34 ms twt (15-30 m) and widths of 400-900 m), low-sinuosity (SI=1.1), SE-flowing channels are developed (Figures 5.9A & B). In cross section, the wide range of seismic facies within

the major incision feature is different from those outside the incision (Figure 5.5B). Furthermore, reflection events within sub-unit 4.1 are truncated at the margin of this deep incision. Sub-unit 4.2 displays a wide range of seismic facies and is characterised by a variety of lithologies. Based on these variations, this sub-unit has been sub-divided into three sub-units:

5.5.1.1.2.1 Sub-unit 4.2A

Description: Sub-unit 4.2A has an average thickness of 12-15 ms twt (10-13 m; Table 5.3) and is located just above the surface (Horizon D.1) defining the base of sub-unit 4.2. Internally, sub-unit 4.2A is characterised by a series of chaotic, lenticular bodies (Figure 5.5B). Due to the poor imaging caused by seismic multiples generated by an overlying channel (see below), the planview morphology of these lenticular bodies is difficult to confidently define.

Lithology: 75 m below the sea-bed and directly above the basal erosion surface (Horizon D.1), a 10 metre thick unit of pebbles, gravel and possibly cobbles are reported (see also Isa, et al. 1992; Figure 5.7). This unit is overlain by a 3 -5 m thick unit of fine-grained sands. Together, the 10 m thick very coarse-grained unit and the 3-5 thick sandstone unit appear to correspond to the chaotic, lenticular seismic facies described above (Figures 5.5B & 5.7).

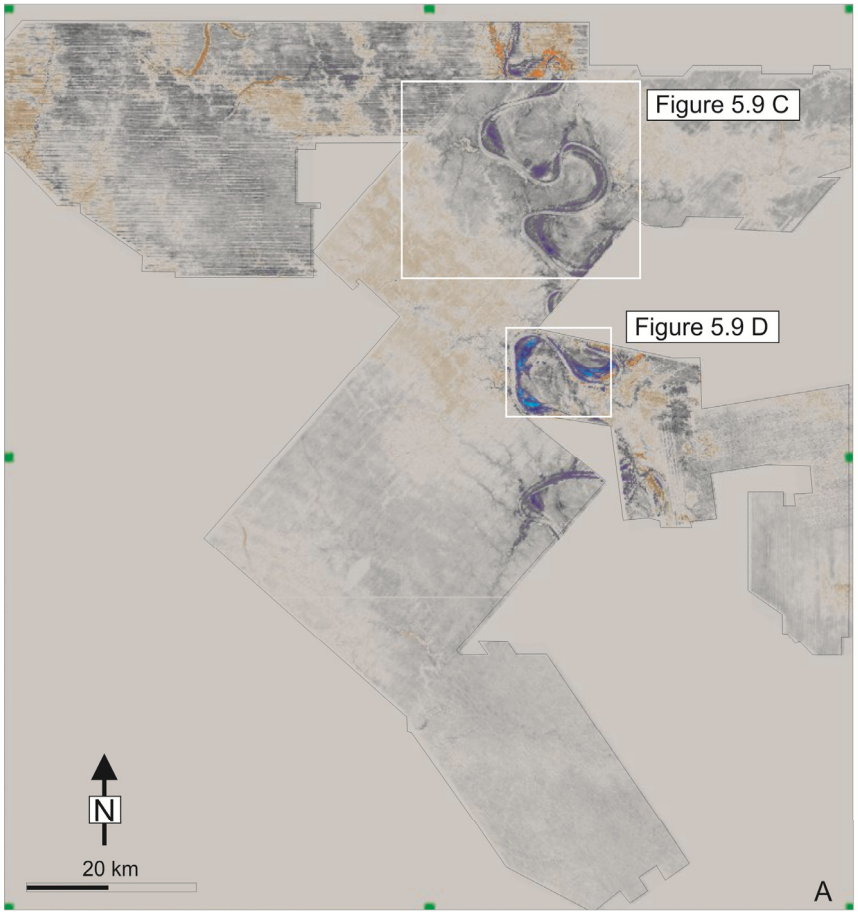
Figure 5.9 C
Figure 5.9 D
N
20 km
A

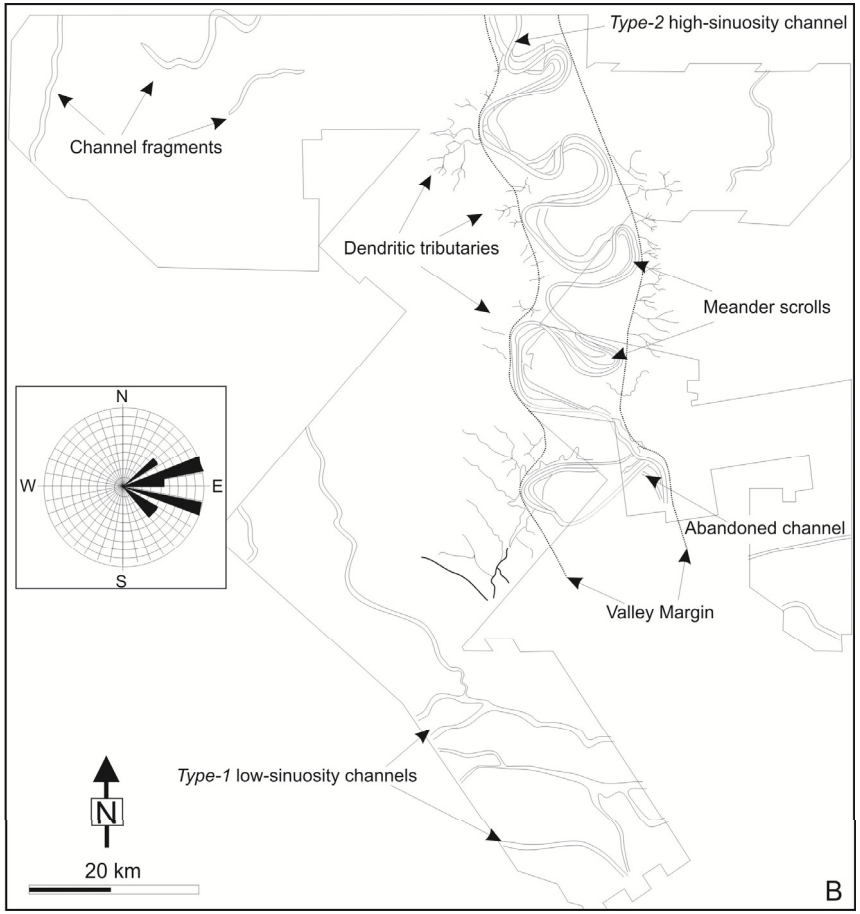
Type-2 high-sinuosity channel
Channel fragments
Dendritic tributaries
Meander scrolls
N
W
E
S
Abandoned channel
Valley Margin
Type-1 low-sinuosity channels
N
20 km
B

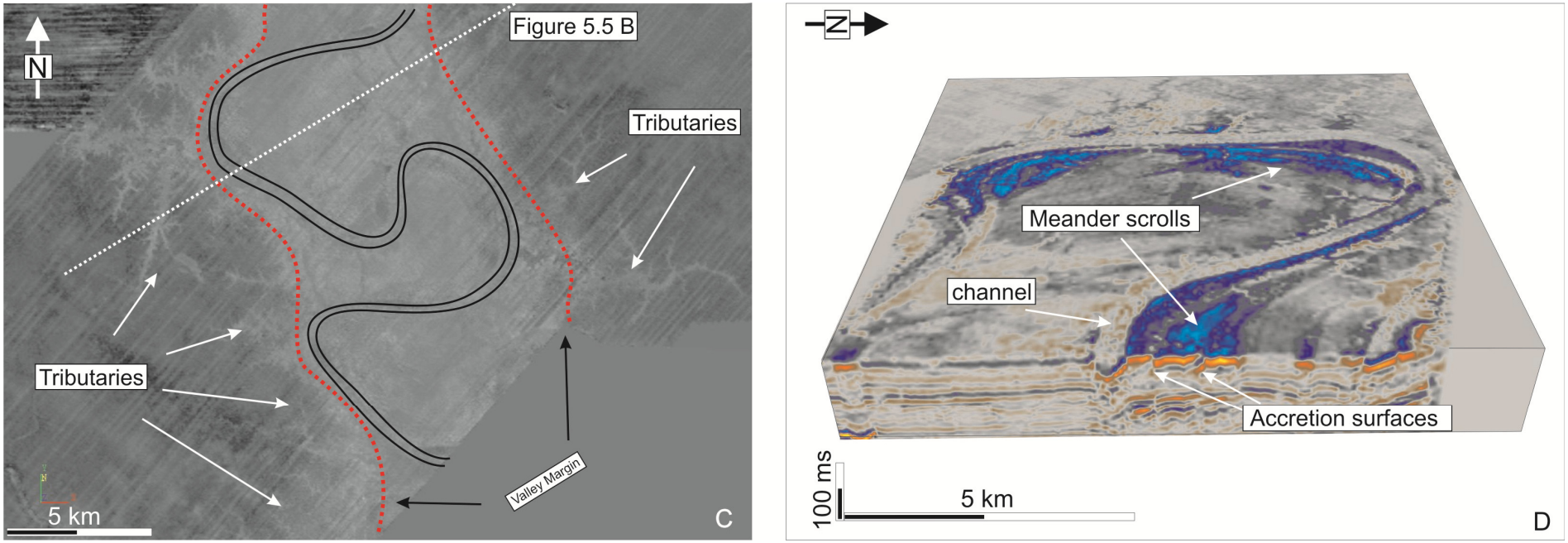

Figure 5.9: A) time-slice 108 twtt and **B)** interpreted map-view showing a large highly-sinuous channel which ran to the south-east and confined within a wide and deep incised valley. This large channel is associated with very well-developed point bars with brighter amplitude. At the margins of these incisions, small tributaries are shown; **C)** Close-up image showing the tributaries that feeding the main incised valley; **D)** 3D seismic cube showing the vertical and lateral seismic expression of the main highly-sinuous channel. The v-shaped channel morphology and the associated well-developed accretion surfaces are clearly imaged. Locations of Figure 5.9C & D are shown in Figure 5.9A. Location of Figure 5.5B is shown on Figure 5.9C.

5.5.1.1.2.2 Sub-unit 4.2B

Description: Sub-unit 4.2B directly overlies the chaotic seismic facies of sub-unit 4.2A and has an average thickness of 22-30 ms twt (20-28 m; Table 5.3). This sub-unit is characterised by laterally-continuous, flat-lying seismic reflections, although inclined reflections, which dips of *ca*. 7° and are up to 25 m deep, are locally observed within this sub-unit. However, it is not possible to determine whether these inclined reflections are real features or multiples associated with features developed within the overlying sub-unit (i.e. sub-unit 4.2C; see below).

Lithology: Sub-unit 4.2B is dominated by a 15-20 m thick unit of fine-grained sands and very-stiff, silty clays containing scattered shell fragments (Figure 5.7). This unit is overlain by a 5-8 m thick unit of very-stiff clay, which contains shell fragments towards its base and organic material towards its top (Figure 5.7).

5.5.1.1.2.3 Sub-unit 4.2C

Description: Sub-unit 4.2C has an average thickness of 25-32 ms twt (23-30 m; Table 5.3). Internally, this sub-unit is characterised by a 27 ms twt (25 m) deep, 'v'-shaped, channel-like incision that is flanked by inclined (up to 7°) reflections which dip into towards the incision (Figure 5.5B). In planview, the 'v'-shaped incision represents a highly-sinuous (SI=2.8) channel, which is filled by a chaotic seismic facies (Figure 5.9A & D). This channel, which flowed towards the SE and which is fully confined within the deep, valley-like incision feature defined by Horizon D.1, is up to 600 m wide and has a meander belt width of 13 km (Figure 5.9B). The inclined reflections adjacent to the channel represent lateral accretion surfaces associated with lateral migration of the main

channel (Figure 5.9D). An abandoned channel, interpreted to be related to 'neck-cutoff' is clearly imaged in the downstream part of the channel (Figure 5.9B).

The architecture of the highly sinuous channel fill is clearly imaged with the boomer data (Figure 5.6B). The basal part of the channel is characterised by a package of high-amplitude reflections with scatterd low-amplitude chaotic character, which is directly overlain by a package of alternating high- and low-amplitude reflections. Toward the top of the channel, low–amplitude, chaotic, and lenticular, high-amplitude reflections occur. Adjacent to the channel fill (i.e. to the right-hand side of the boomer section shown in Figure 5.6), where lateral accretion surfaces are expected based on observations from the 3D seismic data, high-amplitude reflections, with scattered, thin (1 m), low-amplitude reflection are developed. The lack of lateral accretion surfaces within this section may reflect the limited width of the boomer section compared to the full width of the channels (i.e. the section is too narrow to image the accretion surfaces). Finally, the erosional base of the channel is clearly imaged in this boomer section which allows the depth of the channel (*ca*. 23 m) to be precisely determined.

Lithology: 40 m below the sea-bed, at a stratigraphic level which is interpreted to correspond to the base of the uppermost high-sinuosity channel, a 3-5 m thick of rip-up clasts is identified in platform borings (Figure 5.7). This unit, which is interpreted as an interval rich in mudstone rip-up clasts, is overlain by a thick layer (15-18 m) of very-thin, interbedded, sand and shell-bearing stiff clay. This interbedded sand-clay unit corresponds to the lateral accretion surfaces identified on seismic data. The upper 2-3 m of the channel-fill is dominated by stiff clay with shell fragments; scattered fragments of decayed wood are common near the top of the channel fill.

5.5.1.1.3 *Sub-unit 4.3*

Description: The base of sub-unit 4.3 is defined by Horizon D.2. Sub-unit 4.3 has an average thickness of 17-20 ms twt (15-18 m) and is characterised internally by low-amplitude, laterally-continuous seismic reflections. In map-view, no distinct geomorphological patterns have been observed within this sub-unit. On boomer data, the lower part of sub-unit 4.3 is characterised by a 11-13 m thick package of low-amplitude, chaotic reflections with lenses of higher amplitude reflections. The upper part of sub-unit 4.3, directly below the seabed, is characterised by a 3-5 m thick package of high-amplitude, laterally-continuous reflections with lenses of low-amplitude, chaotic reflections.

Lithology: The lower part of sub-unit 4.3 is dominated by a 13 m thick layer of very soft clay with shell fragments, whereas the upper part of the unit is dominated by coarse-grained, unconsolidated sands interbedded with very-soft clay with wood debris. A significant stratigraphic contact, which is defined by a subtle change in lithology but a pronounced change in water content, is identified 16 m below seabed; this surface separates the lower, very-soft clay and that has a water content of 75-100%, from the very-stiff clay that has a water content of 25-50% (Figure 5.7).

5.6 Interpretation and Discussion

Three seismic sub-units (sub-units 4.1, 4.2 and 4.3) have been identified within the Late Pleistocene. The interpretations of these sub-units are given in the following sections.

5.6.1 Sub-Valley Base Depositional Patterns and Sequence Stratigraphy

The prominent incisions along Horizon D at the base of sub-unit 4.1 are interpreted to be related to fluvial erosion and suggest that this horizon represents a sequence boundary (Vail et al., 1977; Van Wagoner et al., 1990; Posamentier and Allen, 1999). This boundary is more likely to be formed in response to incision by several lowstand alluvial bypass systems; these systems are interpreted to have formed during a period of sea-level fall that which was of insufficient magnitude to expose the entire Sunda Shelf (i.e. sea-level did not fall below the shelf edge; see Posamentier, 2001). Due to a lack of well data and uncertainties related to the coupling between lithology and seismic expression, the lithological fill of these low-sinuosity channels has not been determined. However, platform boring data indicate that the units lateral to the main channel incisions correspond to silty-clay-dominated units; these units are, therefore, interpreted to correspond to floodplain deposits. These channels flowed to the south-east towards the South China Sea, and the channels become slightly less sinuous in this direction; this may be interpreted to reflect a decreasing depositional gradient related to closer proximity of the fluvial systems to the coeval shoreline.

Towards the top of sub-unit 4.1, fluvial channels become smaller and more sinuous. However, these channels do not have particularly high sinuosity indices and are not associated with well-developed point bars, perhaps suggesting that these channels formed during the early stages of a marine transgression following the preceding relative sea-level fall. A marine influence on deposition is supported by the presence of shell fragments, lack of distinct geomorphological patterns, and the nature of continuous low-amplitude reflections within the middle and upper parts of this sub-unit (Figure 5.5),

although platform boring data and associated reports do not explicitly state that these shells are fully or marginal marine.

5.6.2 Formation, Geometry and Fill of the Late Pleistocene Incised Valley

Many incised valleys in the rock record contain fully marine deposits, thereby implicating sea-level fluctuations in valley cutting and filling (Gibling, 2006). Several diagnostic criteria have been suggested to aid the identification of incised valleys in the rock record (see Hampson et al 1997; Posamentier, 2001; Fielding and Gibling, 2005): 1) the basal erosion surface that records the lowstand of relative sea-level (sequence boundary) must be of regional (i.e. basin-wide) extent; 2) the basal erosion surface truncates strata which are present beneath the adjacent interfluves; 3) the basal surface is associated with the presence of small tributaries on the main valley interfluves. Posamentier (2001) suggested that incised valleys can be identified and differentiated from 'large' river systems on seismic data based on the presence of small, incised tributary systems which link to the main trunk valley. In contrast, lowstand alluvial bypass systems have no such associated tributaries; 4) the incised valley fill must have a distinctive internal architecture that is commonly multi-storey and which records the progressive rise in base-level during the filling of the valley; therefore the facies within the incised valley must be different from those adjacent to and below the erosional surface; and 5) the depth and width of the incised valley has to be significantly larger (several kilometres wide and several tens of metres deep; Zaitlin et al., 1994; Reynolds, 1999; Gibling, 2006) than expected for a 'normal' fluvial channel system

A model to explain the origin, geometry and infill of the Late Pleistocene incised valley has been developed (Figure 5.10). The large incisional feature developed along Horizon D.1 is significantly larger than those associated with the lowstand alluvial bypass channel systems observed in the underlying stratigraphic unit (i.e. sub-unit 4.1; Figure 5.5B). This feature is, therefore, interpreted as an incised valley formed due to a relative sea-level fall. Correspondingly, Horizon D.1 is interpreted as a sequence boundary (*sensu* Van Wagoner et al., 1988). Furthermore, based on its stratigraphic occurrence towards the top of the Pleistocene succession and by comparison to other similar systems documented in nearby basins (Posamentier, 2001; Miall, 2002, Darmadi et al., 2007), this valley is interpreted to have formed during the Last Glacial Maximum, when sea-level fell *ca.* 120 m below the present-day sea-level and during which the majority of the Sunda Shelf was subaerially exposed (Figure 5.11). The presence of small dendritic tributaries at the main valley margins supports the interpretation of this large incisional feature as an incised valley (cf. Posamentier, 2001). Furthermore, SE-flowing, low-sinuosity channels in the southern part of the study area could be large tributaries that fed the main incised valley as it extended outside of the study area to the E-SE.

Lenticular bodies identified on seismic data and the mud-clasts conglomerate observed in boreholes, directly above the erosional base of the incised valley (sub-unit 4.2A; Figures 5.7 and 5.10A), are interpreted as braided-type channels and associated fluvial lag associated with the lowstand cutting of the incised valley (e.g. Fisk and McFarlan, 1955; Shanley and McCabe, 1994). Similarly, suggested that coarse-grained deposits at the base of the Mississippi River valley system were deposited by braided river systems formed during the initial lowstand period associated with valley incision. Furthermore, Hanebuth et al. (2010) concluded that these types of channel systems (braided rivers) were common

on the Sunda Shelf especially in the western part of the shelf (e.g. Malay Basin, Pattani Basin, Penyu Basin) during the LGM as these areas was highly elevated above sea level.

No clear geomorphological patterns have been identified in sub-unit 4.2B due to the poor imaging caused by the multiples associated with later channel systems; however, the 15-20 m thick, fine-grained sand and very-stiff silty clay with scattered shell fragments may represent the deposits of tidally-influenced point bars which formed during the post-incision transgressive period (Figure 5.10B). This interpretation is supported by the presence of the inclined heterolithic stratification (IHS) (alternating of sands and stiff clay) with shell fragments (Thomas et al., 1987; Allen and Posamentier, 1993; Figure 5.10B). The overlying 5-8 thick of stiff clay with scatterd organic materials may represent the last phase of channel fill which was deposited during the late transgressive system tract.

In a similar manner to sub-unit 4.2B, when the sea-level started to rise slowly again during transgressive times the river observed within sub-unit 4.2C responded by changing its sinuosity to become highly sinuous channel and reoccupied the previous meandering channels of sub-unit 4.2B (Figures 5.9A and 5.10B). It might be that another minor sea-level fall occurred which lead to the formation of the second meandering channel described above. This is expected in areas such as Sunda Shelf where any minor sea-level fall could lead to wide exposure of the Shelf due to its low-gradient. Furthermore, the sea-level curve shown in Figure 5.11 illustrates high-frequency of the sea-level fluctuations in a short time which indicates that this kind of sea-level changes causes dramatic changes in the filling of this incised valley.

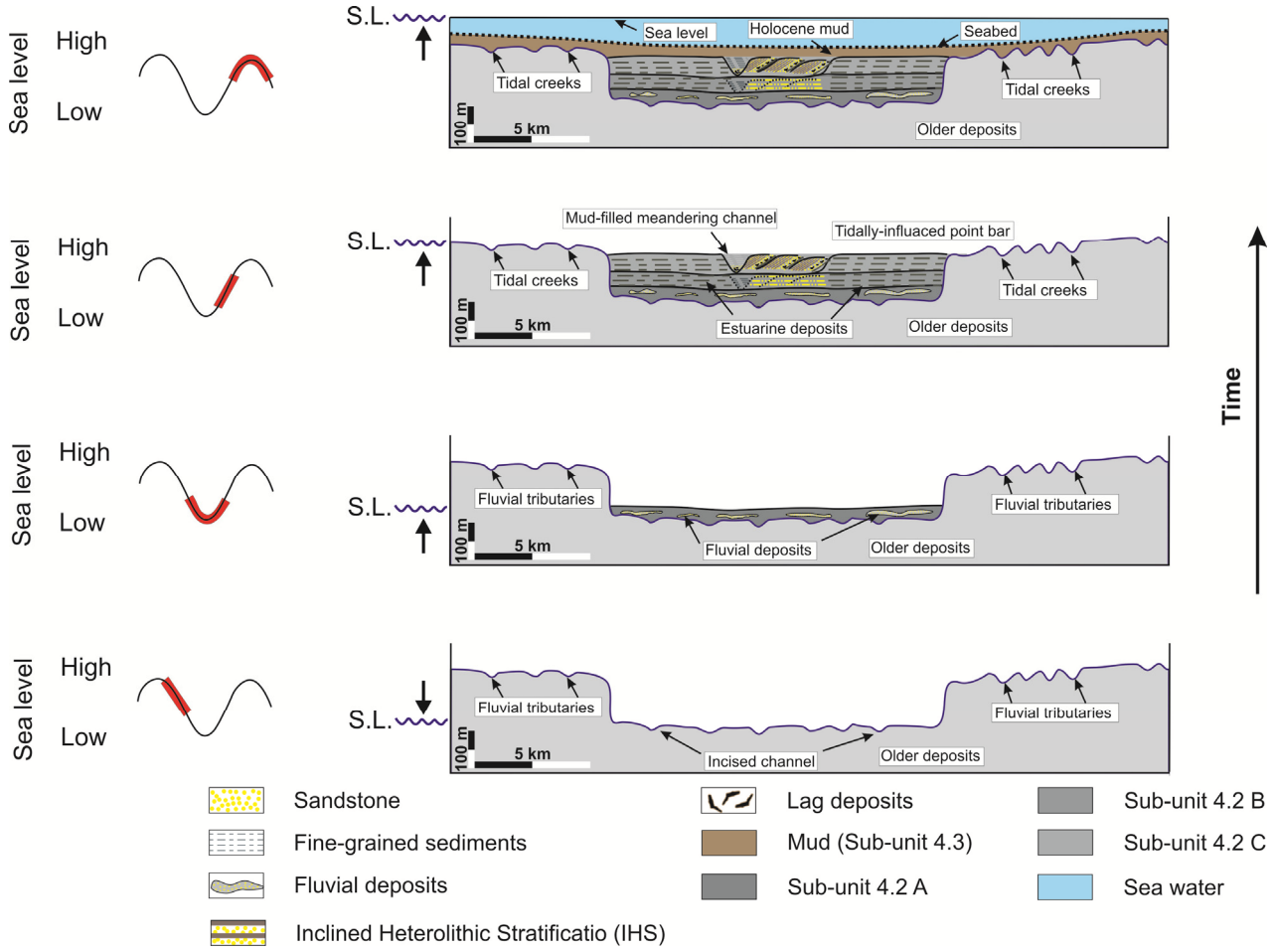

Figure 5.10: A Late Pleistocene Incised Valley model within the Malay Basin. The development of this incised valley is controlled by the variation of the sea-level. **A)** During the LGM when the sea-level fall was at -120 m, the Sunda Shelf was widely exposed and the incised valley was formed; **B)** When the sea-level start to rise slowly, the fluvial deposits of the gravels and cobbles were deposited; **C)** Continued sea-level rise caused the channel to change its sinuosity to become highly-sinuous channel; during this transgressive period, the channel become tidally-influenced and more alternating layers of sand and mud as IHS were deposited; **D)** When the sea-level reached its maximum, the incised valley were drowned and capped by the Holocene mud drape. The vertical scale is approximate.

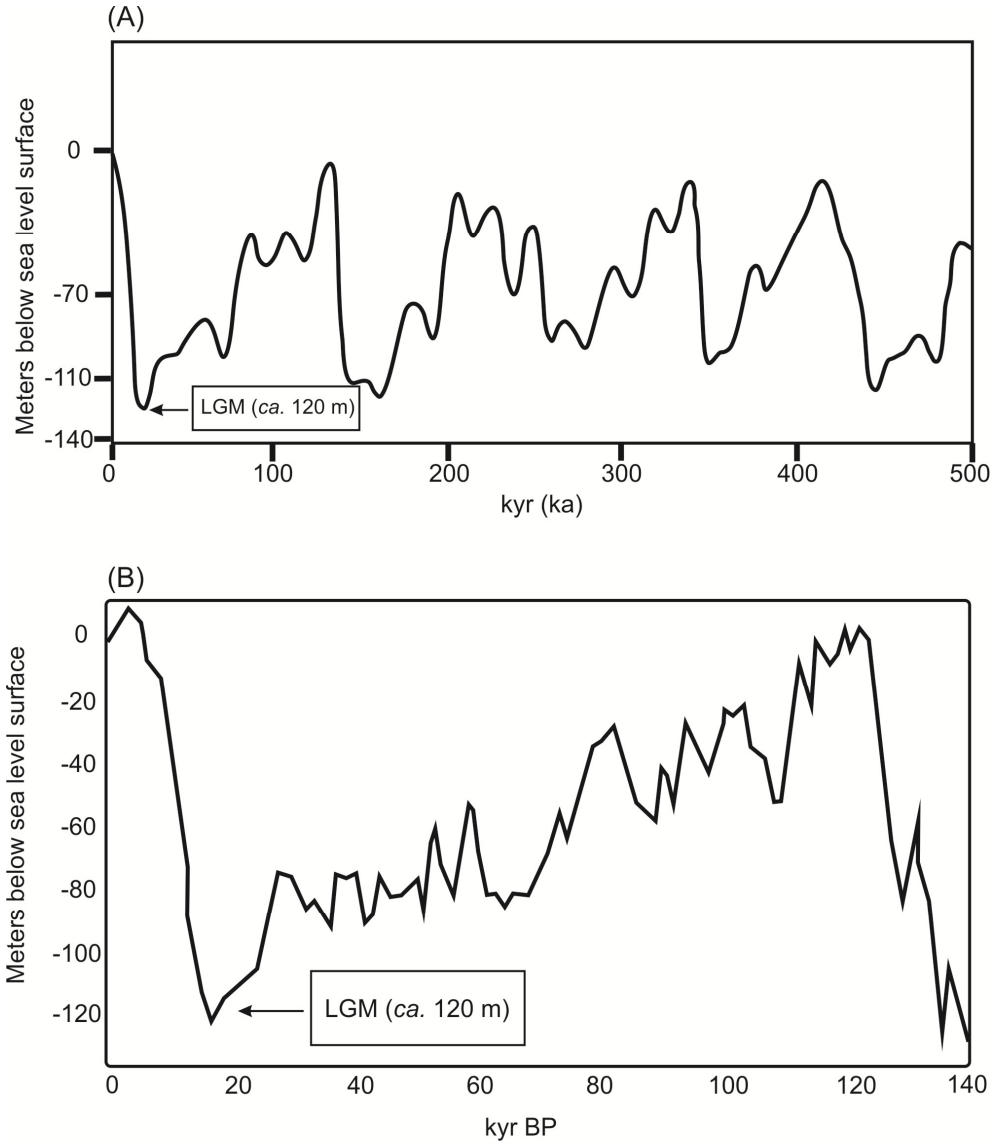

Figure 5.11: Late Pleistocene sea level curves showing the major sea-level fall during the Last Glacial Maximum (LGM) when the sea-level was 120 below the present-day water depth. Numerous minor fluctuations are also shown; **A)** A sea level curve over the past 140 kyr based on estimates obtained from oxygen isotope (Shackleton, 1987) and coral reef records (Chappell et al., 1996; modified from Hanebuth et al., 2003); **B)** A sea level curve over the past 500 kyr based on estimates from oxygen isotope data (Bard et al., modified from Posamentier, 2001).

The 'v'-shaped morphology associated with the inclined reflections within sub-unit 4.2C is interpreted to represent a large meandering river associated with point bar deposits, respectively. The 5 m thick, mudstone clast-rich unit that corresponds to the basal part of sub-unit 4.2C is interpreted as a rip-up clast-rich lag, which was deposited at the base of

the channel (Figure 5.7). This meandering river is interpreted as a tidally-influenced fluvial system that developed during the main period of sea-level rise and transgression.

The presence of the inclined heterolithic stratification (IHS) (i.e. alternating sand and clay) with shell fragments supports the interpretation of tidally-influenced systems (Thomas et al., 1987; Allen and Posamentier, 1993). This meandering channel is associated with very well-developed point bar deposits and very well-imaged lateral accretion surfaces (Figure 5.9D). The point bars are characterised by higher amplitude, especially around the channel bends, whereas the v-shaped channel fill, which is interpreted to document the last phase of active channel activity, is mainly characterised by a low-amplitude, chaotic seismic facies (see Figure 5.9D). An interesting observation is that the site survey boomer data shows sea-bed depressions (Figure 5.6), interpreted by the site survey as the result of shallow gas escape. These depressions seem to be preferentially located at the interface between the abandoned channel and the slightly sandier point bars, presumably picking out sufficient permeability to allow gas migration. Interestingly, this interface also coincides with the bright amplitudes in the point bars immediately adjacent to the abandoned channel (Figure 5.9D). Therefore, this adds strength to the interpretation that the bright amplitudes in the point bars are highlighting some gas charged reservoirs. Equally, the site survey well data suggests that most of this sediment is at best heterolithic and maybe the gas is actually trapped within thin discontinuous sand layers. Furthermore the gas may be still mobile and not just residual saturation.

Parts of the point bars (sub-unit 4.2C) with shell debris in the upper part of the valley fill might represent a fluvially-dominated system with tidal influence. This could be caused by salt-water incursion up the river. Upstream salt-water intrusion is common in many of the modern rivers within Southeast Asia, with a combination of very low river gradients

(< 0.1º) and variable stream flows allowing salt water intrusion to occur. The distance of upstream salt-water reach in fluvial-estuarine systems is generally controlled by the slope of the coastal plain (Reading, 1996). The upstream salt-water intrusion is expected to be large during the dry season at a time when the flux of freshwater to the distal reaches of the fluvial systems is reduced. It has been estimated that the distance of salt-water intrusion in the modern Chao Phraya River is up 200 km and 150 km for Rajang River (Woodroffe, 2000). For larger rivers draining large catchments, but with steep coastal gradients (e.g. the Mekong River), the distance of salt-water intrusion is greatly reduced (e.g. 50-100 km; Woodroffe, 2000). In contrast, in a low-gradient system such as Amazon River, salt-water intrusion can reach 1000 km (Mertes and Dunne, 2007). Based on these observations, it is suggested that the distance of upstream salt-water intrusion in the Late Pleistocene meandering channel might be very large due to the very-low gradient of the Sunda Shelf at this time. Furthermore, the monsoon-driven precipitation rates during the Pleistocene were lower than present-day (Wang, et al. 1999).

The meandering channel of sub-unit 4.2C is geometrically similar to certain reaches of the lower Mississippi River, although it is slightly smaller overall. The channel within sub-unit 4.2C is larger than most if not all of the modern meandering rivers observed in Southeast Asia. Figure 5.12B illustrates a portion of the Purus River, which is one of the main tributaries of the Amazon River and indicates that this river has similar geometric characteristics (e.g. sinuosity, depth, width, meander belt width) to this meandering river within sub-unit 4.2C. Note also the dendritic pattern of the tributaries that drain into the main river. It should be noted that the Purus River is interpreted to occur within an incised valley that was formed in response to tectonically-driven uplift and fluvial incision, and not relative sea-level fall and rise (Mertes and Dunne, 2007).

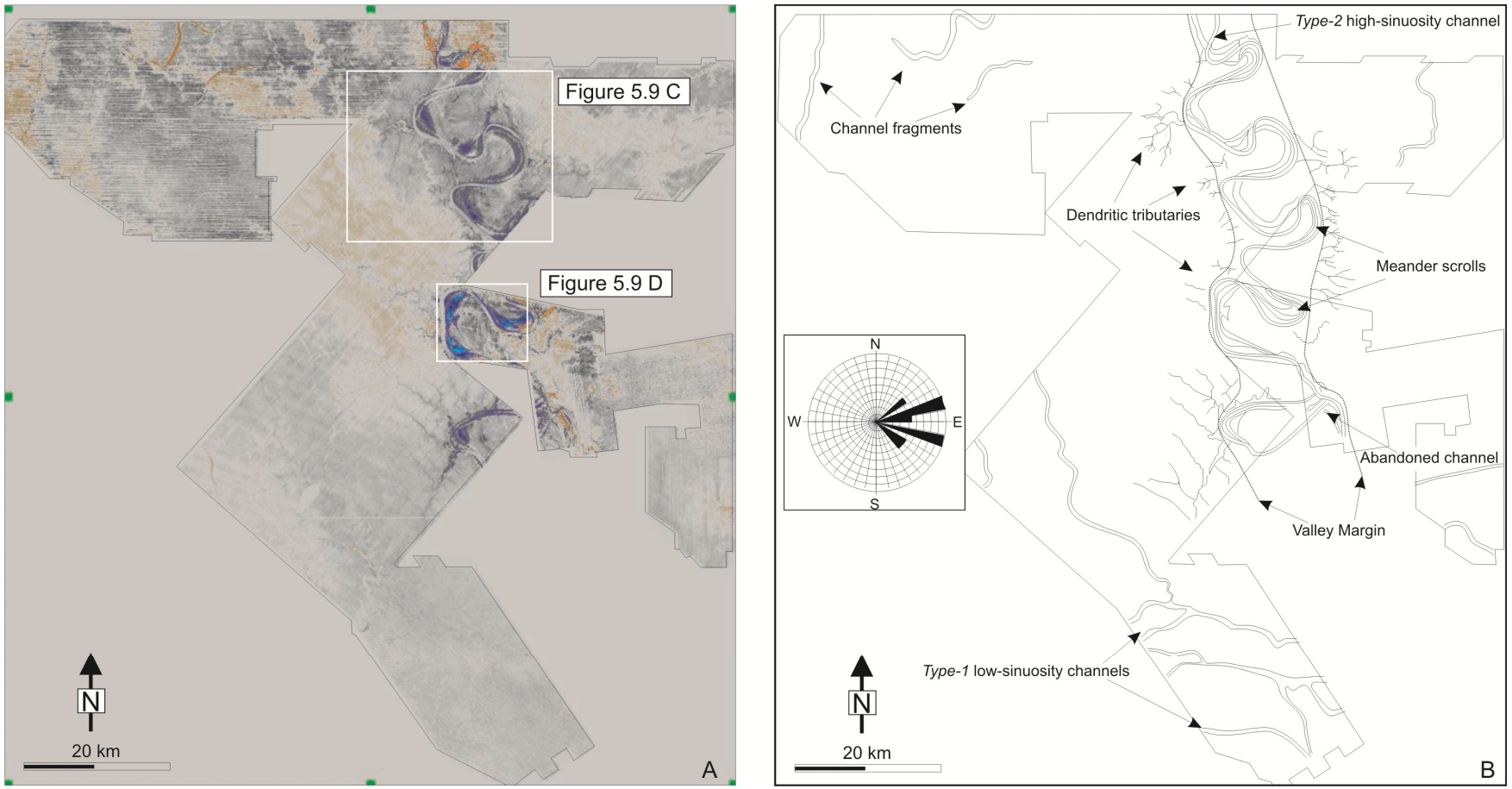

Figure 5.12: A) Time slice at 108 ms twtt showing a large meandering channel with very well-developed scroll bars; **B)** illustrates portion of the Purus River which is one of the main tributary rivers of the Amazon. This river has similar geometric characteristics (width of 500-750, depth of 10-15 m, meander belt width of 14-24 km, and SI of 2.8) that similar to that observed in the time-slice 108 (A). Note the tributaries at the valley margin in both images.

A neck-cut off and associated abandoned channel of sub-unit 4.2C observed in the southern part of the study area suggests that the ongoing sea-level rise caused the channel to reduce its sinuosity via this mechanism (cf. Schumm, 2005). Furthermore, this meandering river became low-sinuosity channel toward the South China Sea which is seen in other datasets (not shown in this study) within the southern part of the Malay Basin (Rapi, 2010, pers. comm.). During this period the former tributaries may have become tidal creeks. Tidal creeks are common in association with the modern rivers on Southeast Asia (e.g. Rajang and Mahakam Rivers).

Continued sea-level rise lead the meandering channel to be drowned and capped by the soft clay of the Holocene succession (Figure 5.11D). The lower part of sub-unit 4.3 is interpreted to correspond to the Holocene mud drape (cf. Allen and Posamentier, 1994) whereas the fine-grained sediments represent sediment deposited on the seabed. The high water content of the very-soft clay layer of sub-unit 4.3 compared to the stiff silty clay of the upper part of sub-unit 4.2C suggests the presence of a significant time gap 16 m below the seabed which separates Late Pleistocene from Holocene sediments (cf. Posamentier, 2001).

5.6.3 Sea-level fall and the formation of incised valleys

Two types of sequence boundaries have been identified within the studied succession: 1) *Type-1:* these are characterised by numerous prominent ‘v’ and/or ‘u’-shaped incisions that are filled with variable-amplitude, chaotic or laterally-continuous reflections (Horizon D; Figure 5.5B); and 2) *Type-2*: these are characterised by a single, wide, deep incision, filled with a range of seismic facies (Horizon D.1). This latter type of sequence

boundary is associated with significant topographic relief (>35-80 m) and numerous smaller incised features at the margins of the main deep incision (Figure 5.5B).

Based on 3D seismic data from the Java Sea, Posamentier (2001) suggested that incised valleys can be identified and differentiated from 'large' river systems on seismic data based on the presence of small, incised tributary systems which link to the main trunk valley. In contrast, lowstand alluvial bypass systems have no such associated tributaries. In addition, as suggested by outcrop examples, incised valleys are typically much larger (e.g. 18000 m wide by 80 m deep) than lowstand alluvial bypass channel systems (e.g. 3000 m wide by 45 deep). Both types of channel systems have been recognised in this study and from other studies conducted on the Sunda Shelf (e.g. Miall, 2002; Darmadi et al, 2006). The study of Posamentier (2001) was based solely on seismic timeslices; in this study, incised valleys are identified in both seismic and boomer cross-sections (Figure 5.5B and 5.6) and horizontal timeslices (Figure 5.9), and their fill has been characterised by site survey borings (Figure 5.7).

Based on the identification of an incised valley within the studied succession, a key question is what drives the formation of this feature in the context of the geographical and geomorphological context of the study area. Standard sequence stratigraphic models described the variation in relative sea-level or base-level as the controlling factor in valley development (e.g. Posamentier and Vail, 1998; Van Wagoner et al., 1990; Shanley and McCabe, 1994). Schumm (1993) indicated that deep river incision may occur in association with a significant fall in relative base-level, and that the geometric characteristics (e.g. width, depth, etc) of the fluvial incision are determined by the magnitude of the base-level fall (Posamentier, 2001). When a significant fall in relative base-level occurs and a former shallow marine shelf is fully exposed, an incised valley may form (Van Wagoner et al., 1990; Posamentier and Allen, 1999; Posamentier, 2001).

When a relative base-level does not expose the entire shelf, a lowstand alluvial bypass channel systems and shelf delta may develop. The Late Pleistocene incised valley observed within the study area within the Malay Basin was formed when sea-level fall was 120 to 160 m below present-day water depth. Although, the sea-level fall did not expose the shelf break, the formation of the incised valley occurred. This is may be because that the Sunda Shelf was a broad and very-low-gradient shelf; therefore when the sea-level fall was 120 m below the present-day depth, most of the Sunda Shelf was exposed. Giving that the Sunda Shelf is a very low-gradient shelf, it is suggested that any minor relative sea-level fall may expose wide part of the shelf area. Additionally, the formation of the relatively wide and deep low-sinuous channels observed along Horizon D is believed to be related to the sea-level fluctuation. The minor relative sea-level fall along with the low-gradient shelf may lead to the formation of these wide and deep channel systems.

5.6.4 Regional Context of the Incised Valley

Miall (2002) identified a wide range of channel style and size within the northern part of the Malay Basin. In particular, a large (500 km wide with meander belt width of 10 km and sinuosity>2) S-flowing meandering channel with well-developed, high-amplitude point bars was identified within the Late Pleistocene succession. This meandering channel is interpreted to be confined within a 10 km wide incised valley and this system was interpreted to be the major channel system developed within the Late Pleistocene succession in the northern part of the Malay Basin (Miall, 2002). The characteristics (width, meander belt width and sinuosity) of both meandering channels and the incised valley within which it is confined are similar to the Late Pleistocene channel systems

observed in this study. Therefore, the meandering channel and the incised valley system observed by Miall (2002) and the one described here are believed to be part of the same system.

To place this study in a regional extent, the valley-confined meandering channel observed in this study has been projected on to the present-day bathymetric map which is superimposed on to the pre-Tertiary, depth map (e.g. top unit 4.2C; Figure 4.9A) of the Malay Basin (Figure 5.13). This visualisation indicates that the meandering river (and the valley which confined it) occupied the axial zone of the Malay Basin. In addition, the system studied here appears to place more accurate constraints on the location of Johore River (Figure 5.13B), the impression of which can be seen in on the seabed (Figure 5.1) (Voris, 2000). Previously, the projection of these large 'trunk' rivers, especially those extending southwards from the Gulf of Thailand, was largely hypothetical due to a thick, predominantly Holocene sedimentary cover and the high-sinuosity of these river systems (Voris, et al. 2000).

The Johore River is thought to have drained from the northern hinterland of Thailand. Morley and Westaway (2006) described a paleo-river system called 'paleo-Chao Phraya River' that ran through the Gulf of Thailand to the South China Sea for much of the Cenozoic (including the Late Pleistocene). This river is believed to be the Johore River presented on the map by Voris (2000). Loe (1997) and Morley and Westaway (2006) suggested that the paleo-Chao Phraya River was one of the major sediment sources for the Malay Basin, along with a series of eastwards-flowing systems draining the Malay Peninsula to the west. Clift (2006) suggested that less sediment was transported to the Sunda shelf through the Gulf of Thailand during the Late Miocene to Recent, especially during the LGM. However, during LGM times, much of the earlier highstand deltaic deposits inland of the modern coastline of the Gulf of Thailand were reworked

downstream and re-deposited, along with material transported directly from the upper reaches of the paleo-river system, within the South China Sea (Sinsakul, 1992; Morley and Westaway, 2006). This study interprets the Late Pleistocene River system identified here as the southern extension of the paleo-Chao Phraya River. This suggests that during the interglacial times, the late Pleistocene river system had a large catchment area (*ca*. 750,000 km²), correspondingly high discharge and sediment flux, and transported eastwards into the South China Sea. Although some thin fluvial lag deposits are observed at the base of the incised valley, it is suggested that the incised valley was mainly a bypass system and that most of the sediments were deposited in the South China Sea. Wonge et al. (2003) concluded that the presence of thick sediment wedge at the shelf break indicates that the sediment bypass was the dominant process on Sunda Shelf. Coarse-grained sediments are common within the Late Pleistocene deposits, especially in the north where the Mekong River transported the sediments into the South China Sea. Hanebuth and Stattegger (2003) predicted that a coarse-grained, Late Pleistocene shelf-edge delta would be developed at the western margin of the South China Sea. Their interpretation was based on boreholes which did not penetrate the base of the incised valley of the North Sunda River or the base of the associated shelf-edge delta; thus it was unknown if significant quantities of coarse-grained material were able to bypass the shelf. In this study we predict that a coarse-grained Late Pleistocene shelf-edge delta was developed at the mouth of this large river as indicated in Figure 5.1.

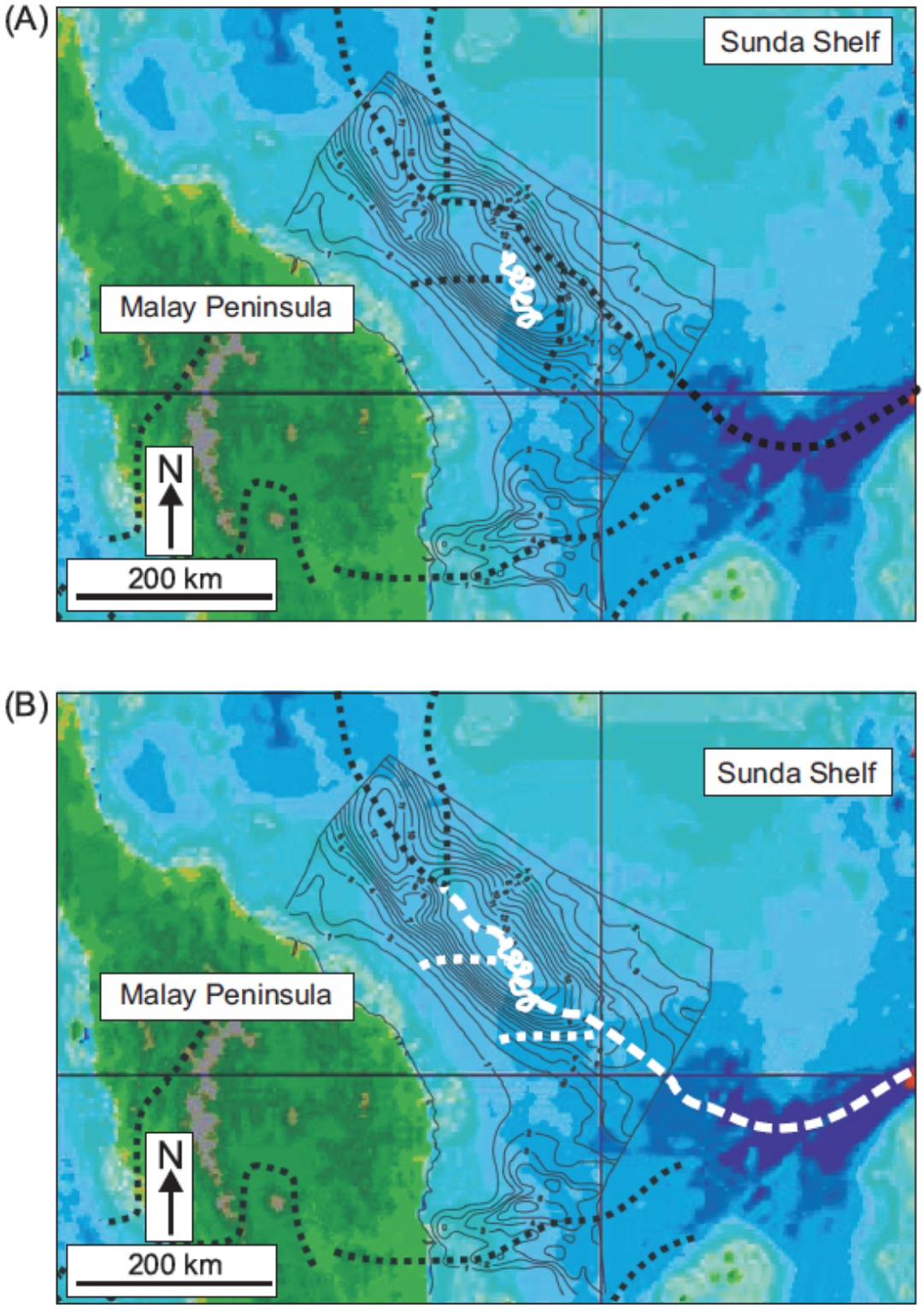

Figure 5.13: A) Close-up map showing the present-day topographic map of the Sunda Shelf (Sathiamurthy and Voris, 2006), superimposed by the pre-Tertiary depth contour of the Malay Basin (Madon, 1999b). The black dashed-lines represent the 'truck' river described by Voris (2000). The white sold-line represents the youngest channel system observed within the Late Pleistocene river systems; **B)** An edited version showing the exact location of the 'trunk' river. This channel was the major channel that occupied the axial zone of the Malay Basin during the Late Pleistocene.

5.7 Conclusions

The mega-merge 3D seismic dataset, supplemented by high-resolution site survey and borehole data, has enabled reconstruction of Late Pleistocene river systems in the Malay Basin. Two different types of incisions have been identified; deep incised valley systems that are associated with smaller tributaries feeding the main valley and weakly incised channel systems that are interpreted as lowstand alluvial bypass channel systems have been recognised.

A large incised valley (80 m deep and 14 km wide) has been identified. This incised valley formed during at or near LGM lowstands when the sea-level fall was significant to widely expose the Sunda Shelf. Borehole data show that the incised valley fill is dominated by mud with shell fragments which overlies cobbles and sands. The cobble layer suggests a fluvial lag deposit, coincident with the lowstand cutting of the valley. Parts of the point bars reflect fluvially-dominated channels, possibly with inclined heterolithic stratification (IHS). Mud with shell debris within the abandoned channel-fill, and parts of the point bars, implies estuarine conditions within the channels. This could be caused by salt-water intrusion in the river upstream. Given the low-gradient character of the shelf, this intrusion can be hundreds of kilometres. The incised valley records a major river system that occupied the axial zone of the Malay Basin, possibly extending from the Gulf of Thailand to the South China Sea (>2,000 km).

Chapter 6

Quantitative Seismic Geomorphology of Fluvial Systems of the Pleistocene to Recent in the Malay Basin, Southeast Asia

6.1 Abstract

Fluvial sandstones constitute one of the major clastic petroleum reservoir types in many sedimentary basins around the world. This is especially true in the Tertiary basins of Southeast Asia, which display a wide range of fluvial channel reservoir types. This study is based on the analysis of high-resolution, shallow (seabed to *ca.* 500 m depth) 3D seismic data which provide exceptional imaging of the geometry, dimension and temporal and spatial distribution of fluvial channels. The Malay Basin comprises a thick (>8 km), rift to post-rift Oligo-Miocene to Pliocene basin-fill. The youngest (Miocene to Pliocene), post-rift succession is dominated by a thick (1-5 km), cyclic succession of coastal plain and coastal deposits, which accumulated in a humid-tropical climatic setting.

This study focuses on the Pleistocene to Recent (*ca*. 500 m thick) succession, which comprises a range of seismic facies, mainly reflecting changes in fluvial channel style and gross stratigraphic architecture. The succession has been divided into four seismic units (Unit 1-4), bounded by basin-wide stratal surfaces. Units 3 and 4 have been further divided into two sub-units (older sub-units 3.1 and 4.1 and younger sub-units 3.2 and 4.2). Each unit displays a predictable vertical change of the channel morphological parameters

including the channel depth, width, and sinuosity. Based on the morphometric parameters of the channels observed in this study, three channel groups (incised valley, alluvial bypass channel systems, and highly sinuous meandering channels) have been identified. The base of each unit is characterised by wide low-sinuosity channels passing gradationally upwards into narrow high-sinuosity channels at the top. The wide variation in channel style and size is interpreted to be controlled mainly by the sea-level fluctuations on the wide, flat and tectonically-quiescent Sundaland Platform. However, climate control along with the channel gradient may have a significant impact on the channel style and size by affecting the discharge and the types of sediment load.

Empirical equations developed for modern rivers have been tested on the humid-tropical coastal plain channels identified in this study. Using these relationships, most of the channel morphological parameters are either underestimated or overestimated. It suggests that these empirical equations cannot be applied to channels whereas morphometric parameters are seismically-derived; however, several new empirical relationships have been established and new empirical equations have been developed.

This study demonstrates how a better understanding of fluvial reservoir variability can be obtained through the analysis of high-resolution, shallow 3D seismic data (seabed to *ca.* 500 m), which can provide exceptional imaging of fluvial channel planform shapes and other geometrical properties and dimensions and allow for new empirical relationships to be developed.

6.2 Introduction

Fluvial channel sandstones are the dominant and most productive reservoirs in many basins around the world; this is especially true in Tertiary basins of Southeast Asia. In these mature basins, exploration and production activities are increasingly concerned with predicting the origin and distribution of fluvial sandstone bodies. Quantitative geometric data of fluvial channel sandbodies, including size, shape, orientation, spatial distribution, proportion and connectedness, is a particularly important aspect of reservoir management that can help to determine reservoir volume productivity (Bryant and Flint, 1993; Reynolds, 1999). These data are also critical to building and conditioning 3D reservoir models in order to determine the most efficient well spacing and production strategy. Furthermore, studying the geometry of the fluvial sandbodies contributes directly to a better understanding of the discipline of sequence stratigraphy (Blum and Törnqvist, 2000) because these systems respond rapidly to changes in climate, tectonics and base-level (Schumm, 1977; Shanley and McCabe, 1994).

6.2.1 Architectural variability and controls on the evolution of fluvial systems

Vertical variability in fluvial channel architecture is indicated in most sequence-stratigraphic models of fluvial systems (e.g. Wright & Marriott, 1993; Shanley & McCabe, 1994) and is controlled by numerous factors including base-level changes, climatic variations, tectonics, sediment calibre and hydrology. Schumm (2005) described three dominant factors that control the architectural variability in fluvial systems: 1) *upstream controls*, including tectonics, climate and bedrock lithology of the source area;

2) *local controls*, including valley morphology, vegetation, active tectonics, number and style of tributaries, and type of bedrock; and 3) *downstream controls*, which include base-level (which for channels that discharge into marine basins corresponds to sea-level) fluctuations and length of upstream extent. Among these factors, base-level variations, syn-depositional tectonics and climate are considered to be the most significant factors that influence the overall fluvial channel architecture and size. Tectonics (uplift or subsidence) and base-level fluctuations are the main controls on the rate of accommodation creation or destruction (Vail et al., 1977; Van Wagoner et al., 1990). Therefore, these factors determine whether fluvial systems incise, aggrade or migrate laterally. Climate change may also have a significant influence on fluvial channel style by affecting the rate and calibre of sediment supply, vegetation cover, precipitation and discharge; however, climate is only rarely cited as a key control on the temporal and spatial evolution of fluvial systems (Blum and Törnqvist, 2000; Ethridge & Schumm, 2007).

6.2.2 Channel Classification and Empirical Relationships

Numerous river classification schemes have been developed and channels can be separated into two major groups depending on their 'freedom' to adjust their shape: (1) *confined channels*, which are bedrock-controlled and are relatively fixed over a relatively significant period of time; and (2) *un-confined channels*, which are free to adjust and avulse (Schumm, 1977). Based on their planform geometry alone, alluvial channels have been traditionally classified as straight, meandering, and braided (Leopold and Wolman, 1957). Another popular classification is that single channels with varying sinuosity are divided into straight and meandering, and that multiple channels with varying sinuosity

are divided into braided and anastomosing (Miall, 1977). Leopold and Wolman (1957) and Rust (1978) have used a sinuosity of 1.5 to separate high-sinuosity rivers from straight rivers. Schumm (1977, 1981) demonstrated that there is a strong relationships between the channel pattern and the type of the sediment transported by the channel, thereby allowing fluvial channels to be classified into three types: 1) *bed-load channels*, which are a straight or of very-low sinuosity; 2) *mixed-load channels*, which are of moderate-sinuosity; and 3) *suspended load channels*, which are of high sinuosity.

There have been numerous attempts to reconstruct the geometry and flow characteristics (e.g. bedload vs. suspended load) of ancient rivers systems; these have relied heavily on the use of several groups of empirical relationships derived from quantitative analysis of modern river systems in a variety of climatic and tectonic settings (e.g. Leopold and Wolman, 1960; Leeder, 1973; Schumm, 1977; Collinson, 1978; Ethridge and Schumm, 1978; Brick, 1984; Lorenz et al., 1985; Fielding and Crane, 1987). These equations have been used to interpreted ancient channels using outcrop and vertical-based data such as well logs and cores; however, these equations have not been used on data that are seismically-derived.

6.2.3 Quantitative seismic geomorphology and previous applications to the analysis of fluvial systems

3D seismic reflection data can provide important insights into the architecture of fluvial systems and allow extraction of quantitative data which can be used to constrain the geometry of fluvial sandbodies in reservoir models (e.g. Posamentier, 2001; Miall, 2002; Carter 2003). Using seismic data in this way has been termed ‘quantitative seismic

geomorphology' (Wood, 2003). The three-dimensional data extracted from seismic reflection datasets cannot typically be obtained from one-dimensional, vertical data tyeps (e.g. wireline logs, core) or two-dimensional outcrops.

To-date, the majority of seismic geomorphologic studies have been largely qualitative (e.g. Posamentier, 2001). Recently, however, geologists and geomorphologists have started to recognise the advantages of quantitative extraction of geomorphological parameters from seismically well-imaged depositional systems in a range of settings (e.g. Carter, 2003; Wood, 2003; Deptuck, et al., 2003). For example, Carter (2003) used quantitative measurements extracted from 3D seismic data in the Widuri Field, offshore Sumatra to improve the pre-existing reservoir model and to allow more accurate placement of future exploration and production wells. In addition, Wood (2007) and Wood and Mize-Spansky (2009) used channel morphometric parameters to establish empirical relationships between variables and to classify the channel systems. Following Schumm (1977, 1981) classification, Wood (2007) classified the fluvial channel systems of the Pliocene and Miocene of the Northern Gulf of Mexico into three classes (bed-load, mixed-load and suspended-load). Miall (2002) provided quantitative data on several Pleistocene to Recent channel systems that are imaged in shallow 3D seismic data from northern Malay Basin. He used these data to compare these ancient systems with modern rivers; this led him to conclude that no large rivers flowed into or through the Malay Basin during the Pleistocene (Miall, 2002).

Darmadi et al., (2007) used quantitative data measured from seismic images from West Natuna Basin, Sunda Shelf to help to determine the vertical changes in fluvial architecture within the Pleistocene Succession of the Muda Formation. He then plotted the channel morphometric parameters (e.g. width, depth and sinuosity) relative to stratigraphic position and to the global sea-level curve of Haq et al., (1987). The plot showed vertical

changes in channel parameters from wide low-sinuosity channels during lowstand and smaller highly sinuous channels during transgression within each identified sequence

6.2.4 Study aims

This study is initiated to investigate and quantitatively describe the temporal and spatial variations in fluvial system architecture within the Pleistocene to Recent fill of the Malay Basin on the Sunda Shelf, situated offshore eastern Malay Peninsula, SE Asia using high-quality, shallow 3D seismic data (Figure. 6.1). The documentation of the dimensions and geometries of Pleistocene fluvial systems will help in the construction of a quantitative database which can be used to help constrain reservoir models for the productive Miocene fluvial reservoirs on the Sunda Shelf. Furthermore, these seismically-derived quantitative data have been also used to establish relationships between the morphometric parameters and to develop new empirical equations.

6.3 Geological Setting

6.3.1 Tectono-stratigraphic evolution

The Malay Basin is situated in the centre of the Sunda Shelf, Southeast Asia, which is one of the largest intracontinental shelf areas in the world (*ca*. 125,000 km²; Figure 6.1) (Madon, 1999). The northwest southeast trending Malay Basin is 500 km long by 250 km wide, and is located between the Penyu and West Natuna basins to the south and the Pattani Basin to the north (Figure 6.1) (Hutchison, 1989; Madon et al., 1999). The basin

formed as a result of tectonic extension during the Late Eocene to Early Oligocene, following the collision of India with the Asian continent (Tapponnier et al., 1986; Hutchison, 1989). The basin comprises a thick succession (>8 km) of Oligo-Miocene to Recent deposits, which overlie a pre-Tertiary basement consisting of metamorphic, igneous and sedimentary rocks (Figures 6.2 & 6.3).

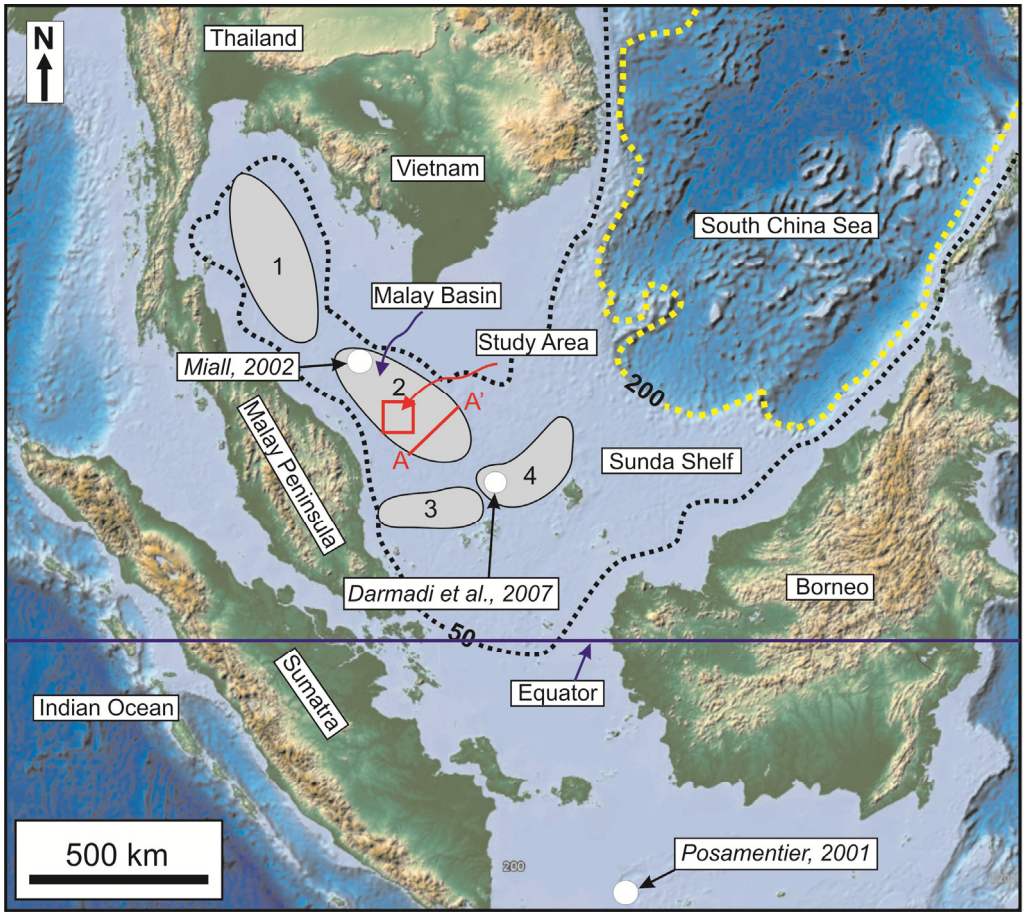

Figure 6.1: Location map of the study area within the Malay Basin (2) on the Sunda Shelf, Southeast Asia. The other basins are Pattani Basin (1), Penyu Basin (3), and West Natuna Basin (4). The yellow and black dashed-lines represent the present-day depth contours at 200 and 50 m, respectively. The water depth within the study area is mainly from 50 to 80 m. The red solid-line represents the regional cross-section shown in Figure 6.3. The blue solid-line represents the equator line. Locations of previous studies of Posamentier (2001), Miall (2002) and Darmadi et al. (2007) that were conducted on SE Asia are shown. Bathymetry data was obtained from National Geophysical Data Centre (NGDC) (http://www.ngdc.noaa.gov).

The structural evolution of the Malay Basin can be divided into three tectono-stratigraphic phases (Tjia, 1994; Madon, 1998; Negah et al., 1996 and Tjia and Liw, 1996): 1) a pre-Miocene syn-rift phase; 2) an Early to Middle Miocene post-rift phase dominated by thermally-induced subsidence and basin inversion; and 3) a Late Miocene to Recent phase dominated by thermally-induced subsidence and lacking inversion-related tectonic uplift (Figure 6.3).

The pre-Miocene phase represents the initial extensional phase of basin development, when subsidence was controlled by normal faulting (Hamilton, 1979; Madon, 1999). Sedimentation was characterised by alternating sand-dominated and shale-dominated fluvio-lacustrine sequences within a series of isolated half-grabens (Madon, 1999). The Early to Middle Miocene post-rift phase was dominated by thermal subsidence that was accompanied by intermittent periods of compressional deformation. This resulted in local inversion of syn-rift half-grabens and re-activation of their bounding faults; this was particularly intense in the southern part of the basin (Madon, 1999). One consequence of this difference in these spatial variations in magnitude of inversion-related uplift is that the south-western flank of the Malay Basin is slightly steeper than its north-eastern flank (Figure 6.3). During this post-rift phase, deposition was characterised by coastal to shallow marine deposits. The Late Miocene to Recent phase was dominated by thermal subsidence, without any significant tectonic activity (Madon et al., 1999). Deposition during this phase was mainly within coastal plain and shallow marine environments (i.e. Pilong Formation; Madon, 1999b). The Upper Pilong Formation within the Malay Basin is time-equivalent to the Muda Formation of West Natuna Basin (Madon, 1999b).

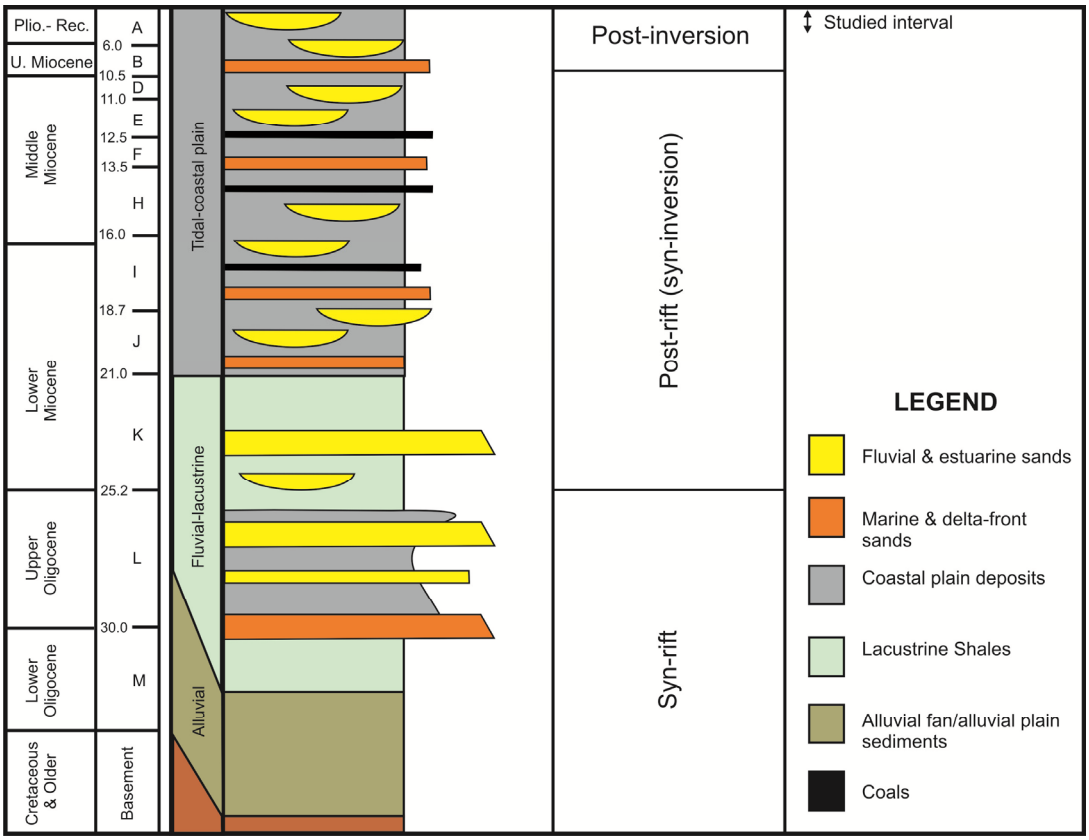

Figure 6.2: Generalised stratigraphic column of the Malay Basin. The second column contains the main regional stratigraphic intervals (labeled A-M) and their approximate ages (in Myr). The studied interval is the upper part of Group A succession which is mainly composed of coastal plain deposits (Modified from Madon, 1999d).

The present-day water depth within the study area ranges from 50-80 m and the average water depth across most of the Sunda Shelf is *ca*. 70 m. The shelf break occurs at *ca*. 180-220 m beneath present-day sea-level. During the middle Pleistocene, the growth of continental glaciers decreased the ocean water volume and caused a maximum reduction in sea-level of between *ca*. 160 m and *ca*. 120 m during the LGM (Gascoyne et al., 1979; Hopkins, 1982; Yang and Xie, 1984; Hanebuth et al., 2003; Hanebuth and Stattegger, 2003; Voris, 2000). Hence, most of the Sunda Shelf was subaerially exposed during the LGM, with the shoreline interpreted to have been located close to the present-day shelf break (Hanebuth et al., 2003; Hanebuth and Stattegger, 2003; Voris, 2000). Consequently, during the LGM, the South China Sea was much smaller than it is present-day and formed a semi-enclosed marginal sea (Sathiamurthy and Voris, 2006).

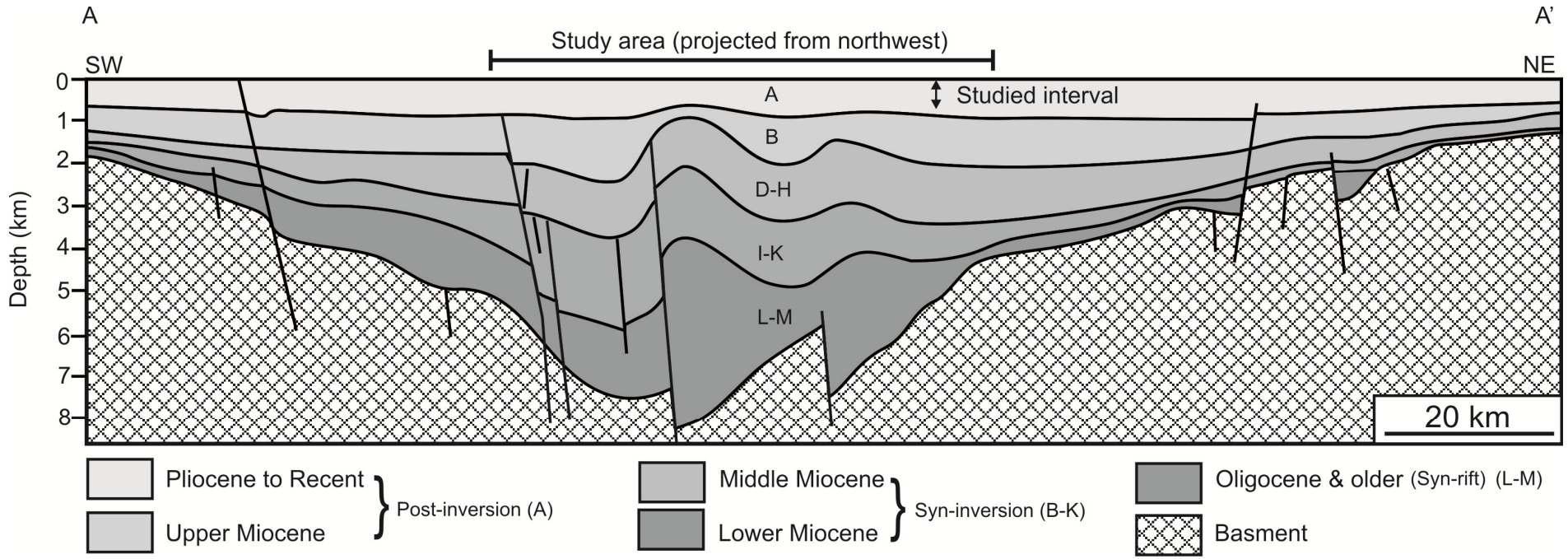

Figure 6.3: Regional cross-section of the Malay Basin. The main regional stratigraphic intervals are labeled A-M. Location of this cross-section is shown in Figure 6.1. The studied interval lies within the Upper post-inversion Pliocene to Recent (Modified from Madon, 1999d).

6.4 Data Sources and Methodology

The data utilised in this study consists of a 3D seismic reflection dataset with a total areal extent of *ca*. 11500 km^2 (*ca*. 115 km wide by *ca.* 100 km long; Figure 6.4). The seismic dataset comprises ten separate seismic surveys that have been merged into a single 3D volume. The dataset is zero-phase processed with SEG normal polarity; a positive (peak) event (black seismic reflection on seismic sections) represents a downward increase in acoustic impedance, and a negative (trough) event (white seismic reflection on seismic sections) represents a downward decrease in acoustic impedance (Brown, 2004). In-line and cross-line spacing within these surveys are 9.38 m and 12.5 m, respectively. The vertical record length is 600 milliseconds two-way time (ms twt). The vertical sampling interval for all surveys is 2 ms, except for one survey which has a sampling interval of 1 ms. The dominant seismic frequency ranges from 60-70 Hz. Unfortunately, only limited well data are available to calibrate the seismic data, as most wells within the area targeted the deeper, productive, Miocene succession. However, depth and thickness measurements were converted from the milliseconds two-way time (ms twt) to metres by using velocity information (i.e. check-shot data) from one reference well (Tunggal-1; Figure 6.4). This well indicates that the average velocity of the shallow part of the basin fill is *ca*. 1880 m sec^{-1}. Based on the estimation of the frequency and velocity, the vertical resolution within the interval of interest ranges from *ca.* 6.7 to 7.8 m and the lateral resolution ranges from *ca.* 11.5 to 15.5 m.

The quality of the seismic data within the studied interval is generally excellent, although exact amplitude values vary between different surveys due to variations in the acquisition and processing parameters. Fortunately, this does not unduly hamper the overall imaging and mapping of fluvial systems. There are also marked ‘acquisition footprints’ in the

upper parts of several of individual datasets within the merged survey. These appear as amplitude stripes on horizontal 'timeslices' through the 3D volumes and are expressed as small breaks or discontinuities along reflection events in seismic cross-sections. Finally, some of the individual surveys within the mega-merge survey have not been optimally merged as observed by minor (<4 ms) vertical offset of corresponding reflection events. Fortunately, most of these minor issues can be overcome by using a combination of map-view and cross-section images; this ensures that only true geological features were interpreted.

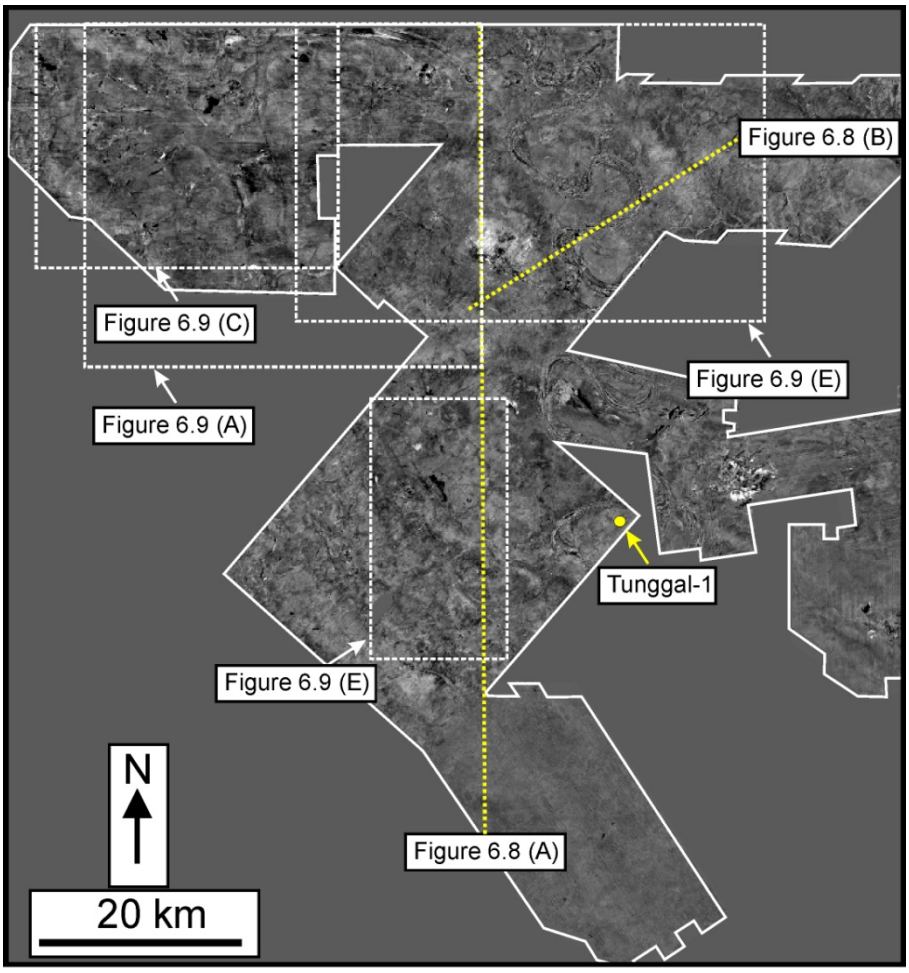

Figure 6.4: Base map of the study area based on a horizontal 'time' slice at 400 ms. The volume consists of ten surveys that have been merged to make a single interpretable volume. The yellow-circle represents the location of the well (Tunggal-1) that was used in the time-depth conversion. The yellow-dashed lines illustrate the locations of the seismic sections shown on Figures 6.8. Locations of time-slices shown on Figure 6.9 are also illustrated.

Interpretation of depositional features and geomorphological patterns has been achieved by the use of a combination of horizontal 'timeslices' and non-horizontal, 'iso-proportional' slices (*sensu* Zeng et al., 1998; Brown, 2004; Posamentier et al., 2007). Time slices are seismic slices taken horizontally through the original 3D seismic reflectivity volume whereas iso-proportional slices are obtained by slicing between two parallel or non-parallel, horizontal or dipping reflection events (see Zeng et al., 1998; Brown, 2004; Posamentier et al., 2007; see Figure 4.5A in Chapter 4). Horizontal 'timeslices' are only useful when the geological features of interest, and the stratigraphic timelines along which they are developed, are horizontal to sub-horizontal; this only occurs in the uppermost part of the studied succession. In the middle and lower part of the studied interval, where the seismic reflections are not horizontal (due to post-depositional deformation), iso-proportional slices have been utilised (see Figure 4.5A in Chapter 4).

Ten interpretive maps were constructed that illustrated the range of fluvial channels styles at various stratigraphic levels within the dataset. Each map is composed of observations from a succession of time and/or iso-proportional slices taken from either the lower half or the upper half of each mapped seismic unit; hence each map illustrates the type of channels that are observed in either the base or the top part of each unit (see Figure 4.5B in Chapter 4). Two examples of the interpretive maps that have been used in this study are shown in Figure 6.5A & B (see Chapter 4 for full description of these plan-view maps). It should be noted that the number of channels shown on these maps within any given stratigraphic interval should be considered a 'minimum'; this reflects the inability to image channels which are below the vertical and lateral resolution of the seismic data or only partial imaging of channels which appear 'fragmented' due to incision by younger channels. Finally, seismic 'multiples' from shallower channels may mask channels imaged at lower stratigraphic levels.

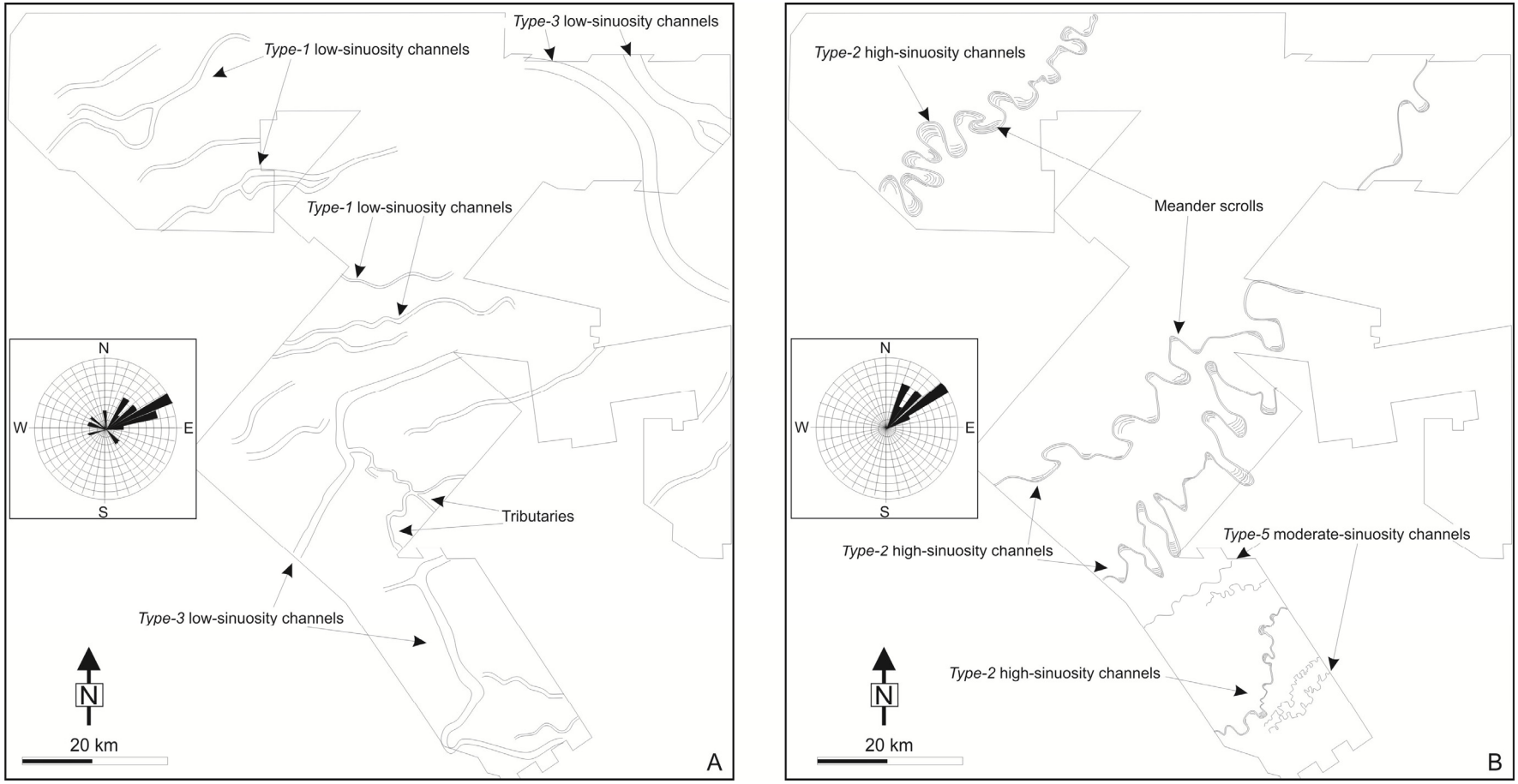

Figure 6.5: Two examples of the interpretive plan-view maps within Unit 1 that have been used in this study; **A)** shows the type of channels observed within the lower part of Unit 1; **B)** shows the type of channels observed within the upper part of Unit 1. Channel orientations are represented as rose diagram for each part of Unit 1. The stratigraphic level of these maps is shown in Figure 6.8 B.

Finally, standard seismic interpretation and visualisation software are not designed to allow extraction of quantitative, spatially-referenced data from seismic reflection volumes. Therefore, seismic interpretation software has been integrated with geographic information system (GIS) software to develop a methodology that can be used to measure and document the various geometric parameters of the studied fluvial systems. In particular, dataset limitations notwithstanding, the ten interpretive maps are treated as 'paleo-satellite', Google Earth-type images, and they have been imported into ArcGIS for quantitative analysis. A semi-automatic data extraction workflow has been developed, which is efficient, fast and flexible (see Chapter 3 for full GIS methodology).

6.5 Fluvial Channel Morphometric Parameters

The morphometric parameters examined in this study include channel width (*CW*), channel depth (*CD*), meander belt width (*MBW*), meander wavelength (*ML*), channel length (*La*), sinuosity (*SI*), and radius of curvature (RC). All of these parameters have been determined using interpretative maps in ArcGIS. The exception to this is depth which was measured directly from vertical slices through the seismic volume. The geometry of a total of 130 channels has been documented and the associated parametric data has been used to establish empirical relationships between these parameters. In this study, these parameters have been measured following the most widely accepted methodology to measure modern rivers using aerial photographs by different authors (e.g. Schumm, 1977, Ethridge & Schumm 2007, Wood 2007; Figure 6.6). The geometric parameters are measured differently depending on the data used in the analysis. Descriptions of these geometric parameters and how these parameters are measured in both modern and ancient rivers are given in the following sections.

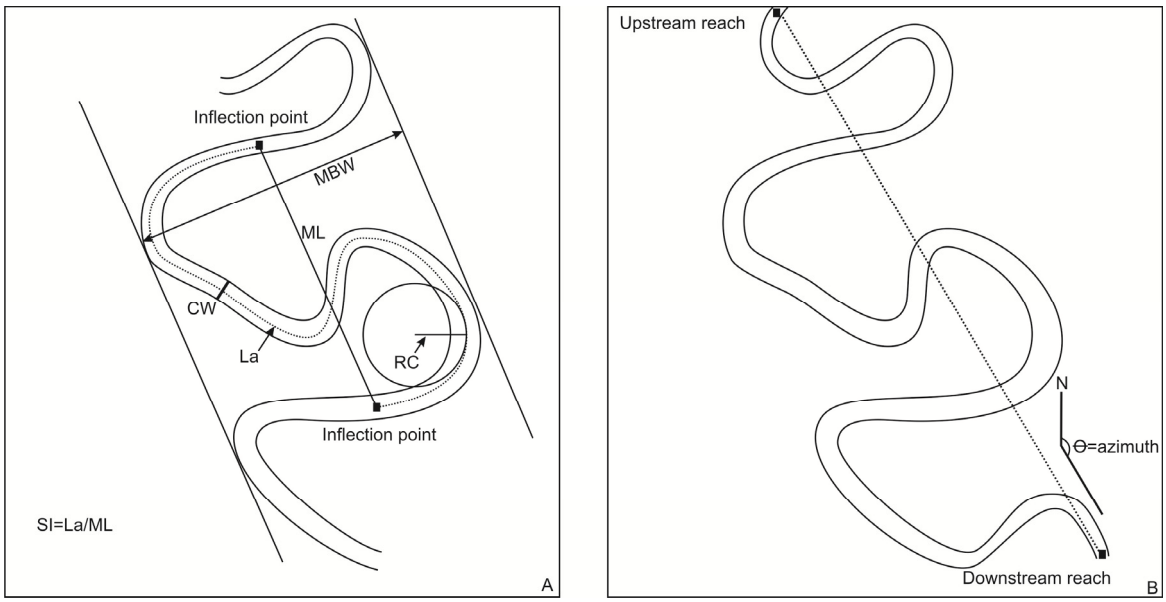

Figure 6.6: Schematic drawing showing the methodology adopted to measure the morphometric parameters of the fluvial systems **(A)** and the channel orientation **(B)**. The morphometric parameters include channel width (*CW*), channel depth (*CD*), meander belt width (*MBW*), radius of curvature (*RC*), meander wavelength (*ML*), and channel length (*La*). Sinuosity (*SI*) is calculated as the length along the channel course (*La*) divided by the meander wavelength (*ML*). The channel orientation is determined by defining the azimuth of a line that has been drawn between two points of the upstream and downstream reaches.

6.5.1 Channel Depth (*CD*)

CD is a measure of the maximum depth of the channel-related incision. This parameter is measured directly from vertical seismic sections and is defined as the vertical distance between the top and base of the channel-related incision (Figure 6.7A); however, in cases where the channel is only visible on time and/or iso-proportional slices, *CD* can be measured by the number of time or iso-proportional slices over which the channel feature appears (e.g. given a 2 ms vertical sampling interval, a channel observed on 4 timeslices would be 6 ms 'thick'). For modern rivers, the maximum bankfull depth, which is measured from the vegetated bank down to the base of the water depth (Figure 6.7B), is the equivalent to the parameter *CD* measured here. Note, however, that the measured

depth in modern rivers does not include the deposited sediments on the river base; this is an important difference which is discussed in detail later.

The *CD* represents the maximum bankfull depth of the channel. In well logs and outcrop, this parameter is measured as the thickness of a complete upward-fining channel-fill. However, the measured thickness is probably less than the original maximum thickness due to post-depositional compaction that reduces the channel-fill thickness during the burial. Ethridge and Schumm (1978) suggested that 10% to be added to estimates of channel-fill thickness (and bankfull depth estimates) to account for post-depositional, burial-related compaction.

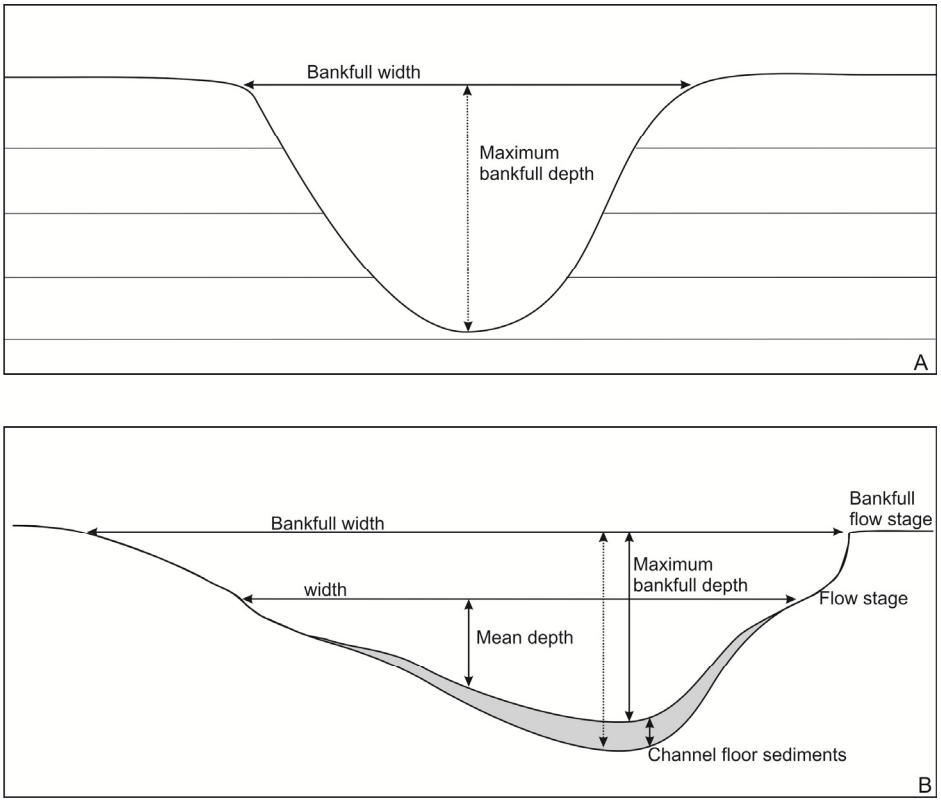

Figure 6.7: Schematic drawing showing the methodology adopted to measure the channel depth (*CD*) from the seismic section **(A)** and from the modern river **(B)**; modified from Bridge, 2003). In this study, the channel depth is measured as the maximum thickness of channel incisions which is the vertical distance between the top and base of the incision feature. In modern rivers the channel depth is measured as the maximum bankfull depth which is the vertical distance between vegetated banks down to the base of the water depth; however, it doesn't take into account the sediments at the base of the channel (dashed-line).

6.5.2 Channel Width (*CW*)

For modern rivers, the channel width (*CW*) is measured as the distance across the channel between vegetated banks. Using outcrop or well data, *CW* is rarely directly measurable for ancient channels, unless both margins of the channel can be unequivocally defined. Where data are more limited, *CW* is usually estimated from the channel depth (derived from the thickness of the channel-fill; see discussion above). Leeder (1973) developed this equation to describe the empirical relationship between depth and width for channels with a sinuosity of >1.7:

$$Wc = 6.8h^{1.54}$$

where the *Wc* is the channel width (*CW*) and the *h* is the channel thickness (*CD*). This relationship is invalid for the low-sinuosity channels (i.e. <1.7).

In this study *CW* is measured directly from the interpretive maps and is defined as the horizontal distance between the erosional margins that bound the channel (Figure 6.6A). *CW* is measured every 500 m on lines which are perpendicular to the channel centreline.

6.5.3 Meander Belt Width (*MBW*)

Meander belt width (*MBW*) describes the width of a fluvial sandbody that forms in response to lateral migration of numerous individual channel systems; in practice, this value defines the width of the 'container' within which the individual channels migrate.

As for *CW* (see above), it is difficult to establish *MBW* for ancient rivers using well log and outcrop datasets, although it may be possible to estimate this parameter from *CW*. For example, Lorenz et al., (1985) developed this empirical relationship between the *CW* and *MBW* for modern rivers:

$$Wm=7.44Wc^{1.01}$$

Where the *Wm* is the meander belt width (*MBW*) and the *Wc* is the channel width (*CW*).

This relationship was established by Lorenz et al., (1985) mainly using data combined from the previous studies of Leopold and Wolman (1960) and Carlston (1965). *MBW* can also be estimated from the *CD*. Based on the quantitative data collated by Carlston (1965), Collinson (1978) established the following empirical relationship relating *MBW* to *CD*:

$$Wm=64.6h^{1.54}$$

In addition, Fielding and Crane (1987) compiled published data on *CD* and *MBW* to produce the following empirical relationship:

$$Wm=12.1\ h^{1.85}.$$

In this study, *MBW* is measured directly from the interpretive maps as the width between two lines that bound outermost visible meander-loop sets (Figure 6.6A). Like *CW*, *MBW* is measured on a line which is perpendicular to the valley centreline every 500 m along the valley axis.

6.5.4 Meander Wavelength (*ML*)

In both modern rivers and in this study of ancient systems, meander wavelength (*ML*) is defined and measured as the length between the upstream and downstream inflection points that define a single, complete meander bend (Figure 6.6A).

In ancient rivers, *ML* is very difficult to be determined from well logs or outcrops alone, although Leopold and Wolman (1960) established an empirical relationship between *ML* and *CW* for high-sinuosity, modern channels:

$$Lm=10.9Wc^{1.01w}$$

where *Lm* is the meander wavelength (*ML* in this study). Another empirical relationship between *ML* and *CD* was proposed by Leeder (1973) and Collinson (1978). This is:

$$Lm=74.1h^{1.54}$$

Although a formal empirical relationship was not proposed, Brice (1984) suggested that the ratio of *ML* to *CW* is *ca*. 1:10 and the ratio of *ML* to radius of curvature (RD) is *ca.* 1:5.

6.5.5 Channel Length (*La*)

Channel length (*La*) is measured as the length of the centreline along the channel course between the uppermost and lowermost inflection points (Figure 6.6A). *La* is measured and used with *ML* to calculate channel sinuosity.

6.5.6 Sinuosity (*SI*)

Sinuosity (*SI*) is an important parameter in describing the overall map-view style (e.g. meandering, braided and straight) of a fluvial system (e.g. Leopold and Wolman, 1957; Schumm, 1977; Rust, 1978). In modern systems, *SI* is calculated by dividing channel length (*La*) by meander wavelength (*ML*) for discrete meander segments of the channel. The overall sinuosity of a channel is calculated by dividing the length along the channel course via the total length of the channel axis; the same methodology is applied here to calculate *SI* (Figure 6.6A).

It is typically very difficult or impossible to determine *SI* from well logs or outcrops alone (see discussion by Bridge and Tye, 2000). Schumm (1977) found a strong empirical relationship between the *SI* and grain-size of sediment transported by the fluvial system. He suggested that fluvial channel systems that have *SI* of 1–1.3 are bedload-dominated system; systems with *SI* of 1.4–2 are mixed-load systems; and systems with *SI* >2.0 are

suspended-load-dominated systems. In the case of single channel fluvial systems, Leopold and Wolman (1956) used an *SI* value of 1.5 to categorise channels as either low-sinuosity (*SI* <1.5) or high-sinuosity (*SI* >1.5). Where multiple active channels are present, the same authors used an *SI* value of 1.5 to separate braided (*SI* <1.5) from anastomosing (*SI* >1.5) channels.

6.5.7 Radius of Curvature (*RC*)

Radius of curvature (*RC*) in modern and ancient systems is calculated by measuring the radius of a best-fit circle located within a meander bend (Figure 6.6A). Similarly to those parameters described above, *RC* is difficult to estimate from the well logs and outcrops. An empirical relationship between the *RC* and *ML* has been proposed by Brice (1984); this states that the ratio of *ML* to *RC* is *ca*. 1:5.

6.5.8 Channel Orientation (*CO*)

The overall trend or orientation for each channel has been determined by defining the azimuth of a line that has been drawn between two points of the upstream and downstream reaches at the limits of the dataset (Figure 6.6B). Since the ultimate source of sediment supply (i.e. the Malay Peninsula and Thailand) and the ultimate depocentre (i.e. the South China Sea) for most if not all of the channels observed within the Malay Basin are known, the upstream and downstream reaches of each channel have been defined. After determining the orientations of all the channels observed on the interpretive maps,

these data have been plotted on rose diagrams to assess the vertical changes in channel orientation for Pleistocene to Recent fluvial systems.

6.5.9 Assessment of Errors Related to Quantifying Morphometric Parameters

Measurement of morphometric parameters of fluvial channel systems has been completed through analysis of time and iso-proportional slices from a 3D seismic reflection dataset; such an approach has only rarely reported in the literature and only few studies have integrated seismic interpretation and GIS software (see Fachmi and Wood, 2003, Wood, 2007, 2009, Kiel, 2009). Extraction of dimensional data from seismic datasets is associated with a number of errors; the derived values (and associated interpretations) are only reliable if they exceed the magnitude of errors associated with that measurement. The errors in quantifying the morphometric parameters are largely related to the initial line spacing of the original seismic survey and any post-processing decimation which is applied.

In this study, there are two types of errors that can be identified. The first error relates to the lateral measurements such as *CW* and *MBW*. This error is estimated to be ±36-48 m, and this is related to decimation of the original 3D seismic survey (i.e. every 4^{th} in-line and cross-line of the original 9.38 m by 12.5 m line spacing). The calculated error for lateral measurements implies that channels <48 m wide are not imaged, thus channels that have been imaged as approximately one pixel wide 'lines' on time or iso-proportional slices (*Type-5*; Table 6.2) and which lack well-defined channel banks, are estimated to have widths of >48 m. Furthermore, because the fine-grained sediments of the overbank

deposit may be less seismically reflective and hence may not be seismically visible, channel width measurements should be considered to be the minimum widths.

The second and more significant error is related to calculation of *CD*. This is related to being able to accurately determine the depth of shallow channels which are at or below the vertical resolution of the seismic data (e.g. *Type-5*; Table 6.2). In addition, the vertical sample spacing of 2 ms (twt) suggests *ca*. 2 m of vertical error. It should be noted that error bars have not been shown in any of the graphical plots presented in this study as many of the error bars lie within the area of the data points shown on these plots. Furthermore, addition of error bars would unnecessarily mask the data points on the plots. Where errors may affect the geological interpretation, this is mentioned in the text.

6.6 3D Seismic Analysis of Pleistocene-Recent Fluvial Systems

6.6.1 Stratigraphic Framework

Based on seismic facies analysis and reflection continuity, the Pleistocene to Recent succession has been divided into four seismic units (Units 1-4; Table 6.1; Figure 6.8). The horizons bounding these units have been mapped throughout the study area (Horizons A-E; Figure 6.4). Two additional horizons, Horizons C.1 and D.1, both of which are strongly erosive, have been mapped within the upper parts of Unit 3 and Unit 4, respectively, to allow further sub-division these units into two sub-units (i.e. sub-units 3.1, 3.2, 4.1 and 4.2; see Table 6.1 and Figure 6.8). Figure 6.8C is a schematic cross-section that illustrates the stratigraphic template and nomenclature used in this study. In addition, the vertical variability of fluvial channels within this framework is illustrated and indicates that a wide range of fluvial channel styles and morphologies have been

observed at multiple stratigraphic levels within the Pleistocene succession. Based on cross-sections and map-view images, six main channel types have been identified (Table 6.2; see Chapter 4 for full description). Examples of time and iso-proportional slices of these channel types are shown in Figure 6.9.

6.6.2 Evaluation of the Depositional Sequences

As described above, four seismic units have been identified within the Pleistocene to Recent succession. The vertical and lateral distribution of the six main channel types discussed above is described fully in Chapter 4. In the following sections, these units and sub-units are summarised and interpreted in terms of the key controls on channel evolution as outlined in the Introduction. This provides the framework for the extraction of quantitative data which follows.

6.6.2.1 Units 1& 2 and Sub-units 3.1 & 4.1

Description: The lower parts of Units 1 & 2 and sub-units 3.1 & 4.1 are characterized by prominent incisions with *Type-1* and *Type-3* channels, which are 16-48 ms twt (15-45 m) deep and 0.5-3 km wide (Figure 6.8). These channels have a low sinuosity index (*SI*=1.05-1.1.3) and are mainly orientated WSW-ESE. *Type-3* channels are associated with smaller (0.5-1 km wide by 25-30 ms twt (20-25 m) deep), low-sinuosity (*SI*=1.15) tributaries. Examples of the low-sinuosity channels are shown in Figures 6.5A and 6.9A & C.

Table 6.1: lists the seismic units and sub-units which are identified within the Pleistocene to Recent succession within the Malay Basin. The basic information data including isochron range and average, channel width (*CW*), channel depth (*CD*) and sinuosity (*SI*) of the channel systems that have been observed in the lower and upper parts of each unit are illustrated.

Unit No.	Base horizon	Top horizon	Thickness range (ms twt)	Average thickness		Channel parameters				Incised valley parameters		
				ms twt	m	Stratigraphic Level	*CW* (m)	*CD* (m)	*SI*	width (m)	depth (m)	SI
4.2	D.1	E	82-192	110	104	Inside IV	600	25	3	13000-18000	55-78	1.1
						Outside IV	320-600	15-32	1.1.15	---------	---------	-------
4.1	D	D.1	108-228	120	112	'U'	75-220	8-20	1.3-1.5	---------	---------	-------
						'L'	300-1300	15-30	1-1.3	---------	---------	-------
3.2	C.1	D	228-290	6	58	Inside IV	150-250	12-25	2.5-3	3500-6500	35-60	1.1
						Outside IV	450-715	18-30	1-1.2	---------	---------	-------
3.1	C	C.1	250-330	80	75	'U'	75-212	8-23	1.5-2.5	---------	---------	-------
						'L'	350-1100	15-32	1-1.17	---------	---------	-------
2	B	C	330-420	90	85	'U'	75-250	10-23	1.4-2.3	---------	---------	-------
						'L'	580-3000	30-50	1-1.25	---------	---------	-------
1	A	B	420-575	155	145	'U'	75-200	8-18	1.6-2.7	---------	---------	-------
						'L'	450-2100	22-30	1-1.2	---------	---------	-------

Table 6.2: illustrate the types of the channel morphologies observed within the Pleistocene to Recent succession. The description and the morphometric parameters including channel width (*CW*), channel depth (*CD*) and sinuosity (*SI*) of these types of channel systems are described.

Channel Type	Seismic facies description	Comments	Morphometric parameters				Examples
			CW (m)	*CD*		*SI*	
				(ms twt)	(m)		
Type-1	v-shaped, infilled with variable-amplitude, laterally-continuous seismic reflections	common in association with large, low-sinuosity channels	450-1500	24-38	22-35	1-1.3	Figure 5.9A
Type-2	v-shaped, infilled with low-amplitude, chaotic seismic reflections	common in association with large, highly sinuous channels	300-600	16-32	15-30	2.5-3.5	Figure 5.9B
Type-3	u-shaped, infilled with variable-amplitude, laterally-continuous seismic reflections	common in association with major low-sinuosity channels	1500-3000	32-54	30-50	1-1.12	Figure 5.9C
Type-4	Narrow, shallow, u-shaped, with a clear erosional base and sub-seismic infill	common in association with medium-scale, high-sinuosity channels	150-300	13-22	12-20	2-3	Figure 5.9D
Type-5	Laterally discontinuous, high-amplitude, seismic reflection 'doublet' lacking on erosional base and with a sub-seismic infill	very common in association with moderate-sinuosity channels and narrow, highly-sinuosity channels	75-200	8-13	6-12	1.5-2	Figure 5.9E
Type-6	Broad, deep and u-shaped, filled with a wide range of seismic facies	commonly associated with incised valleys and association channel fills	3500-13000	38-80	35-78	1.1-1.2	Figure 6.8B

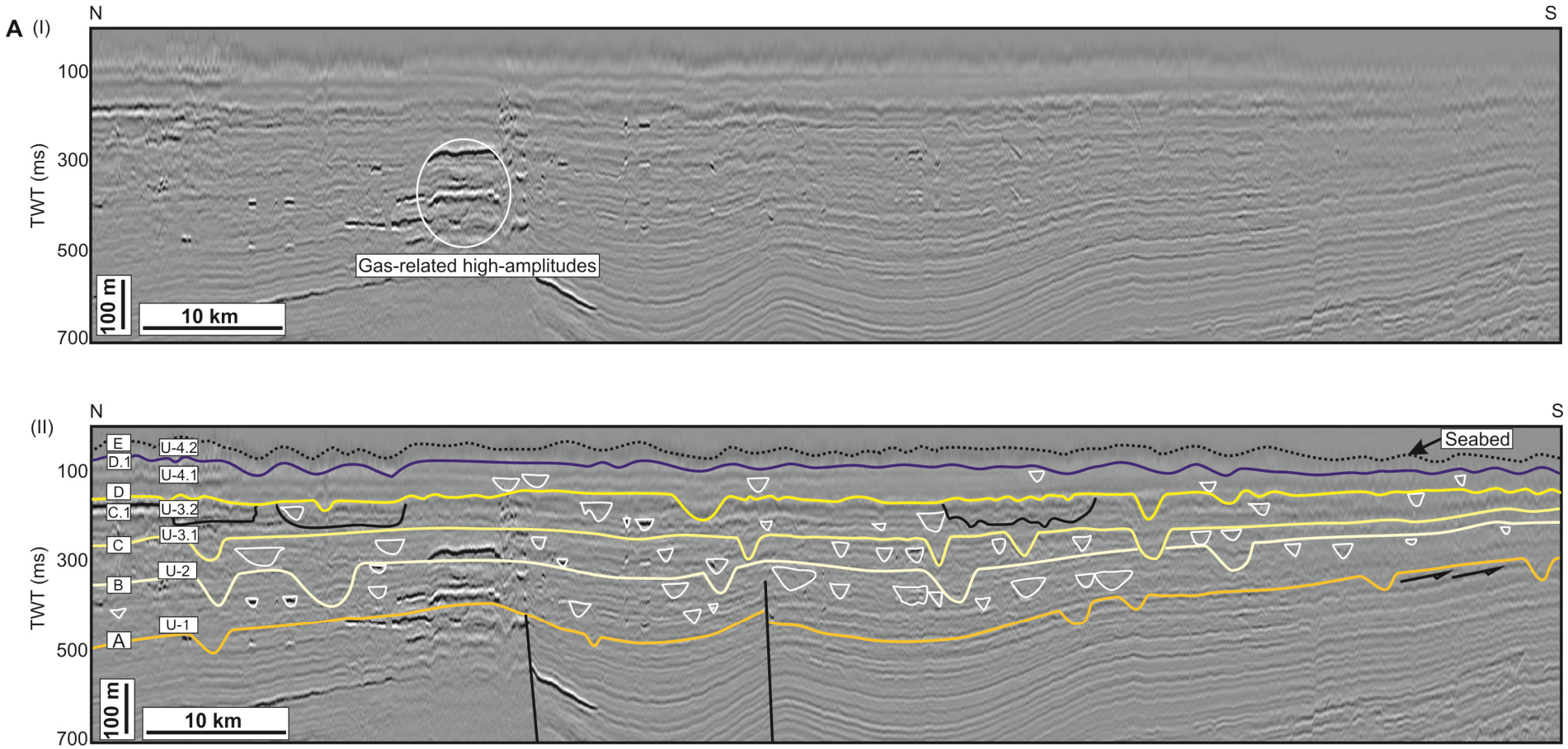
A (I)
N
S
100
300
500
700
TWT (ms)
Gas-related high-amplitudes
100 m
10 km
(II)
N
S
E
D.1
D
C.1
C
B
A
U-4.2
U-4.1
U-3.2
U-3.1
U-2
U-1
Seabed
100
300
500
700
TWT (ms)
100 m
10 km

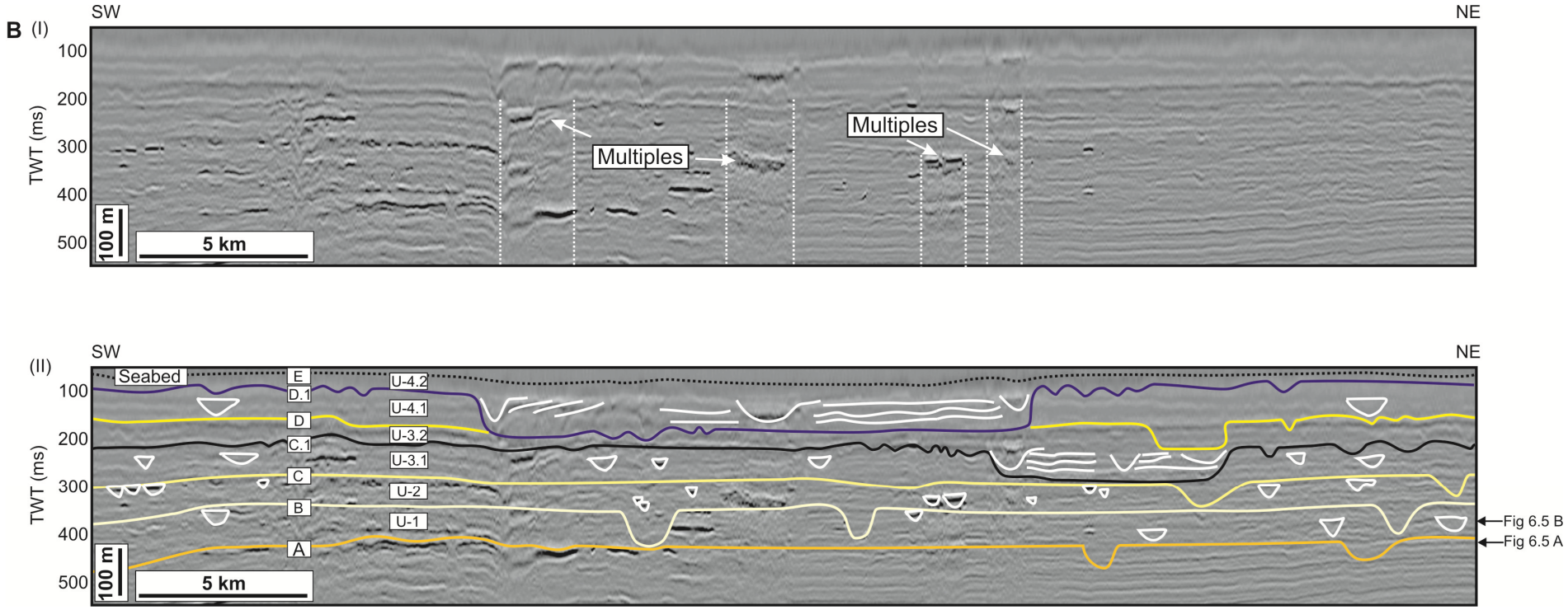
B (I)
SW
NE
100
200
300
400
500
TWT (ms)
Multiples
Multiples
100 m
5 km
(II)
SW
NE
Seabed
E
D.1
D
C.1
C
B
A
U-4.2
U-4.1
U-3.2
U-3.1
U-2
U-1
100 m
5 km
Fig 6.5 B
Fig 6.5 A

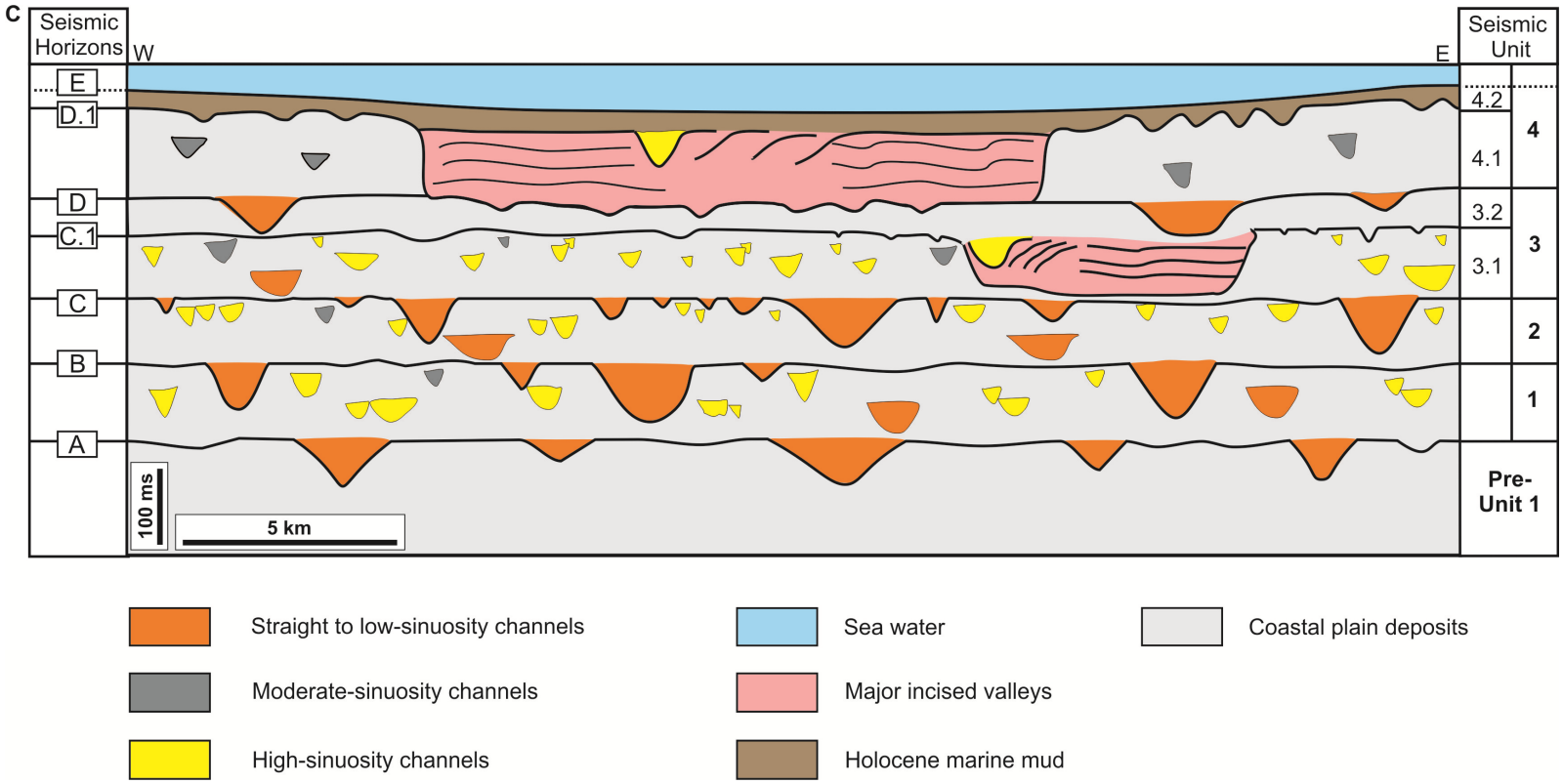

Figure 6.8: A) (I) Un-interpreted and (II) interpreted regional seismic section through the 3D seismic dataset illustrating the seismic units (1-4) and the bounding surfaces (Horizons A-E). Major channel systems are also shown as white 'u' and 'v' shapes. The main bounding surfaces (Horizon A-D) are characterised by prominent incisions. Note the angular discordance between Horizon A and underlying unit at the basin margin (right side of cross-section). Location of this section is shown in Figure 6.4; **B)** Un-interpreted (I) and interpreted (II) seismic section showing the seismic units (1-4) and the bounding surfaces (Horizon A-E). Two additional horizons (Horizon C.1 and D.1) have been picked to show deep and wide incision features. These two horizons divide Unit 3 and 4 into sub-units. Major channel systems are also shown. Note the seismic expression within these deep incisions is different from those adjacent strata. Interpretive planview maps of horizontal 'time' and iso-proportional slices (Figure 6.5) used in this study are shown on the right-hand side of this seismic section as figure numbers. Location of this section is shown in Figure 6.4; **C)** A schematic cross section through the Pleistocene to Recent succession within the Malay Basin showing the seismic units (1-4) and the sub-units 3.1, 3.2, 4.1, and 4.1, the bounding surfaces (A-E) and the channel types observed within each unit. Note the systematic vertical changes in channel patterns and scale in each individual unit.

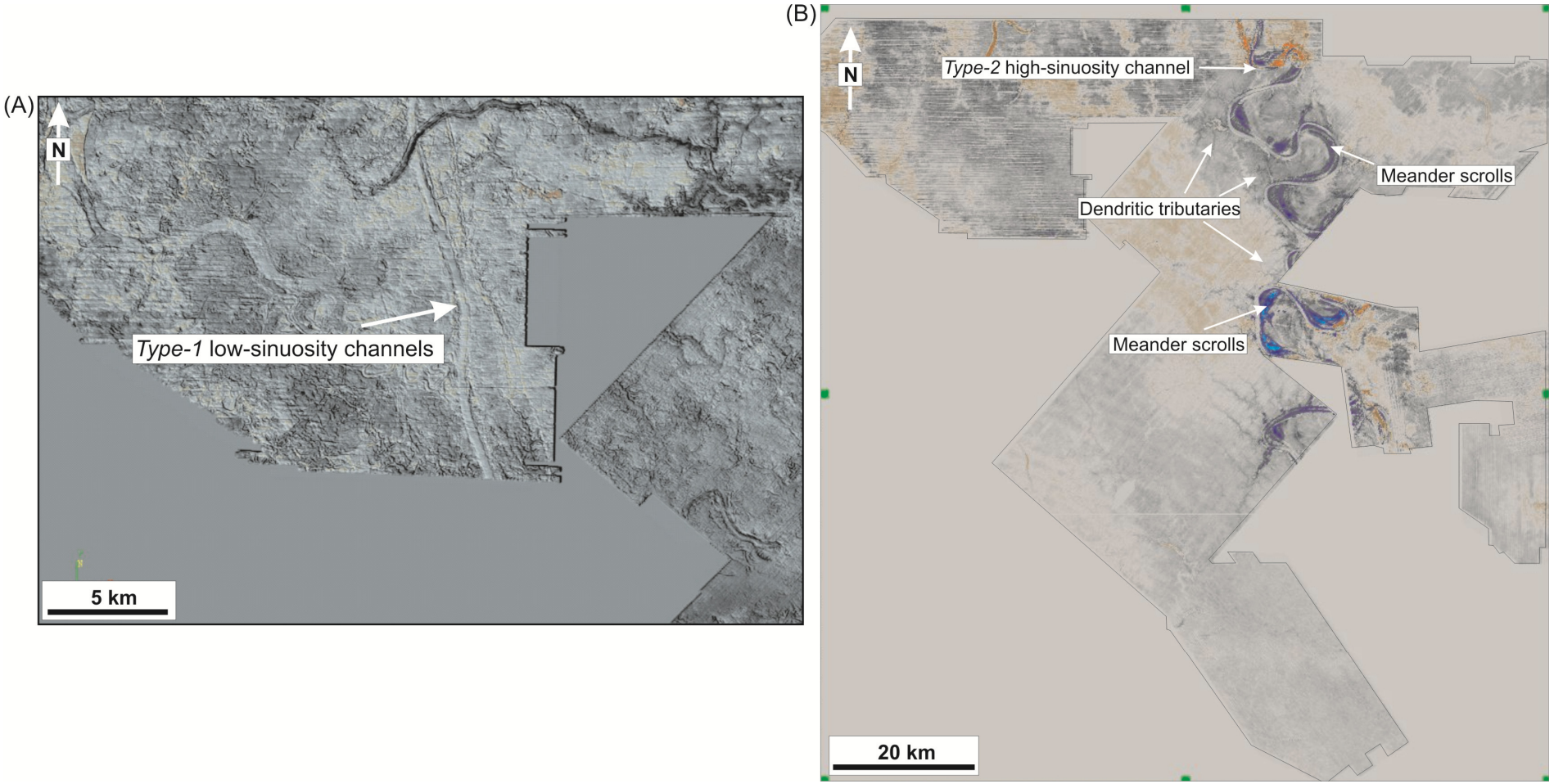
(A)
N
Type-1 low-sinuosity channels
5 km
(B)
N
Type-2 high-sinuosity channel
Meander scrolls
Dendritic tributaries
Meander scrolls
20 km

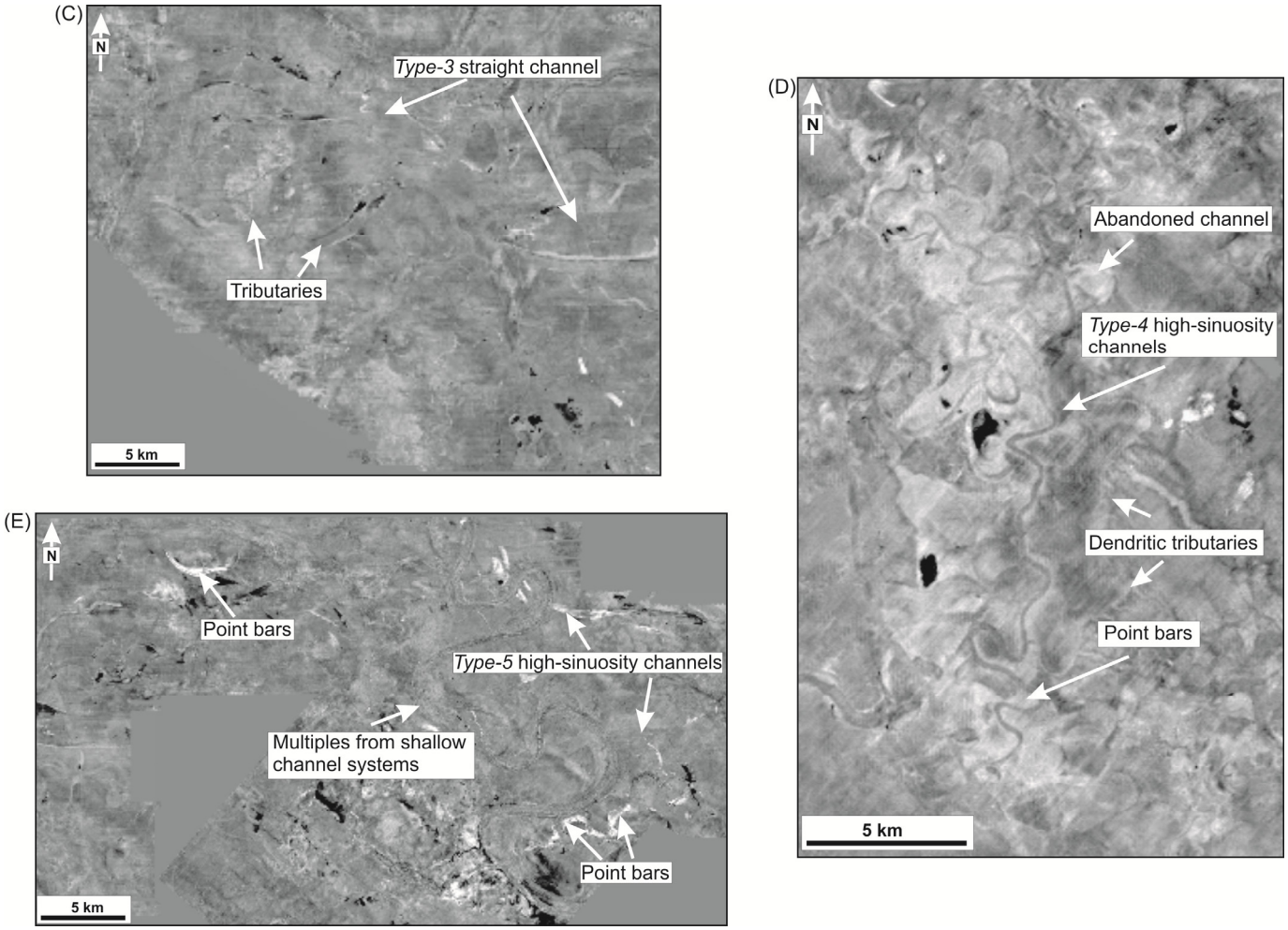

Figure 6.9: Examples of time and iso-proportional slices showing type of channels observed in this study. See Table 6.2 and text for full description.

Within these units and sub-units, channels vary in terms of size and sinuosity. The upper parts of these units and sub-units are characterised by highly-sinuous channels (*SI* =>1.5). These channels are characterised by *Types-2, 4 & 5* morphologies which are up to 20 ms twt (18 m) deep and 50-370 m wide (Figure 6.8). These channels have meander belts of 6-9 km with radius of curvature of up to 1.3 km. These highly sinuous channels are associated with well-developed scrolls and are oriented WNW to ESE. Several abandoned channels are clearly imaged in association with some of these highly-sinuous channels. Examples of the highly sinuous channels are shown in Figures 6.5B and 6.9B, D & E.

Interpretation: The straight and low-sinuosity channels in the lower part of Units 1 & 2 and sub-units 3.1 & 4.2 were broadly flowing eastwards from the high elevated areas in the west and south towards the axial zone of the basin in the east. Based on the lack of smaller dentritic tributaries, channels in the lower parts of these units and sub-units may form part of a 'lowstand alluvial bypass system' (*sensu* Posamentier, 2001), formed during relative sea-level fall. Such systems have been documented in the Java Sea Shelf and are interpreted to form when the magnitude of relative sea-level fall is not great enough to expose wider parts of the previously-flooded continental shelf (e.g. the Sunda Shelf). These channels were flowing from the high elevated areas, which suggest that they were high-gradient channels which also indicate high discharge. Furthermore, the major channel systems are associated with tributary channels that were elongated (up 3 km), possibly due to an overall increase in discharge from the smaller tributary channels.

In contrast to the relatively straight channels within the lower parts of these units and sub-units, channels in the upper parts are dominated by highly-sinuous, meandering channel forms which are associated with point bar deposits. Based on sequence-stratigraphic concepts, these meandering channels may be interpreted as having formed during sea-level rise after the preceding sea-level fall (Shanley and McCabe, 1994). These

meandering channels have different sizes and are of varying sinuosity; these differences may be caused by the type of sediment load and the discharge (c.f. Schumm, 1993). These meandering channels flowed broadly eastwards towards the South China Sea. In association with the larger meandering rivers, abandoned channels were clearly imaged. Channel abandonments would also have been caused by the continued sea-level rise (cf. Bridge, 2003).

6.6.2.2 Sub-units 3.2 and 4.2

The lower parts of sub-units 3.2 and 4.2 are characterised by major incision features (depths 38 to 83 ms twt (35–80 m) and widths of 3.5 and 14 km) with *Type-6* channel morphologies. In cross section, the seismic facies within the incisions are different from those outside them. Outside these major incisions, 50-75 m wide, incised features with 'v'-shaped channels are recognised (Figure 6.8B). Different seismic facies have been observed within these incisions, including laterally-continuous seismic reflections and smaller 'v'-shaped incisions (*Type-2* and *Type-4* channel morphologies; see example from Figure 6.9B & D) associated with inclined seismic reflections which dip inwards towards the incisions.

In planview, these channels have a pronounced dentritic pattern (Figure 6.9B). Channels with *Type-2* morphology which are associated with inclined (up to 7°) reflections. These *Type-2* channels are highly sinuous and are up to 27 ms twt (25 m) deep, 400-600 m wide and have meander belt widths of 6-13 km and radius of curvature of 1.7-3 km. These major channels flowed towards the SE and are fully confined within the deep incisions. Neck-cut off abandoned channels were clearly imaged. In the north-eastern and southern

part of the study area, relatively large (depths of 17-34 ms twt (15-30 m) and widths of 400 to 900 m), low-sinuosity channels which flowed towards the SE are developed.

Interpretation: The large incisional features developed along the base of the sub-units 3.1 and 4.1 are significantly larger than those lowstand alluvial bypass channel systems observed in underlying stratigraphic units (i.e. Units 1 & 2). These features are, therefore, interpreted as incised valleys formed due to a relative sea-level fall. Furthermore, based on its stratigraphic occurrence towards the top of the Pleistocene succession and by comparison to other similar systems documented in nearby basins (Posamentier, 2001; Miall, 2002, Darmadi et al., 2007), the large incised valley of sub-unit 4.1 is interpreted to have formed during the Last Glacial Maximum when sea-level fall was sufficiently great to widely expose the Sunda Shelf. The presence of smaller dentritic tributaries at the valley margin supports the interpretation of this large incisional feature as incised valley (cf. Posamentier, 2001).

After formation of the erosional base and initial deposition, the incised valleys became occupied by large sinuous river systems which appear to represent the major drainage systems occupying the axial zone of the Malay Basin during Late Pleistocene times. Low-sinuosity channels in the north-eastern and southern part of the study area could be large tributaries that fed the main incised valleys. The meandering rivers were associated with point bars and are interpreted to have developed during the main transgressive period. Neck-cut off features and associated abandoned channels suggests that a continued sea-level rise may have caused the channels to reduce thier sinuosity via this mechanism (Schumm, 2005).

6.7 Quantitative Analysis of Pleistocene-Recent Fluvial Systems

A wide range of fluvial channel styles have been imaged. Morphometric parameters of 130 channels have been measured and cross-plotted in order to allow classification of the fluvial channel systems and to establish empirical relationships between these parameters.

6.7.1 Sinuosity (*SI*) and Channel Classification:

SI is one of the main parameters used to classify the channel systems since it allows a first-order classification of the channel map-view morphology to be made. As a result, it has also been plotted against various other morphometric parameters (*CD*, *CW*, *MBW* and *RC*; Figures 6.10). Based on the first-order planform geometry (i.e. sinuosity) and the documented morphometric parameters, the channel systems observed in this study have been classified into three main groups (Table 6.3):

1) *Group-1* – these represent incised valleys and account for 4% of the total channel types observed in this study area. This group of channel systems have very low sinuosity index (*SI* 1-1.12) and have the highest W/D ratio of >100. Incised valleys are the largest fluvial systems type observed within the Malay Basin, being 6000-14000 m wide and 35-78 m deep. These valleys are characterised by *Type-6* channel morphologies that are observed along a sequence boundary (Table 6.2). Within the confines of valleys themselves, *subgroup-3.1* channel systems are developed.
2) *Group-2* – these represent alluvial bypass channel systems and accounts for 64% of the total channels observed in this study area. These channels have a low-sinuosity index (*SI* 1-1.3) and W/D ratio of 20-75. They display a very wide range

of *CW* and *CD*, ranging from 450 to 3000 m to 10-48 m, respectively. These channels types are best-developed in the lower part of the seismic units. Group 2 channels can be further divided into two sub-groups:

a. *Sub-group-2.1* – these are attached to smaller tributary channels and represent the largest alluvial bypass channel systems, accounting for 4% of the channels observed in the study area. These channels are 1800-600 m wide and 30-47 deep and are characterised by *Type-3* channel morphologies. The channels of this sub-group have a wide range of *MBW* (4300-6400 m) with an associated *RC* value of 1800-2600 m.

b. *Sub-group-2.2* - this sub-group represents 60 % of the total channels observed in this study area and represent the majority of the alluvial bypass channel systems. They have a sinuosity index of 1-1.3 and W/D ratio of 20-48, and they are mainly characterised by *Type-1* channel morphologies that are 600-1800 m wide and 30-47 m deep. The channels within this sub-group have a wide range of *MBW* (500 to 4300 m) and *RC (*450-1600 m).

3) *Group-3* - This group accounts for 32 % of the total channels observed in the study area and are characterised by meandering rivers which have high-sinuosity index of 1.5-3 and W/D ratio of <25. These channels are the shallowest (8-25 m deep) of those identified here and are of highly variable *CW* (50-600 m). *Group 3* systems have been observed in the upper parts of the four main seismic units and can be divided into two sub-groups:

a. *Sub-group-3.1* represents the confined highly sinuous channels which have high sinuosity index (*SI* > 2.5) and W/D ratio of 15-25. This sub-group represents 4% of the total channels observed in this study. These channels are the largest among those of *Group-3* with *CW* (300-600 m) and *CD* (15-

25 m) which are characterised by *Type-2* channel morphologies. The channels of this sub-group have *MBW* (6000 to 14000 m), RC (1000-3000 m) and *ML* (6000-14000 m). These confined highly sinuous channels have been observed in the upper part of the incised valleys (*Group-1*).

b. *Sub-group-3.2* represents the unconfined high-sinuosity channels that has a sinuosity index of 1.5-2.5 and W/D ratio of <15. This sub-group represents 28 % of the total channels observed in this study. These channels are the smallest channel systems observed in this study with *CW* (50-250 m) and *CD* (8-20 m). These channels are characterised by *Type-4* and *Type-5* channel morphologies. The channels of this sub-group have *MBW* (800 to 7000 m), *RC* (300-2000 m) and *ML* (1000-7000 m). These channels have been observed within the upper parts of the seismic units.

6.7.2 Channel Orientation (*CO*)

The orientations of the 130 channels identified in the study area have been plotted on a rose diagram and two main orientations have been observed (Figure 6.11). The alluvial bypass channel systems (*Group-2* channels) mainly flowed eastwards from the western basin margin towards the axial zone of the Malay Basin (Figure 6.11A). The majority of highly sinuous channels (*Group-3* channels) flowed towards the south-east, towards the South China Sea (Figure 6.11B).

Table 6.3: illustrates the channel groups observed within the Pleistocene to Recent succession. The description and the morphometric parameters including sinuosity (*SI*) channel width (*CW*), channel depth (*CD*), W/D ratio, meander belt width (*MBW*), radius of curvature (*RC*), meander wavelength (*ML*), and channel length (*La*) are described.

Channel Groups	Channel Types	% of total channels documented	SI	CW (m)	CD (m)	W/D Ratio	MBW (km)	RC (km)	ML (km)	La (km)
1	**Incised valleys**	4%	1-1.12	6000-14000	35-78	>100	----------	----------	20-76	23-78
2.1	**Major alluvial bypass channels**	4%	1-1.2	1300-3000	30-50	50-75	4.5-6.4	1.8-2.6	25-80	20-120
2.2	**Alluvial bypass channels**	60%	1-1.3	450-1300	10-35	20-48	0.5-4.33	0.45-1.6	10-125	11-160
3.1	**Confined, highly sinuous channels**	4%	2.5-3	300-600	15-25	15-25	6-14	1-3	20-76	140-215
3.2	**Unconfined, highly sinuous channels**	28%	1.5-2.3	50-250	8-20	<15	0.8-7	0.3-2	15-68	40-130

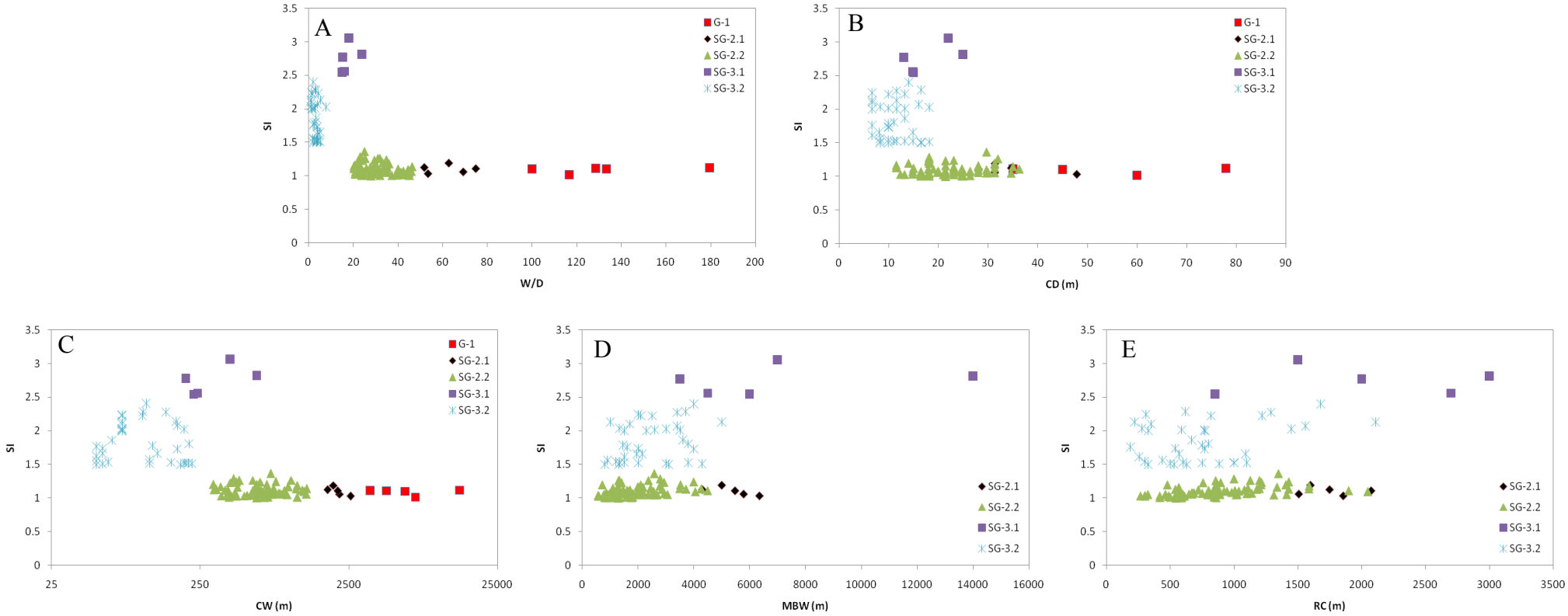

Figure 6.10: Five cross-plots of sinuosity versus W/D ratio (**A**), channel depth (*CD*; **B**), channel width (*CW*; **C**), meander belt width (*MBW*; **D**) and radius of curvature (*RC*; **E**). **A & C)** show clearly three separate populations which are corresponding to the three main groups identified in this study. The low-sinuosity channels of *Groups-1 & 2* display a wide range of *CW*, *CD* and W/D ratio across their range of *CW* (**C**), *CD* (**B**) and W/D ratio (**A**); however, three relatively-small tightly-clustered across their *CW* and W/D separate *Group-1* from *Group-2* and divide *Group -2* into two sub-groups (**A, C**). The confined highly sinuous channels (*sub-group-3.1*) are wider and deeper with considerable *MBW* and *RC* than those of *sub-group-3.2*. **A, B, & C**) shows an inverse relationship between the *SI* and *CW*, *CD* and W/D ratio as *CW* and *CD* increases as the *SI* decreases. **D & C**) show wide range of *MBW* and *RC*; however, the largest are associated with those of *sub-group-3.1*.

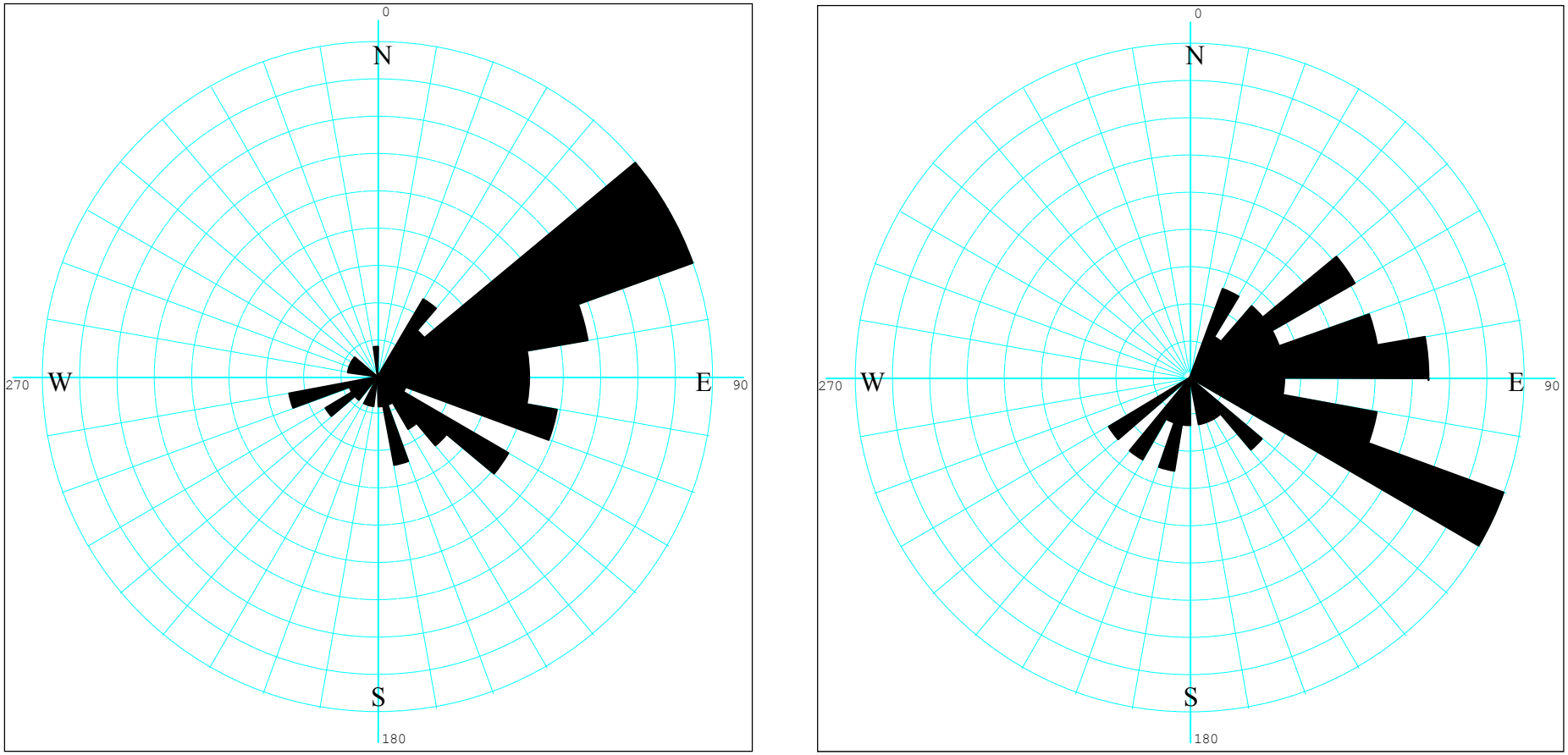

Figure 6.11: Rose diagrams showing the orientation of the channel systems observed in this study. **A)** Shows the orientation of the alluvial bypass channel systems (*Group-2*) which mainly flowed to the east from the high elevated areas towards the axial zone of the basin; **B)** Shows the orientation for the highly sinuous channels (*Group-3*) which mainly flowed towards the south east towards the South China Sea.

6.8 Empirical Relationships

Morphometric parameters of extracted from the 130 studied channels have been cross-plotted against each other to establish empirical relationships. Where a relationship is seen to exist, an empirical equation is then developed to characterise this relationship. The developed empirical equations are compared to equations which have been developed based on analysis of modern rivers; the differences between these equations are described and the reasons for these differences are interpreted.

6.8.1 Sinuosity (*SI*) vs. Channel Width (*CD*) and Channel Depth (*CD*)

A very wide range of values for *CD* (8-78 m) and *CW* (50-14000 m) have been observed. Plotting *SI* against *CD* shows a positive relationship between *CD* and *SI* for the highly sinuous channels (*SI=>1.5)*, where *CD* increases as *SI* increases (Figure 6.10B). There is a very wide range of *CD* for the low-sinuosity channels, and thus a high uncertainty in predicting *CD* from *SI*; however, the plots of Figure 6.10B suggest that low-sinuosity channels are much deeper than those of highly sinuous channels, although the confined highly sinuous channels (*sub-group-3.1*) show considerable depths that are larger than some of those of less sinuous channels.

Plotting *SI* against *CW* shows a positive relationship between *CW* and *SI* for the highly sinuous channels (*SI=>1.5)*, where *CW* increases as *SI* increases (Figure 6.10C). There is a very wide range of *CW* for the low-sinuosity channels, and thus a high uncertainty in predicting *CD* from *SI*; however, the plot of Figure 6.10B suggests that low-sinuosity channels are much wider than those of highly sinuous channels, although the confined

highly sinuous channels (*sub-group-3.1*) show considerable widths that are larger some of those of less sinuous channels.

6.8.2 Channel Depth (*CD*) vs. Channel Width (*CW*)

Plotting *CD* against *CW* defines a moderately-strong (R^2=0.6) positive relationship between these two variables and indicates that as channels get wider they also get deeper (Figure 6.12A). This relationship allows for an empirical equation to be developed which describes the relationship between *CD* and *CW* (dashed-line in Figure 6.12B);

$$CW=0.3CD^{2.54}.$$

The deepest and widest channel systems are those of the incised valleys (*Group-1*) followed by those of the alluvial bypass channel systems (*Group-2*). *Group-3* of the highly sinuous channels are the smallest channels among those groups, although *sub-group 3.1* channels (confined highly sinuous channels) have considerable channel depth and width.

As mentioned above, Leeder (1973) developed an empirical equation (CW=6.8$CD^{1.54}$) to describe the relationship between *CD* and *CW* for high-sinuosity (*SI*>1.7) channels; this equation is tested here against high-sinuosity channels (i.e. *SI* >1.7) identified in the study area (Figure 6.12B). It can be seen that the estimated values of *CW* using Leeder's (1973) equation are overestimated, and a better equation can be developed to fit these specific

data (indicated by a black dashed line on Figure 6.12B). The associated trendline has the same general form as that predicted by Leeder (1973) (black solid-line on Fig. 6.12B), which correctly predicts the trend but overestimates *CW* for the the channels observed in this study. This trend has been edited by changing the constant of 6.8 in Leeder's equation ($CW=6.8CD^{1.54}$) to 3.0 to give a corrected empirical equation of $CW=3.0CD^{1.54}$. The red-dashed line represnts the trendline of the early devolped empirical equation ($CW=0.3CD^{2.54}$) for all channel tyeps. This shows that corrected version of Leeder's equation fits the data used, unlike original eqation of Leeder and the early developed equation in this study.

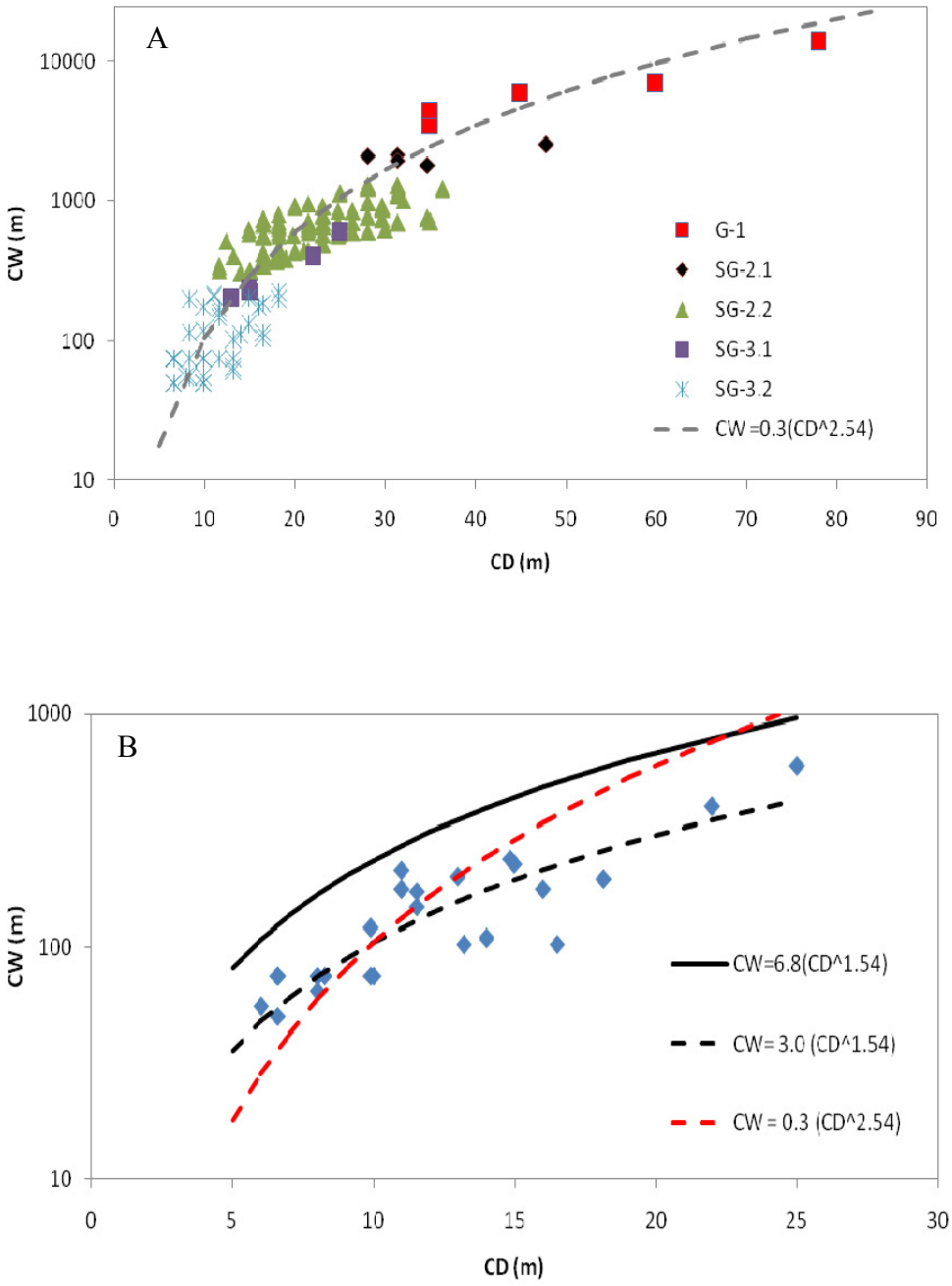

Figure 6.12: A) Cross-plot of channel depth (*CD*) versus channel width (*CW*) shows that a direct relationship exists where *CW* increases as *CD* increases. This relationship allows for a new empirical equation to be developed (dashed-line). The developed equation is $CW=0.3CD^{2.54}$. It can also be seen that the low-sinuosity channels are the widest and the deepest. **B)** Cross-plot of channel depth (*CD*) against channel width (*CW*) for the highly sinuous channels (*SI*>1.7). The red dashed-line is the earlier developed emperical relation. Note while this emperical relation provides good estimation of the dependcy between *CW* and *CD* for the overall range of sinousities observed, we can see that a better relation (black dashed-line) can be developed strictly for highly sinuous channels. This relation has the same form as Leeder's (1973) equation (black solid-line) which correctly predicts the trend but overestimates *CW* for the the channels observed in this study. This trend has been edited by changing the constant of 6.8 in Leeder's equation ($CW=6.8CD^{1.54}$) to 3.0 to give a corrected empirical equation of $CW=3.0CD^{1.54}$.

6.8.3 Channel Width (*CW*) vs. Meander Belt Width (*MBW*)

A very wide range of values for *CW* (50-14000 m) and *MBW* (780-14000 m) have been observed. The largest values for *MBW* (i.e. >6000 m) are those associated with the confined, highly-sinuous channels of s*ub-group-3.2*. Plotting *CW* against *MBW* shows that there is a positive relationship between these parameters, the strength of which varies (R^2=0.5 to 0.9) depending on the exact sub-group of channels; in general, however, the wider channels are associated with overall wider meander belts (Figure 6.13A). In detail, however, two distinct trends appear to be present within the data; 1) one which is associated with low-sinuosity channels (i.e. *Group-2*) that defines a relatively shallow slope; and 2) one which corresponds to highly-sinuous channels (i.e. *Group-3*) that is defined by a steep slope. Empirical equations defining the relationships for these two sub-populations have been developed:

$MBW=4.7CW^{0.92}$ (for the low-sinuosity channels of *Group-2*; red dashed-line in Figure 6.13B)

$MBW=34CW^{0.92}$ (for the highly sinuous channels of *Group-3*; blue dashed-line in Figure 6.13B).

The empirical equation developed by Lorenz et al. (1985) does not seem able to predict *CW* from *MBW* (or vice-versa) (black solid-line in Figure 6.13B). In particular, based on measurements of *CW*, this equation appears to underestimate *MBW* for the highly-sinuous channels (*SI*=>1.5) and overestimate *MBW* for the low-sinuosity channels (*SI*=<1.5).

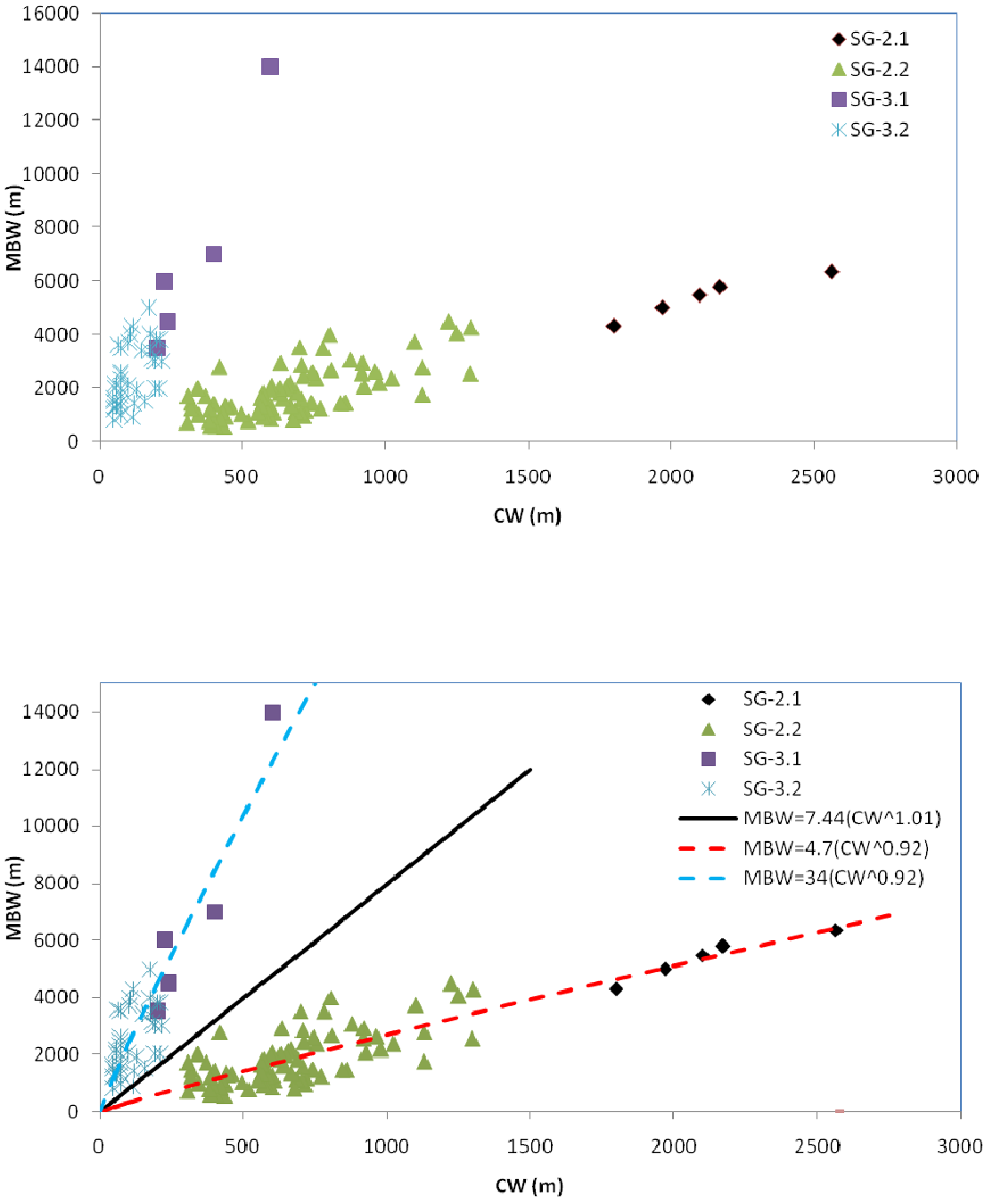

Figure 6.13: Cross-plot of channel width (*CW*) versus meander belt width (*MBW*). This graph shows a direct relationship where *MBW* increases as *CW* increases (**A**). In addition, it shows two main poupulations: one with small slope (rate of increase) corresponding to the low-sinuousity channels (*Group-2*), and another with a larger slope representing highly sinuous channels (*Group-3*). **B**) shows the developed emperical equations defining the relationship for the two poupluations: 1) $MBW=4.7CW^{0.92}$ for the low-sinuosity channels (*Group-2*; red dashed-line) $MBW=4.77CW^{0.92}$ for the highly sinuous channels (*Group-3*; blue dashed-line). The estimated *MBW* (black solid-line) using equation ($Wm=34Wc^{1.01}$) developed by Lorenz et al., (1985) is underestimated for the highly sinuous channels and is overestimated for the low-sinuosity channels.

6.8.4 Channel Width (CW) vs. Meander Wavelength (ML)

ML has been measured for highly-sinuous (*SI*=>1.7) channels only. Most values of *ML* measurements are >600 m, with the largest values (700-14000 m) being associated with those of the confined, highly-sinuous channels (*sub-group-3.1*). Plotting of *CW* against *ML* indicates there is a strong (R^2=0.82), positive relationship between these two variables (i.e. wider channels typically have longer meander wavelengths), thereby allowing an empirical equation to be developed (black dashed-line in Figure 6.14). The equation suggests the relationship between *ML* and *CW* can be defined by a ratio of *ca.* 1:24. This is significantly more than the ratio of 1:10 previously suggested by Brick (1984) that would lead to an underestimation of *ML* for a given *CW* value and an overestimation of *CW* from a given *ML* value.

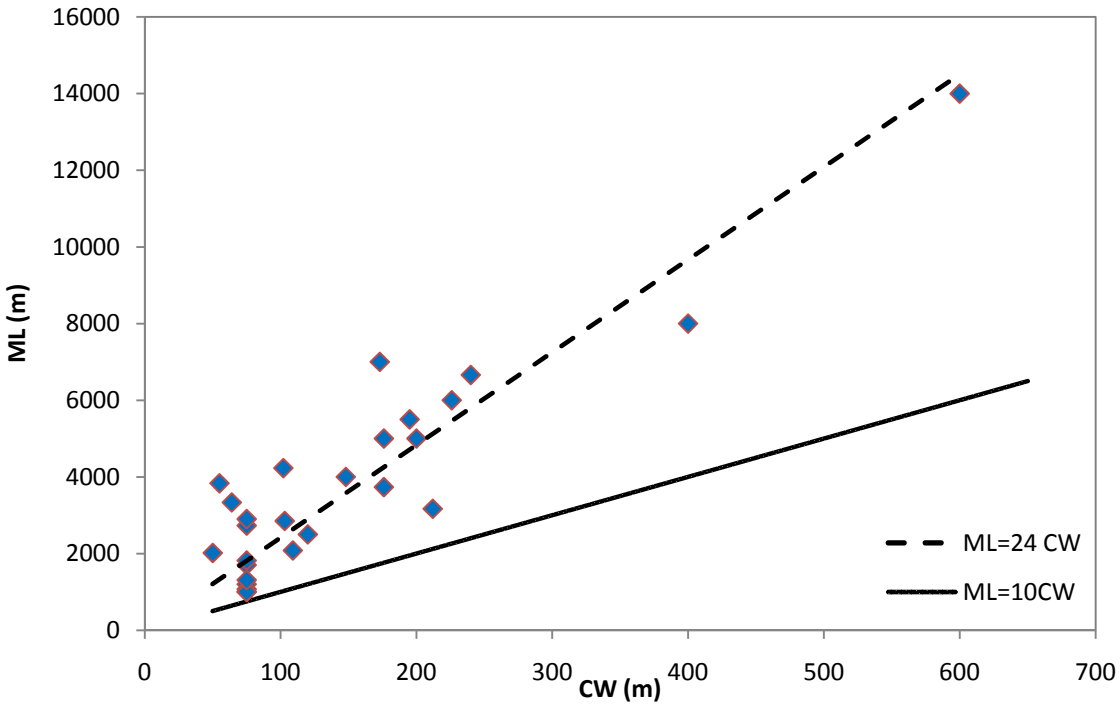

Figure 6.14: Cross-plot of channel width (*CW*) versus meander wavelength (*ML*) for the highly sinuous channels. The plot shows that there is a direct relationship where *ML* increases as *CW* increases. The black solid-line represents the previous relationship proposed by Brick (1984) which is *ML* is 10 times *CW*; however, in this study it has been estimated that the *ML* is 24 times *CW* (black dashed-line).

6.8.5 Meander Wavelength (ML) vs. Meander Belt Width (MBW)

MBW has a strong (R^2=0.74) positive relationship with *ML* for highly-sinuous channels; thus, a channel system with a long meander wavelength is likely to occur within a wider meander belt (black dashed-line; Figure 6.15). The relationship between *MBW* and *ML* can be defined by a linar trendline where *MBW*=0.88ML. No such empirical equation has previously been proposed to define the relationship between these two variables.

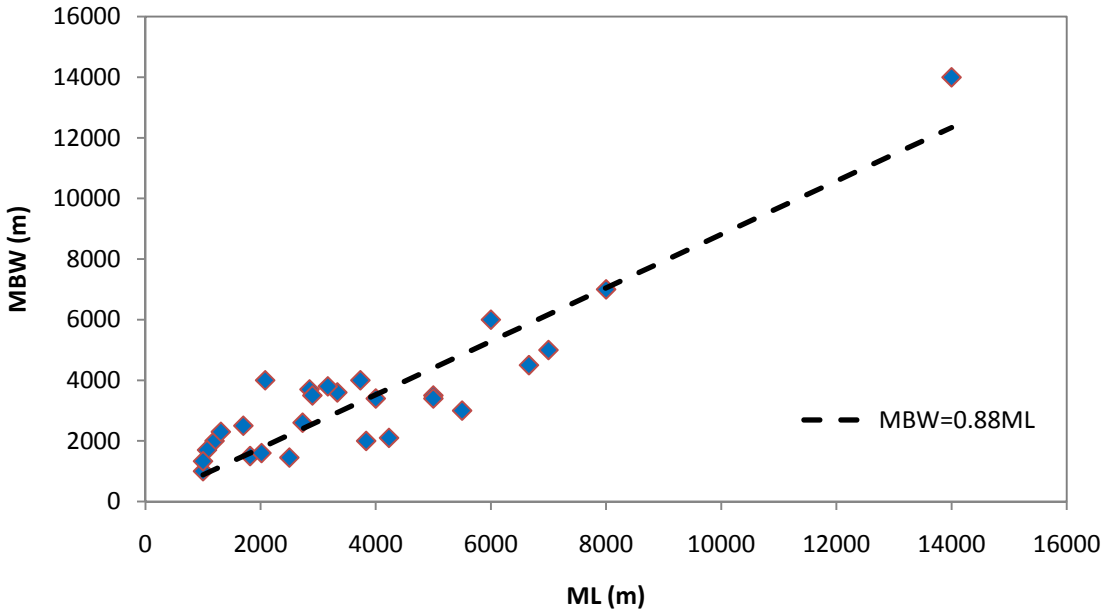

Figure 6.15: Cross-plot of meander wavelength (*ML*) versus meander belt width (*MBW*) for the highly sinuous channels. The plot shows that there is a direct relationship where *MBW* increases as *ML* increases. The dependency can be described by a linar ratio (black dashed-line) where *MBW=0.88ML* .

6.8.6 Meander Wavelength (ML) vs. Radius of Curvature (RC)

ML shows a strong (R^2=0.71) positive relationship with *RC* for highly-sinuous channels; rather intuitively, this indicates that larger channel meanders are associated with larger radius of curvature values and allows for an empirical equation to be developed (black dashed-line; Figure 6.16). The equation (*ML=4RC*) suggests that the ratio of *ML* to *RC* is *ca.* 1:4; this is only slightly less than that previously suggested by Brick (1984) (i.e. *ML=5RC*; black solid-line).

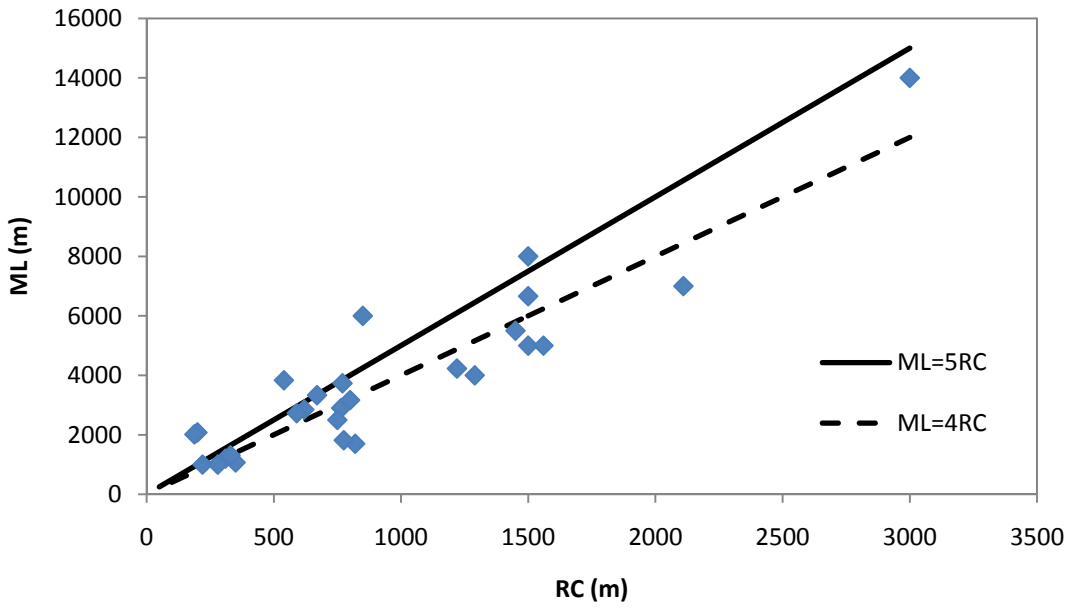

Figure 6.16: Cross-plot of radius of curvture (*RC*) versus meander wavelength (*ML*) for the highly sinuous channels. The plot shows that there is a direct relationship where *ML* increases as *RC* increases. The black solid-line represents the previous estimated *ML* from *RC* for the highly sinuous channels proposed by Brick (1984) which is *ML* is 5 times the *RC*; however, in this study it has been estimated that the *ML* is 4 times the *RC* (black dashed-line).

6.9 Discussion

6.9.1 Empirical Relationship

Vertical profiles from outcrop and well logs datasets provide information on sandbody thickness; however, the lateral dimensions of the channel cannot be constrained and the planform geometry of the channel cannot be unequivocally determined (Bridge and Tye, 2000). Where closely-spaced wells are available and field exposures are aerially and vertically extensive, it may be possible to map the true geometry of entire channel bodies; however, this is rarely possible and it is even more difficult to establish these parameters for ancient rivers in the subsurface. Once the channel thickness (bankfull depth) is determined, several empirical equations can be used to estimate the channel width, meander belt width and sinuosity. There have been numerous attempts to reconstruct the geometry and flow characteristics (e.g. bedload vs. suspended load) of ancient rivers systems; these have relied heavily on the use of several groups of empirical relationships derived from quantitative analysis of modern river systems in a variety of climatic and tectonic settings (e.g. Leopold and Wolman, 1960; Leeder, 1973; Schumm, 1977; Collinson, 1978; Ethridge and Schumm, 1978; Brick, 1984; Lorenz et al., 1985; Fielding and Crane, 1987). These relationships can be applied to the interpretation and classification of ancient fluvial depositional systems (Galloway and Hobday, 1996). Many of these empirical relationships have been tested on data obtained from one-dimensional vertical profiles (e.g. stratigraphic logs from outcrop, wireline logs from subsurface boreholes) in an attempt to link such factors as, for example, channel depth, width and sinuosity, and meander belt width.

The empirical equations discussed above have been tested on humid-tropical, coastal plain channels identified in this study; most of them do not accurately predict the key

morphometric parameters and several new empirical relationships and equation have been established (Figures 6.12-6.16).

Two possible reasons may account for the inability of established empirical equations to accurately predict relationships between channel morphometric parameters in ancient systems. One is related to the type of the channels that were used to develop these empirical equations. The modern rivers used to develop the earlier empirical equations are mainly limited to sand-bed alluvial rivers in semi-arid and sub-humid climate belt from the Great Plains of North America regions, and the Murrumbidgee River, Australia (e.g. Schumm, 1977; Brick, 1984; Ethridge and Schumm, 1978). This contrasts with the channels studied here which were deposited in humid-tropical conditions on the coastal plain. The factors controlling the variability in fluvial architecture in tropical coastal plain rivers are different from those of the alluvial sand-rich alluvial rivers. For example, sea-level variations are a key controlling factors on the architecture of coastal plain rivers, whereas other factors, such as the tectonic, climate, vegetation and bedrock type, may have played a lesser role. In humid environments such as those of Southeast Asia, climate may play a significant role in affecting the amount of erosion and hence sediment supply, amount of rainfall and hence discharge, and the formation overbank sediment (e.g. coal bearing); whereas climate has less influence on semi-arid environments such as those of US.

The second reason for the discrepancy discussed above is related to the methodology used to measure the morphometric parameters of the channels and to the errors involved in these measurements. For example, it has been estimated that the error associated with lateral measurements such as channel width and meander belt width is ± 36-48 m. Furthermore, constraining channel depth is difficult in small channels as their thickness may be at or below the vertical resolution of the seismic data (e.g. *Type-5*; Table 6.2). In

addition, the vertical sampling of the seismic data (i.e. 2 ms twt or *ca*. 2 m) may contribute to errors in calculation of *CD*. As a result, all channel depth measurements have been given an average rather than absolute measurement. These errors could be significant in the resulting data since the relationships between the parameters are affected. For example, a channel may have a smaller width but a larger depth because the lateral measurement (e.g. CW) is considered to be a minimum whereas the vertical measurement (e.g. CD) is considered to be a maximum.

Finally and most critically perhaps, there are several different methods for calculating *CD* in modern and ancient rivers. For example, in modern rivers, *CD* is calculated as the maximum bankfull depth, which is measured from the vegetated river bank down to the base of the channel; hence, *CD* in modern rivers does not include sediment deposited on the river bed above the basal channel scour (Figure 6.7 B). Additionally, measured thickness in ancient rivers is probably less than the original maximum thickness due to burial-related compaction. Ethridge and Schumm (1978) suggested adding 10% to calculations of channel-fill thickness and hence CD to account for burial-related compaction. However, the magnitude of compaction has not been determined for mudstone-rich channels fills.

6.9.2 Vertical changes in fluvial style and sequence-stratigraphic models

Systematic vertical changes are indicated in many stratigraphic models of fluvial systems (e.g. Wright & Marriott, 1993; Shanley & McCabe, 1994). The variability and changes in fluvial architecture are controlled by several factors including sea-level fluctuation, tectonics and climate. During base-level rise and transgression, channels change their

scales and styles, typically becoming more highly-sinuous (meandering) with very well-developed point bars associated with lateral accretion surfaces. During the late highstand, when sea-level starts to fall, channels respond by changing their sinuosity and size, typically becoming narrower and being characterised by low to moderately-sinuous channels.

The channels observed in this study have been classified into three groups. Channel types (e.g. incised valley, low and highly sinuous channels) versus stratigraphic position is shown in Figure 6.8 C. The vertical changes in morphologies and dimensions of the fluvial channels of the Pleistocene succession follow predictable trends.

Channels are widest and deepest immediately above each sequence boundary. These channels represent *Groups-1 & 2* which have a low-sinuosity index (SI<1.3). Where the sequence boundary was formed by an incised valley system, wide channel systems (6-13 km wide; *Group-1*) are probably related to major subaerial exposure during sea-level fall. This sea-level fall was great enough to form valley up 78 m deep and 14000 km wide. Where the sequence boundary was formed by lowstand alluvial bypass systems, wide channels (*Group-2*) are interpreted to form when relative sea-level fall was not rapid or sufficiently large to widely expose the shelf. Given that the Sunda Shelf has a very low-gradient present-day and presumably in the Pleistocene, it is suggested that any minor relative sea-level fall may expose some if not all of the shelf area. This minor relative sea-level fall along with the low-gradient shelf may lead to the formation of wide and deep channel systems. Similar channel types (*Group 2*) have also been observed by Miall (2002), Darmadi et al. (2007) and Wood (2007). Furthermore, the major alluvial bypass channel systems (*sub-group 2.1*) have considerable depth and width (e.g. 45 m deep and 3000 m wide). These channel systems were elongated as these channels had to widen due to increasing discharge from the attached tributary channels. Darmadi et al. (2007),

concluded that the variability in channel pattern within the Pleistocene succession in West Natuna Basin is controlled mainly by variations in discharge during gradual aggradation and that the sea-level fluctuation had less of an influence. This interpretation has also been proposed by Kiel (2009), mainly based on the fact that the study area is *ca.* 1000 km away from the shelf break which has been estimated as the paleo-shoreline in the Sunda Shelf by Darmadi et al. (2007). Furthermore, most of these channels (*Group-2*) were flowing from the high elevated areas in the west towards the axial zone of the basin. This indicates that the low-sinuosity channels may reflect high regional stream gradients during early lowstand. High stream gradients and high discharge during the early lowstand when the sea-level fell caused low-sinuosity channels to develop.

Generally, channel width and depth decrease upsection from the sequence boundary at the base of each depositional sequence. Near the top of each sequence, channels become narrower and highly sinuous (50-600 m wide; *Group-3*). During base-level rise and transgression, channels change their scales and styles, typically becoming more highly-sinuous (meandering) with very well-developed point bars associated with lateral accretion surfaces. During the late highstand, when sea-level started to fall, channels responded by changing their sinuosity and size, typically becoming narrower and being characterised by low to moderately-sinuous channels. Where channels (*sub-group-3.1*) are confined within incised valleys, the fluvial channels have the highest sinuosity (>2.5) and represent the largest systems among those highly sinuous channels. These confined meandering rivers have considerable width (up to 600 m), depth (25 m), and meander belt width (14000 m). In contrast, the unconfined meandering channels (*sub-group-3.2*) are less sinuous but with a wide range of channel depth and width. The orientation for the highly sinuous channels (*Group-3*) is mainly towards the south east towards the South China Sea. These meandering channels (*Group-3*) are probably related to low regional

gradients during sea-level rise and when the axial zone of the basin had been filled by previous low-sinuosity channels.

6.9.3 Predicting channel fill from planform morphology

Various authors have attempted to relate channel planform morphology to the grainsize of sediment transported and ultimately preserved within the channel (e.g. Schumm, 1977; Brick, 1984). Schumm (1977) proposed that a strong empirical link existed between the mode of the sediment transport (e.g. bedload-dominated, mixed-load and suspended load-dominated transport mechanisms) and the planform and cross-sectional geometry of the associated channel. Schumm (1977) suggested that a bedload-dominated river is defined by a sinuosity of 1-1.3 and width-depth ratio of >40, a mixed-load river is defined by a sinuosity of 1.4-2.0 and width-depth ratio of >10, <40, and a suspended load channel is defined by a sinuosity of >2.0 and width-depth ratio <10.

Based on this classification, low-sinuosity channels are more likely to be sandstone-filled and, therefore, represent the best petroleum hydrocarbon reservoirs. Similarly, Miall (2002) suggested that low-sinuosity; lowstand-related channels may provide the greatest volume of potential porous reservoir. The highly-sinuous, meandering channels observed towards the top of the four depositional units studied here display highly-variable seismic amplitude; this contrasts with the straight and low-sinuosity channels which are characterised by low-amplitude, laterally-continuous seismic reflections. For example, the channel point bars are of significantly higher amplitude than the fill of the channel itself, suggesting that the point bars are of a different lithology or lithologies to the channel fill (Figure 6.9 B). However, no well log or core data are available to determine the

lithological variations responsible for these changes in seismic facies although, by comparison to other published examples, it may be speculated the point bars are sandstone-rich and would constitute good-quality reservoirs, whereas the channel fills themselves are mudstone-rich and would constitute non-reservoir (cf. Miall, 2002; Carter, 2003; Darmadi et al., 2007).

6.10 Conclusions

The Pleistocene to Recent successions within the Malay Basin which is about 500 m thick have been divided into four seismic units. The bounding surfaces (sequence boundaries) of these sequences are characterised by prominent fluvial incisions. Two different types of incisions have been identified; deep incised valley systems that are associated with smaller tributaries feeding the main valley and weakly incised channel systems that are interpreted as lowstand alluvial bypass channel systems have been recognised.

A wide variety of channel style and size have been observed within each individual unit. Based on the morphometric parameters of the channels observed in this study, three channel groups (incised valley, alluvial bypass channel systems, and highly sinuous meandering channels) have been identified. The base of each unit is characterised by wide and deep low-sinuosity channels passing gradationally upwards into narrow high-sinuosity channels at the top. The major controlling factor that determines the channel types and their sizes is sea-level fluctuation; however, effects of climate on discharge are also noticed. There are systematic vertical changes in the channel pattern and sizes in response to the sea-level variations.

Empirical equations developed on modern rivers have been tested on the humid-tropical tropical coastal plain channels identified in this study. Using these relationships, most of the channel morphological parameters are either underestimated or overestimated. It suggests that these empirical equations cannot be applied for channels where morphometric parameters are seismically-derived; however, several new empirical relationships have been established and new empirical equations have been developed.

This study demonstrates how a better understanding of fluvial reservoir variability can be obtained through the analysis of high-resolution, shallow 3D seismic data (seabed to *ca.* 500 m), which can provide exceptional imaging of fluvial channel planform shapes and other geometrical properties and dimensions and allow for new empirical relationships to be developed.

Chapter 7

Conclusions and Future Work

7.1 Conclusions

A 'mega-merge' 3D seismic dataset from the Malay Basin, which images down to *ca*. 500 m below the present-day sea-bed, has been used in this study and has enabled reconstruction of fluvial systems within the Pleistocene to Recent succession on the Sunda Shelf, SE Asia. This dataset provides a unique regional overview of the geometry, scale and distribution of fluvial systems that cannot be achieved from interpreting a single 3D seismic survey, or from analysis of spatially-limited outcrops or 'vertical' datasets (e.g. well logs and cores). The results of this study, which have been presented in the preceding chapters, are summarised and discussed here and are structured into four main 'concluding remarks'. After the framework of these concluding remarks, suggestions for future work are made.

7.1.1 Seismic expression and classification of fluvial channel systems

Based on seismic facies analysis and reflection continuity, the Pleistocene to Recent succession has been divided into four seismic units (Units 1-4), bounded by basin-wide stratal surfaces (Horizons A-E). Two additional horizons, Horizons C.1 and D.1, have been mapped within the upper part of Unit 3 and Unit 4, respectively, to allow further

sub-division of these units into two sub-units (i.e. sub-units 3.1, 3.2, 4.1 and 4.2). Horizons C.1 and D.1 are both strongly erosive.

A wide range of fluvial channel styles and morphologies have been observed at multiple stratigraphic levels within the Pleistocene succession. In cross-section, these channels are characterised by different seismic expressions and six main types, including 'v' and 'u'-shaped with different scale have been identified. Each type, in plan-view, has a distinct shape and size.

Ten interpretive maps were constructed that illustrated the range of fluvial channel styles at various stratigraphic levels within the dataset. Each map is composed of observations from a succession of time and/or iso-proportional slices taken from either the lower half or the upper half of each mapped seismic unit; hence each map illustrates the type of channels that are observed in either the basal or the top part of each unit.

Morphometric parameters, including channel width, depth, meander belt width, radius of curvature, channel length, and sinuosity of 130 channels have been quantified. A quantitative database for the Pleistocene river systems has been developed. Based on these data, three channel groups have been recognised. These are incised valley systems, alluvial bypass channel systems with low-sinuosity index, and highly sinuous channels. The largest systems observed in this study are those of the incised valleys with width up to 14000 m and depth up to 80 ms twt (78 m). The lowstand bypass channel systems display a wide range of channel width (450-3000 m) and depth (10-48 m). The highly sinuous channels have been further divided into: 1) confined highly sinuous channels with channel width up to 600 m, meander belt width of up to 14000 m and depth of up to 25 m; and 2) unconfined highly sinuous channels which are the smallest systems observed in

this study with channel width of 50-250 m, meander belt width of 800 to 7000 m and depth of 8-20 m.

7.1.2 Temporal and Spatial Variations and Controls on Fluvial System Architecture

Two different types of incisions have been identified; (i) deep incised valley systems that are associated with smaller tributaries feeding the main valley; and (ii) weakly-incised channel systems that are interpreted as lowstand alluvial bypass channel systems.

Overlying these fluvial incisions within each seismic unit are a wide range of fluvial channel architectures and sizes within a relatively limited (<500 m) stratigraphic interval. Systematic vertical changes in fluvial channel architecture and styles have been observed within each individual unit and sub-unit. This vertical variability in fluvial channel architecture and style is indicated in most sequence-stratigraphic models of fluvial systems (e.g. Wright and Marriott, 1993; Shanley and McCabe, 1994). This suggests that these previous developed models can be used to interpret the subsurface fluvial systems.

At the base of each unit, several straight to low-sinuosity channels are observed. Toward the top of the each unit, the channels change their pattern and size, typically becoming smaller (narrower and shallower) and of higher sinuosity. Given that; (i) the Malay Basin is located in the centre of the Sunda Shelf, a relatively large distance from the main sediment source area(s); and (ii) the extremely broad (up to 800 km at its widest point) and very low-gradient (<0.1º) Sunda Shelf was tectonically quiescent during the Pleistocene to Recent (Madon et al., 1999), it is considered unlikely that climatic variations and/or tectonics are the primary controls on the variation in channel

architecture observed within the Pleistocene succession in this study (see discussion by Miall, 2002). Based on available data it is not possible to determine exactly how far the predominantly non-marine Malay Basin was from coeval palaeo-shoreline(s) during the Pleistocene. However, a series of maps presented by Voris (2000) suggest that the Sunda Shelf was exposed during the Late Pleistocene to Recent and indicate that the study area within the Malay Basin was not far (i.e. a few hundreds of kilometres away) from the palaeo-shoreline. It is considered most likely, therefore, that sea-level was the major factor controlling the types and stratigraphic organisation of fluvial channels within the Pleistocene to Recent succession within the Malay Basin; however, there are variations in the size and the degree of sinuosity within each part (lower or upper) of each individual unit. For examples the low-sinuosity channels at the base of Unit 2 have wide range of widths (500-3000 m) and depths (15-45 m). These variations in morphometric parameters are interpreted to be controlled by the variation of discharge between these channels. It has been observed that the major alluvial bypass channel systems were elongated as these channels had to widen due to increasing in the discharge from the attached tributary channels. Darmadi et al. (2007), concluded that the variability in channel pattern within the Pleistocene succession in West Natuna Basin is controlled mainly by variations in discharge during gradual aggradation and that the sea-level fluctuation had less of an influence. This interpretation has been also proposed by Kiel (2009) which was mainly based on the fact that the study area is *ca*. 1000 km away from the shelf break which has been estimated as the palaeo-shoreline in the Sunda Shelf by Darmadi et al. (2007). Furthermore, the low-sinuosity channels within the study area were flowing from the high elevated areas in the west and southwest. This implies that the channels had steeper gradients and hence higher discharge.

In summary, the sea-level changes are interpreted to be the main controlling factor and may have driven the overall stratigraphic changes within the Pleistocene succession of the Malay Basin, although sediment loads and discharge which are controlled by climate may play a significant role in determining the variability of the channel type and size among each stratigraphic level. Due to a lack of age constraints on the studied stratigraphy in this study (Malay Basin) and that of Darmadi et al. (2007) (West Natuna Basin), it was difficult to confidently tie observations from both areas. However, based on the fact that both successions were deposited in a tectonically inactive basin, the sea-level changes and possibly discharge variation may have driven stratigraphic changes in a similar manner in both areas.

The development of incised valleys or lowstand alluvial bypass systems may depend on the magnitude of the relative sea-level fall. In particular, when the sea-level fall is large and sufficient to widely expose the entire shelf, an incised valley forms whereas the lowstand bypass channel systems may develop when the sea-level fall is minor; however, unlike Posamentier's (2001) model, the shelf break does not have to be exposed for an incised valley to have been formed and developed (see below for further discussion). During the subsequent transgression, channels responded by changing their style and size, typically becoming smaller and of higher sinuosity.

In agreement with past work (Vail et al., 1977, Van Wagoner et al., 1990, Hampson et al 1997, Posamentier, 2001, and Fielding and Gibling, 2005), incised valleys can be distinguished from alluvial bypass systems based on: 1) the basal erosion surface that records the lowstand of relative sea-level (sequence boundary) must be of regional (basin wide) extent; 2) the basal erosion surface truncates underlying strata which may be present beneath the adjacent interfluves; 3) the basal surface is associated with the presence of small tributaries on the main valley interfluves.; 4) the incised valley fill must

have a distinctive internal architecture that is commonly multi-storey which records the progressive rise in base-level through the filling of the valley; therefore the facies within the incised valley must be different from those adjacent to and below the erosional surface; 5) the depth and width of the incised valley has to be significantly larger than expected for a 'normal' fluvial channel system. Geometrically, incised valleys are typically several kilometres wide and several tens of meters deep (Zaitlin et al., 1994; Reynolds, 1999; Gibling, 2006). All these distinguishing criteria have been observed in this study. This confirms that these criteria are critical for identifying incised valleys.

Following the classification proposed by Schumm (1977), it is speculated that the low-sinuosity channels may be filled with sands and the higher–sinuosity (meandering) channels may be filled with finer-grained sediments; however, the bright amplitudes which characterise point bars adjacent to the low-amplitude channel fill may be indicative of sandstone-rich, good-quality reservoirs. Similarly, Miall (2002) suggested that low-sinuosity; lowstand-related channels may provide the greatest volume of potential porous reservoir. However, no well log or core data are available to determine the lithological variations responsible for these changes in seismic facies although, by comparison to other published examples, it may be speculated the point bars are sandstone-rich and would constitute good-quality reservoirs, whereas the channel fills themselves are mudstone-rich and would constitute non-reservoir (cf. Miall, 2002; Carter, 2003; Darmadi et al., 2007).

7.1.3 Late Pleistocene Incised Valley

The mega-merge 3D seismic dataset, supplemented by high-resolution site survey and borehole data, has enabled reconstruction of Late Pleistocene river systems on the Sunda Shelf, Malay Basin. In particular, these data have allowed documentation of a major incised valley on Sunda Shelf. The incised valley is 80 m deep and 14 km wide, and is interpreted to have formed during or near the LGM lowstand period when a eustatic sea-level fall was sufficient to widely expose the Sunda Shelf; however, as stated above, this sea-level fall did not expose the shelf break. The shelf break is located at 180-220 m below present sea-level whereas the sea level fall during the LGM was at 120 m below present sea-level. This suggests that Posamentier's (2001) model can be modified and that an incised valley may form even if the shelf break has not been exposed. Other important factors such as basin physiography and sediment supply may have controlled valley formation.

Hanebuth and Stattegger (2004) concluded that the largest incised valley system on the Sunda Shelf (North River System which is located in the southeastern part of Malay Basin) was formed by the interplay of three major factors: 1) rapid sea-level changes; 2) locally pronounced physiography; and 3) changes in sediment supply that determined the distribution and accumulation pattern. Locally pronounced physiography on the shelf may lead to formation of a deep incised valley during sea-level fall (Talling, 2010). Talling (2010) proposed that the widely used sequence stratigraphic models (e.g. Van Wagoner et al., 1988; Emery and Myers, 1996) are simplistic as the physiography of a basin used in the development of these models is either unrealistic or only qualitatively defined. He suggests that these models do not include the importance of the coastal prism topography as one of these factors that controlling the river incision. Talling (2010) indicates that

pronounced topography may lead to an incision that may exceed 100 m in depth during sea-level fall. In this study, the south-western flank of the Malay Basin is slightly steeper than the north-eastern flank, hence during any minor sea-level fall, a large area of this part (west and south-west) of the basin is widely exposed leading for deep channel and valley systems to be formed.

Given that the study area is away from the sediment sources (Thailand) and during the LMG there was a reduction in the sediment budget (Clift, 2007), the sediment supply, which is affected by the climate, may had less influence in the formation and development of the Late Pleistocene incised valley system identified in this study. In contrast, the ultimate sediment sources for West Natuna Basin (e.g. Malay Peninsula; Hanebuth and Stattegger, 2004) were not far away from the study area. In summary, the interplay of sea-level variation along with the physiography of the basin during the LMG may have been responsible for the formation and development of the Late Pleistocene incised valley within the Malay Basin.

The absence of the terraces within the Late Pleistocene incised valley within the Malay basin may be caused by the widening process of the channel system during the start of sea-level rise (Blum & Törnqvist, 2000). Talling (2010) further suggests that during sea-level fall the channel tends to be very narrow and deep and terraces would be formed during this period. These terraces would be removed when the valley started to widen during the start of sea-level rise (Talling, 2010). Strong (2006) suggests the same the process based on extensive experimental study.

Borehole data indicate that the incised valley fill consists of shell-bearing heterolithics which overlies a unit composed of cobbles and sands. The cobble-rich layer is interpreted as a fluvial lag deposit, deposited during lowstand cutting of the valley. The shell-bearing

heterolithics correspond to inclined reflection events on seismic and boomer data and are interpreted as inclined heterolithic stratification (IHS) associated with the deposition of tidally-influenced point bars. Shell debris within the abandoned channel-fill and parts of the point bars imply estuarine conditions within the channels, which may have been related to salt-water intrusion up the valley during flooding. Given the low-gradient of the Sunda Shelf at this time, this intrusion could have been up to several hundreds of kilometres.

Seismically, the point bars are of higher amplitude than the adjacent channel fill. This suggests that the point bars may be sand-bearing and possibly gas-charged, implying that the mudstone-rich, abandoned channel fill may have acted as lateral seal and the gas is trapped within thin sand layers within the point bar. This highlights the important role that sediment portioning in meandering river systems may have on stratigraphic trap development.

This meandering channel is *ca*. 600 m wide and 23 m deep, with meander belt width of up to 14 km. This channel is confined within the walls of the incised valley and is interpreted to be tidally-influenced (see below). A neck-cut off and associated abandoned channel is observed in the southern part of the study area, suggesting that a continued sea-level rise may have caused the channel to reduce its sinuosity via this mechanism. This channel is similar in geometry to portions of the downstream part of the Mississippi river, although it is slightly smaller. This channel is bigger than most if not all the meandering rivers in Southeast Asia.

At the top of this incised valley, a 16 m thick shell-bearing, mudstone layer is identified and is interpreted to be a Holocene age unit that was deposited above and capped the incised valley when the sea-level reached its present-day highstand A significant

stratigraphic contact, which is defined by a subtle change in lithology but a pronounced change in water content, is identified 16 m below seabed; this surface separates the lower, very-soft clay that has a water content of 75-100%, from the very-stiff clay that has a water content of 25-50% Similar observation has been made by Posamentier (2001).

This channel system is interpreted to have represented a major river system that occupied the axial zone of the Malay Basin, possibly extending from the Gulf of Thailand to the South China Sea (>2000 km). This system is one of the 'trunk rivers' identified on present-day bathymetric maps of the Sunda Shelf (Johore/palaeo-Chao Phraya River) reported by Voris (2000) and Morley and Westaway (2006). This river is interpreted to be the downstream extension of the same major, valley-confined meandering river observed in the study of Miall (2002).

7.1.4 Empirical Relationships

Previous empirical equations developed on modern have been tested on the humid-tropical coastal plain channels identified in this study; these relationships constantly either overestimate or underestimate one of the channel morphological parameters. The inability of published empirical equations to predict fluvial channel geometry may reflect; (i) *the type of the channels studied.* The majority of the modern rivers used in the development of the earlier empirical equations are mainly limited to sand-bed alluvial rivers in semi-arid and sub-humid climate belts from the Great Plains of North America regions, and the Murrumbidgee River, Australia (e.g. Schumm, 1977; Brick, 1984; Ethridge and Schumm, 1978). The majority of these rivers are Holocene systems which occur at elevations of about 800-1500 m above the sea level and are far from the coast. In addition, these

channels are moderate or small rivers. The majority of the previous empirical equations have not been tested on coastal plain river systems which have different climatic belts and/or tectonic setting (North, 1996). This contrasts with channels studied here which were much larger and deposited in humid-tropical conditions on the coastal plain. The factors controlling the variability in fluvial architecture in tropical coastal plain rivers are different from those of the alluvial sand-rich alluvial rivers. For example, sea-level fluctuations are the key controlling factors on the architecture of coastal plain rivers, whereas other factors, such as the tectonic and bedrock type, may have played a lesser role. In humid environments such as those of Southeast Asia, climate may play a significant role in affecting the amount of erosion and hence sediment supply, amount of rainfall and hence discharge and vegetation, and the formation of overbank sediment (e.g. coal bearing); whereas climate has less influence on semi-arid environments such as those of US Great Plains. It has been noted that modern tropical rivers have different morphological parameters in comparison with those of semi-arid and sub-humid channel systems. For example, tropical channels tend to be deeper than those of semi-arid and sub-humid channels. These tropical channels may have had to incise deeper to accommodate the high discharge they receive during the monsoon season. Furthermore, the river banks of tropical channels are more stable and less erodible which affects the overall the channel width and hence the meander belt width; (ii) *the methodology used to measure the morphometric parameters of the channels and the errors involved in these measurements*. It has been estimated that the error associated with lateral measurements using time and iso-proportional slices of this study such as channel width and meander belt width is ± 36-48 m. Additionally, constraining channel depth is difficult in small channels as their thickness may be at or below the vertical resolution of the seismic data. Furthermore, the vertical sampling of the seismic data (i.e. 2 ms twt or *ca*. 2 m) may contribute to errors in calculation of channel depth.

Finally and most critically perhaps, there are several different methods for calculating channel depth in modern and ancient rivers. For example, in modern rivers, channel depth is calculated as the maximum bankfull depth, which is measured from the vegetated river bank down to the base of the channel; hence, channel depth in modern rivers does not include sediment deposited on the river bed above the basal channel scour. Furthermore, using wells logs, there are different methods for calculating the channel thickness (depth). Many researchers used the top of sand beds (e.g. blocky-shaped gamma ray for low-sinuosity channels and the fining-upward cycle for the high-sinuosity channels) as the top of the channel deposit; however, Bridge and Tye (2000) suggested that the thin mud bed at the top of the these blocky-shaped gamma ray or fining-upward should be included as the upper part of the channel. These differences in calculating the channel thickness (depth) may contribute to errors in calculation of channel depth. Additionally, measured thickness in ancient rivers is probably less than the original maximum thickness due to burial-related compaction. Ethridge and Schumm (1978) suggested adding 10% to calculations of channel-fill thickness and hence channel depth to account for burial-related compaction. However, the magnitude of compaction has not been determined for mudstone-rich channels fills. North (1996) concluded that one of the major issues with these previous empirical equations is that there is no clear definition of how the researchers define and differentiate the mean and maximum channel depth from well logs and/or cores.

Despite all these errors related to the seismic resolution, compaction and channel-floor deposition, these errors may be systematic and could be estimated and their magnitude relative to other sources of error could be then assessed. For example, the channel width (*CD*) and meander belt width (*MBW*) can be given lower and upper limits (ranges). For instance, if the channel has *CD* of 100 m and *MBW* of 3000 m, the *CD* for the channel

would range from 52 to 148 m and *MBW* would range between 2952 m to 3048m. Compaction could also be estimated if the corrected depth (mean or maximum depth) is determined; however, as stated above, some of these previous empirical equations have not explicitly defined how the channel depth has been estimated and whether the mean or maximum depth have been used. The influence of channel-floor deposition could also be small; however, this need to be explored and hence it could be estimated as well.

As a result, several new empirical relationships have been established and new empirical equations have been developed. It has been shown that the derived empirical relationships are most applicable to highly sinuous channels. This is because the low-sinuosity channels display a wide range of morphometric parameters. Similar observation has been made by several authors (e.g. Leeder, 1973; Fielding and Crane, 1987).

There are some sources of uncertainties with the application of these new empirical equations on building reservoir models. One of these uncertainties is that the planform geometry of the channels that would be used in building the reservoir model needs to be determined before using these equations. As stated above, the majority of these new empirical equations are valid only for highly-sinuous channels. If the channels used in the building of reservoir model are low-sinuosity, these empirical equations are invalid and could cause significant errors as the low-sinuosity channels display a wide range of channel depth and width.

Secondly and more importantly, the climatic and tectonic settings in which the channel systems are formed and developed are very important to be determined. These new empirical equations have been developed on humid-tropical coastal plain channels in an inactive tectonic area. As stated above, one of the possible problems of using the previous empirical equations is the differences in the channel characteristics caused by the

differences of the climate and tectonic conditions. In detail, these differences are caused by the different controlling factors that determine the channel type. The interplay of these controlling factors on the development of the fluvial systems is complex and would lead channels to have different morphometric parameters. This suggests that similar channel types from different climatic and/or tectonic settings may have different channel parameters such as width, depth and meander belt width. For example, the depths of tropical channels tend to be deeper in comparison with those of semi-arid and sub-humid channels.

Finally, in order to validate them, these equations need to be first tested on similar modern rivers in Southeast Asia such as Baram and Mahakam Rivers. These modern rivers have similar tectonic and climatic settings which will be very useful to test these equations. If these empirical equations show promising results, then they can be then tested on similar types (e.g. high-sinuosity channels) of modern rivers but from different climatic and/or tectonic settings (e.g. Mississippi and Nile Rivers). Additionally, these empirical equations need to be tested on ancient fluvial channel systems from the Miocene succession within the Malay Basin which were developed under a similar climatic setting but different tectonic setting. This will help to determine the application of these empirical equations to producing reservoirs.

7.2 Future Work

This study can be extended to include other 3D seismic surveys within the south-eastern part of the Malay Basin. This will provide a unique opportunity to evaluate and to better understand the Pleistocene to Recent evolution of the Sunda Shelf fluvial to coastal plain

on a basin-scale. Most importantly, a basin-scale study will help to determine the geometric variability of the fluvial channels along their courses, which may aid identifying the controlling factors on their evolution. For example, the large meandering channel which is confined within the Late Pleistocene incised valley has different patterns along its course toward the South China Sea. Furthermore, this river and the incised valley may have different characteristics (e.g. width, depth, sinuosity, etc). Additional site survey data from the south-eastern part will provide important lithological information of the incised valley fill. This will help to determine the lithological changes along the valley course as indicated in Zaitlin et al.'s (1994) model. For example, the coarse-grained deposits observed within the base of this incised valley may not be found in the southern part which may suggest increased marine influence within the downstream reaches. Finally, these data will help to determine the influence of sea-level variation on the development of this incised valley and its fill.

Biostratigraphic data from the Malay Basin is essential to confidently tie the observation of this study to observations from previously published materials conducted on Sunda Shelf (e.g. Miall, 2002, Darmadi et al., 2007). This will help to reconstruct the fluvial systems across the Sunda Shelf.

Future work should also aim to apply the results of this study to the deeper, productive Miocene succession within the Malay Basin. In regions such as the Sunda Shelf, where climate has remained relatively uniform over the last *ca*. 20 Myr, the shallow parts of large 3D seismic datasets may provide an extremely valuable source of analogue data for the deeper, prospective parts. In particular, the documentation of the dimensions and geometries and the construction of a quantitative database of Pleistocene fluvial systems will help to constrain reservoir models for the productive Miocene fluvial reservoirs on the Sunda Shelf. Furthermore, the classification of the channel systems and the types of

the seismic expression of the channel morphologies observed in this study can be applied for the channels of the Miocene succession of the Malay Basin where the channels are poorly-imaged. Additionally, the availability of well logs and cores from the Miocene will aid in the interpretation of the channel fill of the Pleistocene river systems.

Finally, the new empirical relationships and equations developed in this study can be tested on similar channels observed on Sunda Shelf (e.g. Miall, 2002; Darmadi et al., 2007). Furthermore, these equations can also be tested on rivers from different settings. Additionally, the GIS methodology developed in this study can be used to measure the morphometric parameters of modern humid-tropical rivers of Southeast Asia (e.g. Rajang River; Mahakam River) using Google Earth images. Morphometric parameters of rivers from different settings can also be determined. This will provide a large quantitative database which can be used to validate these developed equations.

References

Allen, J. R. L., 1970, Physical processes of sedimentation: London Allen and Unwin, p. 284.

Allen, J. R. L., 1979, Studies in fluviatile sedimentation: an exploratory quantitative model for architecture of avulsion-controlled alluvial suites: Sedimentary Geology, v. 9, p. 235-267.

Arshad, A. M., M., Dashuki, and H. D., Tjia, 1995, A deep seismic section across the Malay Basin; processing of data and tectonic interpretation. Abstracts of the Geological Society of Malaysia Petroleum Geology Conference 1995, Warta Geologi 21, P. 412.

Bard, B., R. G. Hamelin, and R. G. Fairbanks, 1990, U-Th obtained by mass spectrometry in corals from Barbados: sea level during the past 130,000 years: Nature, v. 346, p. 456–458.

Beauboeuf, R.T., and S.J. Friedmann, High-resolution seismic/sequence stratigraphic framework for the evolution of Pleistocene intra slope basins. Western Gulf of Mexico: depositional models and reservoir analogs: GCSSEPM Foundation 20th Annual Research Conference, Deepwater reservoirs of the world (2000) p. 40–60.

Best, J.L., and P.J., Ashworth, 1997, Scour in large braided rivers and the recognition of sequence stratigraphic boundaries: Nature, v. 387, p. 275–277.

Blum, M.D., and T.E. Törnqvist, 2000, Fluvial responses to climate and sea level change: a review and look forward: Sedimentology, v. 47, p. 2-48.

Brice, J. C. 1975, Air photo interpretation of the form and behavior of alluvial rivers. Final Report to the U.S. Army Research Office, Durham.

Brice, J. C. 1981, Stability of relocated stream channels. Federal Highway Administration Report no. FHWA/RD-80/021, Washington, DC.

Brice, J. C. 1982, Stream channel stability assessment. Federal Highway Administration Report no. FHWA/RD-82/021, Washington, DC.

Brice, J. C. 1984, Planform properties of meandering rivers. In: Elliott, C. M. (ed.) River Meandering. American Society of Civil Engineers, New York, 1–15.

Bridge, J. S., 1997, Thickness of sets of cross strata and planar strata as a function of formative bed-wave geometry and migration, and aggradation rate: Geology, v. 25, p. 971-974.

Bridge, J. S., 2003, Rivers and Floodplains: Forms, Processes, and Sedimentary Record, Blackwell Science, New York, p.491.

Bridge, J. S., 2006, Fluvial facies models: recent developments: Society for Sedimentary Geology SEPM Special Publication 84, p. 85-170.

Bridge, J. S., and S. D. Mackey, 1993, A theoretical study of fluvial sandstone body dimensions: in. Flint, S. S and I. D. Bryant (eds.), Geological Modelling of Hydrocarbon Reservoirs: International Association of Sedimentologists, Special Publication 15, Utrecht, Netherlands, p. 213-236.

Bridge, J. S., and R. S. Tye, 2000, Interpreting the dimensions of ancient fluvial channel bars, channels, and channel belts from wireline-logs and cores: American Association of Petroleum Geologists Bulletin, v. 84, p. 1205-1228.

Bristow, C.S., and H. M., Jol, 2003, An introduction to ground penetrating radar (GPR) in Sediments: In Bristow, C.S., and H. M., Jol (eds.), Ground Penetrating Radar in Sediments: Geological Society Special Publication 211, p. 1-7.

Brown, A. R., 2004 Interpretation of three-dimensional seismic data: AAPG Memoir, v. 42: United States, American Association of Petroleum Geologists: p. 541.

Bryant, I. D., and S. S. Flint, 1993, Quantitative clastic reservoir geological modelling: problems and perspectives: in. Flint, S.S and I.D. Bryant (eds.), The geologic Modelling of Hydrocarbon Reservoirs and Outcrop Analogues: International Association of Sedimentologists, Special Publication 15, p. 3-20.

Burnett, M., 1996, 3D seismic expression of a shallow fluvial system in west central Texas: in Weimer, P., and T. L. Davies (eds.) American Association of Petroleum Geologists Bulletin Studies in Geology 42 and SEG Geophysical Development Series 5, American Association Petroleum Geologists / Society for Exploration Geophysics, Tulsa, OK, p. 45-56.

Carlston, C. W., 1965, The effect of climate on drainage density and streamflow: Internat. Assoc. Sci. HydroI. Bull., v. 11, No.3, p. 62-69.

Carter, D. C., 2003, 3D seismic geomorphology: insights into fluvial reservoir deposition and performance, Widuri field, Java Sea, American Association of Petroleum Geologists Bulletin, v. 87, p. 909-934.

Cartwright, J. A., and M. Huuse, 2005, 3D seismic technology: the geological “Hubble”: Basin Research, v. 17, p. 1-20.

Chappell, J., A., Omura, T., Esat, M., McCulloch, J., Pandol, Y., Ota, and B., Pillans, 1996, Reconciliation of late Quaternary sea levels derived from coral terraces at Huon Peninsula with deep-sea oxygen isotope records. Earth Planet. Sci. Lett. 141, p. 227-236.

Clift, P. C., 2006, Controls on erosion of Cenozoic Asia and the flux of the clastic sediment to the ocean, Earth and Planetary Science, p. 571-580.

Collinson, J. D., 1978, Vertical sequence and sand body shape in alluvial sequences, in A. D. Miall, ed., Fluvial Sedimentology: Canadian Society of Petroleum Geologists Memoir 5, p. 577-586.

Cornish, F.G., 1984, Fluvial environments and paleohydrology of Upper Morrow 'A' (Pennsylvanian) meanderbelt sandstone, Beaver County, Oklahoma: Shale Shaker, v. 34, p. 70-80.

Dalrymple, M., 2001, Fluvial reservoir architecture in the Statfjord Formation (northern North Sea) augmented by outcrop analogue statistics: Petroleum Geosciences, v. 7, p. 115-122.

Dalrymple, R.W., B.A., Zaitlin, and R., Boyd, 1994, History of research, valley types and internal organization of incised-valley systems: in Dalrymple, R.W., Boyd, R., and Zaitlin, B.A., eds., Incised-Valley Systems: Origin and Sedimentary Sequences: SEPM, Special Publication 51, p. 3–11.

Darmadi, Y., B. J. Willis, and S. L. Dorobek, 2007, Three-dimensional seismic architecture of fluvial sequences on the low gradient Sunda Shelf, offshore Indonesia: Journal of Sedimentary Research, v. 77 no. 3, p. 225-238.

Davies R. J., S. A. Stewart, J. A. Cartwright, M. Lappin, R. Johnston, S. I. Fraser, and A. R. Brown, 2004, 3D seismic technology: are we realising our full potential?: in Davies R. J., J. A. Cartwright, S. A. Stewart, M. Lappin, and J. R. Underhill (eds.), 3D Seismic Technology: Application to the Exploration of Sedimentary Basins, Geological society Memoirs 29, p. 1-9.

Deptuck, M. E., G. S. Steffens, M. Barton, and C. Pirmez, 2003, Architecture and evolution of upper fan channel-belts on the Niger Delta slope and in the Arabian Sea: Marine and Petroleum Geology, v. 20, p. 649-676.

Ebanks, W. J., and J. F. Weber, 1987, Development of a shallow heavy oil deposits in Missouri: Oil and Gas Journal, p. 222-234.

Ethridge, F. G., and S. H. Schumm, 1978, Reconstructing paleochannel morphologic and flow characteristics: methodology, limitations and assessment. In: Miall AD (ed), Fluvial Sedimentology. Canadian Soc Petrol Geol Mem 5: p. 703-721

Ethridge, F.G., and S. A. Schumm, 2007, Fluvial seismic geomorphology: A view from the surface: in Davies, R. J., H. W. Posamentier, L. J. Wood, and J. A. Cartwright, (eds.), Seismic Geomorphology: Geological Society of London, Special Publication 27, p. 205-222.

Fachmi, M., 2003, Quantitative seismic geomorphology of Gabus and Belanak Fields, West Natuna Basin, Indonesia: Unpublished Thesis, University of Texas at Austin: Austin, TX, United States, p. 74.

Fachmi, M., and L. J., Wood, 2003, Quantitative seismic geomorphology of Belanak, and Gabus Fields, west Natuna Basin, Indonesia, 2003 Annual Meeting: American Association of Petroleum Geologists Program and Abstract Volume, A51-A52.

Fielding, C.R., and R.C., Crane, 1987, An application of statistical modeling to the prediction of hydrocarbon recovery factors in fluvial reservoir sequences, in Ethridge, F.G., Flores, R.M., and Harvey, M.D., eds., Recent Developments in Fluvial Sedimentology: SEPM, Special Publication 39, p. 321–327.

Fielding, C. R., and M.R., Gibling, 2005, Distinguishing between channel and valley fills: definitions, diagnostic criteria and dimensional data (abstract): 8th International Conference on Fluvial Sedimentology: Delft, Netherlands, Abstracts, p. 101.

Fisk, H.N., E. Jr., McFarlan 1955, Late Quaternary deltaic deposits of the Mississippi River. Geological Society of America, Special Paper 62, p. 279– 302.

Fowler, J. N., E. Guritno, P. Sherwood, M. J. Smith, S. Algar, I. Busono, G. Goffey, and A. Strong, 2004, Depositional architectures of Recent deepwater deposits in the Kutei Basin, East Kalimantan: in Davies R. J., J. A. Cartwright, S. A. Stewart, M. Lappin, and J. R. Underhill, (eds.), 3D Seismic Technology: Application to the Exploration of Sedimentary Basins, Geological society Memoirs 29, p. 25-33.

Galloway, W. E., and D. K. Hobday, 1996, Terrigenous clastic depositional systems: applications to petroleum, coal, and uranium exploration (2ed.): New York, Springer-Verlag, p. 489.

Gascoyne, M., G. J. Benjamin, and H. P. Schwartz, H. P., 1979, Sea-level lowering during the Illinoian glaciations: evidence from a Bahama “Blue Hole”, Science 205, p. 806-808.

Geehan, G., 1993, The use of outcrop data and heterogeneity modeling in development planning: in Eschard, R. and B. Doligez (eds.), Subsurface Reservoir

Characterization from Outcrop Observations: Institute François du Pétrole: Paris, Éditions Technip, p. 53-64.

Green A. N., 2009, Palaeo-drainage, incised valley fills and transgressive systems tract sedimentation of the northern KwaZulu-Natal continental shelf, South Africa, SW Indian Ocean. Marine Geology. 263(1–4): p. 46–63.

Ghosh, D. P., M. F. Abdul Hakim, M. Brewer, B. Viratno, and N Darman, 2010, Geophysical issues and challenges in Malay and adjacent basins from an E & P perspective: The Leading Edge, p. 436-449.

Gibling, M. R., 2006, Width and thickness of fluvial channel bodies and valley fills in the geological record; a literature compilation and classification: Journal of Sedimentary Research, v. 76 (5-6), p. 731-770.

Hamilton, W., 1979. Tectonics of the Indonesian region. United States Geological Survey Professional Paper, No. p.1078.

Hampson G. J., T. Elliot, and S. J. Davies, 1997, The application of sequence stratigraphy to Upper Carboniferous fluvio-deltaic strata of the onshore UK and Ireland: implications for the southern North Sea, Journal of the Geological Society, 1997, v.154, p. 719-733.

Hanebuth, T.J.J., Stattegger, K. and P.M., Grootes, 2000, Rapid Flooding of the Sunda Shelf: A Late-Glacial Sea-level Record. Science, 288: p. 1033-1035.

Hanebuth, T.J.J, and K. Statteger, 2003, The stratigraphic evolution of the Sunda Shelf during the past fifty thousand years, in F.H. Sidi, D. Nummedal, P. Imbert, and H.

Darman, eds., Tropical deltas of Southeast Asia; sedimentology, stratigraphy, and petroleum geology: SEPM Special Publications 76, p. 189-200.

Hanebuth, T.J.J., K., Stattegger, A., Schimanski, T., Lüdmann, and H.K., Wong, 2003, Late Pleistocene forced regressive deposits on the Sunda Shelf (SE Asia). Marine Geology, p. 139-157.

Hedage, B. A., R. A. Levey, V. Pendleton, J. Simmons, and R. Edson, 1994, A 3D seismic case history evaluating fluvially deposited thin-bed reservoirs in a gas-producing property, Geophysics, v. 59, p. 1650-1665.

Hopkins, D. M., 1982, Aspects of the paleoecology of Beringia during the Late Pleistocene, in: D. M. Hopkins, J. V. Matthews, C. E. Schweger, and S. B. Young (eds), Paleoecology of Beringia, Academic Press, New York, p. 3-28.

Haq, B.U., J. Hardenbol, and P.R. Vail, 1987, Chronology of fluctuating sea levels since the Triassic: Science, v. 235, p. 1156-1167.

Hutchison, C.S., 1989, Geological Evolution of South East Asia. Oxford monographs on Geology and Geophysics no. 13, Clarendon Press, Oxford.

Isa, Z. M., F. W. Richard, and H. Yunus, 1992, Integration of 3D and site survey seismic data in analysis of near-surface hazards to platform location at Dulang field, Malay Basin: Geological Society of Malaysia Bulletin, v. 32, p. 165-184.

Johnson, H. D., and D. J. Stewart, 1984, Geological modeling of a heterogeneous sandstone reservoir: Lower Jurassic Statfjord Formation, Brent Field: in 59th Annual Technical Conference and Exhibition, Houston, SPE paper 13050, (12).

Keogh, K. J., A. W. Martinius, O. Rune, 2007, The development of fluvial stochastic modeling in the Norwegian oil industry: A historical review, subsurface implementation and future directions: Sedimentary Geology, v. 202, p. 249-268.

Kiel, B., 2009, Three-dimensionality, Seismic Attributes, and Long Profile Setting of Valleys in recent sequences of the Sunda Shelf, Indonesia, Unpublished Thesis, University of Texas at Austin.

Kolla, V., Ph. Bourges, J. M. Urruty, and P. Safa, 2001, Evaluation of deep-water Tertiary sinuous channel offshore Angola (West Africa) and implication for reservoir architecture: American Association of Petroleum Geologists Bulletin, v. 85, p. 1373-1405.

Lang, S. C., J. Kassan, J. M. Benson, C. A. Grasso, and L. C. Avenell, 2000, Application of modern and ancient geological analogues in characterization of fluvial and fluvial-lacustrine deltaic reservoirs in the Cooper Basin: Australian Petroleum Exploration Association Journal, v. 40, p. 393-415.

Leclair, S. F., and J. S. Bridge, 2001, Quantitative interpretation of sedimentary structures formed by river dunes: Journal of Sedimentary Research, v. 71; p. 713-716.

Leeder, M. R., 1973, Fluviatile fining-upward cycles and the magnitude of palaeochannels, Geological Management, v. 110, p. 265-276.

Leopold, L. B., and M. G. Wolman, 1975, River channel patterns: braided, meandering, and straight, US Geological Survey professional paper 282-B.

Leopold, L. B., and M. G. Wolman, 1960, River meanders: Bulletin of the Geological Society of America, v. 71, p. 769–774.

Loe, C. T., 1997, Exploration in the Gulf of Thiland in deltaic reservoirs, related to the Bangkot Field, in: Fraser, A. J., Matthews, S. J., & Murphy, R. W. (eds), Petroleum Geology of Southeast Asia, Geological Society Special Publication No. 126, p. 77-87.

Lorenz., J. C., Henzed, . M., Clark. J,. A., and Searlsc . A., 1985, Determination of widths of meander-belt sandstone reservoirs from vertical downhole data, Mesaverde Group, Piceance Creek Basin, Colorado: American Association of Petroleum Geologists Bulletin, v. 69.

Lorenz, J. C., N. R. Warpinski, and P. T. Branagan, 1991, Subsurface characterization of Mesaverde reservoirs in Colorado: Geophysical and reservoir-engineering checks on predictive Sedimentology, in Miall, A. D., and N. Tyler (eds.), The Three-Dimensional Facies Architecture of Terrigenous Clastic Sediments, and its Implications for Hydrocarbon Discovery and Recovery: SEPM Concepts in Sedimentology and Palaeontology, v. 3, p. 57-79.

Lunt, I. A., and J. S. Bridge, 2004, Evaluation and deposits of a gravely braid bar, Sagavanirktok River, Alaska: Sedimentology, v. 51, p. 415-414.

Madon, M., 1999, Basin types, tectono-stratigraphic provinces, structural styles. In: Petronas (ed.) The Petroleum Geology and Resources of Malaysia. Petronas, Kuala Lumpur, p. 77-111.

Madon, M.B., and A.B. Watts, 1998, Gravity anomalies, subsidence history and the tectonic evolution of the Malay and Penyu basins (offshore Peninsula Malaysia): Basin Research, v. 10, p. 375-392.

Madon, M., P. Abolins., M., Jamaal Hoesni.,and M., Bin Ahmad, 1999, Malay Basin. In: Petronas (ed.) The Petroleum Geology and Resources of Malaysia. Petronas, Kuala Lumpur, p. 173–217.

Martinis, A. W., 2000, Labyrinthine facies architecture of the Tórtola fluvial system and controls on deposition (late Oligocene-early Miocene, Loranca Basin, (Spain): Journal of Sedimentary Research, v. 70, p. 850-867.

Me´tivier, F., Y. Gaudemer, P. Tapponnier, M. Klein, Mass accumulation rates in Asia during the Cenozoic, Geophys. J. Int. 137(1999) 280– 318.

Martinez, K. F., J. A. Cartwright, S A. Stewart, M. Lappin, and J. R. Underhill, 2004, 3-D seismic interpretation of the Messinian unconformity in the Valencia basin: in Davies R. J., J. A. Cartwright, S. A. Stewart, M. Lappin, and J. R. Underhill (eds.), 3D Seismic Technology: Application to the Exploration of Sedimentary Basins, Geological society Memoirs 29, p. 91-100.

Martinsen, O.J., A. Ryseth, H.W. Helland, H. Flesche, G. Torkildsen, and S. Idil, 1999, Stratigraphic base level and fluvial architecture: Ericson Sandstone (Campanian), Rock Springs Uplift, SW Wyoming, USA: Sedimentology, v. 46, p. 235-259.

Mertes L.A.K, T. Dunne, 2007, Effects of Tectonism, Climate Change, and Sea-level Change on the Form and Behaviour of the Modern Amazon River and its Floodplain, in Large Rivers (ed by S. Gupta), p. 115-144.

Miall, A. D., 1977, Facies Models for Alluvial Fans and Braided Rivers, Association of Petroleum Geologists Bulleting, v. 20 p. 23 – 32.

Miall, A. D., 1996, The Geology of Fluvial Deposits: Spring-Verlag, New York, 582 p.

Miall, A. D., 2002, Architecture and sequence stratigraphy of Pleistocene fluvial systems in the Malay Basin, based on seismic time-slice analysis, American Association of Petroleum Geologists Bulleting, v. 86, p. 1201-1216.

Molengraaff, G.A.F., Weber, M., 1921. On the relation between the Pleistocene glacial period and the origin of the Sunda Sea (Java- and South China Sea), and its influence on the distribution of coral reefs and on the land- and freshwater fauna. Proceedings Royal Academy 23, 395–439.

Morgan, R., 2004, Structural controls on the positioning of submarine channels on the lower slopes of the Niger Delta : in Davies R. J., J. A. Cartwright, S. A. Stewart, M. Lappin, and J. R. Underhill (eds.), 3D Seismic Technology: Application to the Exploration of Sedimentary Basins, Geological society Memoirs, 29, p. 45-51.

Morley, R.J. 2000. Origin and Evolution of Tropical Rain Forests. John Wiley & Sons, Ltd., Chichester, p.xiii-362

Morley, C. K. And R., Westaway, 2006, Subsidence in the super-deep Pattani and Malay basins of Southeast Asia: A coupled model incorporating lower-crustal flow in response to post-rift sediment loading. Basin Research, 18, 51–84.

Nakanishi, T., and S. C. Lang, 2003, Towards an efficient exploration frontier: Constructing a portfolio of stratigraphic traps in fluvial-lacustrine successions, Cooper-Eromanga Basin: Australian Petroleum Exploration Association Journal, v. 42, no. 1, p. 65-82.

National Geophysical Data Center (NGDC), 2009, http://www.ngdc.noaa.gov.

Negah, K., Madon, M., and Tjia, H.D., 1996, Role of pre-Tertiary fractures in formation and development of the Malay and Penyu basins. In: Hall, R. and Blundell, D.J., eds., Tectonic Evolution of Southeast Asia. Geological Society of London Special Publications, 106, 281-289.

Nordfjord, S., Goff, J.A., Austin, J.A.J. and Gulick, S.P.S. (2006) Seismic facies of incised-valley fills, New Jersey continental shelf: implications for erosion and preservation processes acting during latest Pleistocene–Holocene transgression. J. Sed. Res., 76, 1284–1303.

North, C. P., 1996, The prediction and modeling of subsurface fluvial stratigraphy: In Carling, P. A., and M. R., Drawson (eds.), Advances in Fluvial Dynamics and Stratigraphy, Wiley, Chichester, p. 395-508.

Olsen, T., R. Steel, K. Hogseth, T. Skar, and S. Roe, 1995, Sequential architecture in a fluvial succession: sequence stratigraphy in upper Cretaceous mesaverde group, Price Canyon, Utah: Journal of Sedimentary Research, v. B65, p. 265-280.

Paquet, F., D. Menier, G. Estournès, J.F. Bourillet[b], P. Leroy[c] and F. Guillocheau, 2010, Buried fluvial incisions as a record of Middle–Late Miocene eustasy fall on the Armorican Shelf (Bay of Biscay, France), Marine Geology, V. 268, issue 1-4, P. 137-151.

Posamentier, H. W., 2000, Seismic stratigraphy into the next millennium: a focus on 3D seismic data: American Association of Petroleum Geologists Annual Conference, New Orleans, LA, p. 16-19, April, 2000, A 118.

Posamentier, H. W., 2001, Lowstand alluvial bypass systems: incised vs. unincised, American Association of Petroleum Geologists Bulletin, v. 85, p. 1771-1793.

Posamentier, H. W., 2004, Seismic geomorphology: imaging elements of depositional systems data: implication for exploration and development: in Davies R. J., J. A. Cartwright, S. A. Stewart, M. Lappin, and J. R. Underhill (eds.), 3D Seismic Technology: Application to the Exploration of Sedimentary Basins, Geological society Memoirs 29, p. 11-24.

Posamentier, H.W., and G.P. Allen, 1993, Variability of the sequence stratigraphic models: effects of local basin factors: Sedimentary Geology, v. 86, p. 91-109.

Posamentier, H. W., G. Allen, 1999, Siliciclastic sequence stratigraphy: concepts and applications: SPEM Society for Sedimentary, p. 204

Posamentier, H. W., R. J. Davies, L. J. Wood, and J. A. Cartwright, 2007, Seismic geomorphology-an overview: in Davies, R. J., H. W. Posamentier, L. J. Wood, and J. A. Cartwright (eds.), Seismic Geomorphology: Geological Society of London, Special Publication 27, p. 1-14.

Posamentier, H. W., and V. Kolla, 2003, Seismic geomorphology and stratigraphy of depositional elements in deep-water settings: American Association of Petroleum Geologists Bulletin, v. 71, p. 367-388.

Rabelo, I. R., S. M. Luthi, and L. J. Van Vliet, 2007, Parameterization of meander-belt elements in high-resolution three-dimensional seismic data using the GeoTime cube, and modern analouges: in Davies, R. J., H. W. Posamentier, L. J. Wood, and J. A. Cartwright (eds.), Seismic Geomorphology: Geological Society of London, Special Publication 27, p. 121-138.

Reading, H. G., 1996, Sedimentary environments: processes, facies, and stratigraphy: Oxford, Blackwell Science, p. 5-36.

Reynaud, J., Tessier, B., Proust, J., Dalrymple, R., Bourillet, J., De BatistATIST, M., Lericolais, G., Berne´ , S., and Marsett, T., 1999, Architecture and sequence stratigraphy of a late Neogene incised valley at the shelf margin, southern Celtic Sea: Journal of Sedimentary Research, v. 69, p. 351–364.

Reynolds, A.D., 1999, Dimensions of paralic sandstone bodies: American Association of Petroleum Geologists, Bulletin, v. 83, p. 211–229.

Robinson, J. W., and P. J. McCabe, 1997, Sandstone-body and shale-body dimensions in a braided fluvial system; Salt Wash Sandstone Member (Morrison Formation), Garfield County, Utah: American Association of Petroleum Geologists Bulletin, v. 81, p.1267-1291.

Rust, B. R., 1978, A classification of alluvial channel systems, In: Miall AD (ed), Fluvial Sedimentology. Canadian Soc Petrol Geol Mem 5: 187-198.

Sathiamurthy, E., and H. K., Voris, 2006, Maps of Holocene sea level transgression and submerged lakes on the Sunda Shelf: The Natural History Journal of Chulalongkorn University, Supplement 2, p. 1-44.

Schumm, S.A., 1977, The Fluvial System: New York, Wiley-Interscience, 338 p.

Schumm, S.A., 1981, Experimental Fluvial Geomorphology: New York, Wiley & Sons, 376 p.

Schumm, S.A., 1993, River response to baselevel change: implications for sequence stratigraphy: The Journal of Geology, v. 101, p. 279-294.

Schumm, S.A., 2005, River Variability and Complexity. Cambridge University Press, Camridge.

Schumm, S.A., and Ethridge, F.G., 1994, Origin, evolution and morphology of fluvial valleys, in Dalrymple, R.W., Zaitlin, B.A., and Scholle, P.A., eds., Incised-Valley Systems: Origin and Sedimentary Sequences, SEPM, Special Publication 51, p. 11–27.

Shackleton, N.J., 1987. Oxygen isotopes, ice volume and sea level. Quat. Sci. Rev. 6, 183-190.

Shanley, K.W., and P.J. McCabe, 1991, Predicting facies architecture through sequence stratigraphy – an example from the Kaiparowits Plateau, Utah: Geology, v. 19, p. 742-745.

Shanley, K.W., and P.J. McCabe, 1993, Alluvial architecture in a sequence stratigraphic framework; a case history from the Upper Cretaceous of southern Utah, USA, in S.S. Flint, and A.D. Bryant, eds., The geological modelling of hydrocarbon reservoirs and outcrop analogues: Special Publication of the International Association of Sedimentologists, p. 21-55.

Shanley, K. W., 2004, Fluvial reservoir description for a giant, low-permeability gas field; Jonah field, Green River Basin, Wyoming, U.S.A: in Robinson, J. W., and K.W. Shanley (eds.), Jonah field: A Case Study of a Tight-Gas Fluvial Reservoir: American Association of Petroleum Geologists Studies in Geology 52, p. 159-182.

Shanley, K.W., and P.J. McCabe, 1994, Perspectives on the sequence stratigraphy of continental strata: AAPG Bulletin, v. 78, p. 544-568.

Sinsakul, 1992, evidence of quaternary sea level changes in the coastal areas of Thailand, Journal of Southeast Asian Earth Science, v.7, p. 23-37.

Staub, J. R., and Gastaldo, R. A., 2003 In: Sidi, F.H., Nummedal, D., Posamentier, H.W., Darman, H., Imbert, P. (Eds.), Deltas of Southeast Asia and Vicinity—Sedimentology, Stratigraphy and Petroleum Geology, SEPM Special

Steffens, G. S., R. C. Shipp, B. E. Prather, J. A. Nott, J. L. Gibson, and C. D. Winker, 2004, The use of near-seafloor seismic data in deepwater exploration and production, in Davies R. J., J. A. Cartwright, S. A. Stewart, M. Lappin, and J. R. Underhill (eds.), 3D Seismic Technology: Application to the Exploration of Sedimentary Basins, Geological society Memoirs 29, p. 35-43

Strong, P.C., G. R. Wood, S. C. Lnage, A. Jollands, E. Karalaus, and J. Kassan, 2002, High resolution palaeogeographic mapping of the fluvial-lacustrine Patchawarra Formation in the Cooper Basin, South Australia: Australian Petroleum Exploration Association Journal, v. 42, p. 65-82.

Sun, X., Li, X., Luo, Y. and Chen, X. 2000. The vegetation and climate at the last glaciation on the emerged continental shelf of the South China Sea. Palaeo, 160: p. 301-316

Swanson, D. C., 1976, Meandering stream deposits, Cygnet Group Inc.

Tapponnier, P., G. Peltzer, and R. Armijo, 1986, On the mechanics of the collision between India and Asia, in M. P. Coward and A. C. Ries, eds., Collision tectonics: Geological Society Special Publication 19, p. 115-157

Thomas, R.G., Smith, D.G., Wood, J.M., Visser, J., Calverley-Range, A., and Koster, E.H., 1987. Inclined heterolithic Stratification – Terminology, Description, Interpretation and Significance, Sedimentary Geol., 53: 123-179.

Thompson, C., G. McMechan, R. Szerbiak, and N. Gaynor, 1995, 3-D GPR imaging of complex stratigraphy within the Ferron sandstone, Castle Valley, Utah: in Proc., Symposium on the Application of Geophysics to Engineering and Environmental Problems, 18-22 April 1995, Orlando, FL, p. 435-443.

Thorp, M.B., Thomas, M.F., Martin, T., Whalley, W.B., 1990. Late Pleistocene sedimentation and landform development in western Kalimantan (Indonesian Borneo). Geologie en Mijnbouw 96, 133–150.

Tjia, H.D., 1980, The Sunda shelf, Southeast Asia: Annals of Geomorphology, v. 4, p.405–427.

Tjia, H.D., 1994a. Origin and tectonic development of Malay-Penyu West Natuna Basins. Paper presented at PRSS Technology Day 21 June 1994, Kuala Lumpur. (unpublished manuscript).

Tjia, H.D., 1994b. Inversion tectonics in the Malay Basin: evidence and timing of events. Bulletin of the Geological Society of Malaysia, 36, 119-126.

Tjia, H.D. and K.K., Liew, 1996. Changes in tectonic stress field in northern Sunda Shelf basins. In: Hall, R. and Blundell, D.J., eds., Tectonic Evolution of Southeast Asia. Geological Society of London Special Publication, 106, 291-306.

Tornqvist, T.E., 1993, Holocene alternating of meandering and anastomosing fluvial system in Rhine-Meuse delta (central Netherlands) controlled by sea level rise and subsoil erodibility: Journal of Sedimentary Petrology, v. 63, p. 683-693.

Tye, R. S., 1991 Fluvial-sandstone reservoirs of the Travis Peak Formation, East Texas basin: in Miall, A. D., and N. Tyler (eds.), The three-dimensional facies

architecture of terrigenous clastic sediments, and its implications for hydrocarbon discovery and recovery: SEPM Concepts in Sedimentology and Palaeontology, v. 3, p. 172-188.

Tye, R. S., 2004, Geomorphology: an approach to determining subsurface reservoir dimensions: American Association of Petroleum Geologists Bulletin, v. 88, p. 1123-1147.

Vail, P. R., R.M. Mutchum, and S. III. Thompson, 1977, Seismic stratigraphy and global changes of sea level, part 3: relative changes of see level from coastal onlap: in Payto, C. E. (ed.), Seismic Stratigraphy – Applications to Hydrocarbon Exploration, American Association of petroleum Geologists Memoir 26, 63-81.

Van Wagoner, J. C., R. M. Mitchum, K. M. Campion, and V. D. Rahmanian, 1990, Siliciclastic sequence stratigraphy in well logs, cores, and outcrops: concepts for high-resolution correlation of time and facies: AAPG Methods in Exploration Series, p. 55.

Voris, H.K. 2000. Maps of Pleistocene sea levels in Southeast Asia: shorelines, river systems and time durations. Journal of Biogeography, 27: p. 1153-1167.

Wang, L., Sarnthein, M., Erlenkeuser, H., Grimalt, J., Grootes, P., Heilig, S., Ivanova, E., Kienast, M., Pelejero, C., P flaumann, U., 1999. East Asian monsoon climate during the Late Pleistocene: high-resolution sediment records from the South China Sea. Marine Geology 156, 245–284.

Weber, K. J., and L. C. van Geuns, 1990, Framework for constructing clastic reservoir simulation models: Society of Petroleum Engineers, 64th Annual Technical Conference and Exhibition, Paper 19582, p. 109-118.

Wong, H.K., Haft, C., Paulsen, A.M., Lu¨dmann, T., Hu¨bscher, C., Geng, J., 2003. Late Quaternary sedimentation and sea-level fluctuations on the northern Sunda Shelf, southern South China Sea. In: Sidi, F.H., Nummedal, D., Posamentier, H.W., Darman, H., Imbert, P. (Eds.), Deltas of Southeast Asia and Vicinity—Sedimentology, Stratigraphy and Petroleum Geology, SEPM Special Publication 76.

Wood, L. J., 2003, Quantitative seismic geomorphology and reservoir architecture of clastic depositional systems; the future of uncertainty analysis in exploration and production, Annual Meeting Expanded Abstracts - American Association of Petroleum Geologists, United States, AAPG and SEPM: Tulsa, OK, United States, p. 182.

Wood, L. J., 2007, Quantitative seismic geomorphology of Pliocene and Miocene fluvial systems in the northern Gulf of Mexico, U.S.A.: Journal of Sedimentary Research, v. 77, p. 713–730.

Wood, L. J., and Mize-Spansky, K. L., 2009, Quantitative seismic geomorphology of a Quaternary leveed-channel system, offshore eastern Trinidad and Tobago, northeastern South America: AAPG Bulletin, v. 93, no. 1, p. 101–125

Wood, J. M., and J.C. Hopkins, Reservoir sandstone bodies in estuarine valley fill: Lower Cretaceous Glauconitic Member, Little Bow Field, Alberta, Canada, Bull. Amer. Ass. Petrol. Geol. 73 (1989), pp. 1361–1382

Woodroffe, C. D., 2000, Deltaic and estuarine environments and their Late Quaternary dynamics on the Sunda and Sahul shelves, Journal of Asian Earth Sciences, p 393-413

Wright, V.P., and S.B. Marriott, 1993, The sequence stratigraphy of fluvial depositional systems: the role of floodplain sediment storage: Sedimentary Geology, v. 86, p. 203-210.

Yalin, M. S., 1964, Geometrical properties of sand waves, Journal of the Hydraulics Division, American Society of Civil Engineers, v. 90, p. 105-119.

Yang, H. and Xie, Z.: 1984, Sea-Level Changes in East China over the Past 20 000 Years ", in R. O. Whyte (ed.), The Evolution of the East Asian Environment, Univ. Hong Kong, Cent. Asian Stud., pp. 288–308.

Zaitlin, B.A., Dalrymple, R.W., and Boyd, R., 1994, The stratigraphic organization of incised-valley systems associated with relative sea-level change, in Dalrymple, R.W., Boyd, R., and Zaitlin, B.A., eds., Incised-Valley Systems: Origin and Sedimentary Sequences: SEPM, Special Publication 51, p. 45–60.

Zeng, H., M. M. Backus, K. T. Barrow, and N. Tyler, 1998, Stratal slicing; Part 1, Realistic 3-D seismic model: Geophysics, v. 63, p. 502-513.

Zeng, H., 2007, Seismic imagining for seismic geomorphology beyond the seabed: potential and challenges: in Davies, R. J., H. W. Posamentier, L. J. Wood, and J. A. Cartwright (eds.), Seismic Geomorphology: Geological Society of London, Special Publication 27, p. 15-28.

Zeng, H., and T. F. Hentz, 2004, High-frequency sequence stratigraphy from seismic sedimentology: applied to Miocene Vermilion Block 50, Tiger Shoal area, offshore Louisiana: American Association of Petroleum Geologists Bulleting, v. 88, p. 153-174.

Appendices

8.1 Quantitative Database

Unit 1 Base

Channel No.	*CD* (ms)	*CD* (m)	IV d. (ms)	IV d. (m)	*CW* (min., m)	*CW* (max., m)	CW (ave., m)	*MBW* (ave., m)	*La* (km)	*ML* (km)	*SI*	*RC* (m)	*CO*	*ML* (ave., km)	*W/D*
1	36	29.7	-------	-------	711	1291	878	3062	17.3	16.3	1.1	945	SW-NE	-------	29.6
2	38	31.35	-------	-------	465	1180	700	3528	42.0	35.0	1.2	1407	SW-NE	-------	22.3
3	42	34.65	-------	-------	441	754	631	1825	19.7	18.5	1.1	873	SW-NE	-------	18.2
4	42	34.65	-------	-------	592	1100	758	2375	39.2	37.3	1.1	1017	SW-NE	-------	21.9
5	34	28.05	-------	-------	1625	2430	2100	5482	47.7	43.2	1.1	2075	NW-SE	-------	74.9
6	38	31.35	-------	-------	1730	2500	2172	5789	18.8	17.8	1.1	1509	NW-SE	-------	69.3
7	26	21.45	-------	-------	290	505	370	1711	17.8	17.0	1.0	1007	SW-NE	-------	17.2
8	30	24.75	-------	-------	384	758	565	1643	38.1	34.5	1.1	922	SW-NE	-------	22.8
9	28	23.1	-------	-------	450	903	668	2193	21.2	19.5	1.1	982	SW-NE	-------	28.9
10	26	21.45	-------	-------	461	800	658	2112	13.3	12.6	1.1	829	SW-NE	-------	30.7
11	28	23.1	-------	-------	757	1067	926	2076	13.5	12.2	1.1	1038	SW-NE	-------	40.1
12	34	28.05	-------	-------	1005	1826	1297	2551	44.0	40.0	1.1	1024	SW-NE	-------	46.2
13	26	21.45	-------	-------	260	732	445	1298	17.6	15.1	1.2	567	SE-NW	-------	20.7
14	32	26.4	-------	-------	523	1041	707	1584	32.5	32.0	1.0	564	SW-NE	-------	26.8
15	26	21.45	-------	-------	1017	1243	1130	1763	7.9	7.8	1.0	860	SW-NE	-------	52.7
16	26	21.45	-------	-------	564	834	720	1177	15.0	13.9	1.1	685	SW-NE	-------	33.6
17	38	31.35	-------	-------	488	1872	1130	2790	53.3	45.0	1.2	1590	SW-NE	-------	36.0
18	28	23.1	-------	-------	486	617	576	1614	13.1	12.4	1.1	647	SE-NW	-------	24.9
19	30	24.75	-------	-------	243	434	320	1471	11.3	10.0	1.1	720	SE-NW	-------	12.9

Unit 1 Top

Channel No.	*CD* (ms)	*CD* (m)	IV d. (ms)	IV d. (m)	*CW* (min., m)	*CW* (max., m)	CW (ave., m)	*MBW* (ave., m)	*La* (km)	*ML* (km)	*SI*	*RC* (m)	*CO*	*ML* (ave., km)	*W/D*
1	22	18.15	-------	-------	116	324	185	6000	122.5	44.2	2.8	2000	SW-NE	5.0	10.2
2	20	16.5	-------	-------	75	150	115	4300	30.2	22.2	1.4	800	NE-SW	5.2	7.0
3	22	18.15	-------	-------	125	300	195	7110	107.8	54.3	2.0	1400	SW-NE	7.8	10.7
4	18	14.85	-------	-------	95	290	160	10840	130.5	42.7	3.1	1500	SW-NE	6.1	10.8
5	8	6.6	-------	-------	50	50	50	1500	21.0	16.5	1.3	250	SW-NE	4.1	7.6
6	8	6.6	-------	-------	50	50	50	1600	17.7	10.1	1.8	180	SW-NE	2.0	7.6
7	18	14.85	-------	-------	50	254	130	1950	40.4	24.4	1.7	570	SW-NE	4.1	8.8
8	10	8.25	-------	-------	50	50	50	1330	26.1	13.3	2.0	280	SW-NE	1.0	6.1
9	8	6.6	-------	-------	50	50	50	2000	27.5	12.3	2.2	300	SW-NE	1.2	7.6

Unit 2 Base

Channel No.	*CD* (ms)	*CD* (m)	IV d. (ms)	IV d. (m)	*CW* (min., m)	*CW* (max., m)	CW (ave., m)	*MBW* (ave., m)	*La* (km)	*ML* (km)	*SI*	*RC* (m)	*CO*	*ML* (ave., km)	*W/D*
1	58	47.85	-------	-------	1442	3800	2565	6358	120.0	116.5	1.0	1857	NW-SE	-------	53.6
2	44	36.3	-------	-------	710	1740	1222	4500	83.5	75.0	1.1	1900	NW-SE	-------	33.7
3	24	19.8	-------	-------	1170	2120	1325	4273	27.4	24.0	1.1	1588	NW-SE	-------	66.9
4	46	37.95	-------	-------	320	988	713	2457	19.6	17.0	1.2	1109	N-S	-------	18.8
5	38	31.35	-------	-------	1327.3	2869	1970	5007	72.5	61.0	1.2	1600	W-E	-------	62.8
6	36	29.7	-------	-------	790	1119	918	2563	14.3	13.0	1.1	945	SW-NE	-------	30.9
7	26	21.45	-------	-------	743	1563	965	2635	34.4	32.8	1.0	1313	NW-SE	-------	45.0
8	24	19.8	-------	-------	469	615	573	1818	14.8	13.9	1.1	843	SW-NE	-------	28.9
9	20	16.5	-------	-------	122	370	209	725	12.6	12.1	1.0	477	SW-NE	-------	12.7
10	26	21.45	-------	-------	135	679	386	1212	14.6	13.1	1.1	570	SW-NE	-------	18.0
11	34	28.05	-------	-------	606	1344	979	2185	23.6	20.3	1.2	1338	SW-NE	-------	34.9
12	36	29.7	-------	-------	473	1050	745	2588	13.7	10.0	1.4	1349	SW-NE	-------	25.1
13	22	18.15	-------	-------	378	810	564	1336	27.1	21.4	1.3	1128	SW-NE	-------	31.1

Unit 2 Top

Channel No.	*CD* (ms)	*CD* (m)	IV d. (ms)	IV d. (m)	*CW* (min., m)	*CW* (max., m)	CW (ave., m)	*MBW* (ave., m)	*La* (km)	*ML* (km)	*SI*	*RC* (m)	*CO*	*ML* (ave., km)	*W/D*
1	28	23.1	-------	-------	378	1066	805	4450	68.0	54.7	1.2	1430	SW-NE	9.1	34.8
2	28	23.1	-------	-------	78	275	176	3400	58.0	28.0	2.1	1500	W-E	4.0	7.6
3	26	21.45	-------	-------	55	102	55	2150	84.6	51.0	1.7	1000	NW-SE	5.1	2.6
4	20	16.5	-------	-------	100	141	125	1500	21.6	18.5	1.2	1040	NW-SE	6.2	7.6
5	12	9.9	-------	-------	55	137	55	2000	40.0	23.0	1.7	500	NW-SE	3.8	5.6
6	16	13.2	-------	-------	55	80	60	1350	53.6	36.5	1.5	1000	SW-NE	4.6	4.5
7	10	8.25	-------	-------	55	119	55	1300	39.1	28.0	1.4	600	W-E	3.5	6.7
8	16	13.2	-------	-------	55	265	102	2100	144.6	55.0	2.6	1200	SW-NE	4.2	7.7
9	12	9.9	-------	-------	55	209	120	1450	26.8	15.0	1.8	700	W-E	2.5	12.1
10	14	11.55	-------	-------	116	257	173	5000	45.3	21.2	2.1	2100	SW-NE	5.3	15.0
11	18	14.85	-------	-------	123	406	240	4650	46.1	20.0	2.3	2700	SW-NE	6.7	16.2

Sub-unit 3.1Base

Channel No.	*CD* (ms)	*CD* (m)	IV d. (ms)	IV d. (m)	*CW* (min., m)	*CW* (max., m)	CW (ave., m)	*MBW* (ave., m)	*La* (km)	*ML* (km)	*SI*	*RC* (m)	*CO*	*ML* (ave., km)	*W/D*
1	26	21.45	-------	-------	375	827	601	1300	16.1	16.1	1.0	545	NW-SE	-------	28.0
2	42	34.65	-------	-------	600	3000	1800	4312	90.6	80.6	1.1	1750	W-E	-------	51.9
3	32	26.4	-------	-------	688	1000	844	1454	14.0	13.0	1.1	670	NW-SE	-------	32.0
4	14	11.55	-------	-------	200	486	343	2000	16.4	14.0	1.2	870	SW-NE	-------	29.7
5	22	18.15	-------	-------	550	805	677.5	813	14.5	14.4	1.0	590	NW-SE	-------	37.3
6	32	26.4	-------	-------	483	712	597.5	1950	65.9	61.0	1.1	800	NW-SE	-------	22.6
7	20	16.5	-------	-------	283	408	345.5	1008	14.0	13.5	1.0	550	W-E	-------	20.9
8	18	14.85	-------	-------	550	711	630.5	2000	21.7	20.2	1.1	1139	SW-NE	-------	42.5
9	18	14.85	-------	-------	714	1127	920.5	2951	22.5	21.0	1.1	1101	SW-NE	-------	62.0
10	20	16.5	-------	-------	563	814	688.5	1819	27.6	27.1	1.0	843	SW-NE	-------	41.7
11	30	24.75	-------	-------	543	864	703.5	1100	13.5	13.1	1.0	611	NW-SE	-------	28.4
12	36	29.7	-------	-------	278	341	309.5	1717	15.0	13.3	1.1	1082	SW-NE	-------	10.4
13	32	26.4	-------	-------	326	553	439.5	944	20.3	19.7	1.0	484	SW-NE	-------	16.6
14	38	31.35	-------	-------	980	1225	1102.5	3724	21.6	19.0	1.1	1429	SW-NE	-------	35.2
15	30	24.75	-------	-------	438	900	669	1345	17.7	17.5	1.0	419	SW-NE	-------	27.0
16	16	13.2	-------	-------	302	508	405	600	16.2	15.7	1.0	302	SW-NE	-------	30.7

Sub-unit 3.1Top

Channel No.	*CD* (ms)	*CD* (m)	IV d. (ms)	IV d. (m)	*CW* (min., m)	*CW* (max., m)	CW (ave., m)	*MBW* (ave., m)	*La* (km)	*ML* (km)	*SI*	*RC* (m)	*CO*	*ML* (ave., km)	*W/D*
1	26	21.45	-------	-------	110	383	212	3800	51.6	28.5	1.8	800	W-E	3.2	9.9
2	28	23.1	-------	-------	315	1067	782	4500	61.8	54.0	1.1	1200	W-E	13.5	33.9
3	12	9.9	-------	-------	50	50	50	2500	30.0	8.5	3.5	800	W-E	1.7	5.1
4	12	9.9	-------	-------	118	264	176	4000	38.8	22.4	1.7	700	N-S	3.7	17.8
5	20	16.5	-------	-------	71	144	103	3700	45.7	20.0	2.3	620	W-E	2.9	6.2
6	12	9.9	-------	-------	50	50	50	2600	120.0	60.1	2.0	590	SW-NE	2.7	5.1
7	8	6.6	-------	-------	50	50	50	1700	21.0	7.5	2.8	350	W-E	1.1	7.6
8	20	16.5	-------	-------	118	290	186	3100	35.7	27.6	1.3	531	W-E	3.5	11.3
9	16	13.2	-------	-------	50	107	75	3500	75.0	37.8	2.0	765	NW-SE	2.9	5.7
10	16	13.2	-------	-------	55	147	64	3600	93.1	50.0	1.9	670	NW-SE	3.3	4.8
11	8	6.6	-------	-------	50	50	50	2300	42.0	21.0	2.0	300	W-E	1.3	7.6
12	8	6.6	-------	-------	50	50	50	1000	32.0	15.0	2.1	200	NW-SE	1.0	7.6
13	14	11.55	-------	-------	50	50	50	1500	40.0	20.0	2.0	700	SW-NE	1.8	4.3

Sub-unit 3.2

Channel No.	*CD* (ms)	*CD* (m)	IV d. (ms)	IV d. (m)	*CW* (min., m)	*CW* (max., m)	CW (ave., m)	*MBW* (ave., m)	*La* (km)	*ML* (km)	*SI*	*RC* (m)	*CO*	*ML* (ave., km)	*W/D*
1	14	11.55	42	34.65	100	238	148	3.4	50.0	22.0	2.3	1290	SW-NE	3.1	12.8
2	32	26.4	66	54.45	55	208	109	4	180.0	62.5	2.9	1680	SW-NE	2.1	4.1
3	10	8.25	34	28.05	100	412	226	6.5	140.0	60.5	2.3	850	NW-SE	2.3	27.4
4	36	29.7	-------	-------	470	711	590.5	1251	22.8	21.1	1.1	550	NE-SW	-------	19.9
5	28	23.1	-------	-------	343	650	496.5	1043	22.1	21.4	1.0	490	NE-SW	-------	21.5
6	28	23.1	-------	-------	346	420	383	780	14.0	13.3	1.1	324	NE-SW	-------	16.6
7	22	18.15	-------	-------	385	755	602	2100	14.5	10.0	1.4	1212	NE-SW	-------	33.2
8	22	18.15	-------	-------	495	950	650	1979	27.5	26.0	1.1	800	NW-SE	-------	35.8
9	22	18.15	-------	-------	340	578	435	572	7.9	7.6	1.0	300	SW-NE	-------	24.0
10	22	18.15	-------	-------	300	845	460	1309	14.4	9.6	1.5	856	SW-NE	-------	25.3
11	22	18.15	-------	-------	270	635	440	1350	14.2	11.5	1.2	895	SW-NE	-------	24.2
12	26	21.45	-------	-------	640	740	686	1129	19.7	19.5	1.0	567	SW-NE	-------	32.0
13	22	18.15	-------	-------	552	785	715	973	17.7	17.4	1.0	500	SW-NE	-------	39.4

Sub-unit 4.1Base

Channel No.	*CD* (ms)	*CD* (m)	IV d. (ms)	IV d. (m)	*CW* (min., m)	*CW* (max., m)	CW (ave., m)	*MBW* (ave., m)	*La* (km)	*ML* (km)	*SI*	*RC* (m)	*CO*	*ML* (ave., km)	*W/D*
1	30	24.75	-------	-------	208	230	285	300	18.4	17.8	1.0	300	N-S	-------	11.5
2	30	24.75	-------	-------	400	1145	860	1468	27.0	25.1	1.1	886	N-S	-------	34.7
3	26	21.45	-------	-------	300	995	633	2936	154.8	125.0	1.2	1216	N-S	-------	29.5
4	28	23.1	-------	-------	485	958	707	2869	71.5	63.0	1.1	1179	N NW-SE	-------	30.6
5	38	31.35	-------	-------	850	1500	1297	4061	27.8	26.3	1.1	2050	NW-SE	-------	41.4
6	22	18.15	-------	-------	550	1168	810	2689	86.3	81.7	1.1	890	W-E	-------	44.6
7	12	9.9	-------	-------	255	280	280	300	6.5	6.2	1.1	320	SW-NE	-------	28.3
8	22	18.15	-------	-------	305	637	420	3000	35.0	22.5	1.6	1000	W-E	-------	23.1
9	18	14.85	-------	-------	410	925	585	1217	15.1	14.5	1.0	545	SW-NE	-------	39.4
10	15	12.375	-------	-------	450	600	520	780	6.0	5.8	1.0	417	SW-NE	-------	42.0

Sub-unit 4.1Top

Channel No.	*CD* (ms)	*CD* (m)	IV d. (ms)	IV d. (m)	*CW* (min., m)	*CW* (max., m)	CW (ave., m)	*MBW* (ave., m)	*La* (km)	*ML* (km)	*SI*	*RC* (m)	*CO*	*ML* (ave., km)	*W/D*
1	10	8.25	-------	-------	100	320	195	2000	148.2	120.0	1.2	700	NW-SE	3.8	23.6
2	14	11.55	-------	-------	100	260	160	1500	44.6	35.3	1.3	600	NW-SE	3.5	13.9
3	22	18.15	-------	-------	100	446	220	3000	122.8	82.8	1.5	500	NW-SE	4.0	12.1
4	10	8.25	-------	-------	80	190	115	600	22.7	19.0	1.2	400	N-S	1.7	13.9
5	18	14.85	-------	-------	140	420	200	3800	68.6	48.1	1.4	1100	NW-SE	4.0	13.5
6	26	21.45	-------	-------	190	500	210	2000	28.9	23.9	1.2	1000	NW-SE	3.6	9.8
7	12	9.9	-------	-------	50	50	50	1200	17.0	12.5	1.4	300	NE-SW	2.4	5.1
8	12	9.9	-------	-------	50	50	50	800	24.0	17.0	1.4	320	NE-SW	2.0	5.1
9	16	13.2	-------	-------	80	205	165	500	21.6	21.0	1.0	250	W-E	2.3	12.5
10	14	11.55	-------	-------	80	160	145	800	24.0	22.3	1.1	330	W-E	2.6	12.6
11	14	11.55	-------	-------	110	420	320	1250	18.4	16.2	1.1	540	W-E	4.0	27.7

Sub-unit 4.2

Channel No.	*CD* (ms)	*CD* (m)	IV d. (ms)	IV d. (m)	*CW* (min., m)	*CW* (max., m)	CW (ave., m)	*MBW* (ave., m)	*La* (km)	*ML* (km)	*SI*	*RC* (km)	*CO*	*ML* (ave., km)	*W/D*
1	38	32	-------	-------	345	525	430	1115	18.4	17.0	1.1	670	N-S	-------	13.4
2	38	32	-------	-------	330	390	560	1200	23.0	16.0	1.4	500	SW-NE	-------	17.5
3	38	32	-------	-------	220	390	307	500	12.0	10.0	1.2	360	SW-NE	-------	9.6
4	25	20	88	78	430	780	560	14000	214.0	76.0	2.8	3000	NW-SE	13.0	28.0
5	38	32	-------	-------	265	361	200	500	18.7	13.0	1.4	350	N-S	-------	6.3
6	30	24.75	-------	-------	515	685	600	860	7.9	7.3	1.1	560	NW-SE	-------	24.2
7	30	24.75	-------	-------	482	674	578	1000	65.0	60.5	1.1	552	NW-SE	-------	23.4
8	34	28.05	-------	-------	546	1000	773	1244	27.3	25.7	1.1	672	NW-SE	-------	27.6
9	34	28.05	-------	-------	417	798	607.5	1104	7.0	6.1	1.2	846	NW-SE	-------	21.7
10	20	16.5	-------	-------	336	510	423	845	8.7	8.3	1.1	793	NW-SE	-------	25.6
11	20	16.5	-------	-------	200	380	290	300	8.8	8.5	1.0	260	NW-SE	-------	17.6
12	20	16.5	-------	-------	550	934	742	1454	25.0	23.3	1.1	750	NW-SE	-------	45.0
13	20	16.5	-------	-------	304	480	392	909	11.4	11.3	1.0	585	NW-SE	-------	23.8
14	20	16.5	-------	-------	400	708	554	1100	7.3	6.9	1.1	600	NW-SE	-------	33.6
15	30	24.75	-------	-------	536	748	642	1612	19.0	17.0	1.1	800	NW-SE	-------	25.9
16	20	16.5	-------	-------	306	468	387	600	15.0	13.5	1.1	266	E-W	-------	23.5
17	20	16.5	-------	-------	538	606	572	925	9.0	8.5	1.1	461	E-W	-------	34.7

8.2 Channel Classification

Group-1: Incised valleys

Channel No.	Ch d. (m)	CW (m)	MBW (m)	La (km)	ML (km)	SI	RC (m)	W/D
1	78	14000	18000	84.0	75.0	1.1	0.0	179.5
2	60	7000	10840	42.7	42.0	1.0	0.0	116.7
3	45	6000	6500	60.5	55.0	1.1	0.0	133.3
4	35	3500	6500	44.2	40.0	1.1	0.0	100.0
5	35	4500	6000	20.0	18.0	1.1	0.0	128.6

Sub-group-2.1: Major low-sinuosity channels

Channel No.	Ch d. (m)	CW (m)	MBW (m)	La (km)	ML (km)	SI	RC (m)	W/D
1	47.85	2565	6358	120.0	116.5	1.0	1857.0	53.6
2	31.35	2172	5789	18.8	17.8	1.1	1509.0	69.3
3	28.05	2100	5482	47.7	43.2	1.1	2075.0	74.9
4	31.35	1970	5007	72.5	61.0	1.2	1600.0	62.8
5	34.65	1800	4312	90.6	80.6	1.1	1750.0	51.9

Sub-group-2.2: Low-sinuosity channels

Channel No.	Ch d. (m)	CW (m)	MBW (m)	La (km)	ML (km)	SI	RC (m)	W/D
1	28.05	1300	4273	27.4	24.0	1.1	1588.0	46.3
2	28.05	1250	4061	44.0	40.0	1.1	2050.0	44.6
3	31.35	1297	2551	27.8	26.3	1.1	1024.0	41.4
4	36.3	1222	4500	83.5	75.0	1.1	1900.0	33.7
5	31.35	1130	2790	53.3	45.0	1.2	1590.0	36.0
6	25	1130	1763	7.9	7.8	1.0	860.0	45.2
7	31.35	1102.5	3724	21.6	19.0	1.1	1429.0	35.2
8	32	1023	2378	21.5	17.0	1.3	1200.0	32.0
9	28.05	979	2185	23.6	20.3	1.2	1338.0	34.9
10	21.45	965	2635	34.4	32.8	1.0	1313.0	45.0
11	23.1	926	2076	13.5	12.2	1.1	1038.0	40.1
12	20	920.5	2951	22.5	21.0	1.1	1101.0	46.0
13	29.7	918	2563	14.3	13.0	1.1	945.0	30.9
14	29.7	878	3062	17.3	16.3	1.1	1413.0	29.6
15	24.75	860	1468	27.0	25.1	1.1	886.0	34.7
16	26.4	844	1454	14.0	13.0	1.1	670.0	32.0
17	18.15	810	2689	86.3	81.7	1.1	890.0	44.6

18	23.1	805	4000	68.0	54.7	1.2	1430.0	34.8
19	23.1	782	3500	61.8	54.0	1.1	1200.0	33.9
20	28.05	773	1244	27.3	25.7	1.1	672.0	27.6
21	34.65	758	2375	39.2	37.3	1.1	1017.0	21.9
22	29.7	745	2588	13.7	10.0	1.4	1349.0	25.1
23	16.5	742	1454	25.0	23.3	1.1	750.0	45.0
24	21.45	720	1177	15.0	13.9	1.1	685.0	33.6
25	18.15	715	973	17.7	17.4	1.0	500.0	39.4
26	35	713	2457	19.6	17.0	1.2	1109.0	20.4
27	23.1	707	2869	71.5	63.0	1.1	1179.0	30.6
28	26.4	707	1584	32.5	32.0	1.0	564.0	26.8
29	24.75	703.5	1100	13.5	13.1	1.0	611.0	28.4
30	31.35	700	3528	42.0	35.0	1.2	1407.0	22.3
31	16.5	688.5	1819	27.6	27.1	1.0	843.0	41.7
32	21.45	686	1129	19.7	19.5	1.0	567.0	32.0
33	18.15	677.5	813	14.5	14.4	1.0	590.0	37.3
34	24.75	669	1345	17.7	17.5	1.0	419.0	27.0
35	23.1	668	2193	21.2	19.5	1.1	982.0	28.9
36	21.45	658	2112	13.3	12.6	1.1	829.0	30.7
37	18.15	650	1979	27.5	26.0	1.1	800.0	35.8
38	24.75	642	1612	19.0	17.0	1.1	800.0	25.9
39	21.45	633	2936	154.8	125.0	1.2	1216.0	29.5
40	30	631	1825	19.7	18.5	1.1	873.0	21.0
41	14.85	630.5	2000	21.7	20.2	1.1	1139.0	42.5
42	28.05	607.5	1104	7.0	6.1	1.2	846.0	21.7
43	18.15	602	2100	12.0	10.0	1.2	1212.0	33.2
44	21.45	601	1300	16.1	16.1	1.0	545.0	28.0
45	24.75	600	860	7.9	7.3	1.1	560.0	24.2
46	26.4	597.5	1950	65.9	61.0	1.1	800.0	22.6
47	25	590.5	1251	22.8	21.1	1.1	550.0	23.6
48	14.85	585	1217	15.1	14.5	1.0	545.0	39.4
49	24.75	578	1000	65.0	60.5	1.1	552.0	23.4
50	23.1	576	1614	13.1	12.4	1.1	647.0	24.9
51	19.8	573	1818	14.8	13.9	1.1	843.0	28.9
52	16.5	572	925	9.0	8.5	1.1	461.0	34.7
53	24.75	565	1643	38.1	34.5	1.1	922.0	22.8
54	18.15	564	1336	27.1	21.4	1.3	1128.0	31.1
55	16.5	554	1100	7.3	6.9	1.1	600.0	33.6
56	12.375	520	780	6.0	5.8	1.0	417.0	42.0
57	23.1	496.5	1043	22.1	21.4	1.0	490.0	21.5
58	18.15	460	1309	12.0	9.5	1.3	856.0	25.3
59	21.45	445	1298	17.6	15.1	1.2	567.0	20.7
60	18.15	440	1350	14.2	11.5	1.2	895.0	24.2
61	21	439.5	944	20.3	19.7	1.0	484.0	20.9
62	18.15	435	572	7.9	7.6	1.0	300.0	24.0

63	20	430	1115	18.4	17.0	1.1	670.0	21.5
64	16.5	423	845	8.7	8.3	1.1	793.0	25.6
65	18.15	420	2800	29.0	22.5	1.3	1000.0	23.1
66	13.2	405	600	16.2	15.7	1.0	302.0	30.7
67	18	400	1415	16.0	13.0	1.2	757.0	22.2
68	16.5	392	909	11.4	11.3	1.0	585.0	23.8
69	16.5	387	600	15.0	14.5	1.0	266.0	23.5
70	19	386	1212	14.6	13.1	1.1	570.0	20.3
71	18	383	780	14.0	13.3	1.1	324.0	21.3
72	18	370	1711	17.8	16.0	1.1	1007.0	20.6
73	16.5	345.5	1008	14.0	13.5	1.0	550.0	20.9
74	11.55	343	2000	16.4	14.0	1.2	870.0	29.7
75	15	320	1471	11.3	10.0	1.1	720.0	21.3
76	11.55	320	1250	16.2	18.4	1.1	540.0	27.7
77	15	309.5	1717	15.0	13.3	1.1	1082.0	20.6
78	14	307	725	12.0	10.0	1.2	477.0	21.9

Sub-group-3.1: Confined highly sinuous channels

Channel No.	Ch d. (m)	CW (m)	MBW (m)	La (km)	ML (km)	SI	RC (m)	W/D
1	25	600	14000	214.0	76.0	2.8	3000.0	24.0
2	22	400	7000	130.5	42.7	3.1	1500.0	18.2
3	15	226	6000	140.0	55.0	2.5	850.0	15.1
4	13	200	3500	122.5	44.2	2.8	2000.0	15.4
5	14.85	240	4500	46.1	18.0	2.6	2700.0	16.2

Sub-group-3.2: Unconfined highly sinuous channels

Channel No.	Ch d. (m)	CW (m)	MBW (m)	La (km)	ML (km)	SI	RC (m)	W/D
1	16	176	3400	58.0	28.0	2.1	1560.0	4.0
2	11.55	173	5000	45.3	21.2	2.1	2110.0	5.3
3	11.55	148	3400	50.0	22.0	2.3	1290.0	3.1
4	14	109	4000	180.0	75.0	2.4	1680.0	2.1
5	16.5	103	3700	45.7	20.0	2.3	620.0	2.9
6	13.2	102	2100	144.6	65.0	2.2	1220.0	4.2
7	13.2	75	3500	76.0	37.8	2.0	765.0	2.9
8	8.25	75	1330	27.0	13.3	2.0	280.0	1.0
9	9.9	75	2600	121.0	60.1	2.0	590.0	2.7
10	6.6	75	2300	42.0	21.0	2.0	330.0	1.3
11	11.55	75	1500	40.0	20.0	2.0	775.0	1.8
12	6.6	75	1000	32.0	15.0	2.1	220.0	1.0
13	6.6	75	2000	27.5	12.3	2.2	310.0	1.2
14	6.6	75	1700	21.0	10.0	2.1	350.0	1.1
15	9.9	75	2500	30.0	13.5	2.2	820.0	1.7
16	18.15	195	3000	110.0	54.3	2.0	1450.0	7.8
17	18.15	220	3000	122.8	81.0	1.5	500.0	4.0
18	11	212	3800	51.6	28.5	1.8	800.0	3.2
19	14.85	200	3800	68.6	45.0	1.5	1100.0	4.0
20	8.25	195	2000	160.0	105.0	1.5	750.0	3.8
21	16.5	186	3100	36.0	24.0	1.5	531.0	3.5
22	9.9	176	4000	38.8	22.4	1.7	770.0	3.7
23	11.55	160	1500	46.0	30.0	1.5	600.0	3.5
24	14.85	130	1950	40.4	24.4	1.7	570.0	4.1
25	9.9	120	1450	26.8	15.0	1.8	750.0	2.5
26	8.25	115	900	25.0	16.0	1.6	440.0	1.7
27	16.5	115	4300	30.2	20.0	1.5	885.0	5.2
28	13.2	64	3600	93.1	50.0	1.9	670.0	3.3
29	13.2	60	1350	53.6	35.0	1.5	1000.0	4.4
30	8.25	55	1300	39.1	26.0	1.5	630.0	3.5
31	8	55	2150	84.6	51.0	1.7	1090.0	5.1
32	9.9	55	2000	40.0	23.0	1.7	540.0	3.8
33	6.6	50	1500	21.0	13.0	1.6	256.0	4.1
34	9.9	50	1200	17.0	11.0	1.5	300.0	2.4
35	9.9	50	800	24.0	16.0	1.5	328.0	2.0
36	6.6	50	1600	17.7	10.1	1.8	188.0	2.0
37	11	210	2000	32.0	21.0	1.5	1000.0	3.6

8.3 Lithological Logs

LEGEND

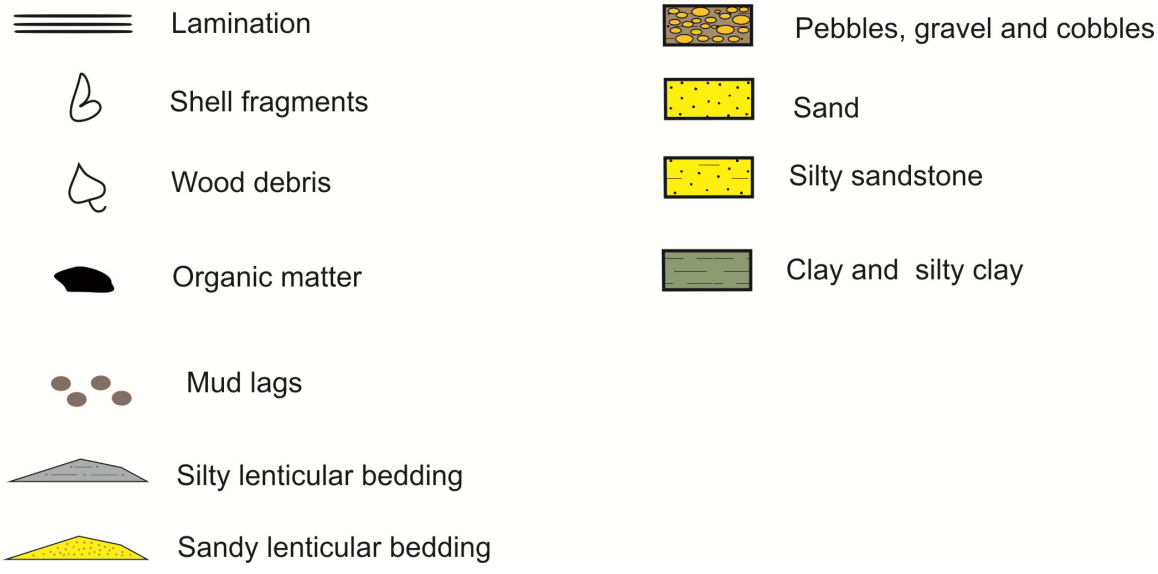
Lamination
Shell fragments
Wood debris
Organic matter
Mud lags
Silty lenticular bedding
Sandy lenticular bedding
Pebbles, gravel and cobbles
Sand
Silty sandstone
Clay and silty clay

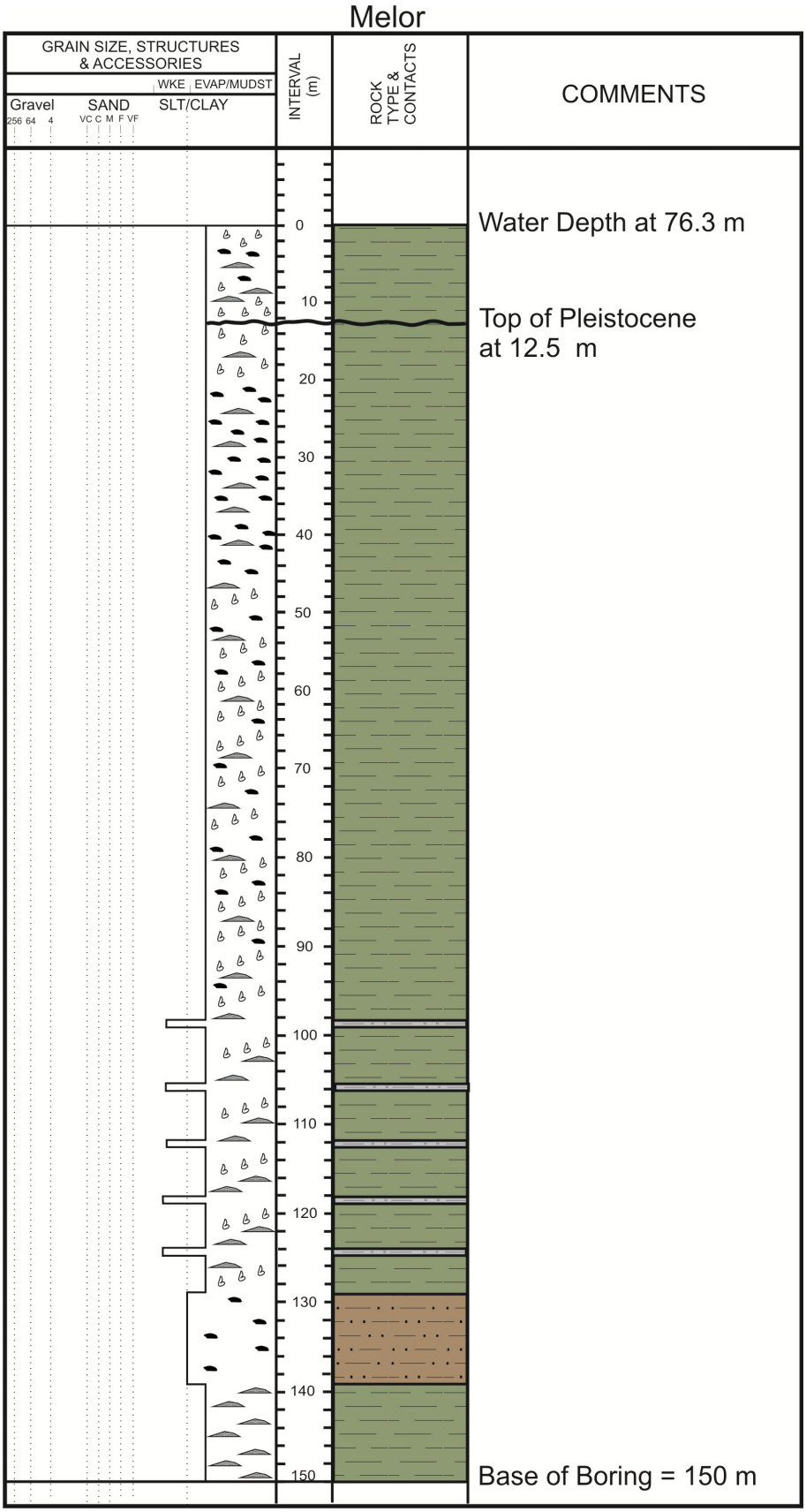
Melor
GRAIN SIZE, STRUCTURES & ACCESSORIES
WKE
EVAP/MUDST
Gravel
SAND
SLT/CLAY
256 64 4
VC C M F VF
INTERVAL (m)
ROCK TYPE & CONTACTS
COMMENTS
0
10
20
30
40
50
60
70
80
90
100
110
120
130
140
150
Water Depth at 76.3 m
Top of Pleistocene at 12.5 m
Base of Boring = 150 m

Tanga Barat-1A

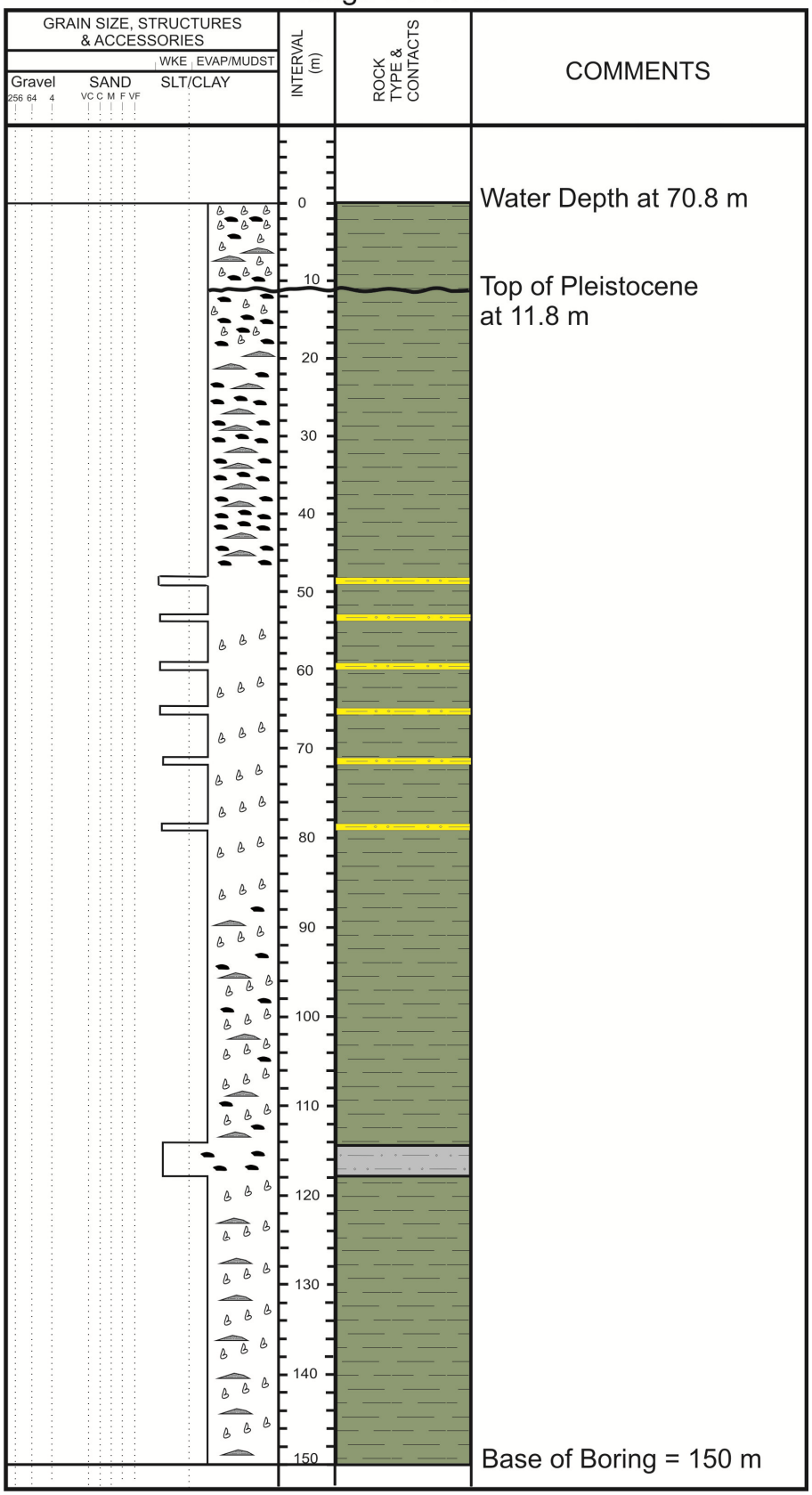

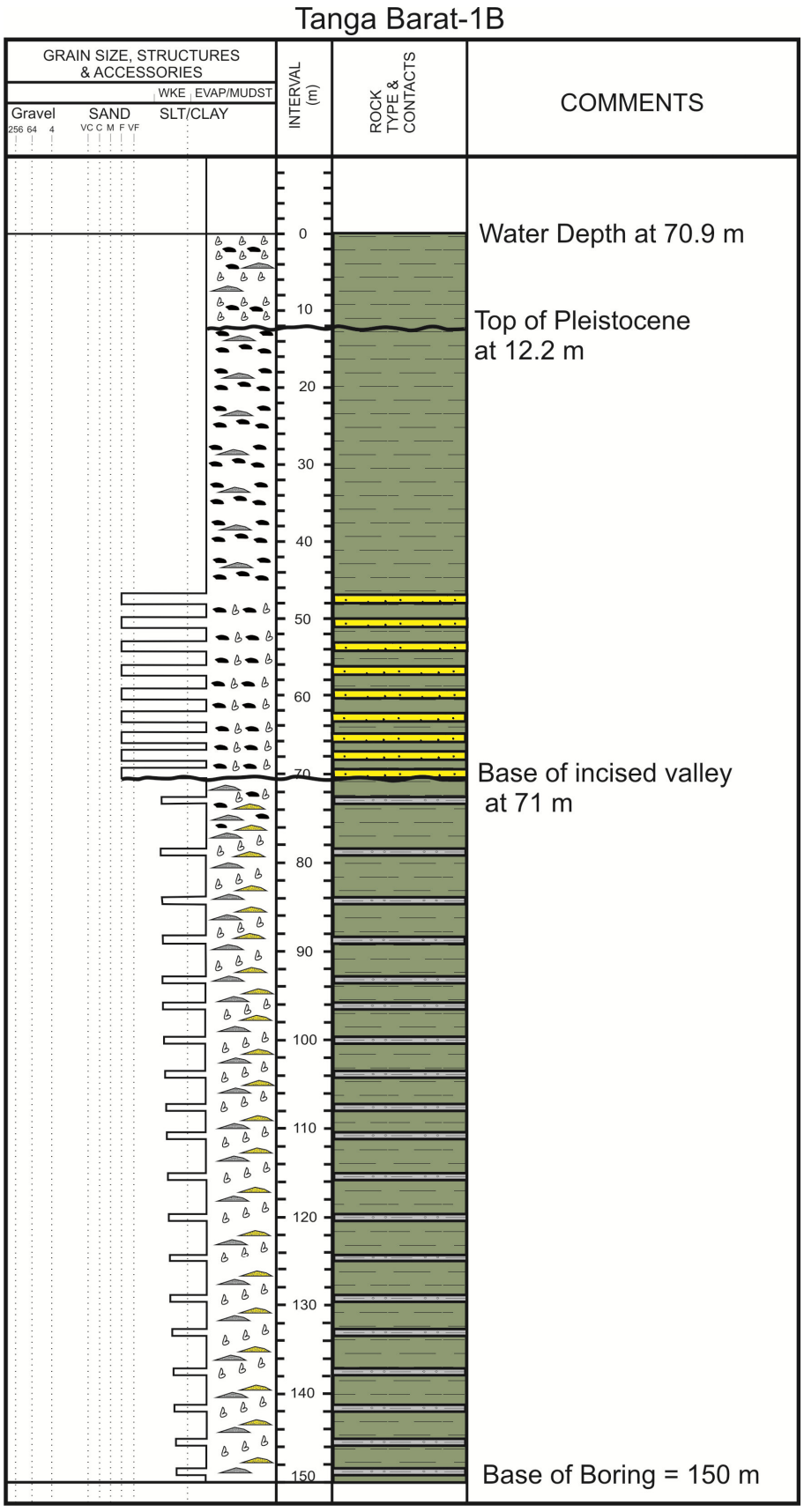
Tanga Barat-1B
GRAIN SIZE, STRUCTURES & ACCESSORIES
WKE
EVAP/MUDST
Gravel
SAND
SLT/CLAY
256 64 4
VC C M F VF
INTERVAL (m)
ROCK TYPE & CONTACTS
COMMENTS
0
10
20
30
40
50
60
70
80
90
100
110
120
130
140
150
Water Depth at 70.9 m
Top of Pleistocene at 12.2 m
Base of incised valley at 71 m
Base of Boring = 150 m

Dulang A-Primary

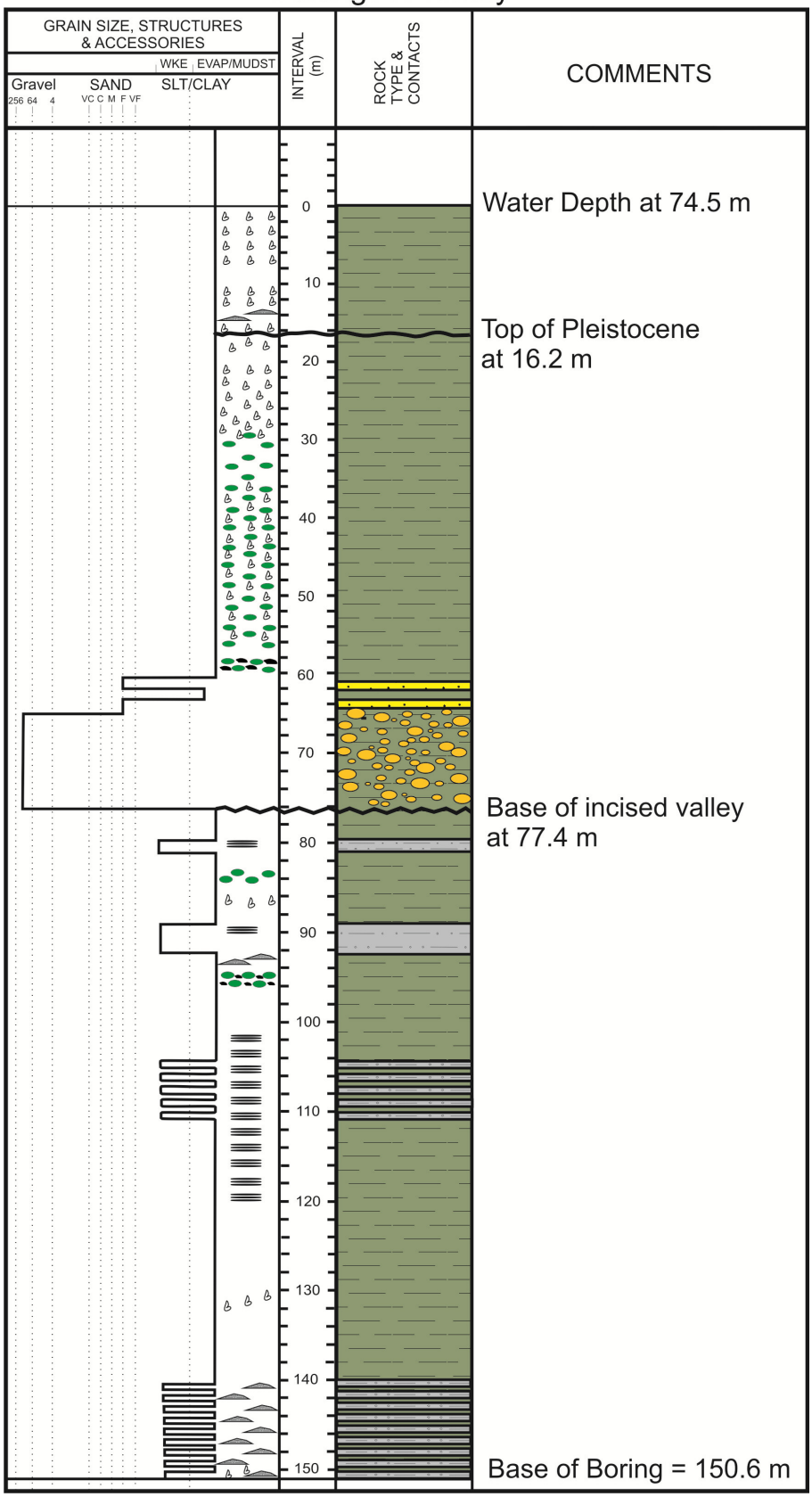

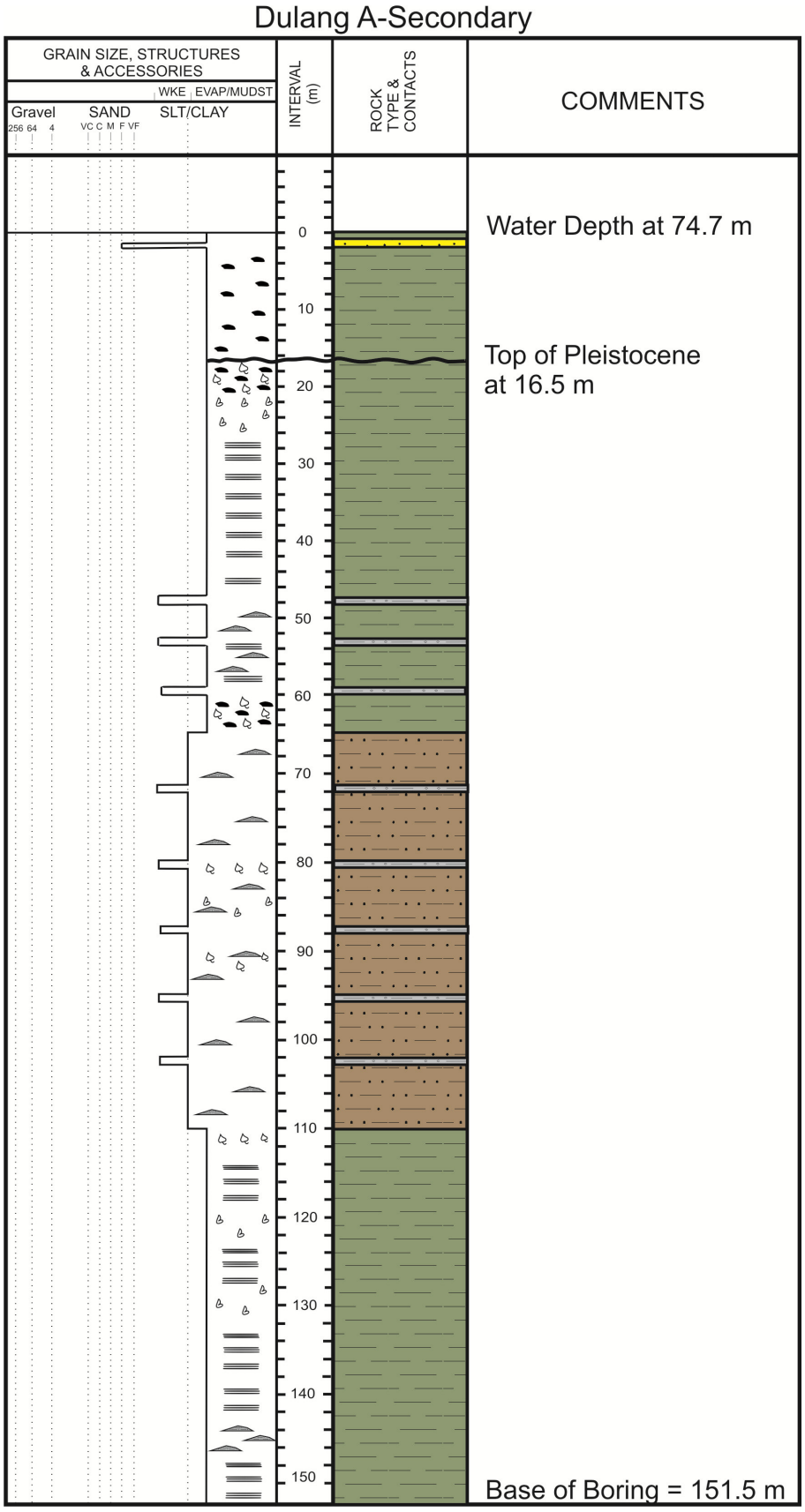
Dulang A-Secondary
GRAIN SIZE, STRUCTURES & ACCESSORIES
WKE
EVAP/MUDST
Gravel
SAND
SLT/CLAY
256 64 4
VC C M F VF
INTERVAL (m)
ROCK TYPE & CONTACTS
COMMENTS
0
10
20
30
40
50
60
70
80
90
100
110
120
130
140
150
Water Depth at 74.7 m
Top of Pleistocene at 16.5 m
Base of Boring = 151.5 m

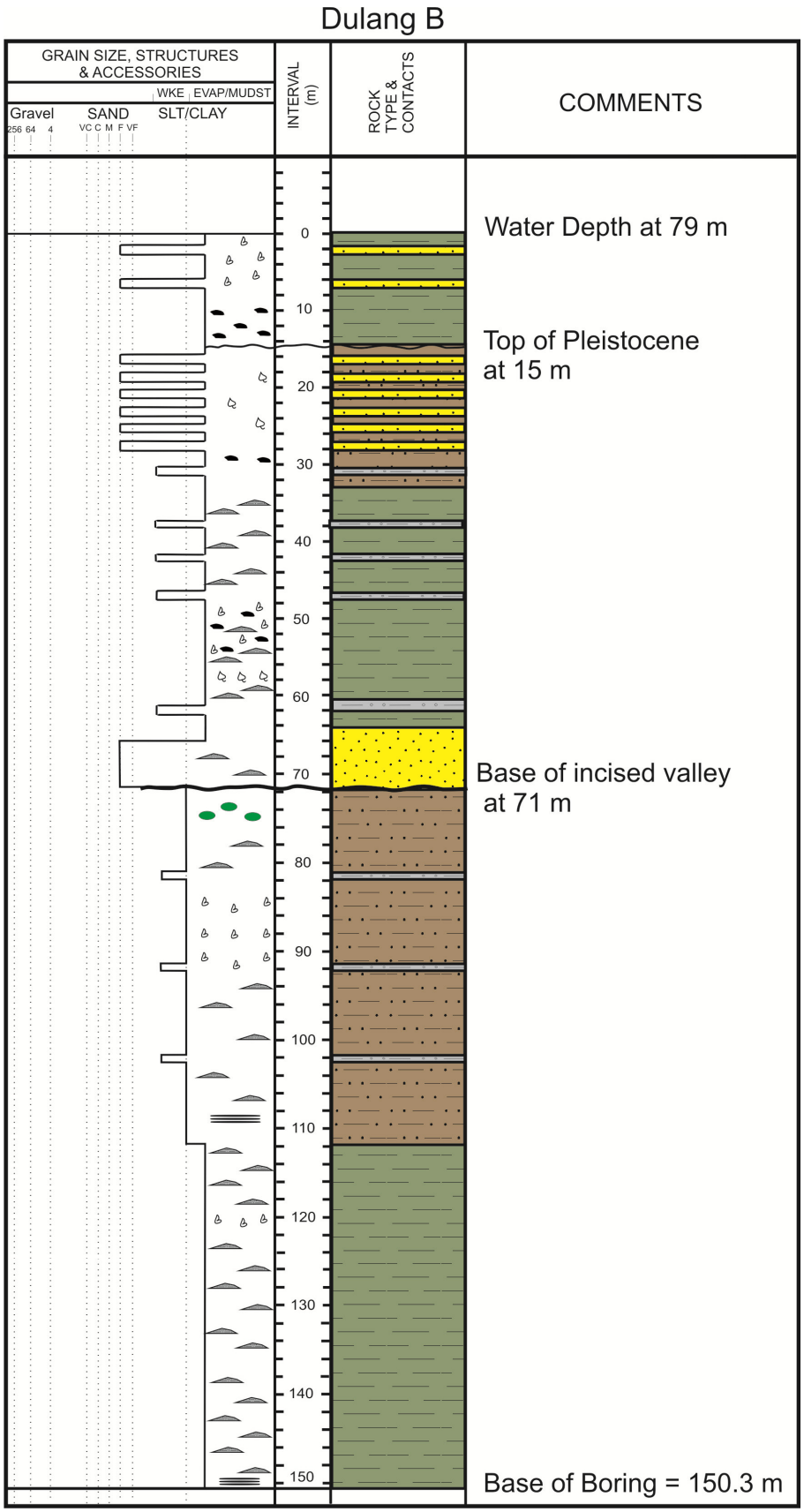
Dulang B
GRAIN SIZE, STRUCTURES & ACCESSORIES
WKE
EVAP/MUDST
Gravel
SAND
SLT/CLAY
256 64 4
VC C M F VF
INTERVAL (m)
ROCK TYPE & CONTACTS
COMMENTS
0
10
20
30
40
50
60
70
80
90
100
110
120
130
140
150
Water Depth at 79 m
Top of Pleistocene at 15 m
Base of incised valley at 71 m
Base of Boring = 150.3 m

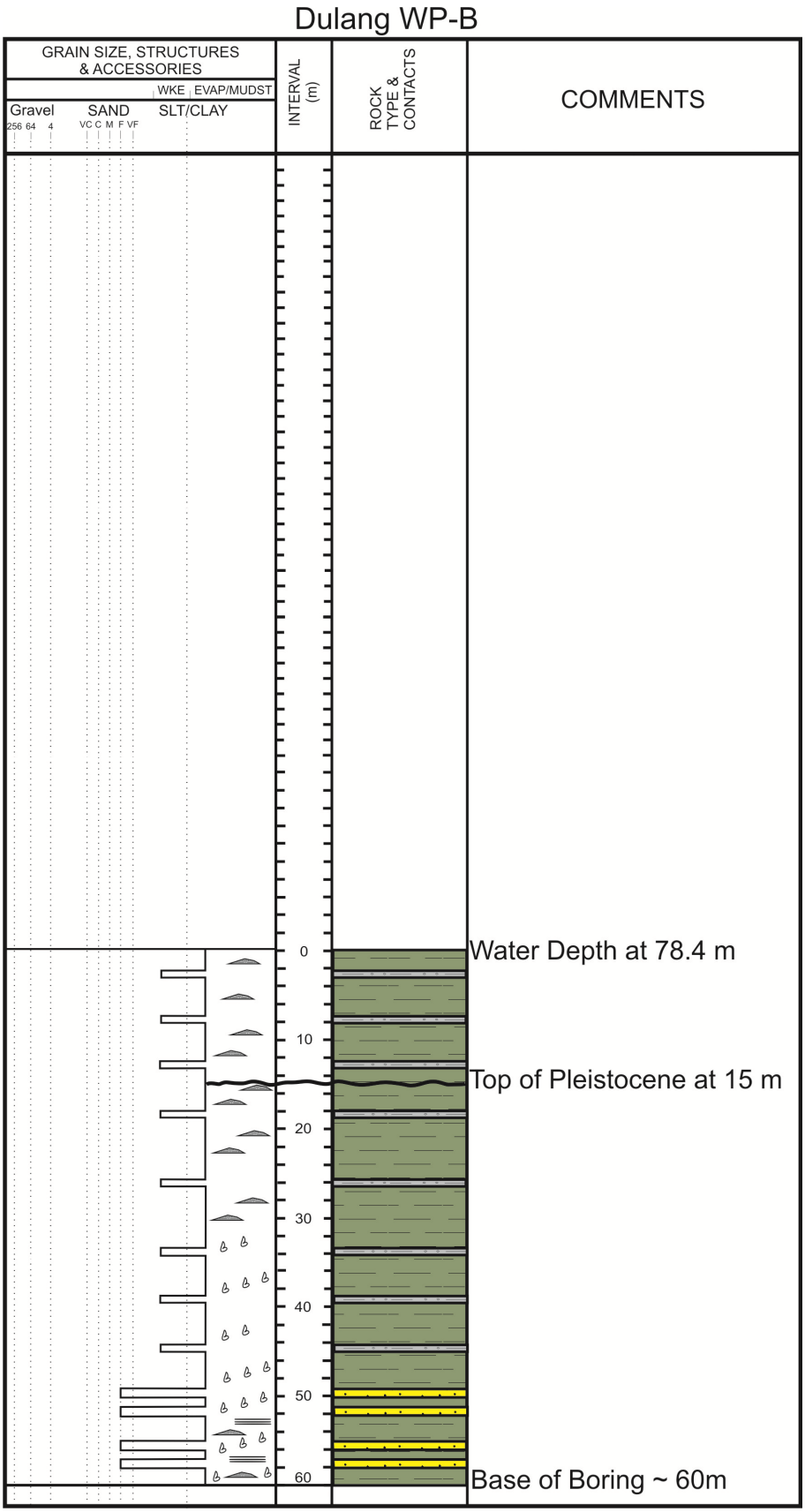
Dulang WP-B
GRAIN SIZE, STRUCTURES & ACCESSORIES
WKE
EVAP/MUDST
Gravel
SAND
SLT/CLAY
256 64 4
VC C M F VF
INTERVAL (m)
ROCK TYPE & CONTACTS
COMMENTS
0
10
20
30
40
50
60
Water Depth at 78.4 m
Top of Pleistocene at 15 m
Base of Boring ~ 60m

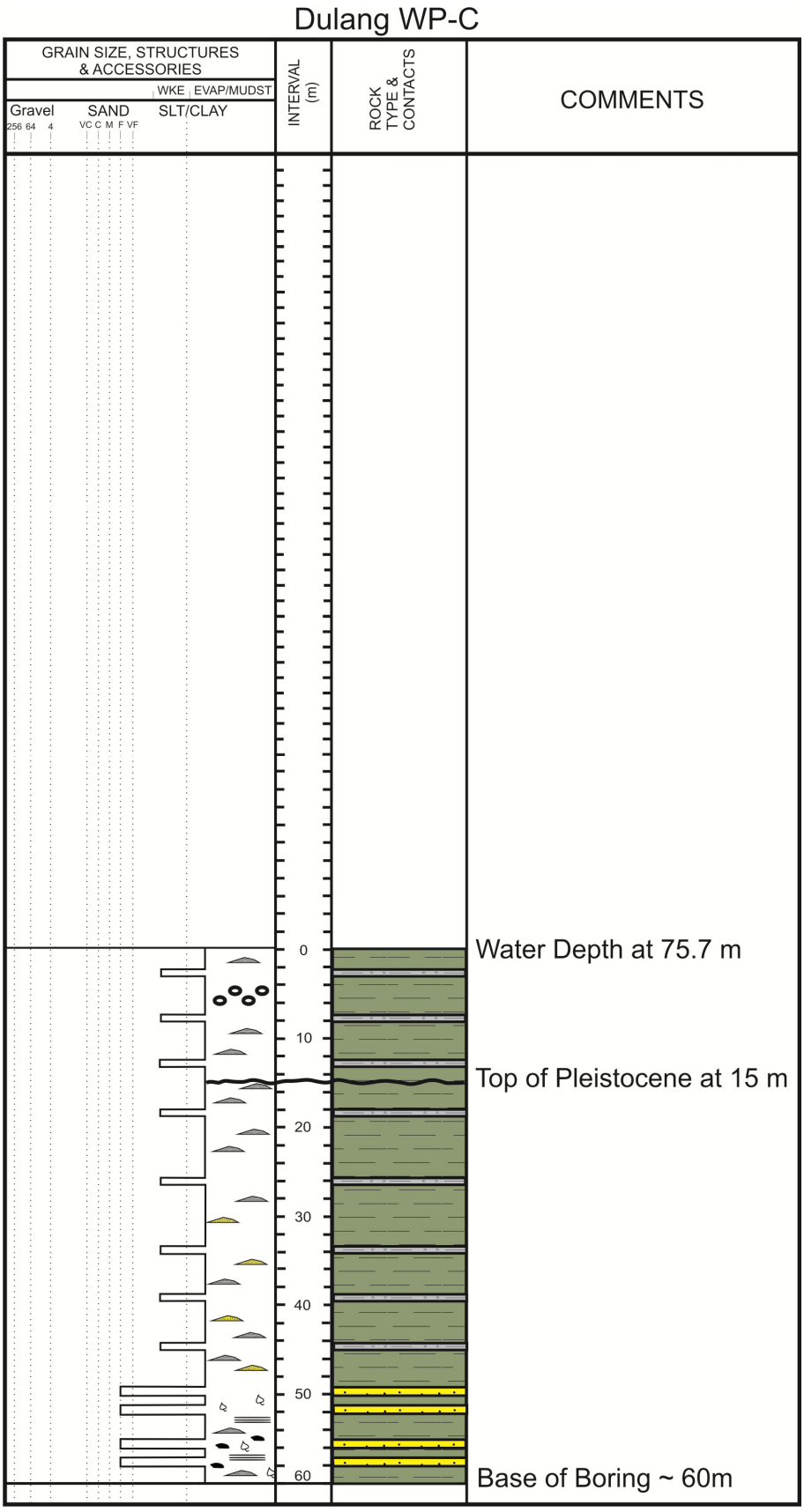
Dulang WP-C
GRAIN SIZE, STRUCTURES & ACCESSORIES
WKE
EVAP/MUDST
Gravel
SAND
SLT/CLAY
256 64 4
VC C M F VF
INTERVAL (m)
ROCK TYPE & CONTACTS
COMMENTS
0
10
20
30
40
50
60
Water Depth at 75.7 m
Top of Pleistocene at 15 m
Base of Boring ~ 60m

Dulang WP-D

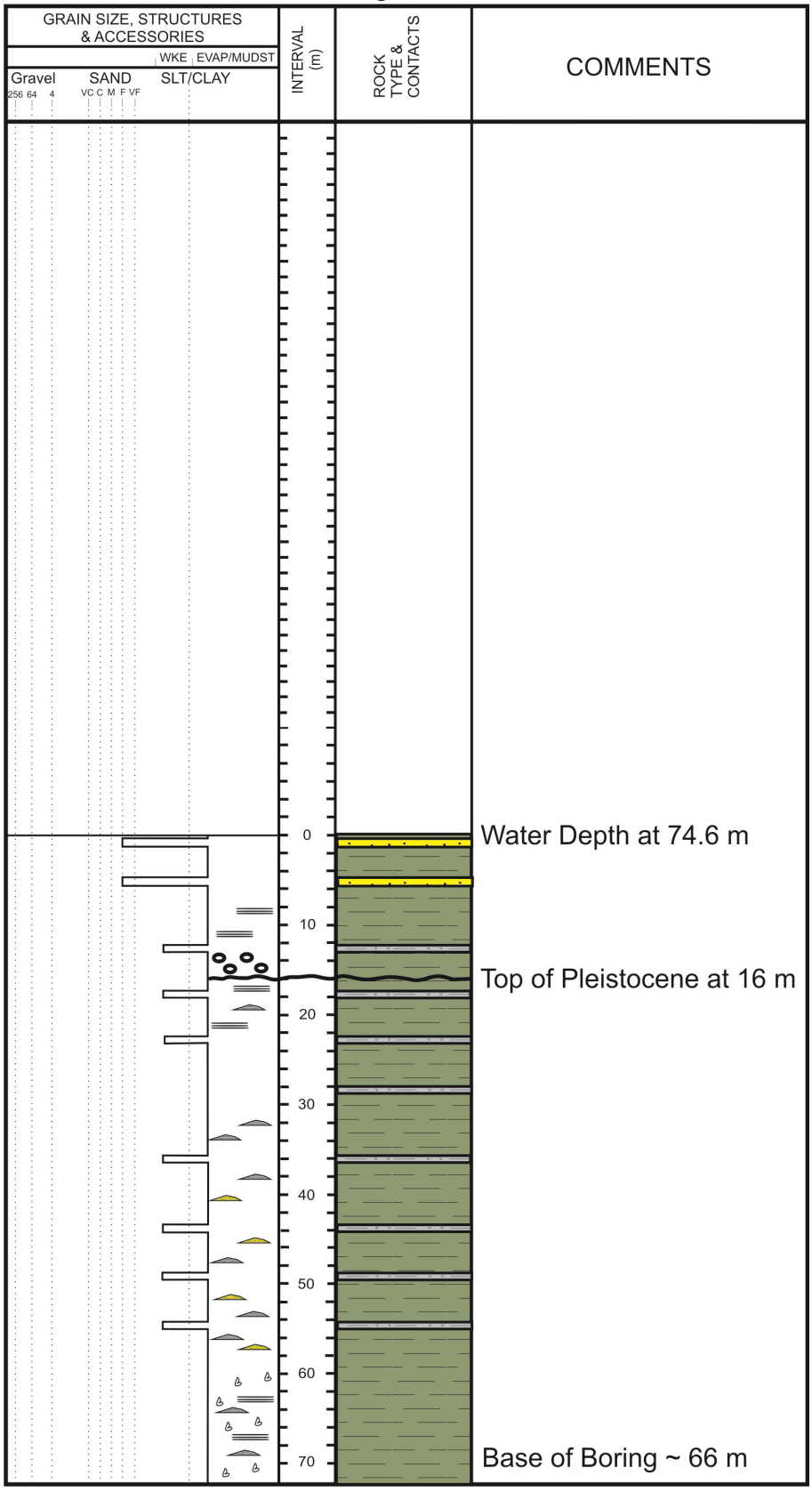
GRAIN SIZE, STRUCTURES & ACCESSORIES
WKE
EVAP/MUDST
Gravel
SAND
SLT/CLAY
256 64 4
VC C M F VF
INTERVAL (m)
ROCK TYPE & CONTACTS
COMMENTS
0
10
20
30
40
50
60
70
Water Depth at 74.6 m
Top of Pleistocene at 16 m
Base of Boring ~ 66 m

Dulang SPM-1

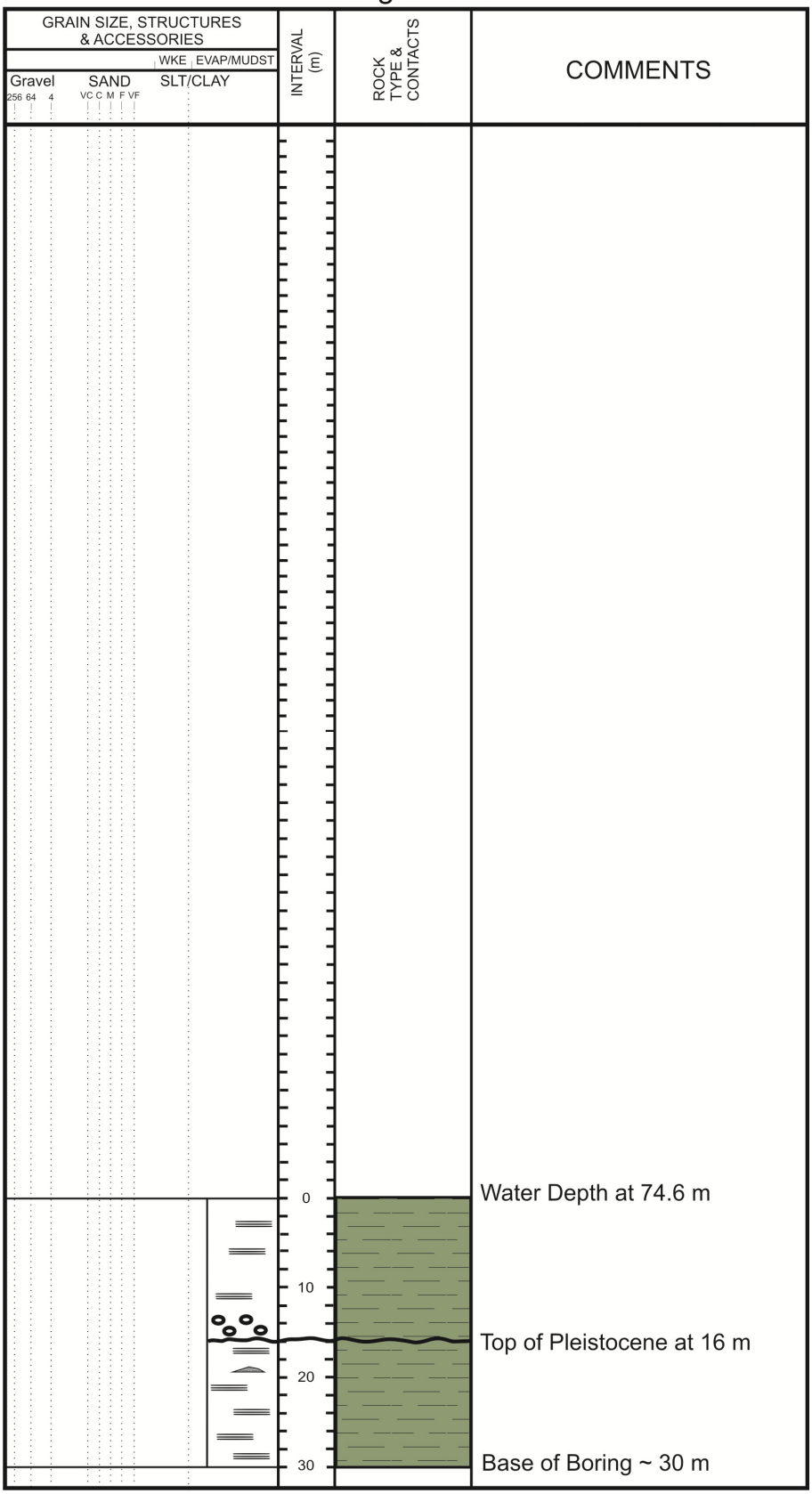
GRAIN SIZE, STRUCTURES & ACCESSORIES
WKE
EVAP/MUDST
Gravel
SAND
SLT/CLAY
256 64 4
VC C M F VF
INTERVAL (m)
ROCK TYPE & CONTACTS
COMMENTS
0
10
20
30
Water Depth at 74.6 m
Top of Pleistocene at 16 m
Base of Boring ~ 30 m

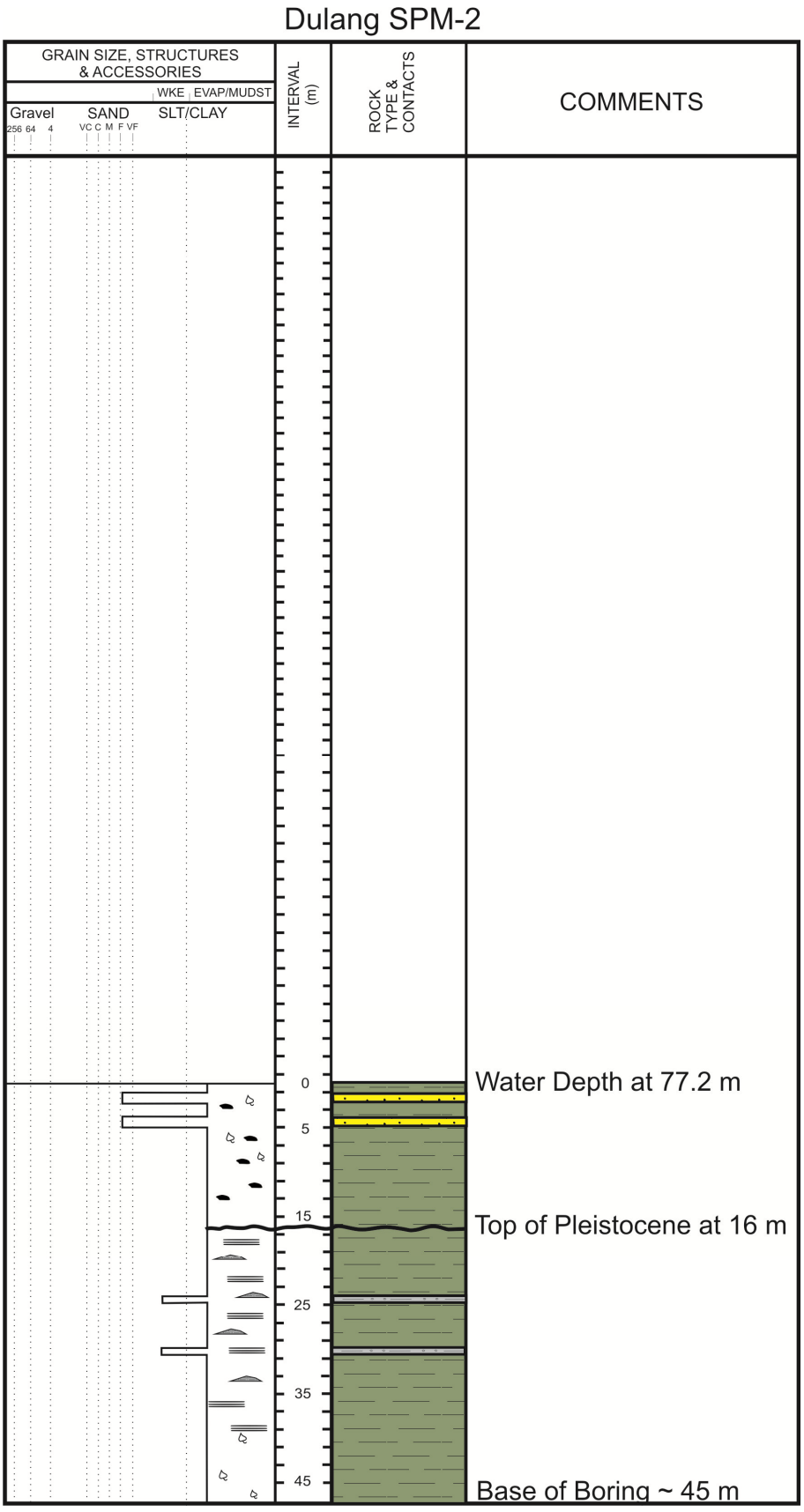
Dulang SPM-2
GRAIN SIZE, STRUCTURES & ACCESSORIES
WKE
EVAP/MUDST
Gravel
SAND
SLT/CLAY
256 64 4
VC C M F VF
INTERVAL (m)
ROCK TYPE & CONTACTS
COMMENTS
0
5
15
25
35
45
Water Depth at 77.2 m
Top of Pleistocene at 16 m
Base of Boring ~ 45 m

Dulang SPM-3

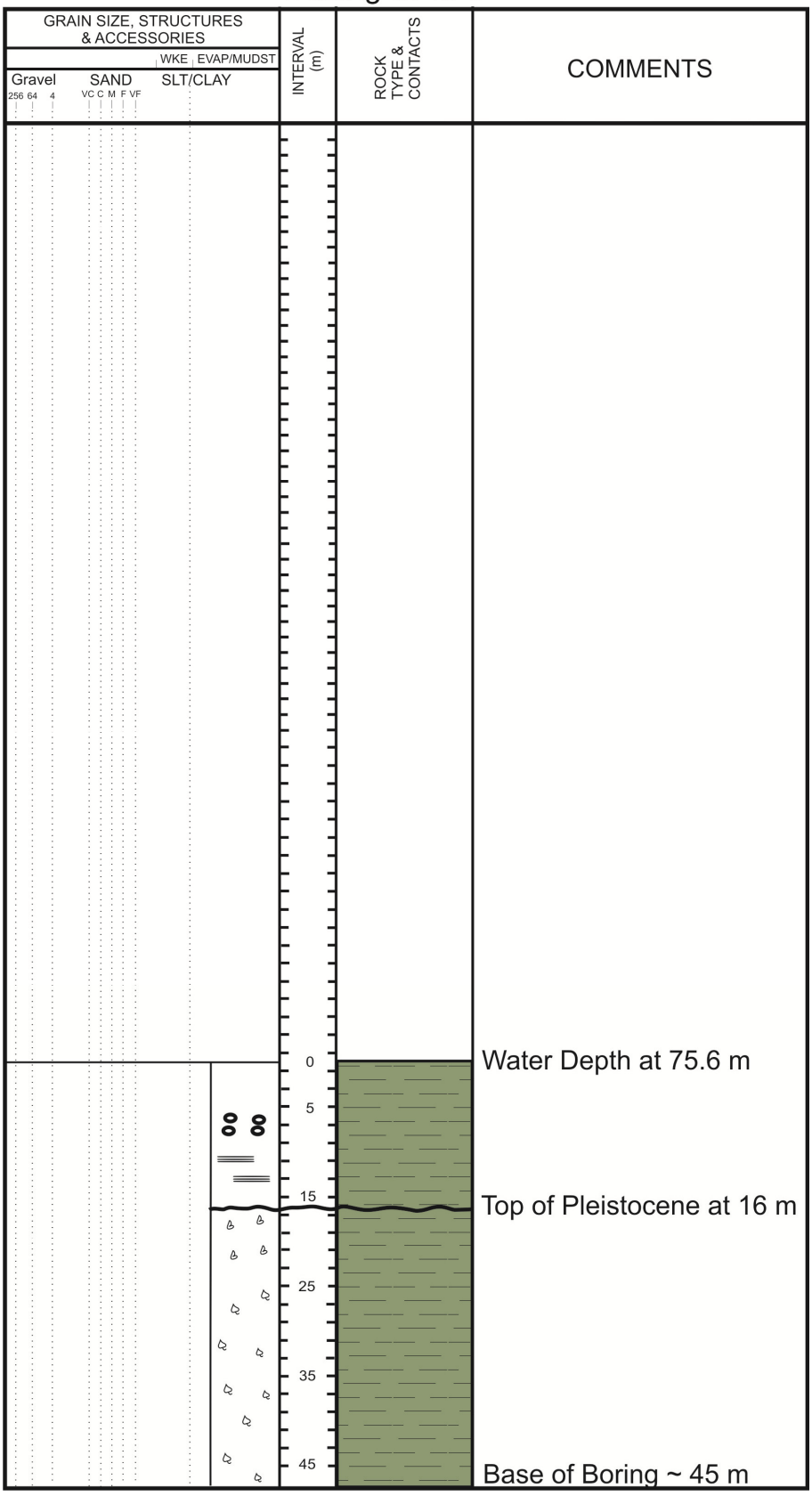
GRAIN SIZE, STRUCTURES & ACCESSORIES
WKE
EVAP/MUDST
Gravel
SAND
SLT/CLAY
256 64 4
VC C M F VF
INTERVAL (m)
ROCK TYPE & CONTACTS
COMMENTS
0
5
15
25
35
45
Water Depth at 75.6 m
Top of Pleistocene at 16 m
Base of Boring ~ 45 m

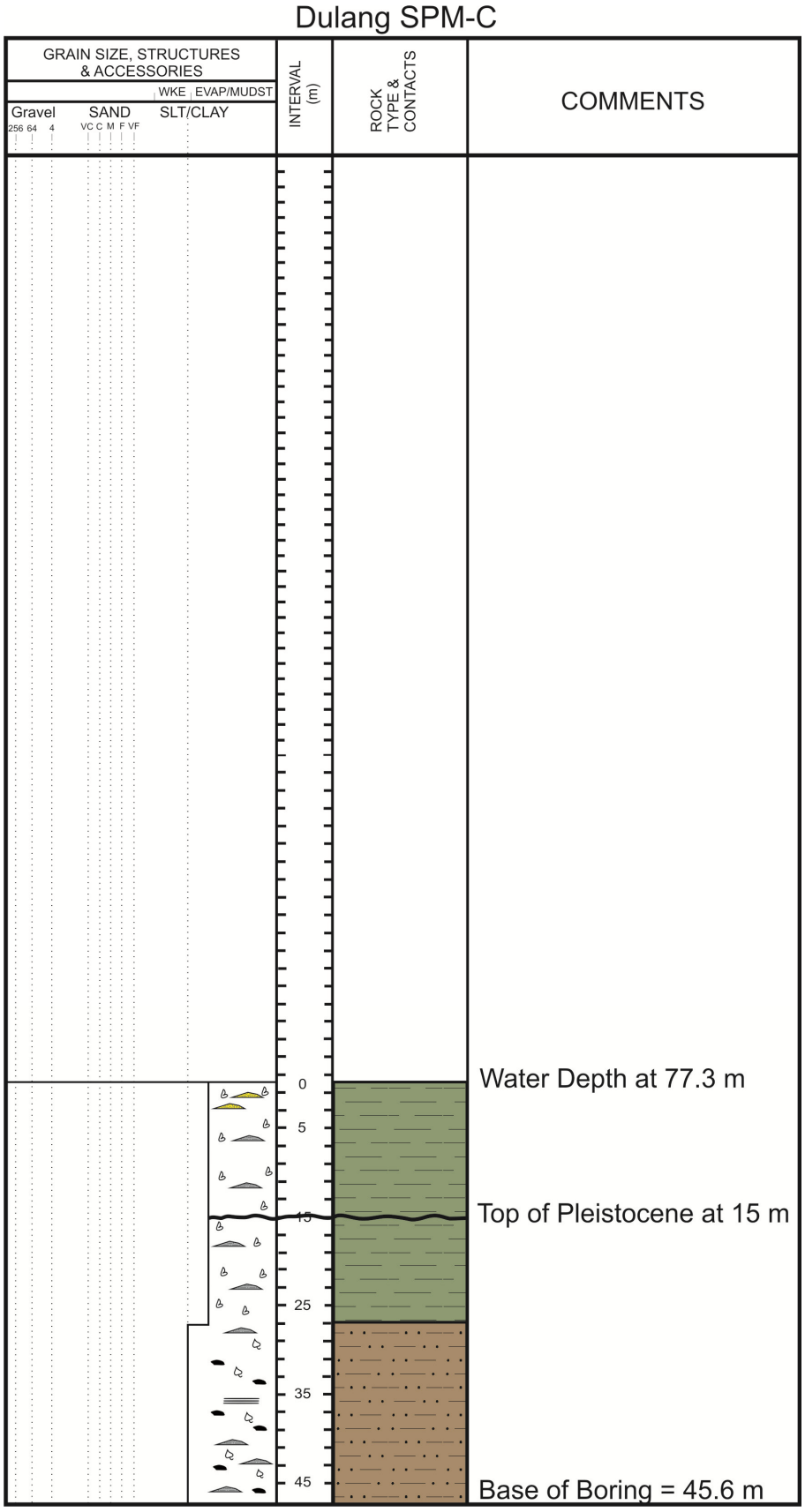
Dulang SPM-C
GRAIN SIZE, STRUCTURES & ACCESSORIES
WKE
EVAP/MUDST
Gravel
SAND
SLT/CLAY
256 64 4
VC C M F VF
INTERVAL (m)
ROCK TYPE & CONTACTS
COMMENTS
0
5
15
25
35
45
Water Depth at 77.3 m
Top of Pleistocene at 15 m
Base of Boring = 45.6 m